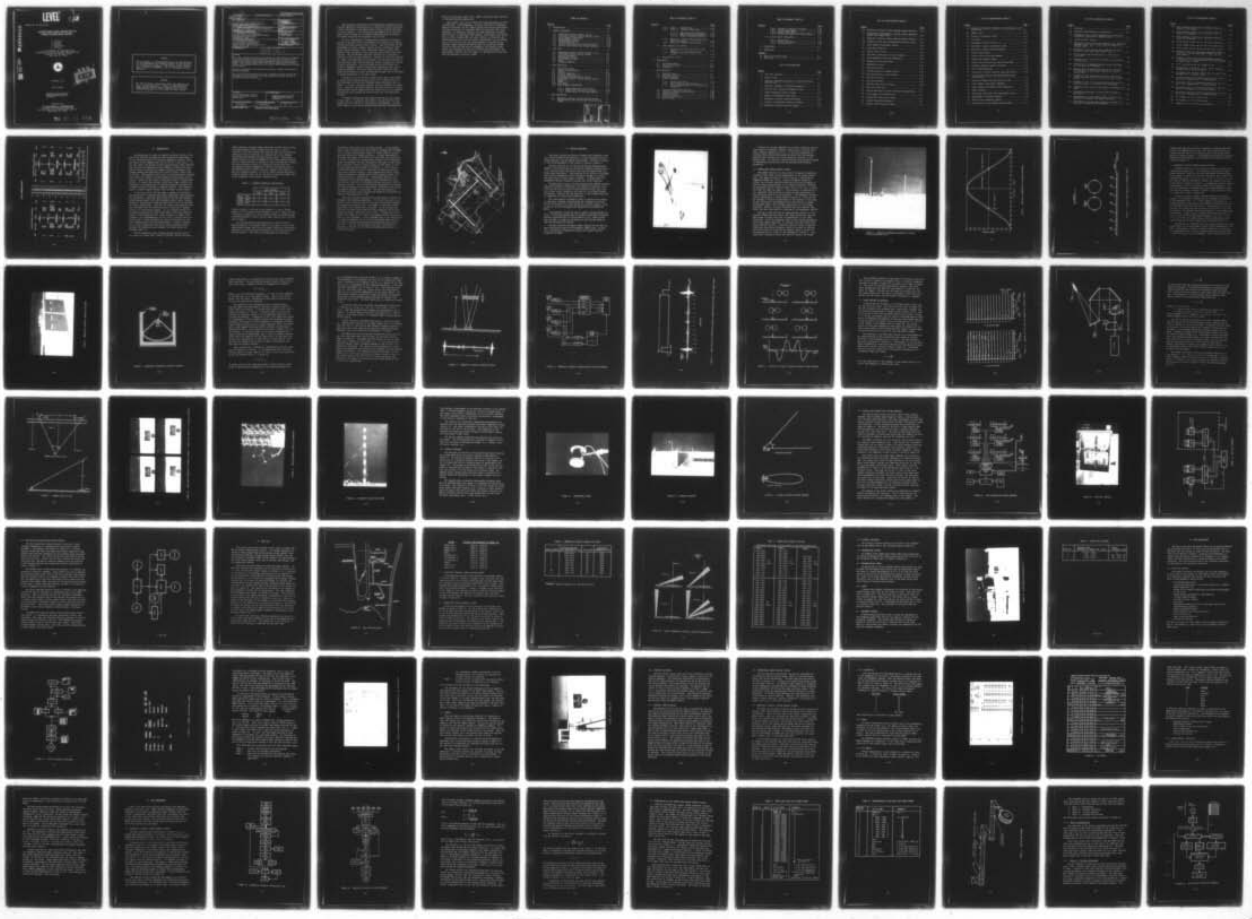
AD-A068 925 TRANSPORTATION SYSTEMS CENTER CAMBRIDGE MASS F/G 1/2
AIRCRAFT WAKE VORTEX TAKEOFF TESTS AT TORONTO INTERNATIONAL AIR--ETC(U)
FEB 79 T SULLIVAN, J HALLOCK, B WINSTON

UNCLASSIFIED TSC-FAA-79-9 FAA-RD-78-143 NL

1 OF 3
AD
AD 68925



LEVEL II

B.S. 13

AD A068925

DDC FILE COPY

REPORT NO. FAA-RD-78-143

AIRCRAFT WAKE VORTEX TAKEOFF TESTS AT TORONTO INTERNATIONAL AIRPORT

T. Sullivan
J. Hallock
B. Winston
I. McWilliams
D. Burnham

U.S. DEPARTMENT OF TRANSPORTATION
RESEARCH AND SPECIAL PROGRAMS ADMINISTRATION
Transportation Systems Center
Cambridge MA 02142



DDC
RECEIVED
MAY 24 1979
C

FEBRUARY 1979

FINAL REPORT

DOCUMENT IS AVAILABLE TO THE PUBLIC THROUGH THE NATIONAL TECHNICAL INFORMATION SERVICE, SPRINGFIELD, VIRGINIA 22161

Prepared for

U.S. DEPARTMENT OF TRANSPORTATION
FEDERAL AVIATION ADMINISTRATION
Systems Research and Development Service
Washington DC 20591

79 05 24 012

NOTICE

This document is disseminated under the sponsorship of the Department of Transportation in the interest of information exchange. The United States Government assumes no liability for its contents or use thereof.

NOTICE

The United States Government does not endorse products or manufacturers. Trade or manufacturers' names appear herein solely because they are considered essential to the object of this report.

Technical Report Documentation Page

1. Report No.	2. Government Accession No.	3. Recipient's Catalog No.
FAA-RD-78-143		

4. Title and Subtitle

AIRCRAFT WAKE VORTEX TAKEOFF TESTS AT TORONTO INTERNATIONAL AIRPORT

5. Report Date
February 1979

6. Performing Organization Code
DTS-521

7. Author(s)
T. Sullivan, J. Hallock, B. Winston, I. McWilliams, D. Burnham

8. Performing Organization Report No.
DOT-TSC-FAA-79-9

9. Performing Organization Name and Address
U.S. Department of Transportation
Research and Special Programs Administration
Transportation Systems Center
Cambridge MA 02142

10. Work Unit No. (TRAIS)
FA905/R9111

11. Contract or Grant No.

12. Sponsoring Agency Name and Address
U.S. Department of Transportation
Federal Aviation Administration
Systems Research and Development Service
Washington DC 20591

13. Type of Report and Period Covered
Final Report - June 1976-June 1977

14. Sponsoring Agency Code

15. Supplementary Notes
210p.

16. Abstract

This report describes the collection and analysis of data related to the behavior of the wake vortices of departing aircraft. The test site was located on the departure end of Runway 23L at Toronto International Airport, Toronto, Ontario, Canada. Three arrays of Ground Wind Vortex Sensing Systems and one Monostatic Acoustic Vortex Sensing System were used to detect, track and measure the strength of the vortices.

The data were analyzed to determine vortex lifetimes, transport characteristics and decay mechanism.

The results of the data analysis were used to generate an elliptical wind rose criterion similar to that used in the Vortex Advisory System for reduction in interarrival aircraft spacings.

17. Key Words	18. Distribution Statement
Vortex Sensing Tests, Acoustic Sensors, Wind Sensors, Aircraft Wake Vortices	DOCUMENT IS AVAILABLE TO THE PUBLIC THROUGH THE NATIONAL TECHNICAL INFORMATION SERVICE, SPRINGFIELD, VIRGINIA 22161

19. Security Classif. (of this report)	20. Security Classif. (of this page)	21. No. of Pages	22. Price
Unclassified	Unclassified	216	

Form DOT F 1700.7 (8-72) Reproduction of completed page authorized

407 082

PREFACE

The increased interarrival and interdeparture spacings between aircraft imposed by the potential of a wake vortex hazard have been a major contributor to aircraft delays at major airports operating at or near capacity. The problem has been emphasized in the last several years because of the rapidly increasing costs associated with these delays and the resultant waste of fuel.

The U.S. Department of Transportation initiated a multiphase program in the early 1970's to determine the feasibility of modifying the constraint posed by wake vortices. The first phase was the development of sensor systems, such as arrays of propeller anemometers, pulsed acoustic radars, monostatic acoustic radars and a Doppler laser velocimeter, which could be used to detect and track vortices. The second phase was the collection of a statistical quantity of data on vortex behavior. Analysis of this data resulted in a model for predicting vortex behavior and the identification of wind conditions when vortices would not pose a problem with reduced aircraft separations. The third phase was the development of a system to implement reduced interarrival separations in an operational environment. The first Vortex Advisory System has been installed at Chicago's O'Hare International Airport and is scheduled to become operational in the near future.

Virtually all of the effort in these three phases was devoted to the aircraft landing operation since this is where delays are more important and where most reported vortex encounters were recorded. In theory, similar procedures could be developed for departures. Using the same sensor systems, the test facility at Toronto International Airport demonstrated the feasibility of this approach by detecting and tracking the vortices from over 5000 departing aircraft.

It should be noted that both English and metric units appear in this report. In general, the format is to use English as the primary unit with the metric equivalent in parentheses. In some cases, however, the data processing output has been developed with

metric as the primary units (e.g., MAVSS circulation data) and this is followed wherever appropriate.

The authors would like to thank the following people for their contributions: Chuck Radgowski, Illinois Institute of Technology Research Institute, for his support during the system installation, training of Ministry of Transport (MOT) site operators and, most important, his immediate response to system modification requirements during site operation; Mike Ahoorai, Leon Thomas, Bert Drenth and K.C. Howe, Canadian MOT, for their efforts in operating and maintaining the test site; Ron Brash, Canadian MOT, for his management of the test site and his rapid response in resolving site problems; Rigby Stamison and Rob Milliken for providing TSC/MOT liaison and overall MOT project management; the Canadian Armed Forces for providing the services of the Chinook helicopter; and John Winkler, Kentron, for his support in the analysis of the data from the monostatic acoustic system.

TABLE OF CONTENTS

Section			Page
1.	INTRODUCTION		1-1
2.	SENSOR SUBSYSTEMS		2-1
	2.1	Ground-Wind Vortex-sensing System	2-3
	2.2	Monostatic Acoustic Vortex-sensing System	2-7
	2.3	Laser Doppler Velocimeter	2-18
	2.4	Photographic System	2-23
	2.5	Meteorological System	2-23
	2.6	Aircraft Detector	2-28
	2.7	Digital Data-Acquisition System Hardware	2-32
	2.8	Digital Data-Acquisition System Software	2-38
3.	TEST SITE		3-1
	3.1	Monostatic Acoustic Vortex-sensing System	3-3
	3.2	Ground-Wind Vortex-sensing System	3-3
	3.3	Aircraft Detectors	3-7
	3.4	Photographic System	3-7
	3.5	Meteorological Tower	3-7
	3.6	Laser	3-7
	3.7	Equipment Shelter	3-7
4.	DATA COLLECTION		4-1
	4.1	Real-Time Display	4-1
	4.2	System Initialization	4-3
	4.3	Camera	4-8
	4.4	Aircraft Detectors	4-10
	4.5	Aircraft Identification	4-10
	4.6	Ground-Wind Vortex-sensing System	4-11
	4.7	Monostatic Acoustic Vortex-sensing System	4-11
	4.8	Diagnostics	4-12
	4.9	DEBUG	4-12
	4.10	Log Sheets	4-12
	4.11	Laser Doppler Velocimeter	4-15
		4.11.1 Data Collection in the Ravine	4-16
		4.11.2 Finger-Scan Tracking of Vortices	4-16
		4.11.3 Second Series of LDV Measurements	4-16
5.	DATA PROCESSING		5-1
	5.1	Monostatic Acoustic Vortex-sensing System	5-1
	5.2	Meteorological and Ground-Wind Vortex-sensing System	5-6

ACCESSION for
NTIS White Section
DDC Buff Section
UNANNOUNCED
JUSTIFICATION
BY
DISTRIBUTION/AVAILABILITY CODES
Dist. SPECIAL

TABLE OF CONTENTS (CONT'D.)

Section			Page
	5.2.1	Phase I - Reformatting	5-10
	5.2.2	Phase II - Digital Processing	5-10
		5.2.2.1 - MET Processing Algorithm	5-12
		5.2.2.2 - GWVSS Processing Algorithm	5-13
		5.2.2.3 - Digital Processing Output	5-18
	5.2.3	Phase III - Vortex Track Analysis and MET Verification	5-21
	5.2.4	Phase IV - Punched Card Editing	5-28
5.3		Laser Doppler Velocimeter	5-28
	5.3.1	Processing of Data Collected in the Ravine	5-32
	5.3.2	LDV Data Collected Between Lines 1 and 2	5-33
5.4		Photographic System	5-33
6.		METEOROLOGY	6-1
6.1		Wind Measurements	6-1
6.2		Vertical Wind Shear	6-3
6.3		Turbulence	6-3
7.		DATA ANALYSIS	7-1
7.1		Aircraft Types	7-1
7.2		Reference Corridor	7-2
7.3		Vortex Residence	7-2
7.4		Vortex Lifetimes	7-7
	7.4.1	Vortex Decay Time	7-10
	7.4.2	Vortex-Position Distribution	7-12
	7.4.3	Vortex Characteristics as a Function of Turbulence	7-16
7.5		Aircraft-Height Distributions	7-16
7.6		Predictive Capability and Systems	7-24
7.7		Crossing Vortices	7-29
7.8		Vortex Bouncing	7-30
7.9		Aircraft Separations	7-31
7.10		Vortex Decay	7-35

TABLE OF CONTENTS (CONT'D.)

Section			Page
	7.10.1	Average or Effective Strength.....	7-35
	7.10.2	Vortex Decay Modes.....	7-40
	7.10.3	General Decay Model.....	7-47
	7.10.4	Probability Models for Vortex Decay....	7-54
7.11		Laser Doppler Velocimeter.....	7-57
	7.11.1	Ravine Site.....	7-57
	7.11.2	Finger-Scan Tests.....	7-57
	7.11.3	Arc-Scan Tests.....	7-59
8.		CONCLUSIONS.....	8-1
9.		REFERENCES.....	9-1

Appendix

A.	SPECIAL HELICOPTER TESTS.....	A-1
B.	DATA BASE.....	B-1

LIST OF ILLUSTRATIONS

Figure		Page
1.	Test Site Location.....	1-4
2.	Sensor Layout.....	2-2
3.	Propeller Anemometer Mounted on 10-foot Polyvinyl-chloride Pole.....	2-4
4.	Propeller Anemometer Calibrated Response.....	2-5
5.	Vortices over Propeller Anemometer Array.....	2-6
6.	Single Anemometer Output Voltage.....	2-8
7.	Example of Anemometer Array Data.....	2-9
8.	Monostatic Acoustic Antenna Enclosure.....	2-10
9.	Interior of Monostatic Acoustic Antenna.....	2-11
10.	Monostatic Acoustic Receiver Signal.....	2-14

LIST OF ILLUSTRATIONS (CONT'D.)

Figure		Page
11.	Monostatic Acoustic Vortex-sensing System Hardware..	2-15
12.	Quantization of Monostatic Acoustic Sensor Received Signal Into Range Gates.....	2-16
13.	Monostatic Acoustic Sensor Expected Signal Returns..	2-17
14.	Example of Data from the Monostatic Acoustic Sensor.	2-19
15.	Laser Doppler Velocimeter Optics.....	2-20
16.	Laser-Scan Geometry.....	2-22
17.	Camera Field of View.....	2-24
18.	Four-Photo Sequence of Aircraft Takeoff.....	2-25
19.	Three-Component Propeller Anemometer.....	2-26
20.	Waveguide Glide-Slope Tower.....	2-27
21.	Temperature Sensor.....	2-29
22.	Aircraft Detector.....	2-30
23.	Aircraft-Detector Antenna Pattern.....	2-31
24.	Data-Acquisition System Hardware.....	2-33
25.	Data-Box Interior.....	2-34
26.	Data-Box Hardware.....	2-35
27.	Software Tasks and Interfaces.....	2-39
28.	Test-Site Plan View.....	3-2
29.	Special Monostatic Acoustic Antenna Configurations..	3-5
30.	Laser Doppler Velocimeter Van.....	3-8
31.	Cathode-Ray Tube Display Zones.....	4-2
32.	Typical Recording Procedure.....	4-4
33.	General Status Display Format.....	4-5

LIST OF ILLUSTRATIONS (CONT'D.)

Figure		Page
34.	Display of Propeller Anemometer, Meteorological, and Status Data	4-7
35.	Camera Site	4-9
36.	Display of Diagnostic Data	4-13
37.	Log Sheet	4-14
38.	Topography of Laser Site No. 1	4-17
39.	Monostatic Acoustic System Data Flow	5-2
40.	Monostatic Acoustic System Hardware	5-3
41.	Digital Tape Format	5-9
42.	Digital Tape Processing Sequence	5-11
43.	Single-Run Computer Output	5-14
44.	Vortex Track with Missing Start-of-Run Mark	5-17
45.	Parameter Summary Computer Printout	5-22
46.	Vortex Death Notation	5-24
47.	Correction of Vortex Location Algorithm Errors	5-26
48.	Vortex Track Analysis and Meteorological Data Verification	5-27
49.	Editing of Number One Data Analysis Card	5-29
50.	Laser Doppler Velocimeter Hardware	5-30
51.	Laser Doppler Velocimeter Vortex Spectrum	5-31
52.	Camera Geometry	5-35
53.	Trajectory Calculated from Photographic Data	5-36
54.	Photographic Trajectory Summary	5-38
55.	Sensor Tower-shadowing Example	6-2
56.	Distribution of One-Minute Averaged Winds	6-4

LIST OF ILLUSTRATIONS (CONT'D.)

Figure		Page
57.	Wind Rose	6-5
58.	Turbulence Distributions by Head Wind	6-9
59.	Probability That a Vortex Remained in the Reference Corridor-as a Function of Elapsed Time	7-4
60.	Vortex Velocity Profiles	7-5
61.	Probability That a Vortex Will Remain in the Reference Corridor Longer than a Given Time and Compared to Heathrow Data	7-6
62.	Probability That a Vortex Will Remain in the Corridor for a Time Longer Than Elapsed Time, T	7-9
63.	Vortex Death Time Distribution as a Function of Total Wind	7-11
64.	Probability for a Vortex Not to Decay as a Function of Total Wind	7-13
65.	McGowan Curve of Maximum Observed Vortex Lifetimes as a Function of Wind Speed	7-14
66.	McGowan Curve of Maximum Observed Vortex Lifetimes as a Function of Wind Speed Revised to Include Toronto Data	7-15
67.	Probability That the Death Position of the Vortex Further from the Center Line was Less than or Equal to DP	7-18
68.	Probability That an Observed Vortex Has Decayed in a Time Less than t, as a Function of Turbulence	7-19
69.	Probability That the Aircraft Height was Between h-15 and h	7-20
70.	Cumulative Percentage of Aircraft Whose Height is Less than h	7-21
71.	Percentage of Aircraft Whose Height Is Below h as a Function of Distance from Runway Threshold	7-22
72.	Percentage of Aircraft Whose Height is Between h-15 and h as a Function of the Head Wind	7-23

LIST OF ILLUSTRATIONS (CONT'D.)

Figure		Page
73.	Wind Conditions Which Led to Residence Times in Excess of 120 Seconds	7-25
74.	Wind Conditions Which Led to Residence Times in Excess of 90 Seconds	7-26
75.	Wind Conditions Which Led to Residence Times in Excess of 60 Seconds	7-27
76.	Vortex Height Versus Age for the B-747 and DC-8	7-32
77.	Vortex Height Versus Age for the B-707 and B-727	7-33
78.	Vortex Height Versus Age for the DC-9 and L-1011	7-34
79.	Probability That the Separation Between Aircraft is Less than t for the Cases Where a Heavy was the Lead Aircraft	7-36
80.	Probability that the Separation Between Aircraft is Less than t for the Cases Where the Lead Aircraft is Either Large or Small	7-37
81.	B-707 Circulation for Four Values of b/2	7-41
82.	Circulation for the B-727, B-737, B-747, and DC-8, Averaged Over a 20-Meter Radius	7-42
83.	Circulation for the DC-9, DC-10, BAC-111, and L-1011, Averaged Over a 20-Meter Radius	7-43
84.	Circulation Data in 20-Second Intervals for the B-707 and B-727, Averaged Over a 20-Meter Radius	7-44
85.	Circulation Data in 20-Second Intervals for the B-737 and B-747, Averaged Over a 20-Meter Radius	7-45
86.	Circulation Data in 20-Second Intervals for the DC-8 and DC-9, Averaged Over a 20-Meter Radius	7-46
87.	Circulation Data in 20-Second Intervals for the DC-10 and L-1011, Averaged Over a 20-Meter Radius	7-48
88.	Two Examples of B-747 Vortex Decay	7-49
89.	Two Examples of B-727 Vortex Decay	7-50
90.	Examples of DC-9 and DC-10 Vortex Decay	7-51

LIST OF ILLUSTRATIONS (CONT'D.)

Figure		Page
91.	Two Examples of L-1011 Vortex Decay.....	7-52
92.	Vortex-Strength Probability of Decay Versus Time for B-707, B-727, B-737, and B-747.....	7-55
93.	Vortex-Strength Probability of Decay Versus Time for DC-8, DC-9, DC-10, and L-1011.....	7-56
94.	Fraction of Vortices with a Γ' Greater than a Limiting Circulation.....	7-58
A-1.	Helicopter Takeoff Flight Path.....	A-2
A-2.	Helicopter Landing Flight Path.....	A-3
A-3.	Helicopter Vortex Circulation Versus Elapsed Time...	A-11
A-4.	Example of a Helicopter Ground-Wind Track.....	A-13

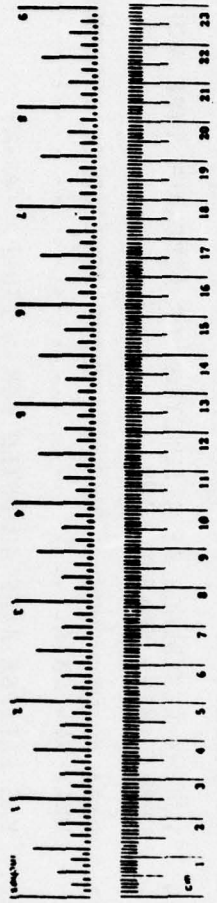
LIST OF TABLES

Table		Page
1.	AIRCRAFT-SEPARATION REQUIREMENTS	1-2
2.	MONOSTATIC ACOUSTIC SENSOR LOCATIONS	3-4
3.	GROUND-WIND SENSOR LOCATIONS	3-6
4.	LASER-SITE LOCATIONS	3-9
5.	GWVSS NINE-TRACK DATA-FRAME FORMAT	5-7
6.	METEOROLOGICAL NINE-TRACK DATA-FRAME FORMAT	5-8
7.	ELAPSED TIME OFFSET FOR UNTRIGGERED BASELINES	5-20
8.	VERTICAL WIND SHEAR	6-6
9.	TURBULENCE DISTRIBUTIONS	6-8
10.	VORTEX RESIDENCE AS A FUNCTION OF AIRCRAFT TYPE AND GROUND-WIND SENSOR LINE	7-8
11.	DATA POINTS OUTSIDE McGOWAN CURVE REVISED TO INCLUDE HEATHROW DATA	7-17
12.	VAS ELLIPSE AXES ADJUSTED FOR A 150-FT (45-M) CORRIDOR	7-28
13.	PROBABILITY THAT A VORTEX WILL REMAIN IN THE CORRIDOR	7-29
14.	MAVSS DATA BASE	7-39
A-1.	HELICOPTER OPERATIONAL PARAMETERS	A-5
A-2.	HELICOPTER TEST RESULT SUMMARY	A-6
A-3.	HELICOPTER VORTICES WHICH WERE OBSERVED TO REMAIN IN THE REFERENCE CORRIDOR LONGER THAN 60 SECONDS	A-12

METRIC CONVERSION FACTORS

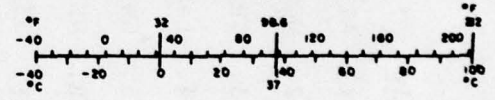
Approximate Conversions to Metric Measures

Symbol	When You Know	Multiply by	To Find	Symbol
		LENGTH		
in	inches	2.5	centimeters	cm
ft	feet	30	centimeters	cm
yd	yards	0.9	meters	m
mi	miles	1.6	kilometers	km
		AREA		
in^2	square inches	6.5	square centimeters	cm^2
ft^2	square feet	0.09	square meters	m^2
yd^2	square yards	0.8	square meters	m^2
mi^2	square miles	2.5	square kilometers	km^2
	acres	0.4	hectares	ha
		MASS (weight)		
oz	ounces	28	grams	g
lb	pounds	0.45	kilograms	kg
	short tons (2000 lb)	0.9	tonnes	t
		VOLUME		
tsp	teaspoons	5	milliliters	ml
Tbsp	tablespoons	15	milliliters	ml
fl oz	fluid ounces	30	milliliters	ml
c	cups	0.24	liters	l
pt	pints	0.47	liters	l
qt	quarts	0.95	liters	l
gal	gallons	3.8	liters	l
ft^3	cubic feet	0.03	cubic meters	m^3
yd^3	cubic yards	0.76	cubic meters	m^3
		TEMPERATURE (exact)		
°F	Fahrenheit temperature	5/9 (after subtracting 32)	Celsius temperature	°C



Approximate Conversions from Metric Measures

Symbol	When You Know	Multiply by	To Find	Symbol
		LENGTH		
mm	millimeters	0.04	inches	in
cm	centimeters	0.4	inches	in
m	meters	3.3	feet	ft
m	meters	1.1	yards	yd
km	kilometers	0.6	miles	mi
		AREA		
cm^2	square centimeters	0.16	square inches	in^2
m^2	square meters	1.2	square yards	yd^2
km^2	square kilometers	0.4	square miles	mi^2
	hectares (10,000 m^2)	2.5	acres	
		MASS (weight)		
g	grams	0.035	ounces	oz
kg	kilograms	2.2	pounds	lb
t	tonnes (1000 kg)	1.1	short tons	
		VOLUME		
ml	milliliters	0.03	fluid ounces	fl oz
l	liters	2.1	pints	pt
l	liters	1.06	quarts	qt
l	liters	0.26	gallons	gal
m^3	cubic meters	35	cubic feet	ft^3
m^3	cubic meters	1.3	cubic yards	yd^3
		TEMPERATURE (exact)		
°C	Celsius temperature	9/5 (then add 32)	Fahrenheit temperature	°F



1. INTRODUCTION

The generation of a pair of counter-rotating vortices in the wake of an aircraft in flight has been observed for many years. It was treated as merely a scientific phenomenon, however, until the advent of the widebody jets (B-747, DC-10, L-1011, etc.). In the late 1960's the Federal Aviation Administration (FAA) realized that the vortices generated by the widebody aircraft could pose a serious threat to smaller and lighter aircraft following at the minimum spacing then applied by Air Traffic Control (three nautical miles). The problem is most acute in the high-density terminal areas where the volume of aircraft produces long periods of full capacity runway use and, hence, sustained periods of minimum separations. To ensure safe aircraft operations, larger interarrival separations are required now for the more dangerous situation of a lighter aircraft following a widebody aircraft. This approach, however, reduces airport capacity and increases aircraft delays.

In the early 1970's the FAA began a program to investigate the possibility of reducing these large separations while ensuring safe operations. Under the sponsorship of the FAA, the Transportation Systems Center (TSC) has developed several sensor systems capable of detecting and tracking vortex motion up to an altitude of several hundred feet. Thus far the primary investigations have been concerned with the characteristics of vortices of landing aircraft for three major reasons: (1) all landing aircraft are following essentially the same flight path in the final approach stages so the probability of a vortex encounter is higher than elsewhere; (2) instrumentation of test sites is easier since sufficient land is often available for sensor installation at the final landing stages from the middle marker to runway threshold; and (3) over 85 percent of the vortex-caused landing accidents occurred for landing aircraft between the middle marker and touchdown (Ref. 1).

TSC has installed vortex tracking systems during the last five years at several major airports (Kennedy, Denver Stapleton,

London Heathrow, Chicago O'Hare) which have yielded vortex tracks from approximately 60,000 landing aircraft (Refs. 2 and 3). Analysis of this data showed that under certain well-defined wind conditions vortices would not be a hazard even if all landing separations were reduced to three nautical miles. These data formed the base for the development of the Vortex Advisory System (Ref. 4) being installed at Chicago's O'Hare International Airport. The Vortex Advisory System is a predictive system which uses strategically placed anemometers to measure the ambient wind in the approach area of runways and uses a green or red light to advise a controller when it is safe to reduce landing separations to three nautical miles for all aircraft or when the present separation standards, listed below, should be used:

TABLE 1. AIRCRAFT-SEPARATION REQUIREMENTS

		LEAD AIRCRAFT		
		SMALL	LARGE	HEAVY
FOLLOWING AIRCRAFT	SMALL	3	4	6
	LARGE	3	3	5
	HEAVY	3	3	4

A Small aircraft is defined as one capable of a gross takeoff weight of 12,500 pounds (5670 kilograms) or less; a Heavy aircraft is defined as capable of a gross takeoff weight of 300,000 pounds (136,000 kilograms) or more; and all other aircraft fall into the Large category.

In a meeting between representatives of the FAA and the Canadian Ministry of Transport (MOT) in the summer of 1975, both organizations agreed that there was mutual interest in developing techniques for investigating the behavior of the vortices of departing aircraft. This data would supplement the data base

obtained for the vortices of arriving aircraft. It was decided that a jointly operated test site would be designed and instrumented at Toronto International Airport to collect data to investigate the behavior of takeoff vortices. A formal memorandum of agreement was signed in the fall of 1975 and the test period was to be for a period of six months after delivery of the equipment. Under the agreement the FAA, through TSC, delivered a wake vortex data collection system to Toronto Airport in the summer of 1976 for the departure end of Runway 23L (Figure 1). The system included meteorological sensors, monostatic acoustic and ground-wind vortex-sensing systems, a laser Doppler velocimeter, photographic equipment, a computer-based data-recording system, associated electronics, cabling, etc. Fabrication, delivery, and installation of the system components were contracted by TSC to the Illinois Institute of Technology Research Institute (IITRI), Chicago, Illinois. A team consisting of representatives from MOT and IITRI performed the site preparation, trenching, cable laying, and general equipment installation. Two one-week periods of training describing system software and hardware were provided by IITRI for representatives of MOT.

Data were collected during the fall and winter of 1976/77 as defined in the bilateral agreement. A review of the data in the winter of 1977 indicated that to reach any statistically meaningful conclusions from the tests, the number of vortices tracked would have to be significantly increased. It was decided that the test site would remain open for data collection for an additional six months, until the fall of 1977. A second review was held in the summer of 1977 and the preliminary results of the data analysis were presented. It was concluded that it was feasible to determine the behavior of the vortices from departing aircraft such that a takeoff system could be developed, the major goal of the tests. The site was therefore officially closed and dismantled in the fall of 1977 with data having been obtained from over 5000 aircraft.

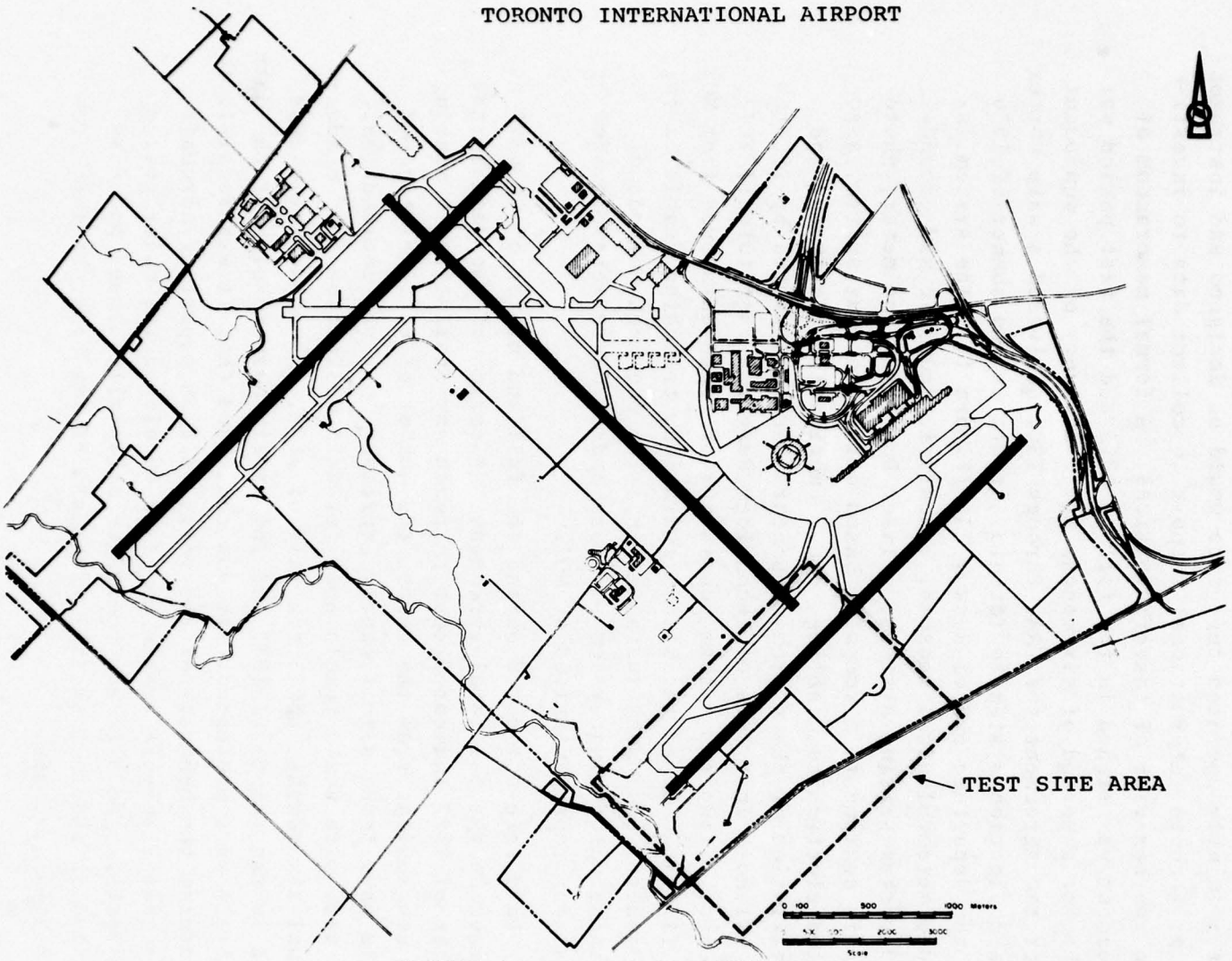


FIGURE 1. TEST SITE LOCATION

2. SENSOR SUBSYSTEMS

The sensor systems installed at Toronto were designed to measure vortex transport characteristics, vortex strength, aircraft-height profiles, and the ambient meteorology. An artist's concept of the field deployment of the sensors is given in Figure 2.

The main function of the Ground Wind Vortex-Sensing System (GWVSS) is to provide data on the vortex transport characteristics (e.g., how fast the vortex moves away from the runway under different wind conditions). The detection of the vortex by the GWVSS gives little information on the strength or height of a vortex, but does locate a vortex along a baseline. A large number of anemometers provide extensive coverage for vortex detection.

The Monostatic Acoustic Vortex-Sensing System (MAVSS) provides some vortex position information (the height and location is provided for one point in time for each detected vortex) and a measure of the vortex strength in the form of a calculated average circulation. Analysis of time histories of the strength data give an indication of vortex decay properties.

The laser Doppler velocimeter (LDV) is theoretically capable of detecting, tracking, and measuring the strength of vortices. The use of the LDV as a vortex sensor was limited, however, since it was not as fully developed and engineered as the MAVSS and GWVSS.

A photographic system was used to obtain aircraft-height profiles. It was anticipated that the profiles would help to explain possible idiosyncrasies in vortex behavior (e.g., when no data were recorded, it might be attributed to the aircraft being too high for the detection system).

Aircraft detectors provided trigger signals for the start of data collection on each of the respective GWVSS lines. In addition, one detector triggered the camera and another detector triggered the MAVSS.

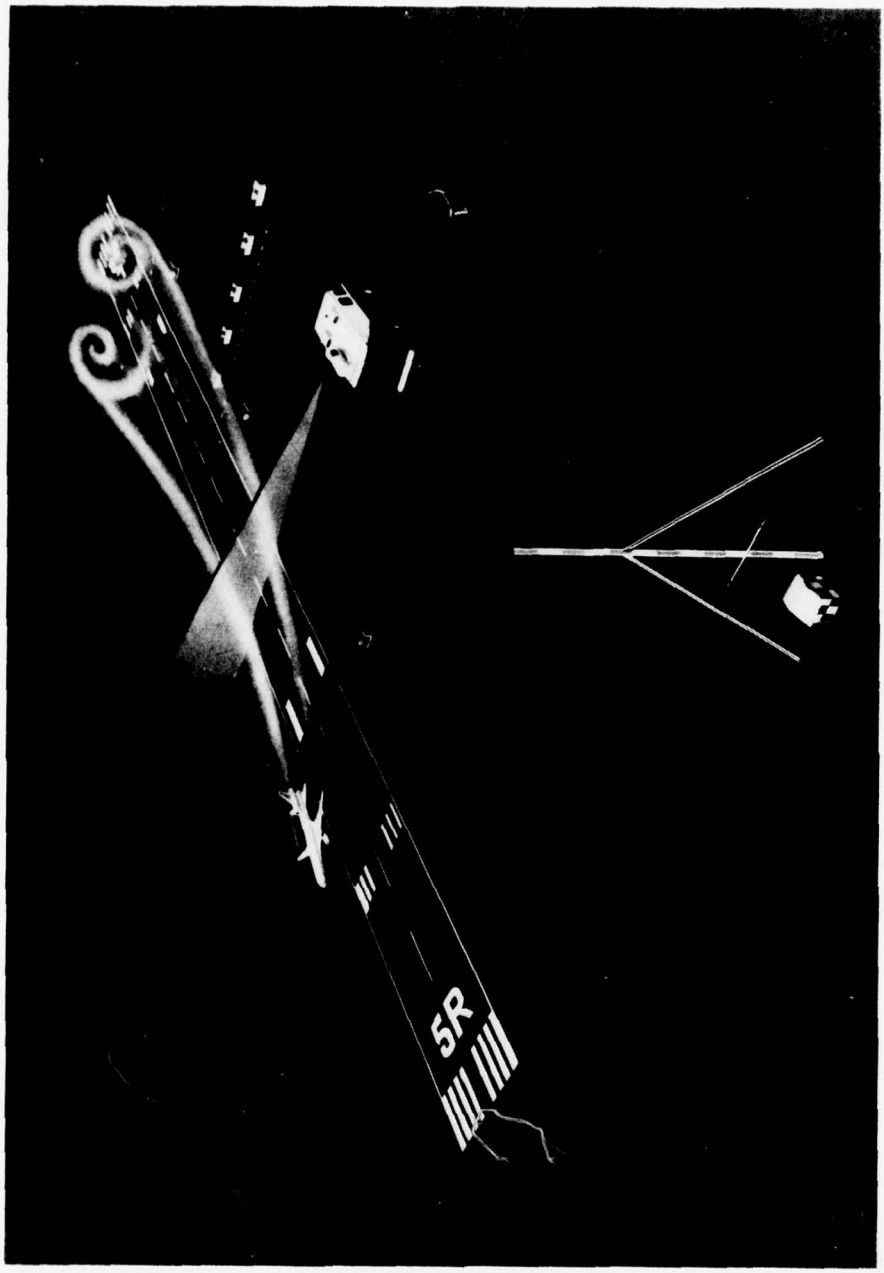


FIGURE 2. SENSOR LAYOUT

Analysis of the data depended on accurately measuring several meteorological parameters (ambient wind velocity, vertical wind shear, ambient temperature, etc.). It has been determined in previous data collection and analysis efforts that the dominant mechanism which affects the vortex transport and decay is the ambient wind. All efforts at characterizing vortex behavior depend on determining correlations with the measured meteorological parameters.

2.1 GROUND-WIND VORTEX-SENSING SYSTEM

Each GWVSS consists of a line array of propeller anemometers located on both sides of and perpendicular to the runway centerline. The sensor consists of a R.M. Young Co., Gill propeller anemometer (Model No. 27101), a plastic propeller (Model No. 27108), and a plastic (polyvinylchloride) pole mount designed to hold the sensor perpendicular to the runway centerline, parallel to the ground, and at a nominal height of 10 ft (3.3 m). A sensor and mount are shown in Figure 3. The propeller is connected to a d.c. generator which provides an output voltage proportional to the rotational velocity of the propeller. The anemometer response closely approximates a cosine function (Figure 4). Thus the output voltage is directly proportional to the component of the wind in the direction of the anemometer axis and consists of random fluctuations about a bias voltage proportional to the average crosswind. However, a vortex influences the local ambient wind field, and this perturbation is detected by the anemometer sensors.

The axes of the vortices are approximately parallel to the aircraft flight path and, hence, the runway centerline; thus the main vortex circular wind flow is perpendicular to the runway centerline. Since the anemometer axis is also aligned perpendicular to the runway centerline, it coincides with the ground level vortex-induced wind flow. Since the vortices rotate in opposite directions, one vortex (downwind) causes an increase in the measured wind while the other vortex (upwind) causes a decrease in the measured wind as sensed by the anemometers (Figure 5). As a vortex pair transports across the array of sensors, the output

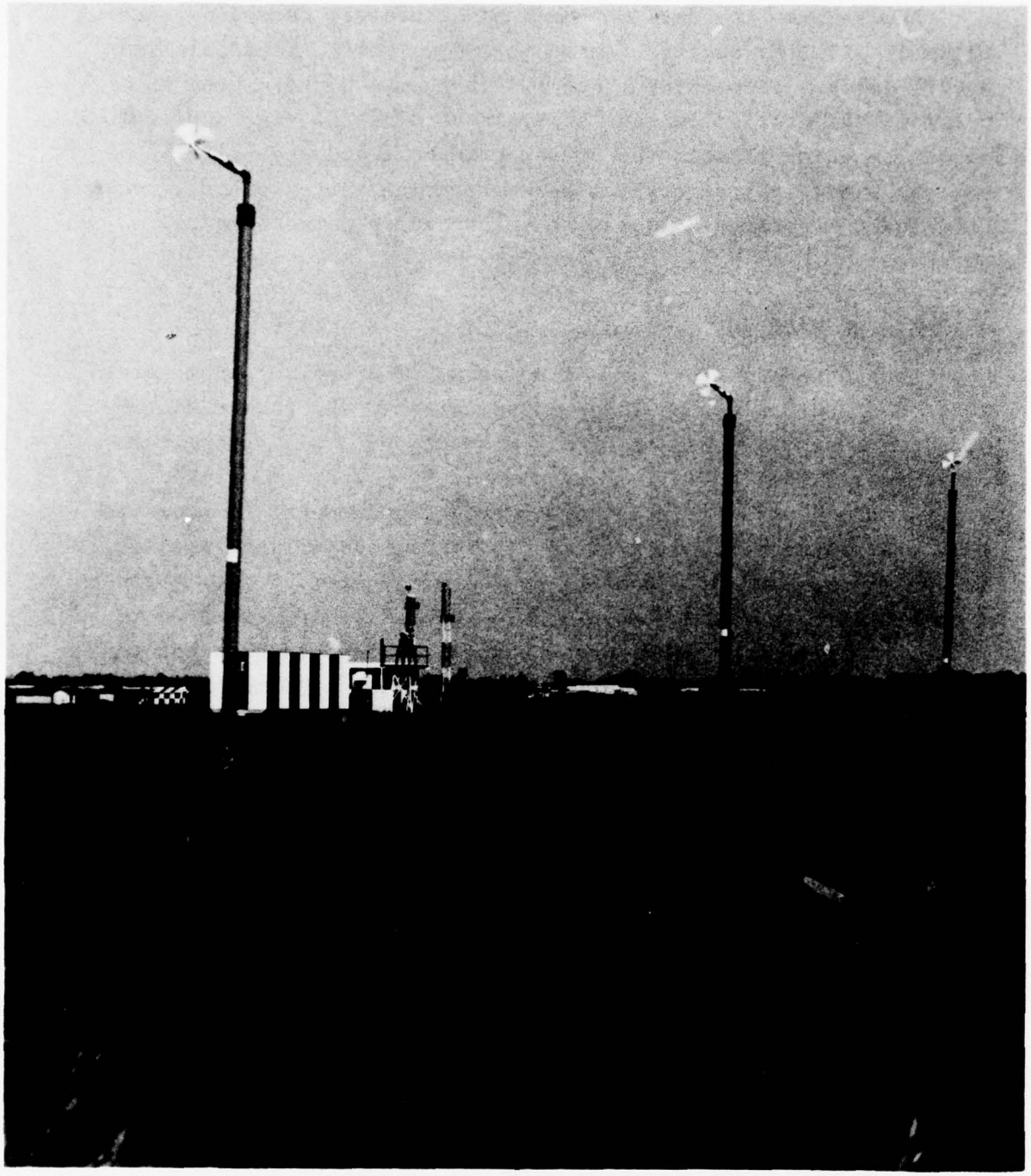


FIGURE 3. PROPELLER ANEMOMETER MOUNTED ON 10-FOOT POLYVINYLCHLORIDE POLE

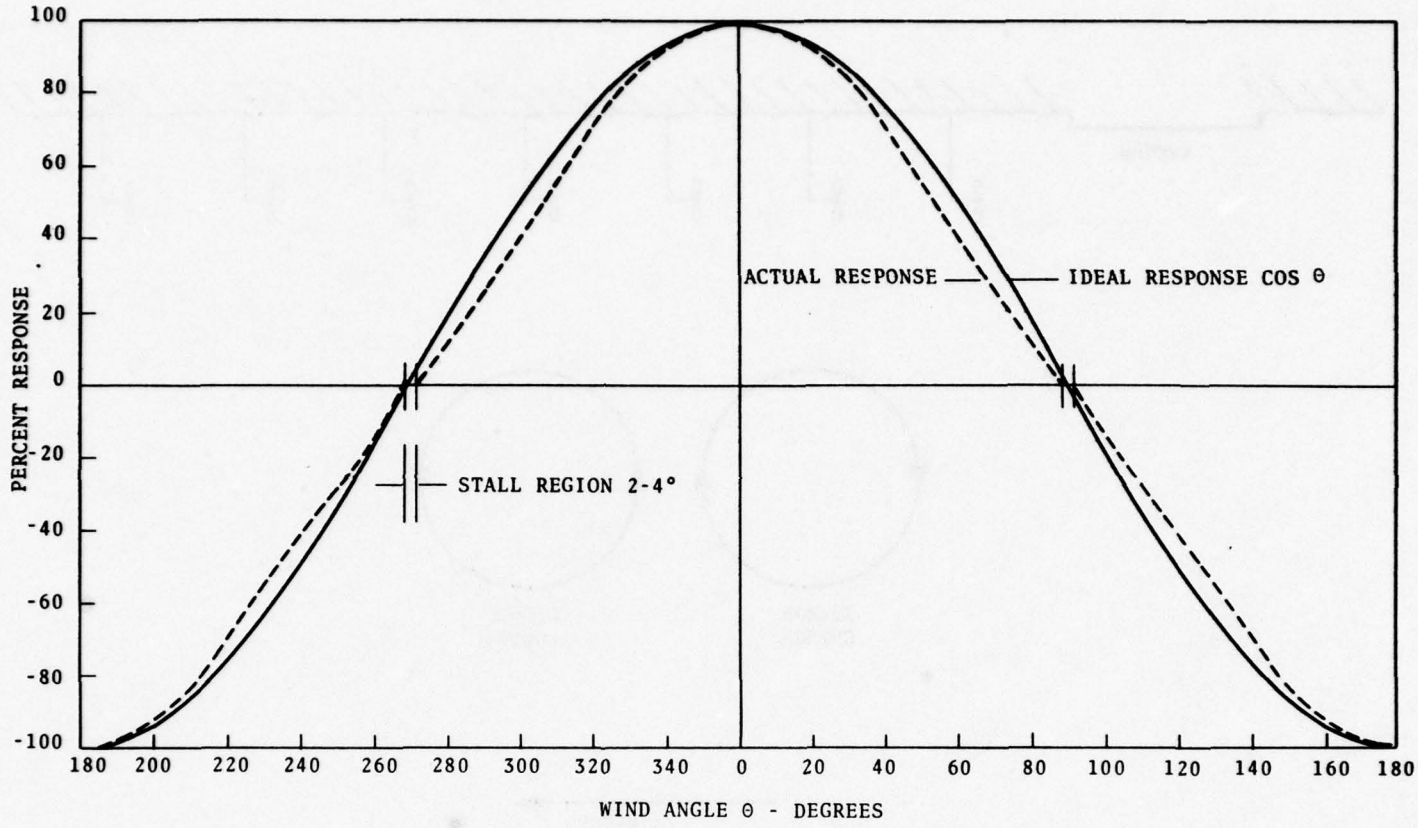


FIGURE 4. PROPELLER ANEMOMETER CALIBRATED RESPONSE

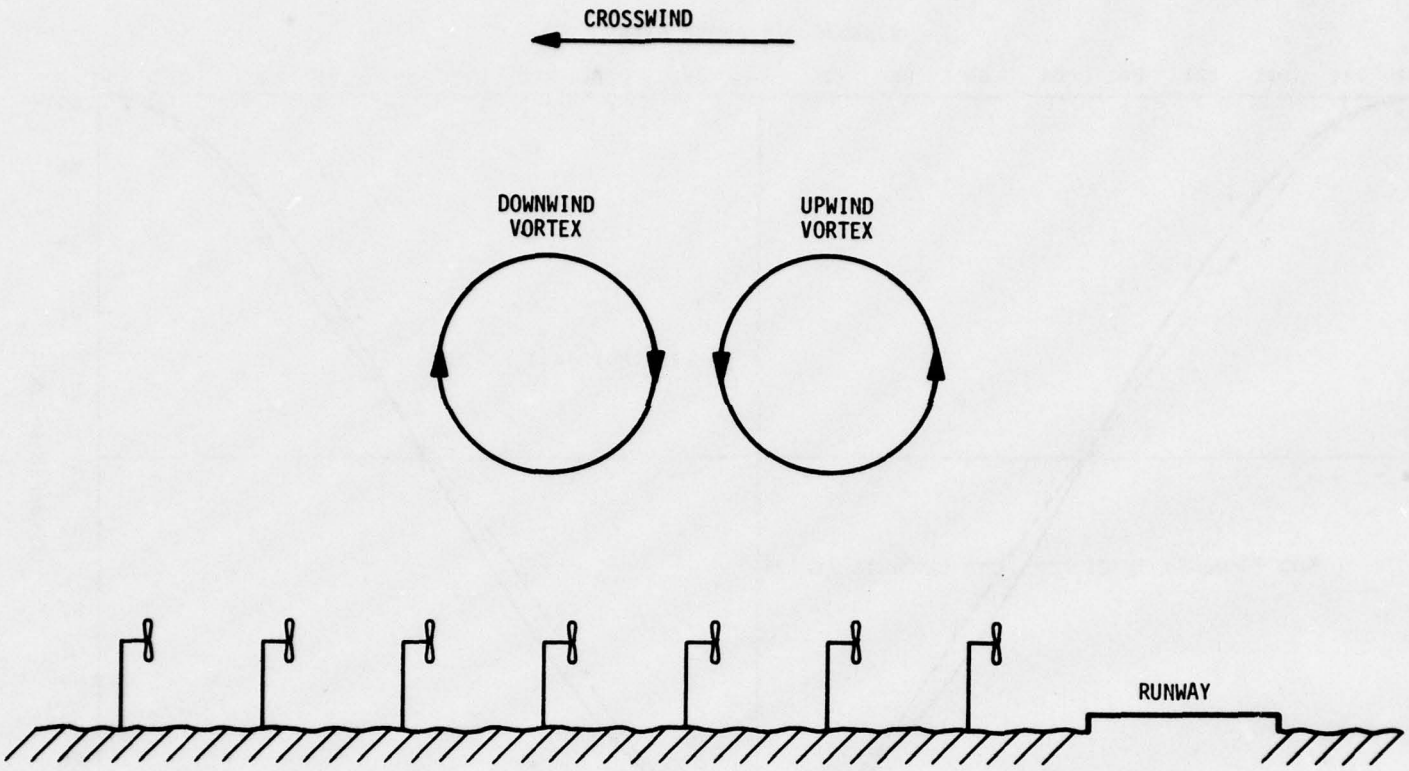


FIGURE 5. VORTICES OVER PROPELLER ANEMOMETER ARRAY

voltage from each sensor would be expected to increase above the level of the ambient wind as the first vortex passes and to decrease below the level of the ambient wind as the second vortex passes as shown in Figure 6. By displaying the outputs of several anemometers simultaneously, the transport of the vortices may be monitored (Figure 7).

2.2 MONOSTATIC ACOUSTIC VORTEX-SENSING SYSTEM

The MAVSS consists of a line array of acoustic receiver and transmitter antenna pairs. The transmitter and receiver appear almost identical since each uses the same molded fiberglass parabolic antenna, a speaker as acoustic transducer, and is housed in a plywood enclosure, 4 ft (1.2 m) by 4 ft (1.2 m) by 4 ft (1.2 m). One receiver and one transmitter assembly are joined to form the vortex sensor as shown in Figure 8. A sponge-type acoustic absorbing material is used to line the insides of the enclosures. The acoustic transducer is mounted above and pointed downward toward the reflector antenna as shown in Figure 9, and directs the acoustic energy into a pencil-shaped beam.

A pulse of acoustic energy, emitted from the transmitter antenna, is scattered by temperature and turbulence fluctuations in the atmosphere (Ref. 5). A small amount of the energy is scattered directly back toward the transmitter (back-scatter) and is collected by the receiver antenna. The theoretical cross section for 180° scattering from turbulent fluctuation is zero (Ref. 5) and hence the dominant scattering mechanism is from temperature fluctuations. Higher signal strengths may be expected from vortices of aircraft with wing-mounted engines (e.g., B-707, DC-8) since some of the hot engine exhaust would be entrained in the vortex resulting in larger temperature fluctuations (Ref. 6).

The antennas are oriented with their beams pointing vertically which results in the measurement of the vertical components of the wind. This geometry provides a natural mechanism for rejecting the background "noise" from the ambient wind which contains only a relatively small vertical component. When a vortex enters the

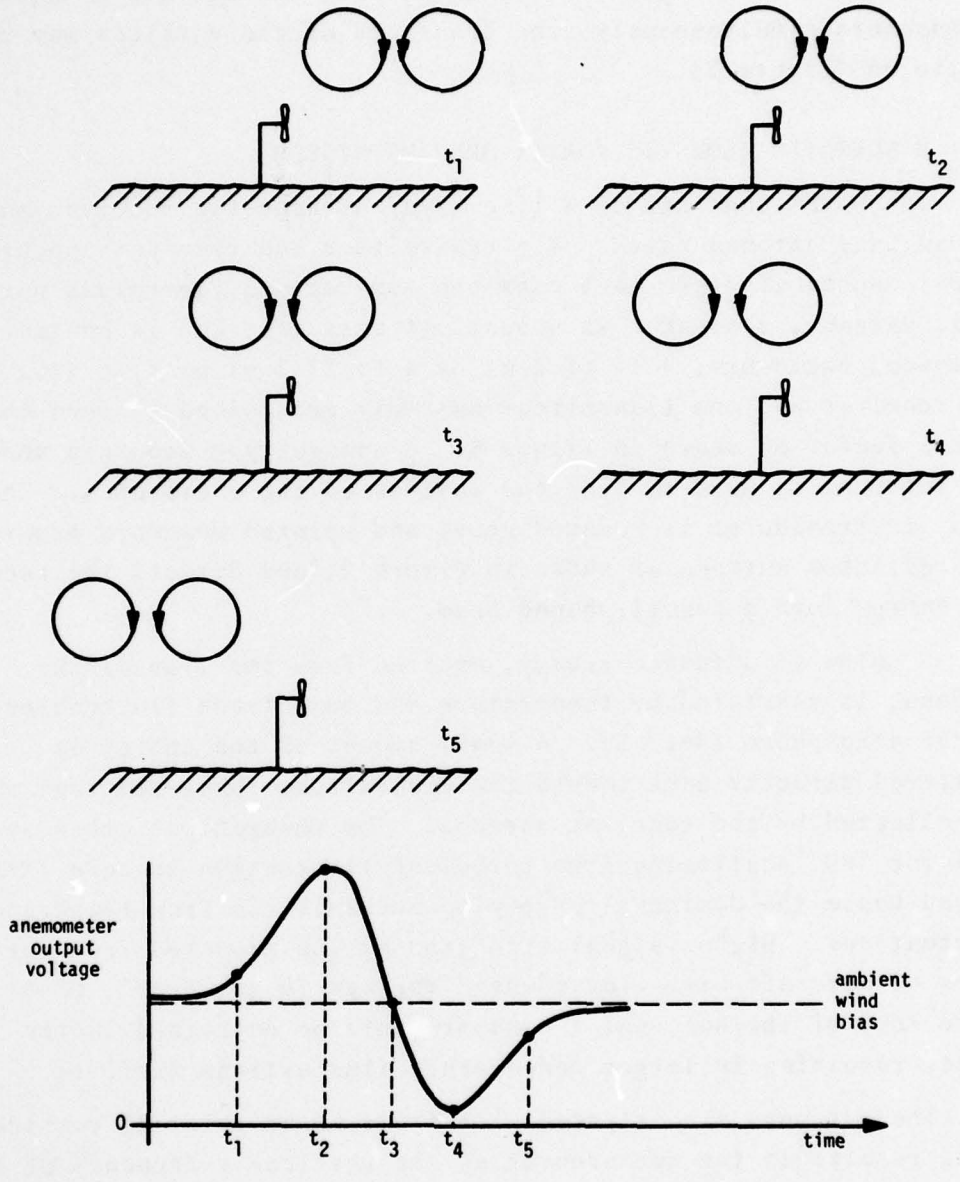


FIGURE 6. SINGLE ANEMOMETER OUTPUT VOLTAGE

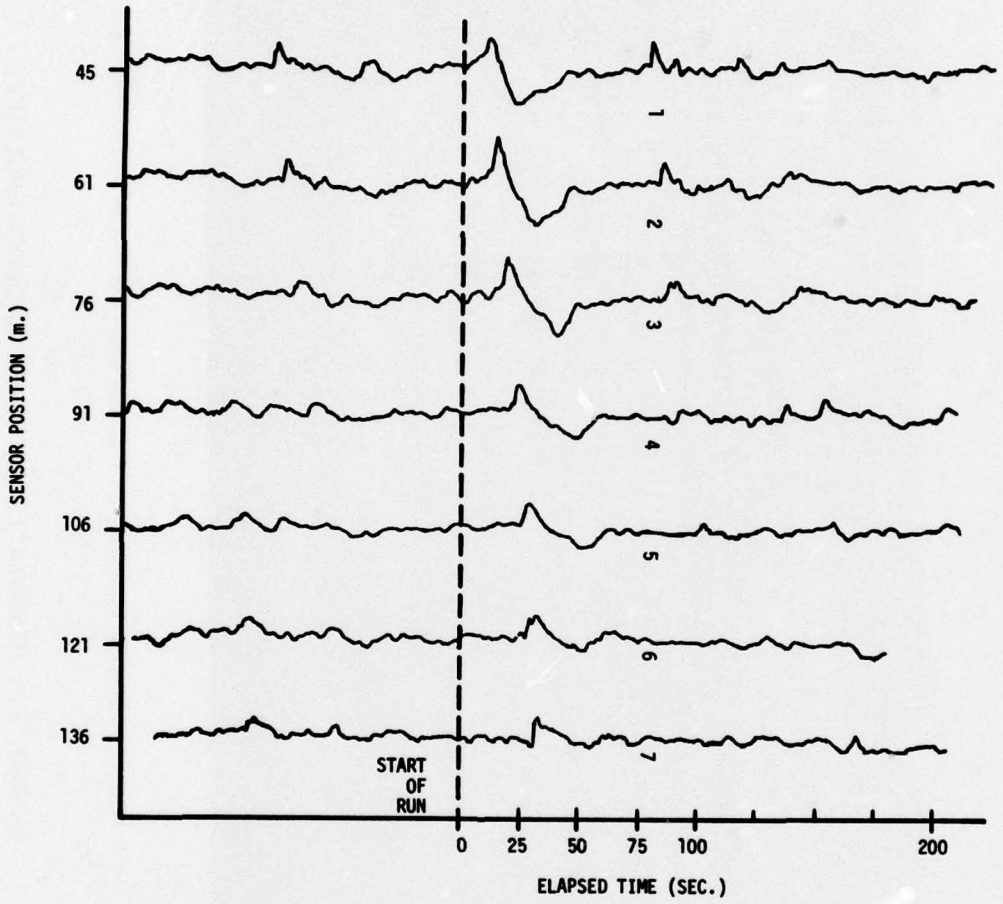


FIGURE 7. EXAMPLE OF ANEMOMETER ARRAY DATA

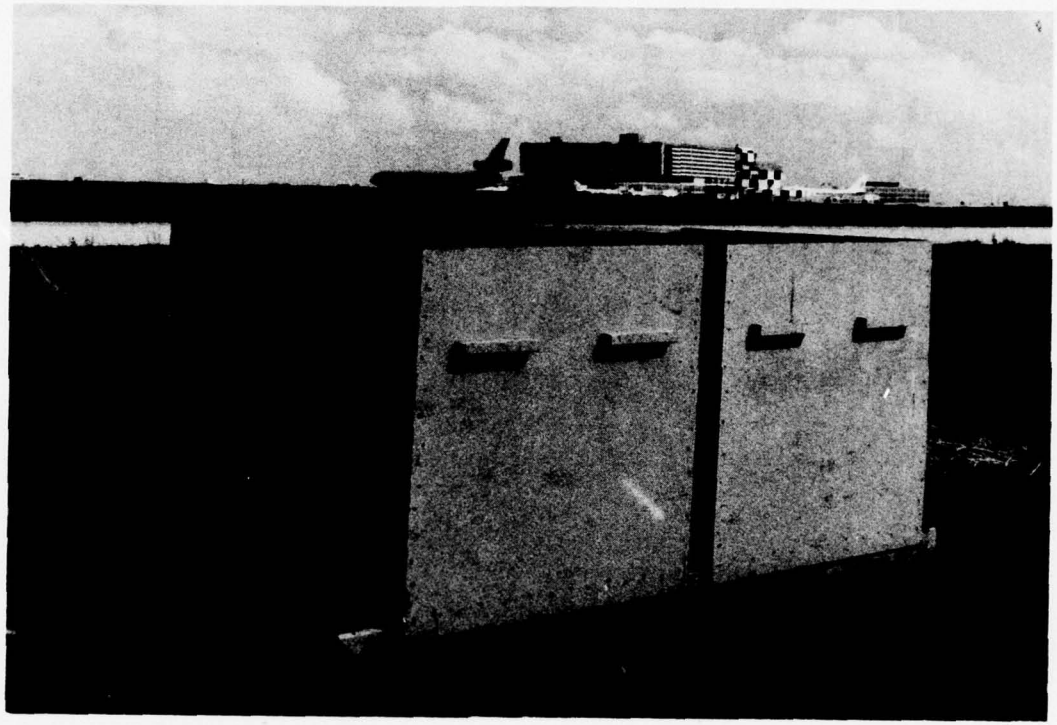


FIGURE 8. MONOSTATIC ACOUSTIC ANTENNA ENCLOSURE

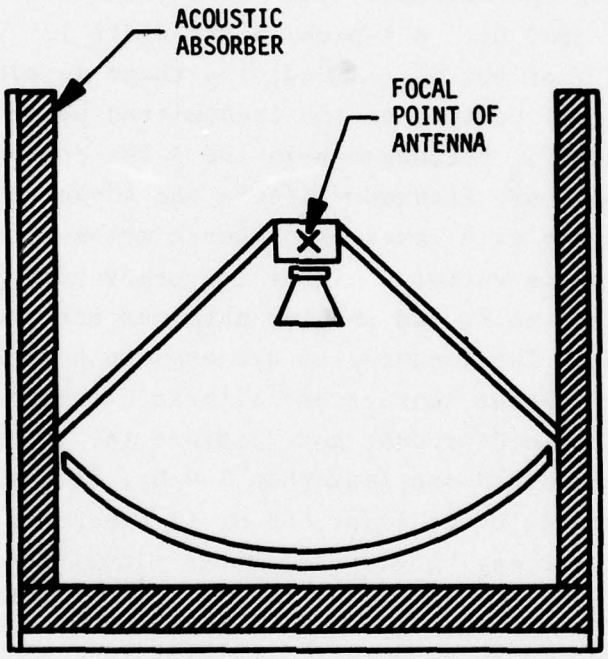


FIGURE 9. INTERIOR OF MONOSTATIC ACOUSTIC ANTENNA

sensed volume there is a component of vertical wind with relatively high velocities. The backscattered acoustic energy received from the vortex winds is Doppler shifted in frequency by an amount

$$\Delta f = 2f_o \frac{v}{v_s} ,$$

where f_o is the transmitted frequency, v is the vertical component of the wind, and v_s is the speed of sound. Thus, as the vortex passes over the sensor, information on the vertical velocity profile of the vortex may be obtained.

The envelope of the transmitted pulse is approximately a Gaussian shape with approximately 100 watts (acoustic) power at either 2950 Hz or 3550 Hz. A typical pulse width is 30 ms with a repetition period T of 600 ms. A Gaussian shape is used to concentrate the spectral content of the transmitted pulse near the transmitted frequency. Frequencies in the 3-kHz region were chosen as a compromise--a lower frequency offers the advantage of higher transducer efficiency with lower atmospheric attenuation and hence higher signal-to-noise ratio; a higher frequency offers the advantage of lower ambient noise and smaller antennas for the same required beam-widths. Two frequencies are used in a MAVSS array for two reasons: 1) adjacent sensors use alternate frequencies to reduce crosstalk or feedthrough; and 2) since the largest spectral shifts which are expected are less than 300 Hz, if the center frequencies are separated by at least 600 Hz (2 times 300 Hz), then one spectrum analyzer may be used to reduce simultaneously the data from two adjacent sensors.

Range information is obtained by transmitting a pulsed signal and time gating the receiver. In the backscatter mode with the receiver gated to accept signals at a time t_r after the transmitted pulse, the sampled range, r, is given by:

$$r = 1/2\ t_r\ v_s .$$

In actual practice the range gating has a finite width Δt_r determined by the processing parameters of the spectrum analyzer and

Δt_r is defined to be within the bounds of t_r as shown in Figure 10. The difference in time between the start of two consecutive range gates is defined as the rangegate spacing, Δt_s (generally not equal to Δt_r) and is determined by the processing parameters of the data-reduction minicomputer to be equal to T/16. The range-gate spacing, Δt_s, and pulse width, t_p, should satisfy the requirements that $t_p \leq \Delta t_s$ to prevent redundancies in the signal return. The pulse width, however, should be as large as possible to maximize the energy in the transmitted pulse and thus to increase the signal-to-noise ratio. In actual practice t_p is chosen to be equal to Δt_r.

For most of the tests at Toronto the parameters chosen were T = 600 ms, t_p = 30 ms, Δt_s = ms, Δt_r = 30 ms, and r = 16 ft (5 m). Thus the maximum height sampled was approximately 330 ft (100 m). A limited amount of data was collected with T = 800 ms and t_p = 40 ms which results in a maximum height of approximately 385 ft (125 m).

A block diagram of the MAVSS electronics is given in Figure 11. Vortices were detected at the upper ranges, but it was decided that this did not increase the data enough to balance the loss of data due to the lower sampling rate with the longer period and, therefore, most of the data were collected at T = 600 ms.

The analog data received between transmitted pulses are divided into timed gates which are multiples of the pulse width as shown in Figure 12. The signal received during any one of these gates (e.g., between t_2 and t_3 where $t_3 - t_2 = t_p$) is passed to a spectrum analyzer where a weighted average of the frequency components is calculated. The result of this operation is a single point which represents the characteristic frequency of the received signal in that gate. The expected characteristic shape of this signal can be seen from the pictorial sequence shown in Figure 13. The leading edge of the first vortex is always an upwash and, therefore, this shape is obtained no matter which direction the vortices are transporting.

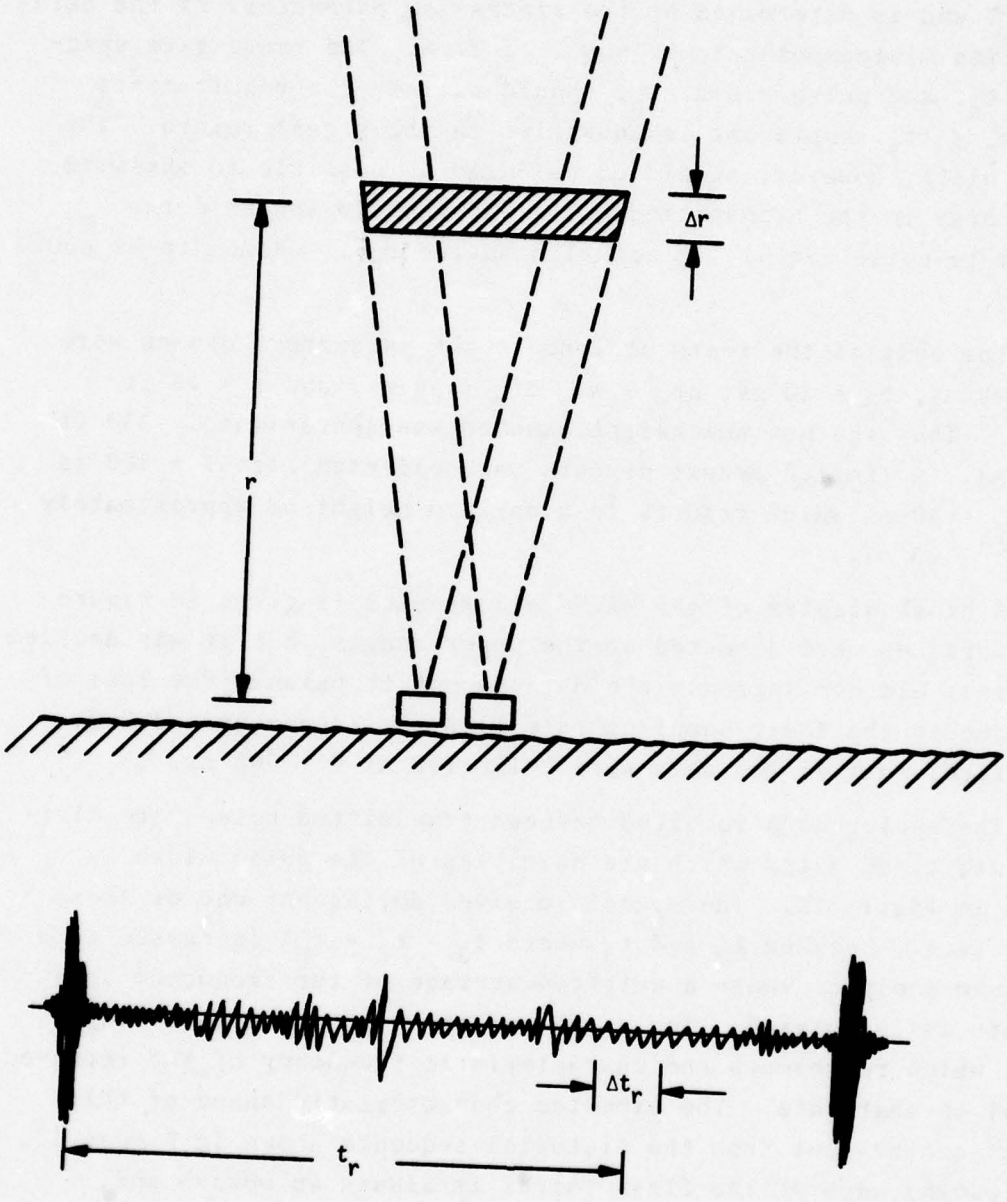


FIGURE 10. MONOSTATIC ACOUSTIC RECEIVER SIGNAL

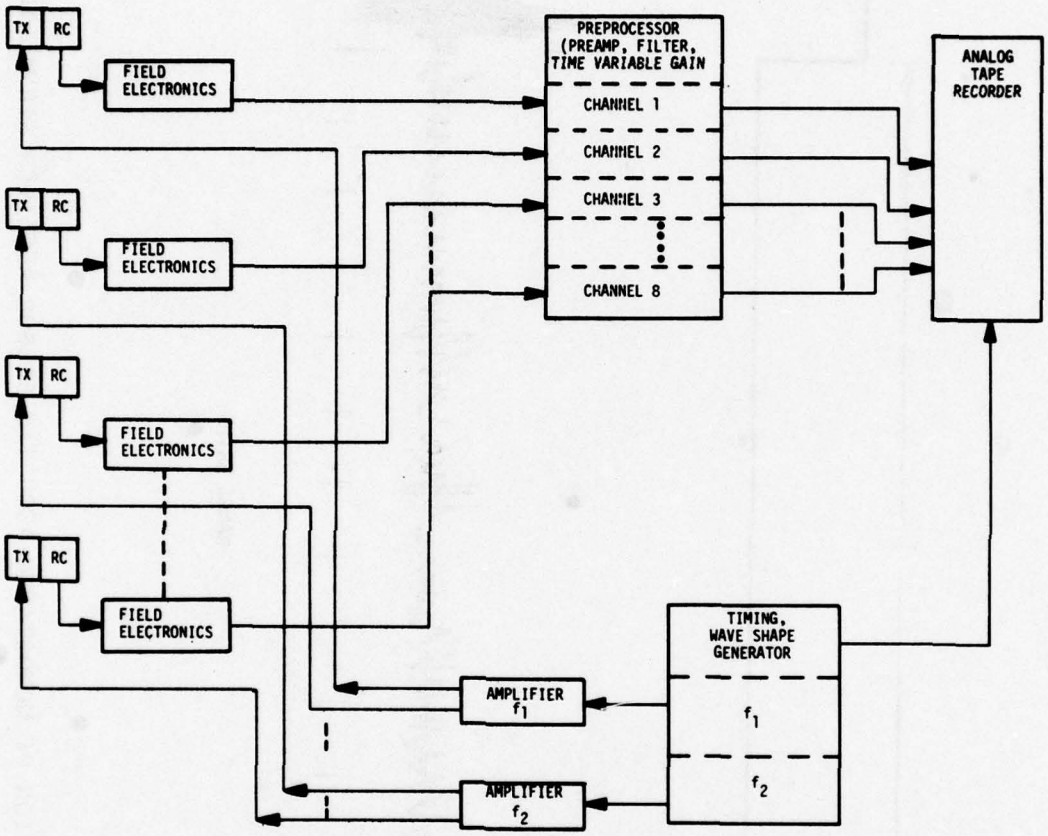


FIGURE 11. MONOSTATIC ACOUSTIC VORTEX-SENSING SYSTEM HARDWARE

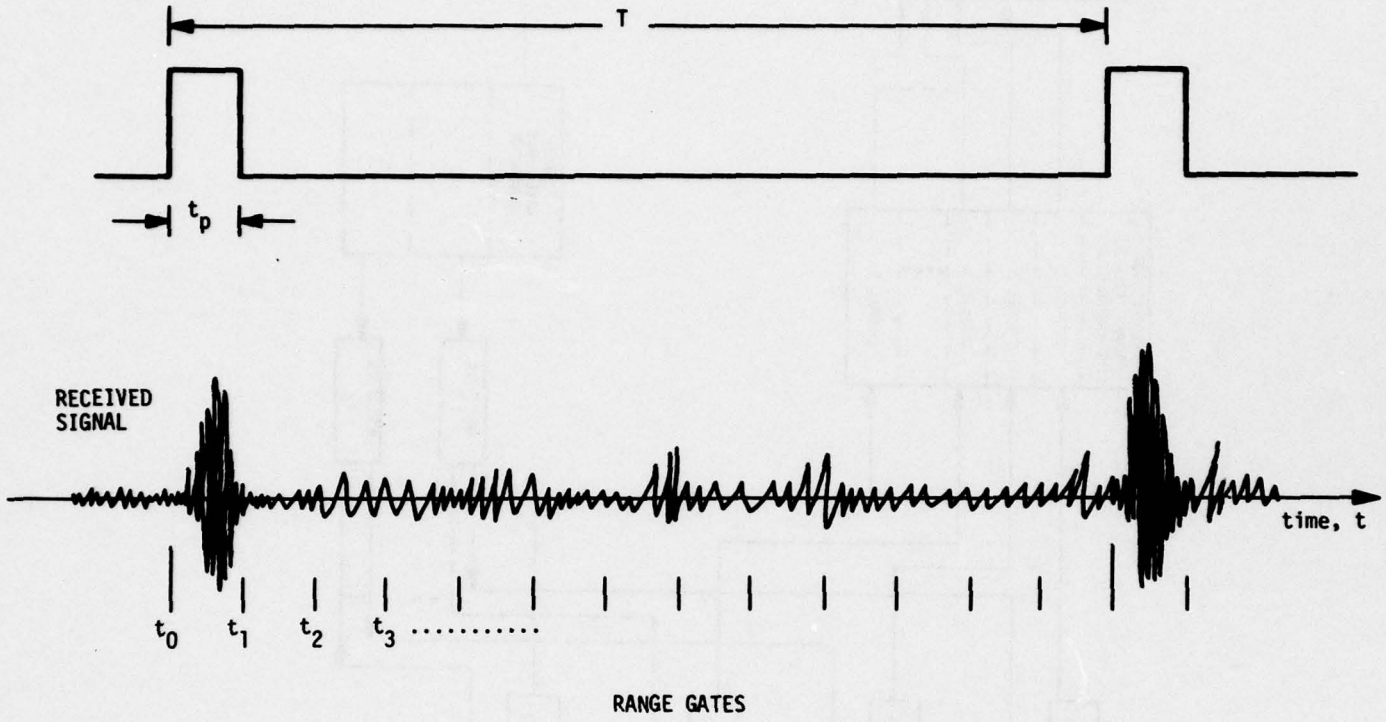


FIGURE 12. QUANTIZATION OF MONOSTATIC ACOUSTIC SENSOR RECEIVED SIGNAL INTO RANGE GATES

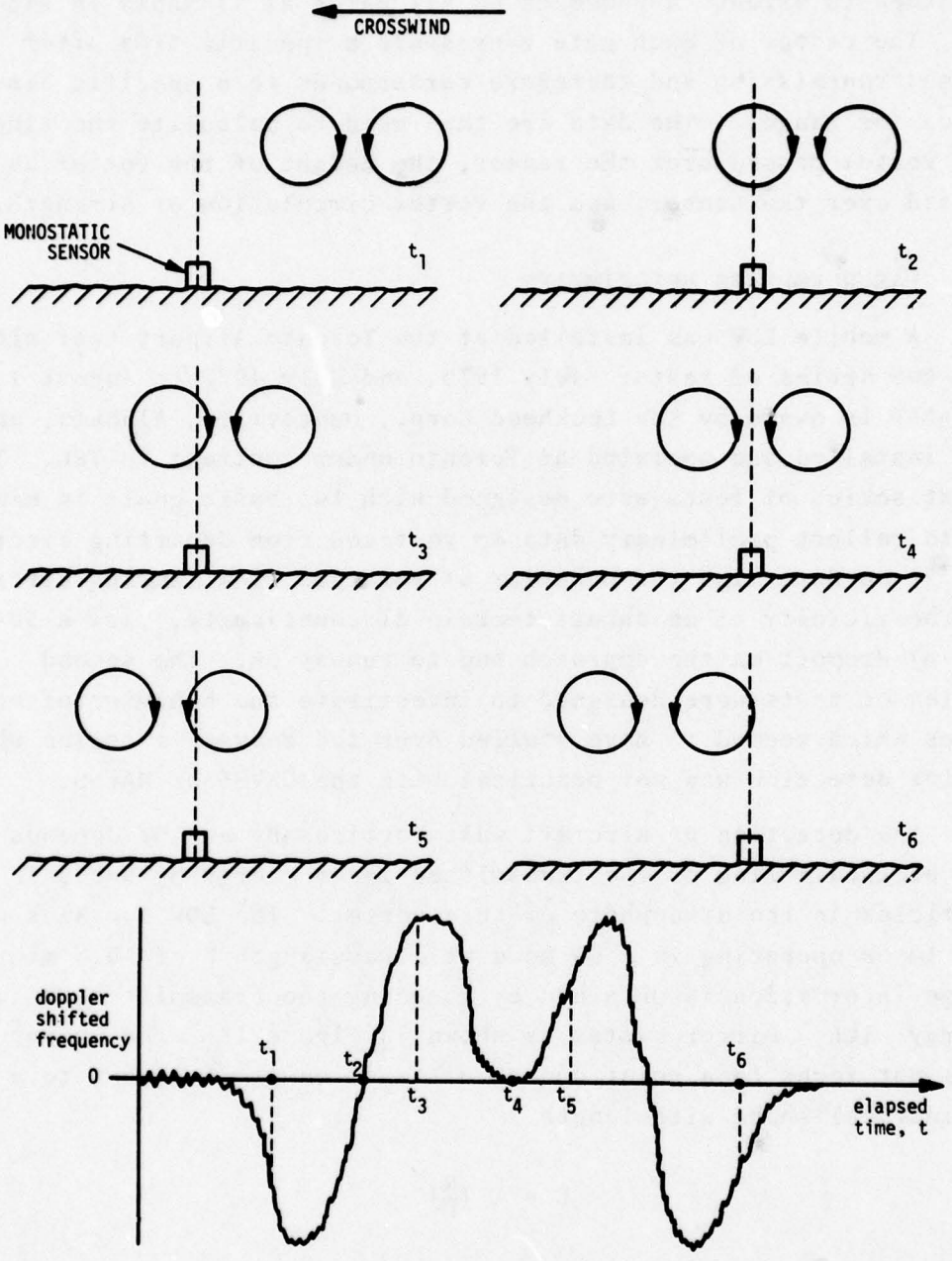


FIGURE 13. MONOSTATIC ACOUSTIC SENSOR EXPECTED SIGNAL RETURNS

One convenient method of displaying all the data for one test run is first to convert the Doppler shifts to velocity components and then to arrange a sequence of all gates as is shown in Figure 14. The center of each gate represents a specific time after pulse transmission and therefore corresponds to a specific distance (or range). The data are then used to calculate the time the vortex passed over the sensor, the height of the vortex as it passed over the sensor, and the vortex circulation or strength.

2.3 LASER DOPPLER VELOCIMETER

A mobile LDV was installed at the Toronto Airport test site for two series of tests: July 1976, and July 1977 to August 1977. The LDV is owned by the Lockheed Corp., Huntsville, Alabama, and was installed and operated at Toronto under contract to TSC. The first series of tests were designed with two basic goals in mind: 1) to collect preliminary data on vortices from departing aircraft, and 2) to determine the behavior of vortices from landing aircraft in the vicinity of an abrupt terrain discountinuity, viz. a 50-ft (15-m) dropoff on the approach end to runway 5R. The second series of tests were designed to investigate the behavior of vortices which seemed to have stalled over the runway--a region where vortex detection was not practical with the GWVSS or MAVSS.

The detection of aircraft wake vortices by an LDV depends on the backscattering of the transmitted laser energy by aerosol particles in the atmosphere or in a vortex. The LDV contains a CO_2 laser operating in a CW mode at a wavelength λ of 10.6 microns. Range information is obtained by focusing the transmitted CW laser energy with a mirror system as shown in Figure 15. The energy does not focus to a point due to diffraction limiting but to a cylindrical shape with length

$$L \cong \lambda \left(\frac{R}{D}\right)^2$$

[R is the range and D is the diameter of the primary mirror (1 ft (3 m))] and diameter (or focused spot size)

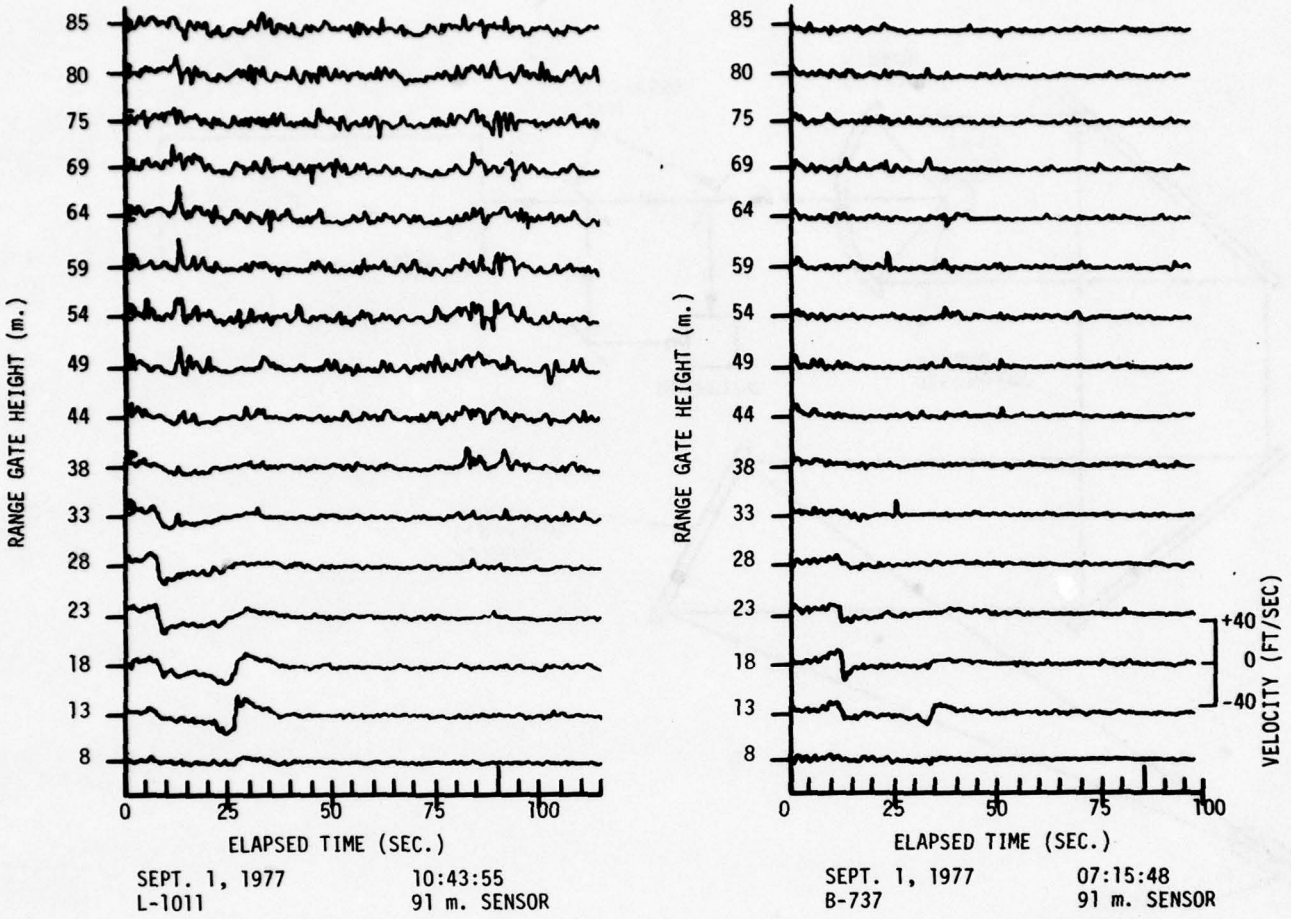


FIGURE 14. EXAMPLE OF DATA FROM THE MONOSTATIC ACOUSTIC SENSOR

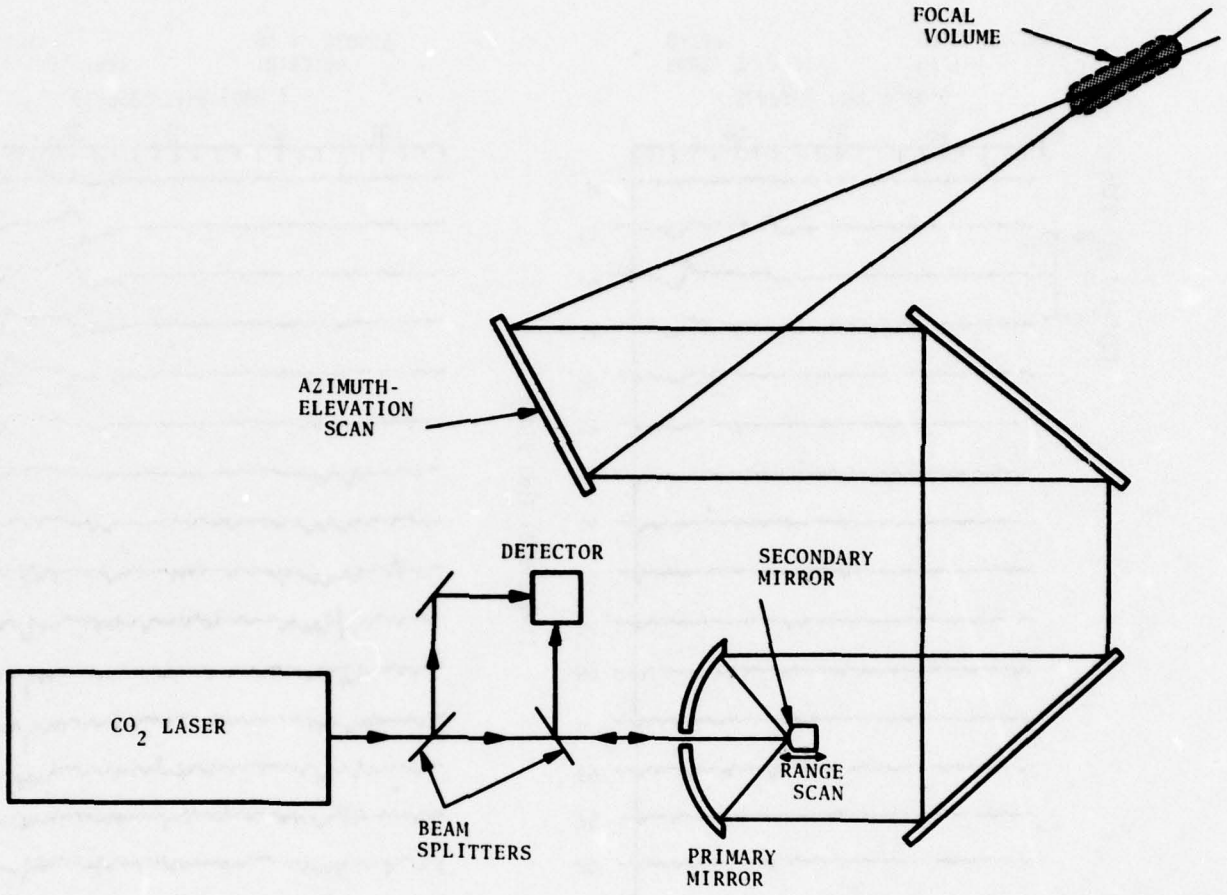


FIGURE 15. LASER DOPPLER VELOCIMETER OPTICS

$$d \cong \lambda \frac{R}{D}.$$

It can be seen that the resolution decreases very quickly as the range is increased. The backscattered energy is collected and focused using the same primary and secondary mirrors and mixed with a local oscillator reference signal taken from the laser output. The frequency of the heterodyned signal depends on the Doppler shift of the backscattered signal given by:

$$f = 2 f_o \frac{|v|}{c} ,$$

where $f_o = 28 \times 10^{12}$ Hz,

v = line-of-sight velocity component of sampled wind.

c = speed of light = 10^9 ft/sec (3×10^8 m/sec).

If the sampled velocity component is 33 ft/sec (10 m/sec), the observed Doppler shift would be 1.9 MHz.

The LDV is capable of operating in several scanning modes. The one selected as the most promising for the second series of tests at Toronto was the arc-scan mode. During one scan the laser is focused at a certain distance and scanned in elevation angle. The range is then stepped and another elevation angle scan is begun. Complete coverage of the tested volume consists of eight arc scans as shown in Figure 16. The heights of each individual scan, the minimum elevation angle, scan speed (continuously variable from 0.1 to 0.5 Hz for a complete cycle, α_μ to α_ℓ and back), and the scan angle limits are all selected by the operator. Figure 16 also shows a typical scan geometry which could be used to investigate remotely the vortices which remain in the area directly over the runway.

The simple heterodyne system just described suffers from a sign ambiguity (i.e., there was no way to distinguish a positive from a negative velocity since both result in the same frequency shift). A "translate" mode would resolve this problem by offsetting the local oscillator frequency so that the observed Doppler shift is:

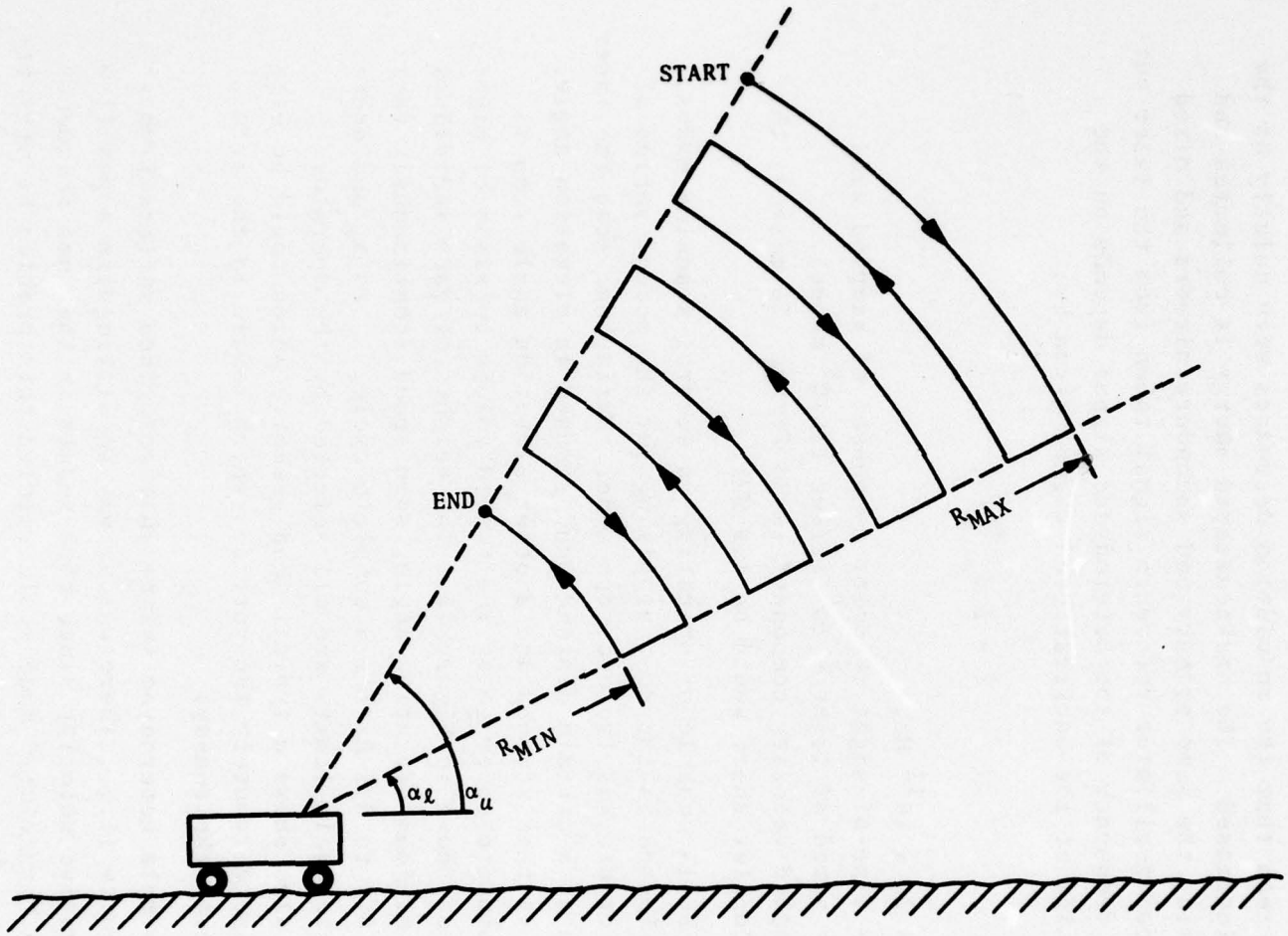


FIGURE 16. LASER-SCAN GEOMETRY

$$f_{Doppler} = f_{offset} + 2f \frac{V}{C} .$$

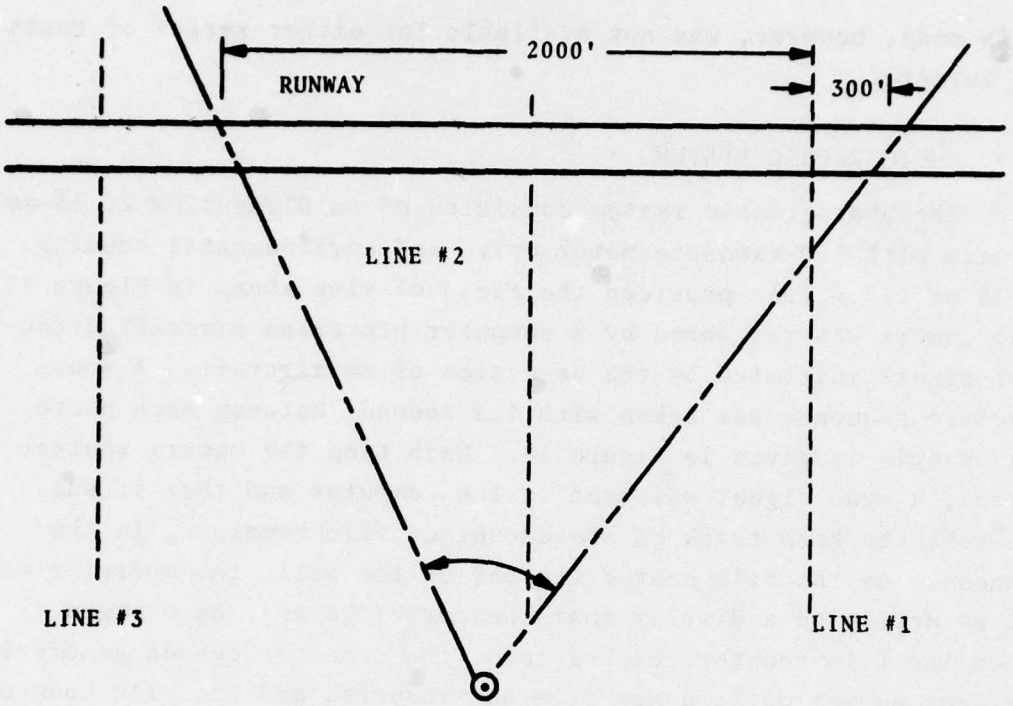
This mode, however, was not available for either series of tests at Toronto.

2.4 PHOTOGRAPHIC SYSTEM

The photographic system consisted of an Olympus OM-2, 35-mm camera with 250-exposure motor drive and environmental housing. A 28-mm f/2.0 lens provided the field of view shown in Figure 17. The camera was triggered by a computer-processed aircraft detector signal initiated by the detection of an aircraft. A four-picture sequence was taken with 1.5 seconds between each photo. An example is given in Figure 18. Each time the camera shutter fired, a sync signal was sent to the computer and thus it was possible to keep track of the amount of film remaining in the camera. As the film neared the end of the roll, the operator was given notice on a display that the cartridge must be changed. When the film counter reached zero, the computer ceased generating trigger pulses until a new film was inserted and the film counter was reset by the operator.

2.5 METEOROLOGICAL SYSTEM

The meteorological parameters measured included ambient wind, absolute temperature, differential temperature, and general weather conditions. The ambient wind was measured with three sets of Gill UVW three-axis anemometers, an example of which is shown in Figure 19. One set was mounted at a height of 100 ft (33 m) at the top of a microwave antenna tower adjacent to the site shelter with the other two sets mounted on crossarms on either side of the tower at the 20-ft (6-m) level, as shown in Figure 20. Two sensors are required at the lower level so that a wind measurement unaffected by tower shadowing may be obtained by choosing the data from the upwind sensor. The sensors consist of three propeller anemometers mounted on the three orthogonal x,y,z axes. The sensor is oriented so that one anemometer is parallel to the runway centerline



CAMERA PLAN FIELD OF VIEW

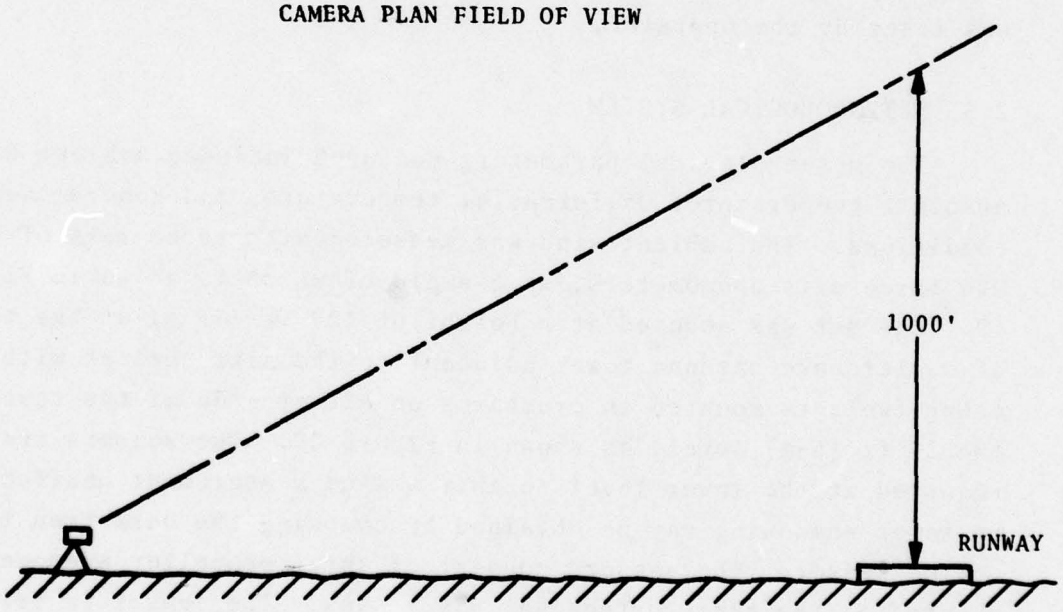


FIGURE 17. CAMERA FIELD OF VIEW



FIGURE 18. FOUR-PHOTO SEQUENCE OF AIRCRAFT TAKEOFF. PHOTOS ARE TAKEN AT 1.5-SECOND INTERVALS

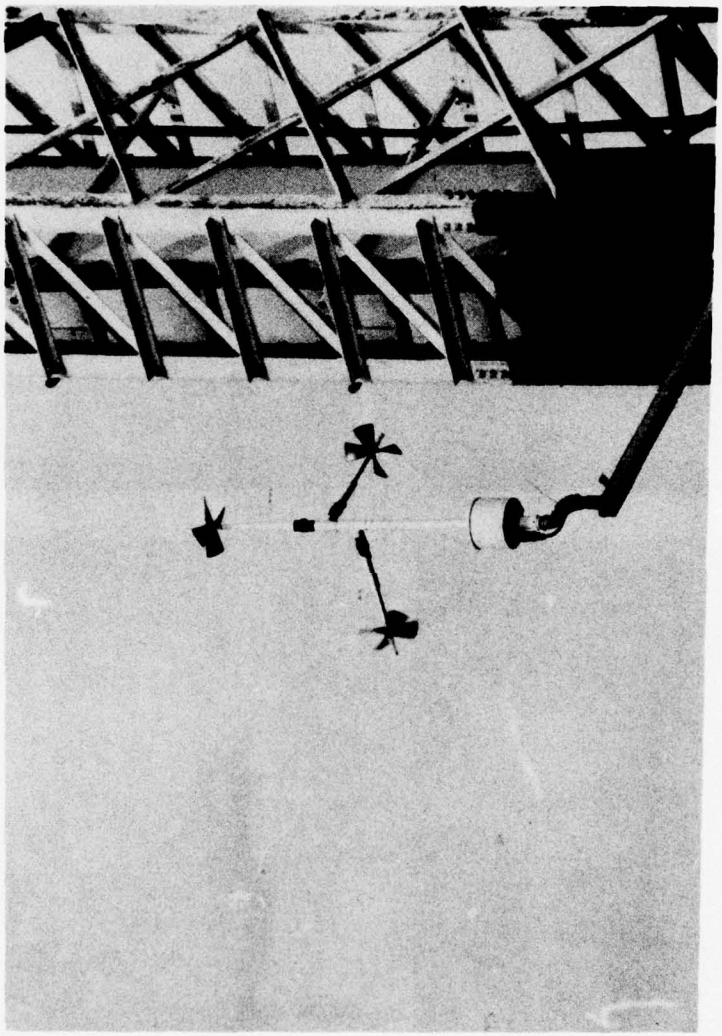


FIGURE 19. THREE-COMPONENT PROPELLER ANEMOMETER

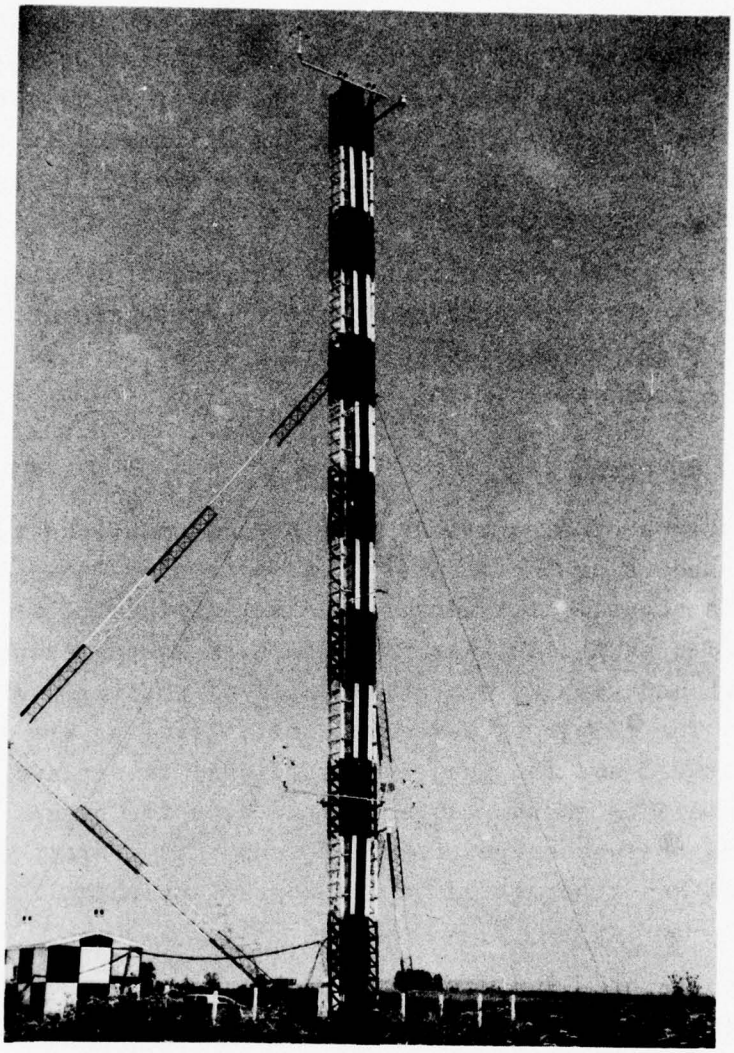


FIGURE 20. WAVEGUIDE GLIDE-SLOPE TOWER

and provides a measurement of the headwind component of the ambient wind. A second anemometer points in a direction perpendicular to the runway and provides a measurement of the crosswind component. The third anemometer points vertically and provides a measurement of the vertical component of the wind.

The absolute and differential temperature measurements are obtained from two aspirated platinum resistance temperature probes (Figure 21). One sensor is mounted at the 20-ft (6-m) level and the other at the 100-ft (30-m) level. The difference in the readings from these two sensors provides a differential temperature measurement (lapse rate).

The general weather conditions are obtained from the daily log sheets. The site operators were required to comment at least twice per log sheet on the general weather (i.e., cloudy, rainy, 50 percent overcast, etc.).

2.6 AIRCRAFT DETECTOR

The detection of aircraft as they passed each sensor baseline was accomplished using the acoustic sensing system shown in Figure 22. An acoustic transducer receiver is located at the focal point of a parabolic antenna whose beam is fan shaped, narrow in azimuth and with an elevation angle of approximately 60° (Figure 23). The change in perceived noise level as the aircraft passes is measured and the peak in this signal is defined as the time the aircraft is in the center of the acoustic beam. The sampled analog voltage output from the sensor is converted to a digital signal and transmitted to the central computer for processing.

The computer uses an operator-controllable threshold which must be exceeded before the signal is a candidate for detection as an aircraft. The setting is critical as too low a level will allow false alarms from other sources (e.g., aircraft on other runways) while too high a level will not detect the quieter aircraft (e.g., general aviation aircraft and, more importantly, in some cases the newer and quieter jets: L-1011, DC-10, etc.).

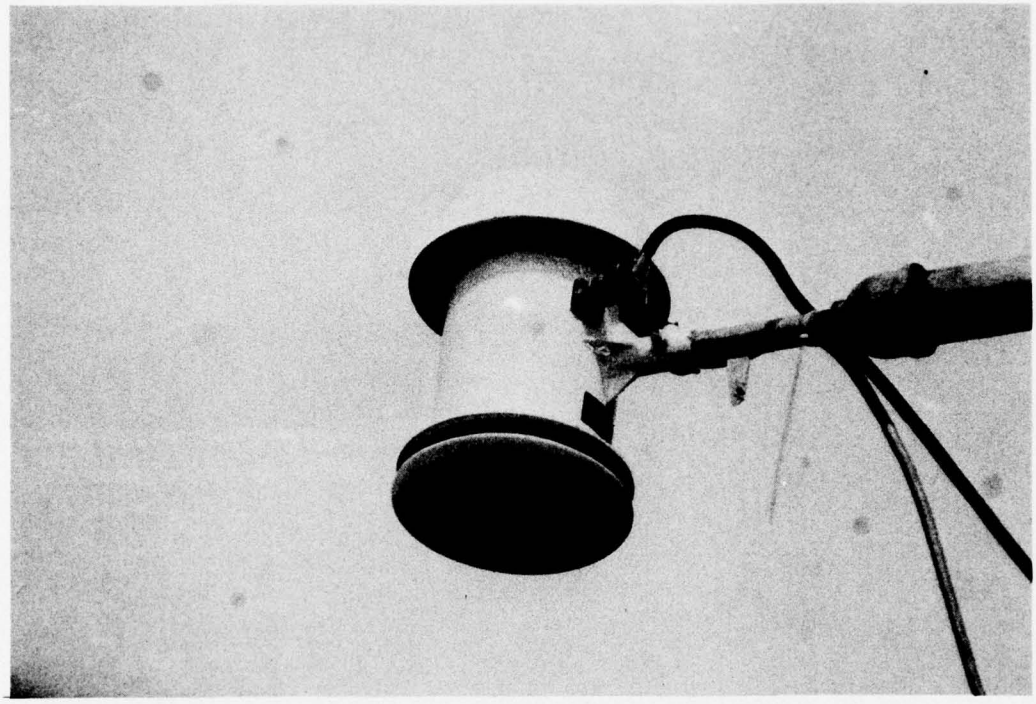
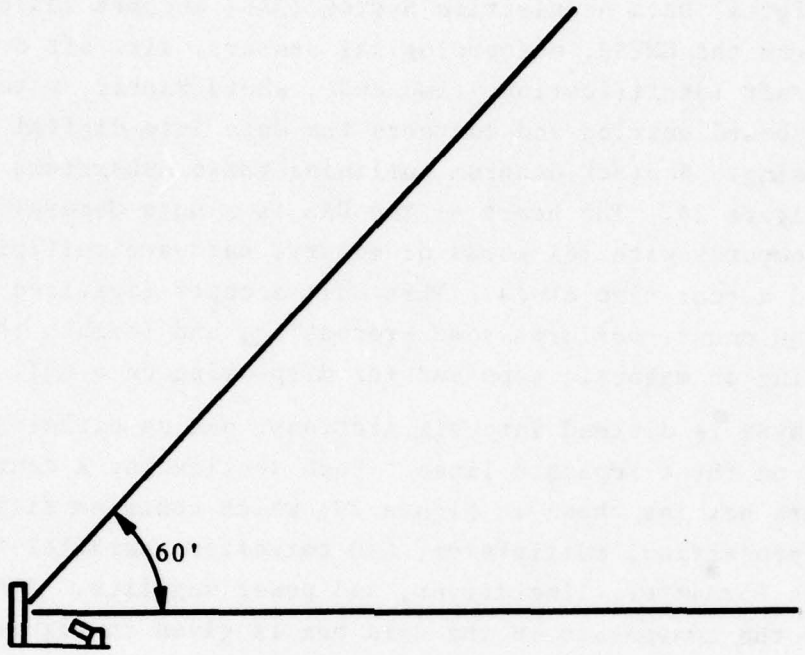


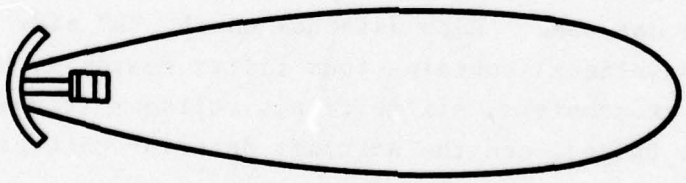
FIGURE 21. TEMPERATURE SENSOR



FIGURE 22. AIRCRAFT DETECTOR



ELEVATION PATTERN



AZIMUTH PATTERN

FIGURE 23. AIRCRAFT-DETECTOR ANTENNA PATTERN

2.7 DIGITAL DATA-ACQUISITION SYSTEM HARDWARE

The digital Data Acquisition System (DAS) accepts analog voltages from the GWVSS, meteorological sensors, aircraft detectors, aircraft identification, time code, photographic system, and console keyboard entries and converts the data into digital signals for processing. A block diagram outlining these subsystems is shown in Figure 24. The heart of the DAS is a Data General NOVA 2/10 minicomputer with 16K words of memory, hardware multiply/divide, and a real-time clock. This unit accepts digitized data from the equipment, performs some processing, and formats the data for recording on magnetic tape and for displaying on a CRT.

The GWVSS is divided into six sections, one on either side of the runway on three separate lines. Each section has a centrally located data box (as shown in Figure 25) which contains filtering, lightning protection, multiplexer, A/D converter, parallel-to-serial data formatter, line driver, and power supplies. A block diagram of the components in the data box is given in Figure 26.

Each filter board has eight input channels with provisions for mounting discrete electronic components for signal conditioning. All signals have zener-voltage clamping at $\pm$15 volts (multiplexer power supply voltage) and lightning protection in the form of a gas discharge overvoltage sensor. Data signals from the anemometers are input to an RC combination which acts as a 2-Hz low-pass filter. Each data box on the "A" side of the field (shorter baselines) contains two filter boards with inputs from eleven anemometers and three reference voltages; the remaining two input ports are not used. Each data box on the "B" side of the field (longer baselines) contains four filter boards with inputs from nineteen anemometers, six reference voltages (three voltages each input twice), and the aircraft detector connected in common to the remaining seven inputs.

The outputs of the filter boards are connected to a sixteen-channel multiplexer-A/D converter. The "B" side requires two multiplexer/converters to accommodate the 32 data inputs. The input channels are sequentially sampled and each channel is

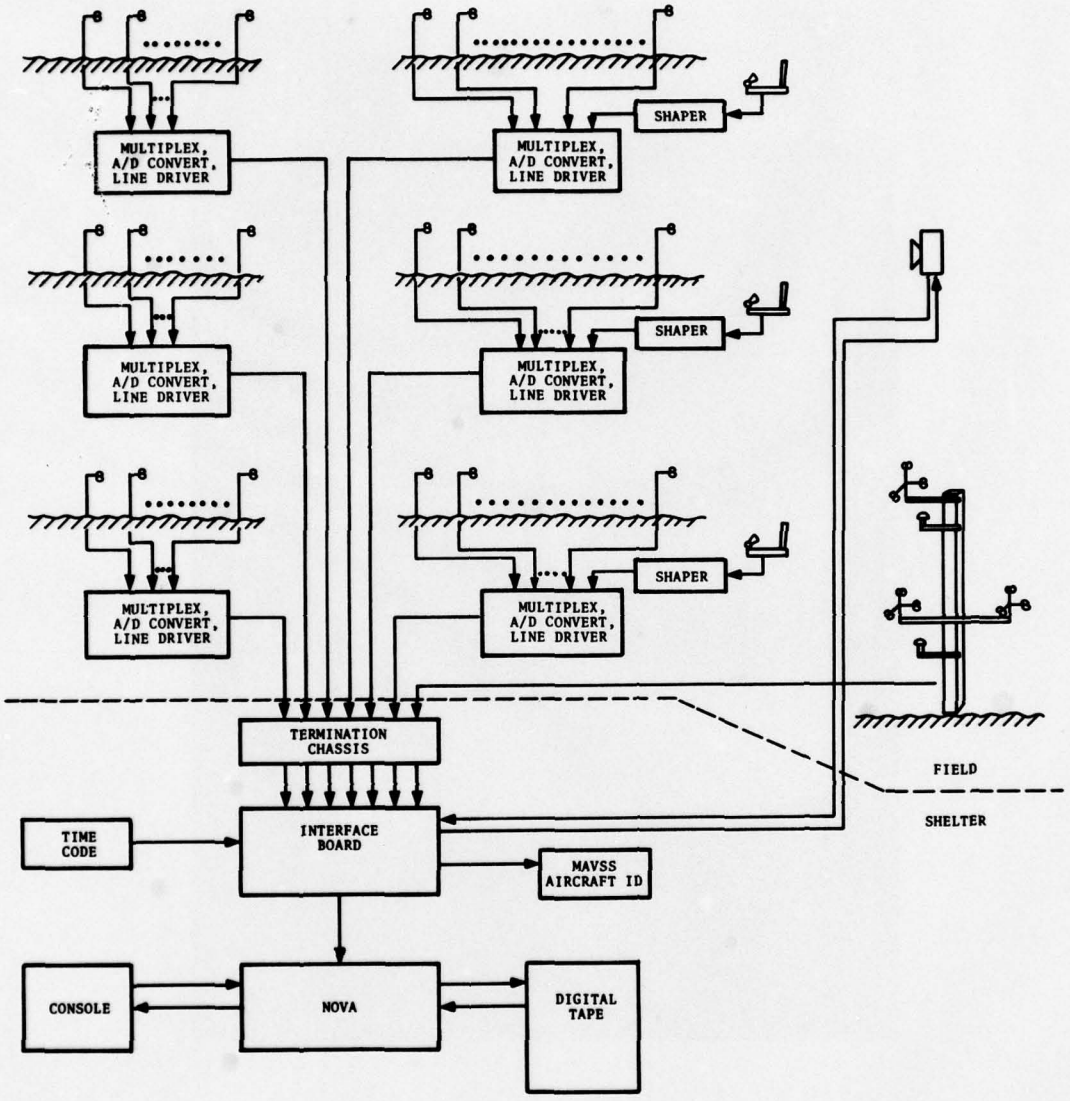


FIGURE 24. DATA-ACQUISITION SYSTEM HARDWARE

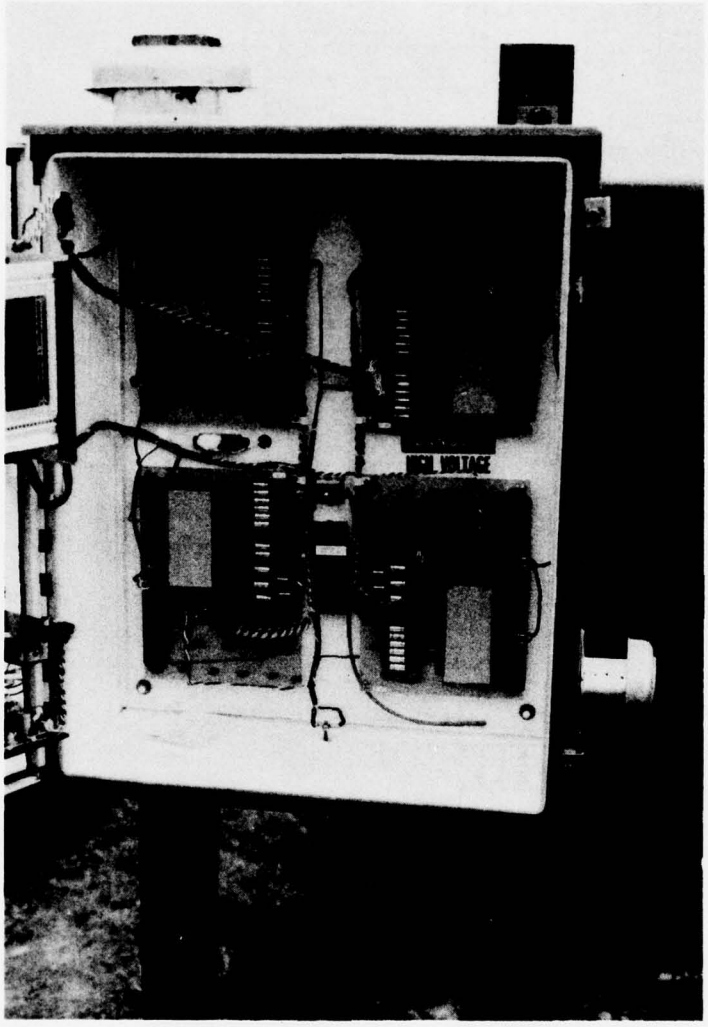


FIGURE 25. DATA-BOX INTERIOR

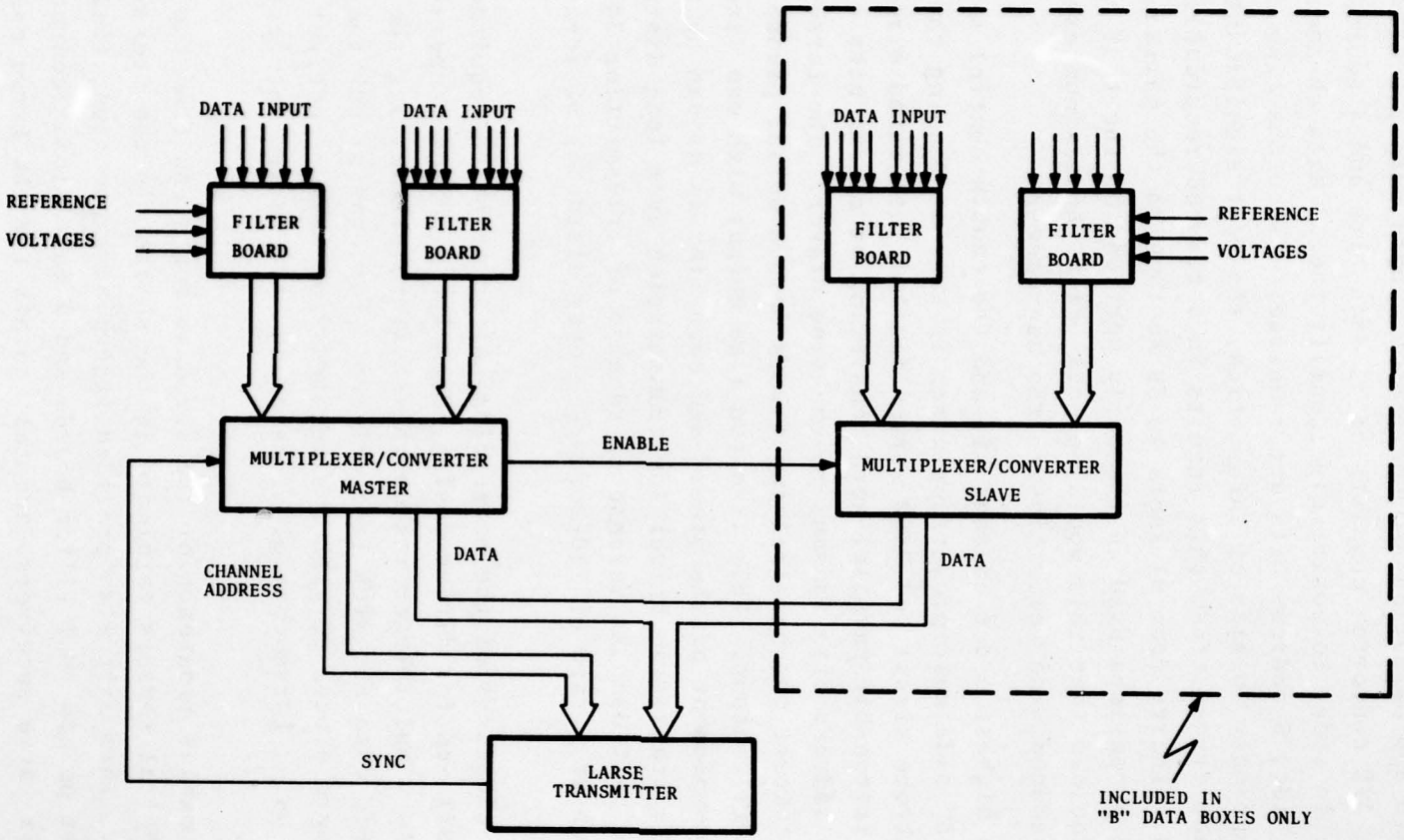


FIGURE 26. DATA-BOX HARDWARE

sampled 5 times per second. Each sample then undergoes a 12-bit successive approximation A/D conversion. Data output available from the A/D converter consists of 12 data bits and 4 address bits. However, in order to positively identify the 32 data channels on the "B" side, 5 address bits are required. Since the line driver can accept only 16 bits of information, the most significant data bit is not transmitted; this results in a reduced recordable maximum wind velocity from 61 knots to 30 knots with the maximum-response propellers used in the early portions of the test period. It was decided that this would be well below the maximum expected vortex-induced wind velocities on the anemometers.

The highest order address bit and the enable control signal on the "B" side multiplexer/converter is generated using the line-driver strobe signal and 7400 series digital integrated circuits. Thus a sixteen-bit parallel word consisting of eleven bits of data and five address bits is sent to the line driver. The Larse line drivers convert the parallel input word into a serial pseudo-differential output. This is a two-line output with one line the logical complement of the other, and each line is driven by a totem-pole transistor driver for transmission over long distances. The Larse unit used at Toronto is capable of transmitting 34 bit data words at a rate of 160 words/sec over distances of several miles.

The closeness of the meteorological tower to the equipment shelter allowed for direct cabling from the wind and temperature sensors to a multiplexer inside the shelter, eliminating the need for a field data box with line drivers. For consistency these signals were processed with a simulated line driver/receiver combination using Larse control signals and 7400 series integrated circuits.

The cables from each of the six data boxes and from the meteorological sensors terminate in the shelter in the "termination chassis". This unit also provided lightning protection, field-cable test points, MET filter boards and a multiplexer/converter board, six Larse receivers, and test points for the Larse end-of-word (EOW) pulse. The Larse receiver converts the transmitted

serial data into a 16-bit parallel word which is sent to the computer interface board. A "FORCE OFF" control input to a Larse receiver forces the output data lines into the "tri-state" mode (looks like an open circuit) and inhibits the transmittal of data from this Larse. A "strobe" control signal is sent to the one Larse which has been selected to transmit its data to the computer interface thus allowing all receiver output data busses to be logically "OR-ed".

The measurement of absolute temperature is accomplished with standard sensors. However, measuring the lapse rate, or temperature gradient between the 20-ft (6-m) sensor and the 100-ft (30-m) sensor, is a very difficult task. Lapse rates of a few tenths of a degree Centigrade can be expected. Therefore, a design goal was set at a maximum total systematic error of 0.01 C° and a maximum error of 0.001°C for a temperature range of -30°C (-22°F) to +50°C (+122°F). The scheme selected consists of using the two temperature sensors as arms of a bridge circuit and measuring the voltage difference between them. The required sensitivity is obtained by chopping the d.c. power supplies and closely matching the resistances leading to the sensors which produces an output voltage proportional to the difference in the sensors alone, excluding the voltage drops in the leads.

The data from all the Larse's and the MET board are demultiplexed by using the larse end-of-word (EOW) control pulses and sent to a computer interface board. This board (printed circuit and wirewrapped) is located in the Central Processing Unit (CPU) housing. It contains most of the flip-flops and gates generally needed to interface external circuits to the Data General computer. This interface board also accepts signals from the camera and the time-code generator and provides two digital output lines to the camera for photo sequence control and to the MAVSS for aircraft identification signals. The interface board is connected directly to the NOVA where the control of data flow resides. The NOVA-processed data are output to the tape recorder and to the operator's CRT display.

2.8 DIGITAL DATA-ACQUISITION SYSTEM SOFTWARE

The Data Acquisition System software is written in NOVA assembly language and is assembled with Data General's Macro Assembler. The program flow control is handled by a software package called RTOS (Real Time Operating System) supplied by Data General which provides scheduling of the software tasks and input/output data control. The tasks perform such functions as acquire data from the Larse, convert the raw data, display and record the converted data, and monitor operator commands from the keyboard. A block diagram showing the interaction of these subroutines is given in Figure 27.

The primary task is EXEC whose main purpose is to monitor the keyboard for operator commands. Upon initial start up or whenever the system has been reset, EXEC is the first and only task created. When the operator exercises a command to acquire data, EXEC initiates the operation of the Larse interrupt service routine and the parallel tasks DPROC, DDIS, and STAT for the processing and display of the data. Another important function of EXEC is to accept aircraft ID commands from the keyboard.

The Larse interrupt service routine is called by the operating system each time an interrupt is transmitted from a Larse REDE interface. When an interrupt occurs, the subroutine determines which Larse has requested service and directs the program flow to a software table called a Device Control Block (DCB) which contains all the pertinent information needed to process the data from this particular unit. The routine also contains simple diagnostics to determine if the correct sequence of data channels is being received.

The DPROC task forms the heart of the software data acquisition system. It coordinates the data conversion, display, and recording. DDIS takes the converted data and arranges it into the proper format for display on the CRT. STAT updates the general-status display field of the CRT once every second. This field includes general system status, time code, aircraft identification, aircraft speed, and camera status.

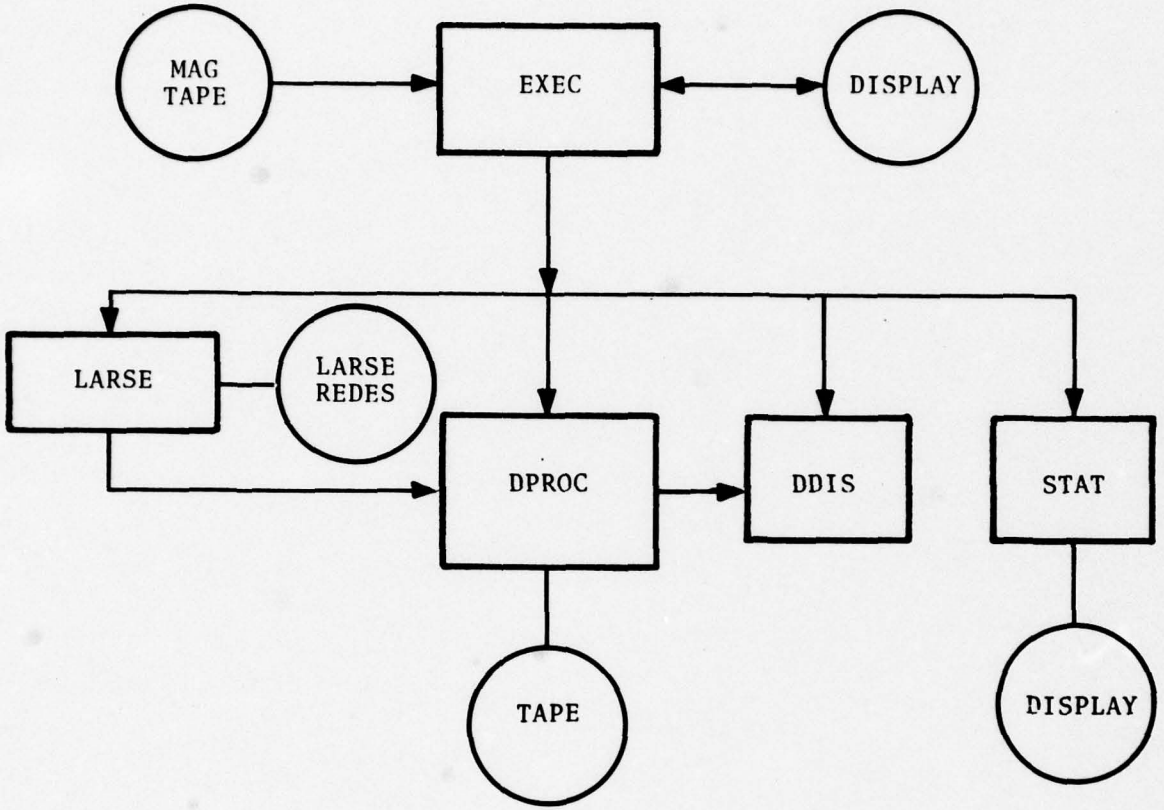


FIGURE 27. SOFTWARE TASKS AND INTERFACES

3. TEST SITE

The vortex sensors were located on both sides of runway 23L/05R at Toronto International Airport. The systems installed consisted of three ground wind vortex-sensing system (GWVSS) lines, one monostatic acoustic vortex-sensing system (MAVSS) line, one laser doppler velocimeter (LDV), three acoustic aircraft detectors, one 35-mm camera system, three sets of ambient wind sensors, and two temperature sensors.

There were several reasons for choosing runway 23L/05R: (1) there was adequate land available for all the vortex sensors, (2) it is one of the major takeoff runways at Toronto, (3) it afforded the possibility of installing vortex sensors on the approach to 05R to investigate vortex behavior in terrain with large height discontinuities, (4) a shelter for equipment and personnel already existed, and (5) a tower of sufficient height for mounting the meteorological sensors already existed (waveguide glide-slope facifacility). An overall plan view of the location of the sensors is given in Figure 28. The locations of the sensors with respect to the threshold of runway 23L are given below. The sign convention used throughout this report is defined as follows: the distances to the right of the runway centerline as observed by a pilot of an aircraft taking off from 23L is defined as positive. Thus, distances to the northwest of the runway are positive while distances measured to the southeast of the runway are negative. The decision to locate the sensors at the listed distances from the threshold was based on the analysis of data on the distribution of aircraft liftoff points and takeoff angles recorded at Philadelphia International Airport (Ref. 7).

The electronics and data recording equipment were housed in a shelter which had been intended for use with a developmental waveguide glide-slope facility. Two windows had to be installed to permit the site operator to identify the aircraft type.

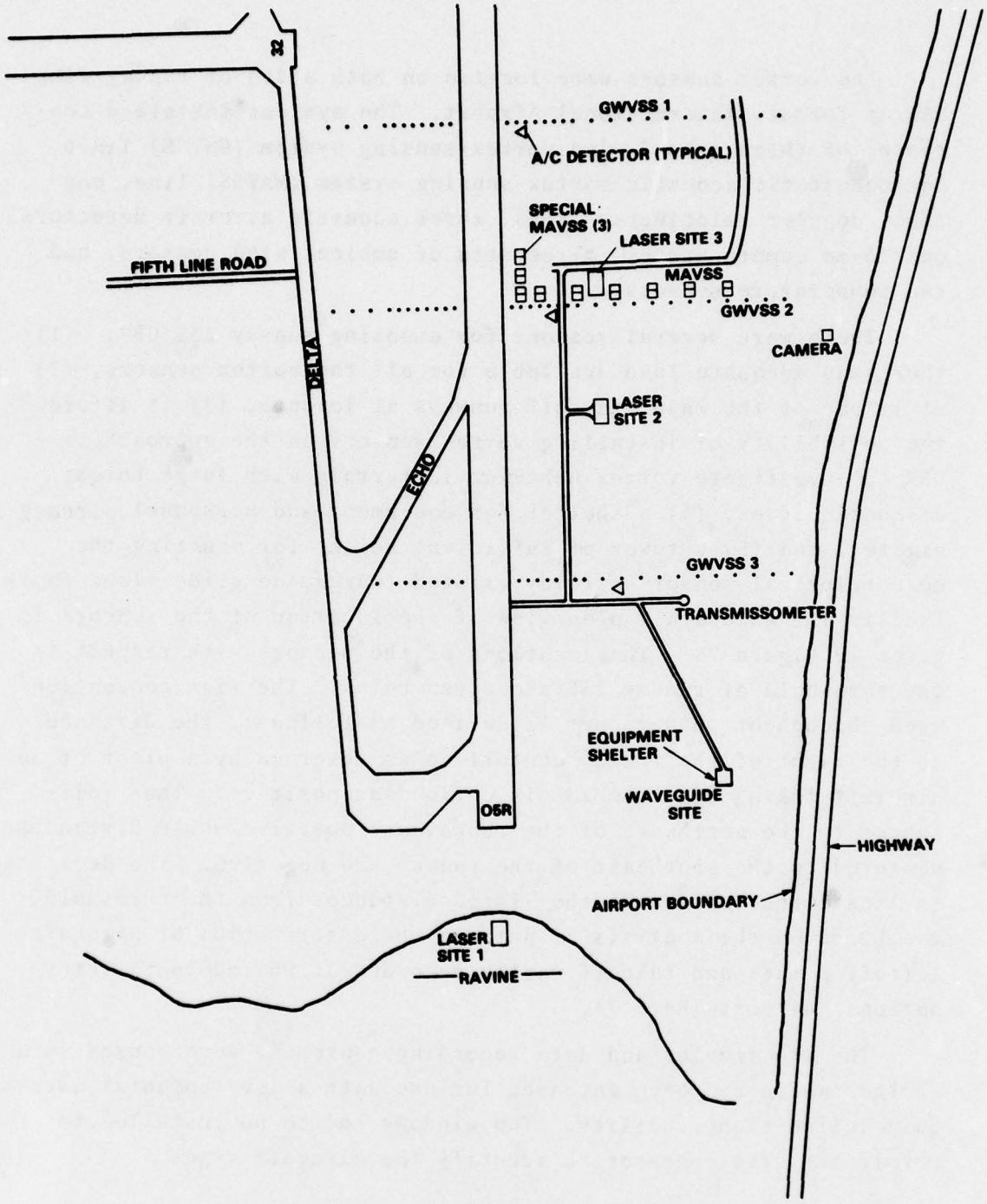


FIGURE 28. TEST-SITE PLAN VIEW

SENSOR	DISTANCE FROM THRESHOLD OF RUNWAY 23L
GWVSS line 1	5810 ft (1770 m)
GWVSS line 2	6800 ft (2070 m)
GWVSS line 3	8260 ft (2515 m)
MAVSS	6760 ft (2059 m)
A/C Detector 1	5820 ft (1773 m)
A/C Detector 2	6790 ft (2068 m)
A/C Detector 3	8279 ft (2519 m)
Camera	7030 ft (2141 m)
Laser Site 2	7325 ft (2231 m)
Laser Site 3	6740 ft (2053 m)

3.1 MONOSTATIC ACOUSTIC VORTEX-SENSING SYSTEM

A detailed description of the locations of the MAVSS sensors is given in Table 2. Sensors 1 through 6 were installed first and collected data in the standard operating mode with the beams pointing straight up and the antennas spaced 200 ft (60 m) apart. The antennas were skewed approximately 45° in azimuth to reduce reflections from adjacent antennas. Sensors 7 through 9 were installed in the summer of 1977 and were oriented at special elevation angles to try to investigate the behavior of vortices which may have stalled over the runway. The area covered by these special sensors is shown in Figure 29.

3.2 GROUND WIND VORTEX-SENSING SYSTEM

A detailed description of the locations of the ground wind sensors is given in Table 3. All the sensors were mounted on 10-ft (3.3-m) PVC poles with the exception of the sensors located 150 ft (45 m) from the runway centerline on all three baselines. These sensors were mounted on 4-ft (1.3-m) poles to conform to obstruction clearance regulations. The length of the sensor lines on the northwest side of the runway was restricted by taxiway Delta. The length of the sensor lines on the southeast side was chosen to be 1600 ft (490 m) since data from the test site at Kennedy has shown vortices from landing aircraft transporting that far.

TABLE 2. MONOSTATIC ACOUSTIC SENSOR LOCATIONS

SENSOR NUMBER	DISTANCE FROM RUNWAY CENTERLINE ft (m)	TILT ANGLE	TRANSMITTER FREQUENCIES (Hz)
1*	1300 (396)	90°	2950
2	1100 (335)	90°	3600
3	900 (274)	90°	2950
4	700 (213)	90°	3600
5	500 (152)	90°	2950
6	300 (91)	90°	3600
7	200 (61)	90°	2950
8*	200 (61)	40°	3600
9	200 (61)	20°	2950

*Antenna 1 became antenna 8 for the special tests.

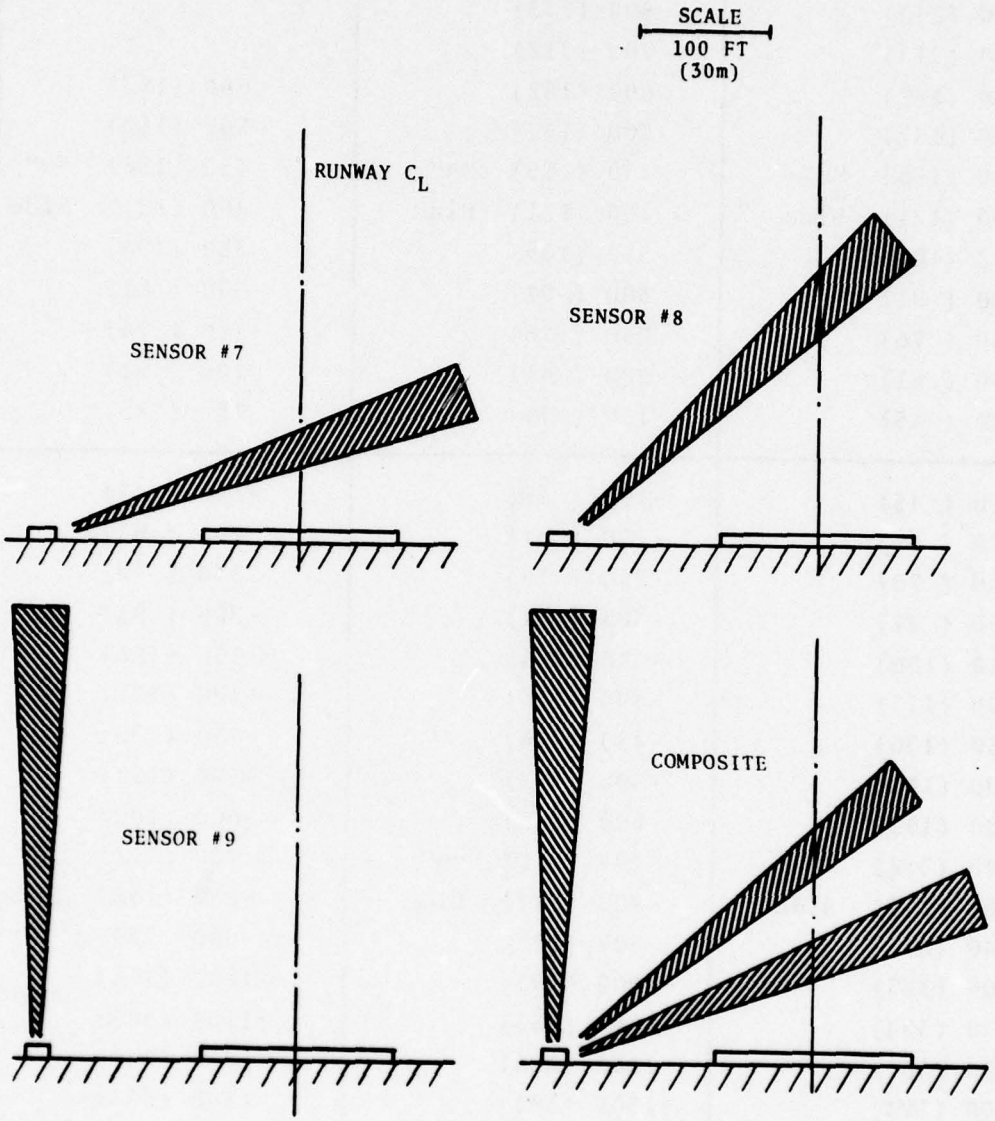


FIGURE 29. SPECIAL MONOSTATIC ACOUSTIC ANTENNA CONFIGURATIONS

TABLE 3. GROUND-WIND SENSOR LOCATIONS

(Distances are given in feet (meters) from runway centerline)

LINE 1		LINE 2		LINE 3	
800 (242)		800 (242)			
700 (212)		700 (212)			
600 (182)		600 (182)		600 (182)	
500 (152)		500 (152)		500 (152)	
450 (136)	"a"	450 (136)	"a"	450 (136)	"a"
400 (121)	Side	400 (121)	Side	400 (121)	Side
350 (106)		350 (106)		350 (106)	
300 (91)		300 (91)		300 (91)	
250 (76)		250 (76)		250 (76)	
200 (61)		200 (61)		200 (61)	
150 (45)		150 (45)		150 (45)	
-150 (45)		-150 (45)		-150 (45)	
-200 (61)		-200 (61)		-200 (61)	
-250 (76)		-250 (76)		-250 (76)	
-300 (91)		-300 (91)		-300 (91)	
-350 (106)		-350 (106)		-350 (106)	
-400 (121)		-400 (121)		-400 (121)	
-450 (136)		-450 (136)		-450 (136	
-500 (152)		-500 (152)		-500 (152)	
-600 (182)		-600 (182)		-600 (182)	
-700 (212)	"b"	-700 (212)	"b"	-700 (212)	"b"
-800 (242)	Side	-800 (242)	Side	-800 (242)	Side
-900 (273)		-900 (273)		-900 (273)	
-1000 (303)		-1000 (303)		-1000 (303)	
-1100 (333)		-1100 (333)		-1100 (333)	
-1200 (364)		-1200 (364)		-1200 (364)	
-1300 (394)		-1300 (394)		-1300 (394)	
-1400 (424)		-1400 (424)		-1400 (424)	
-1500 (455)		-1500 (455)		-1500 (455)	
-1600 (485)		-1600 (485)		-1600 (485)	

3.3 AIRCRAFT DETECTORS

One acoustic aircraft detector was located on the southeast side of each GWVSS line at the locations shown in Figure 28.

3.4 PHOTOGRAPHIC SYSTEM

An Olympus 35-mm single-lens-reflex camera was located 1800 ft (550 m) southeast of the runway centerline and 200 ft (60 m) to the southwest of GWVSS line 2 as shown in Figure 28.

3.5 METEOROLOGICAL TOWER

An unused 100-ft (30-m) waveguide glide-slope antenna was used to mount the UVW ambient wind sensors and the temperature sensors. The tower is located approximately 25 ft (7.6 m) from the south corner of the test-site instrumentation shelter as shown in Figure 28. There are no large obstructions (buildings, terrain discontinuities, etc.) in the immediate area of the tower which could cause biased or distorted wind readings.

3.6 LASER

A mobile laser Doppler velocimeter was installed at the Toronto Toronto Airport test site for two series of tests: July 1976 and July to August 1977. Two sites were used in the first series of tests and are labeled "Laser Site 1" and "Laser Site 2", respectively, on Figure 28. The site used for the second series of tests is labelled "Laser Site 3". A photograph of the laser van at site 3 is given in Figure 30. The locations of the laser sites are given in Table 4.

3.7 EQUIPMENT SHELTER

An MOT building previously used to house the equipment for the waveguide glide-slope facility was used as a shelter for the electronic equipment. The shelter was modified to include two windows to allow the operators to identify the aircraft type. Extra air conditioning was added to control the temperature for the sensitive computer equipment.

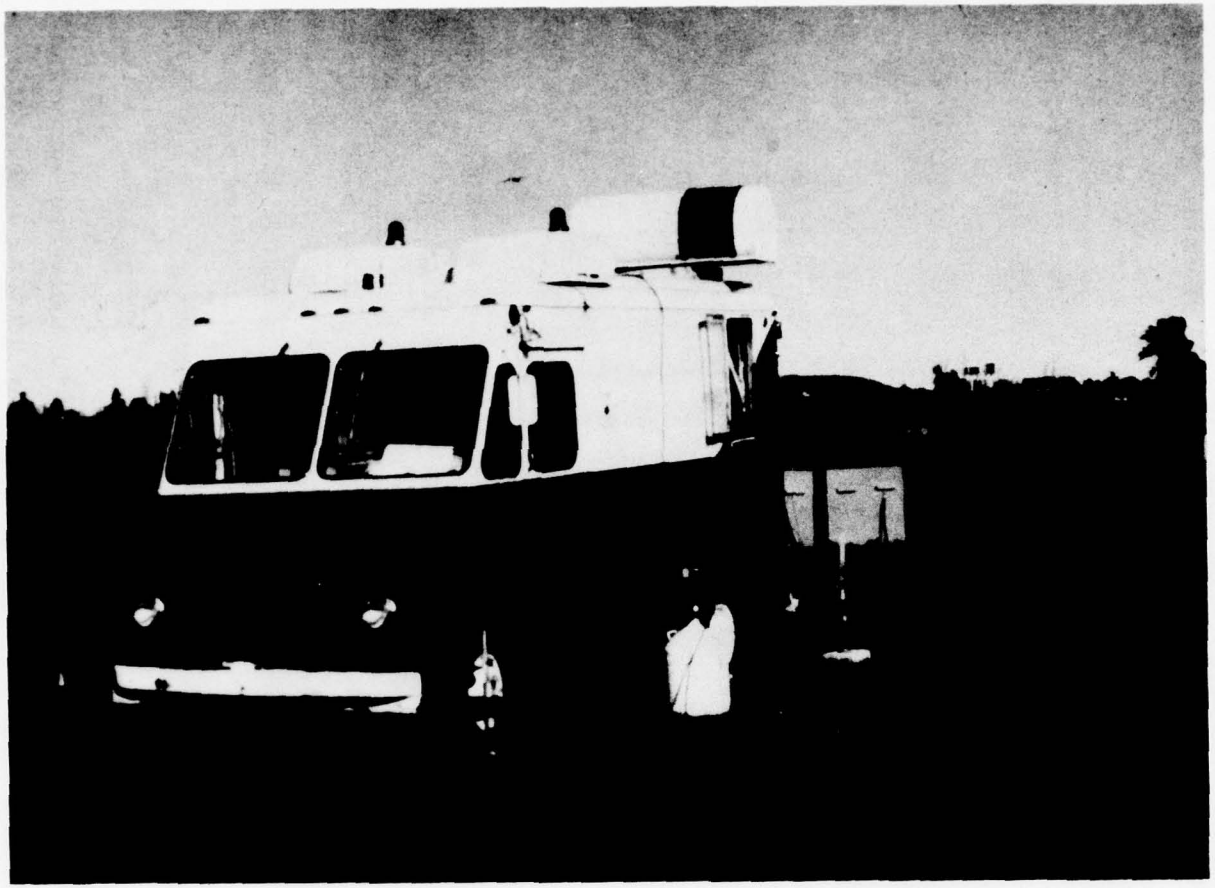


FIGURE 30. LASER DOPPLER VELOCIMETER VAN

TABLE 4. LASER-SITE LOCATIONS

SITE NO.	DISTANCE FROM THRESHOLD OF RUNWAY 23L, ft(m)	OFFSET DISTANCE, ft(m)
1	10,100 (3060)	0
2	7,300 (2212)	600 (182) SE
3	6,750 (2045)	400 (121) SE

4. DATA COLLECTION

The goal of the data collection effort was to acquire accurate and distortion-free data. At least one trained operator was required at the site during all times of data collection. The functions of the operator included: inspection and maintenance of sensors and electronics, adjustment of parameters to fit program needs, aircraft identification, system maintenance, and camera operation. Data collection procedures for individual subsystems are described in the following subsections.

4.1 REAL-TIME DISPLAY

The primary interface the operator has with the components of the system is the cathode ray tube (CRT) display and keyboard. With selectable keyboard instructions the CRT can display the major system parameters which include:

- all meteorological data
- a real-time indication of the analog outputs of a complete GWVSS anemometer line
- status of the signal conditioning and processing equipment in the field
- camera status and amount of film remaining
- aircraft identification
- aircraft detector triggers
- time code
- multiplexed analog data from a field data station (for troubleshooting purposes)
- echoes of keyboard inputs
- false trigger of an aircraft detector
- sensor malfunction
- tape recorder malfunction
- software malfunction.

The CRT is divided into four display zones as shown in Figure 31. Each of the parameters listed above can be displayed in one of these zones.

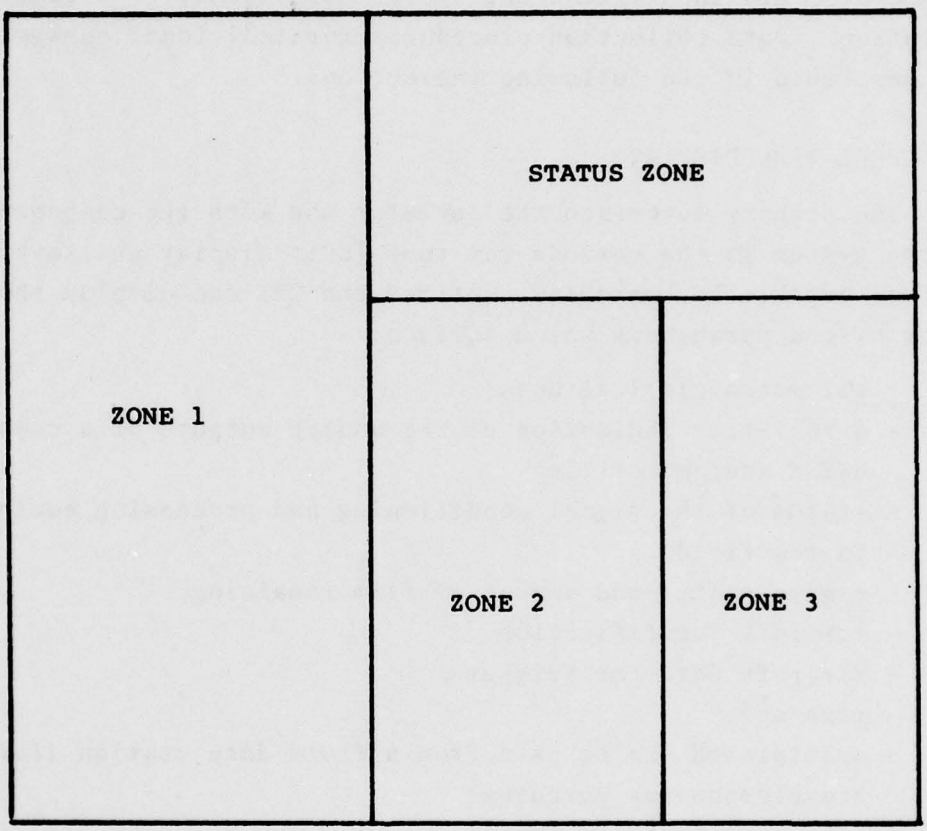


FIGURE 31. CATHODE-RAY TUBE DISPLAY ZONES

4.2 SYSTEM INITIALIZATION

The first step in the operator's daily routine was to load the system program into the computer (if required). This involves mounting a tape and loading the bootstrap program using manual settings of the computer front panel switches. The system verifies the proper completion of this procedure by displaying RTOS REV 3.00 (Real-Time Operating System, Revision 3.00) or its equivalent on the CRT. From this point on, all interactions between the operator and the computer are through the use of keyboard commands which are monitored and executed with the EXECUTIVE subroutine.

After the system program has been loaded, the operator has several choices of displays and data collection modes from which to choose. A typical procedure, which results in the recording of data on magnetic tape and the displaying of the most important system parameters, is presented in Figure 32. To begin data acquisition, the command RECORD is typed on the keyboard. The system will now accept data from the input channels, perform conversions, and display status information in the status zone. The information contained in the status display allows for early identification of system malfunctions from several sources. The format of this display with sample data is shown in Figure 33. The data collection mode selected for each GWVSS subsystem and the meteorological system is displayed in the GW MODE and MT MODE fields. The indication of the detection of one of three types of errors in data transmission by any of these systems was displayed in the GWERR and MTERR fields. If no data are received from a field station, a ? symbol is displayed. If an erroneous block of data is received, a 1 is displayed. If the address of the received data channel does not match the expected address, a code is displayed (See Appendix A for a list of the codes). Triggering of each aircraft detector is indicated by an X displayed under the appropriate device column in the AC DET field. The aircraft speed is computed using the measured times between triggers of the aircraft detectors and is displayed in the VELOCITY field. When only two of the three detectors trigger, only one speed may be calculated; when all three detectors trigger, three speeds V_{12}, V_{13} and

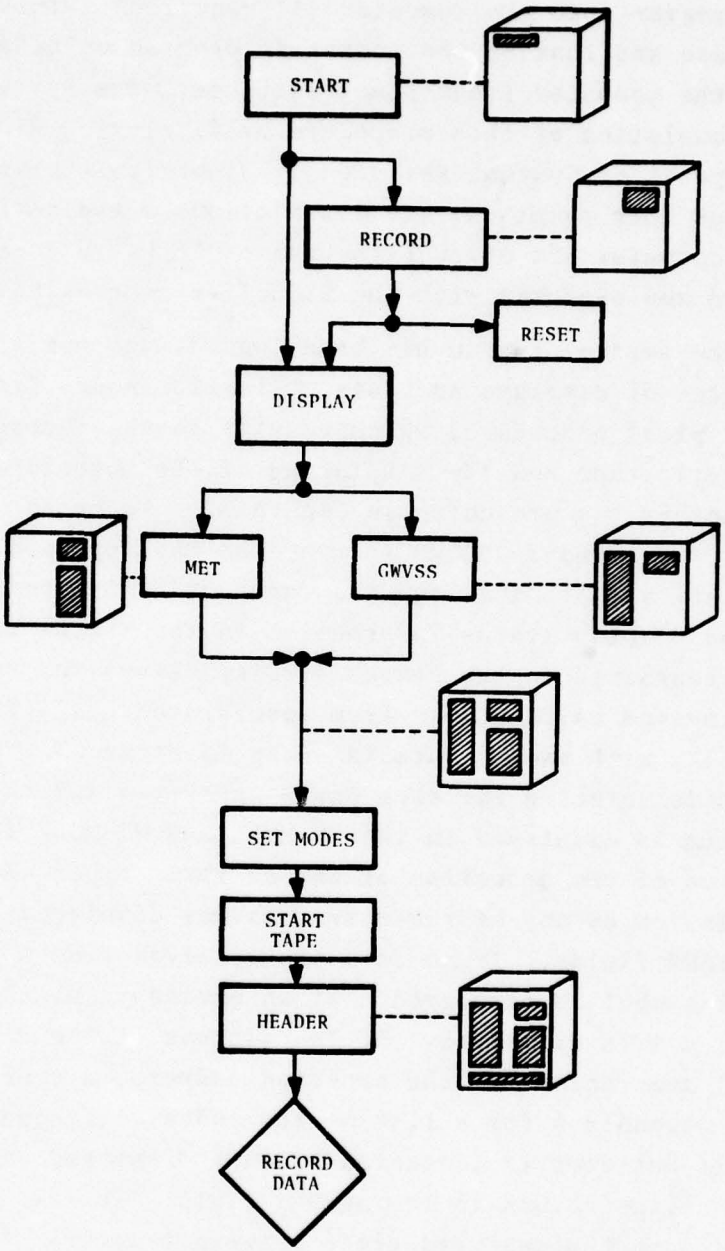


FIGURE 32. TYPICAL RECORDING PROCEDURE

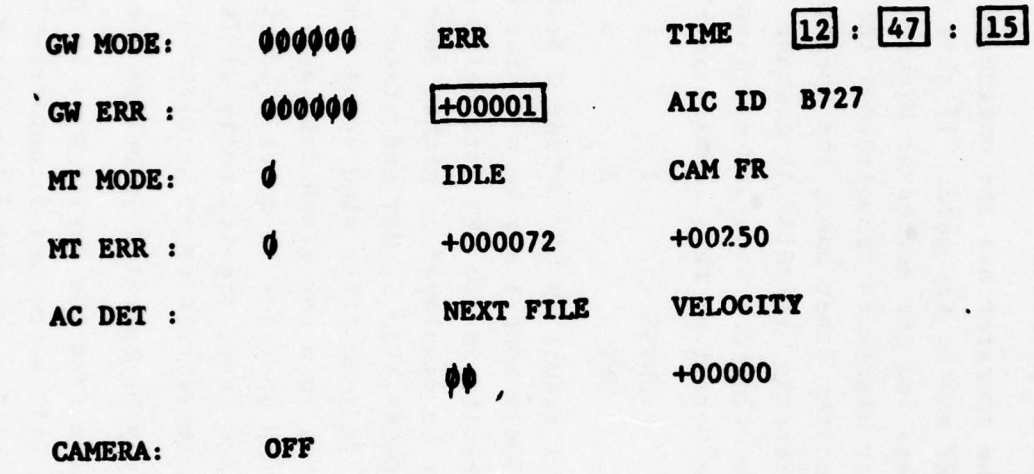


FIGURE 33. GENERAL STATUS DISPLAY FORMAT

V_{23} (where V_{12} is between aircraft detectors 1 and 2, etc.) are calculated and are displayed. The camera status and number of frames remaining before the end of the reel are displayed in the CAMERA and CAM FR fields, respectively. The aircraft type as identified by the operator is displayed in the AC ID field. The time as read by the time-code generator is displayed in the TIME field. The IDLE field indicates the percentage of the time that the CPU is idle; it has been empirically determined that it should always be greater than 50 percent.

At this point the operator has the option of resetting the system by typing RESET on the keyboard. If this mode is chosen, data acquisition ceases and the screen is blanked. This is normally used when the operator wishes to troubleshoot the system using the DEBUG routine. If, on the other hand, the operator wishes to perform normal data collection, the DISPLAY command is used to display in real time all meteorological data and one line of ground-wind data on the CRT. The format of this command is shown below:

DISPLAY	GWVSS	2	1
DISPLAY	MET	1	3

The first command will result in GWVSS line 2 being displayed in zone 1 of the CRT. (Only zone 1 may be used for GWVSS displays.) The second command results in the MET data being displayed in zone 3. (The MET data may be displayed in either zone 2 or 3.) A photo of the display with GWVSS line 1, MET and status information is shown in Figure 34. In zone 1 the wind speed measured by each anemometer is presented in a bar-graph display. An inspection of this display allows the operator to quickly identify a malfunctioning anemometer (voltage level significantly different from the rest of the line, voltage level remains at zero and does not move, etc.)

Each subsystem may be operated in one of four selectable modes:

Mode 0 - no data from the device will be recorded
Mode 1 - data will be recorded continuously
Mode 2 - data will be recorded for four minutes only after the trigger of an aircraft detector (applies to GWVSS only).

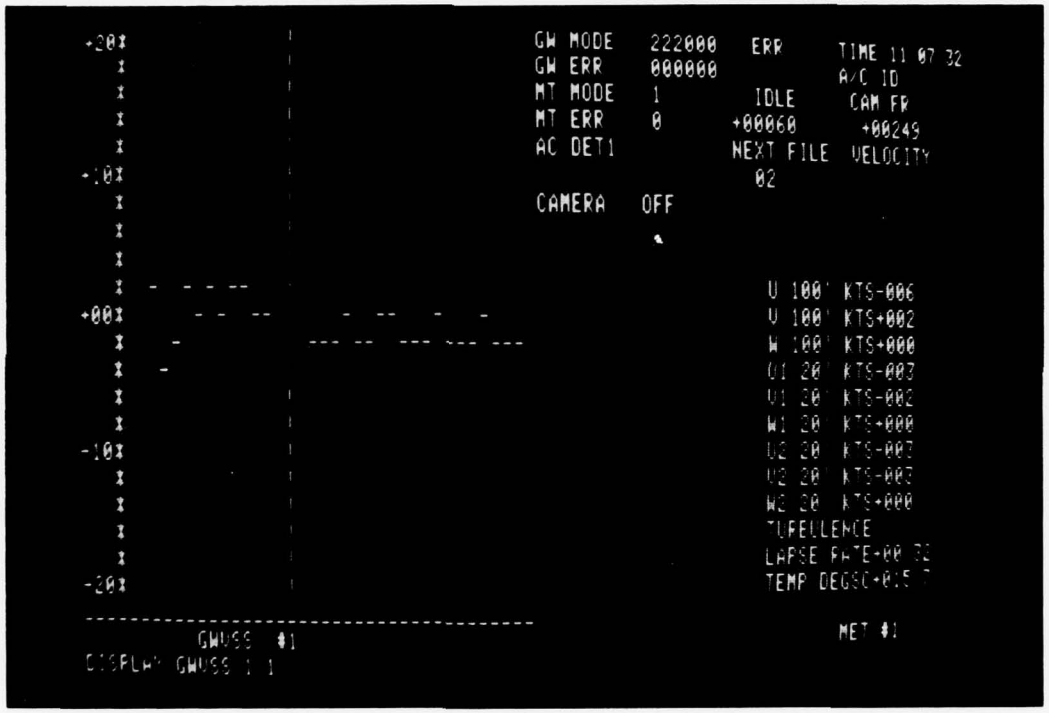


FIGURE 34. DISPLAY OF PROPELLER ANEMOMETER, METEOROLOGICAL, AND STATUS DATA

If a subsequent trigger from another aircraft obtained before the 4 minutes has expired, the 4-minute counter is restarted.

Mode 3 - no data will be recorded until an aircraft identification button is depressed on the keyboard.

It is necessary to set the mode for each subsystem.

The procedure for the actual recording of data on magnetic tape begins with the issuance of the START TAPE command. The system then requires the operator to provide a header message which, for normal data collection, starts with the letters YYZ followed by the tape number, a six-digit month/day/year date, and the operator's name. After this information has been logged, the operator may include other comments that might be helpful in the data reduction. At the end of the header the operator types a "control N" and the recording of data commences.

4.3 CAMERA

When the camera is functioning properly, all operation is under computer control and completely automatic. The operator loads the camera with a 250-exposure film pack and initializes the computer with the SET CAMERA command. The picture-taking sequence is enabled by the operator through the CAMERA ON command. The number of frames remaining in the film pack and the camera on/off status are indicated in the STATUS field of the display. When the film counter reaches zero, the operator must remove the exposed film cassette and replace it with a new roll of film.

Identification information is included in the foreground of each photo with a clock and notice board as shown in Figure 35. The operator is responsible for updating this board with the correct date and film-pack number.

The camera system proved to be the most unreliable of all the subsystems. Constant attention was required to provide reliable operation of the motor drive, particularly in cold weather. A large portion of candidate data was not recorded due to camera system malfunctions.



FIGURE 35. CAMERA SITE

4.4 AIRCRAFT DETECTORS

Like the camera system, when the aircraft detectors are functioning properly, all operation is under computer control and completely automatic. The successful detection of an aircraft by each of the three detectors is indicated in the AC DET field of the status display. This system proved to be very reliable and little operator interaction was required. The operator was required to record in the log sheets whenever a "false" trigger (i.e., an aircraft taking off on another runway, an aircraft landing on runway 23L, etc.) was observed. The electrical detection parameters (threshold voltages, etc.) can be changed by the operator but not simply as a keyboard entry; this requires software modification using the DEBUG routine.

4.5 AIRCRAFT IDENTIFICATION

Identification of the aircraft type is performed by the site operator as the aircraft enters the sensing system. The operators must make the identification and set the corresponding switch on the keyboard console before the aircraft passes line 2 due to the manner in which the monostatic acoustic sensor data are processed. Identification of the aircraft type is done primarily by keying on the engine configuration. When identification is difficult using only engine-placement criteria, other factors are considered (e.g., the top portion of a DC-9 tail section has a hump shape while a BAC-111 has a forward pointing protrusion; some airlines fly only one type of aircraft in each class such as Air Canada owns only DC-8's and no B-707's, while American Airlines owns only B-707's and no DC-8's, etc.). The computer interprets the switch on the console and transmits the appropriate aircraft-type code to the magnetic-tape recording system at regular intervals for 30 seconds after the first setting of the switch. If the operator decides a mistake in identification was made, the correct ID button could be pressed any time during these 30 seconds and the corrected ID would be recorded. The selected aircraft type is also indicated in the status field of the display permitting confirmation of the proper selection.

4.6 GROUND-WIND VORTEX-SENSING SYSTEM

The only operator interactions required for the GWVSS are selecting the data collection modes, repairs of malfunctioning parts, and routine maintenance. The mode selection has been described in Section 4.2. A fragile four-bladed polystyrene propeller was used initially. An unusually high frequency of propeller blade breakage was recorded and was attributed to hawks alighting on the anemometer and hitting the blade with their wings. This problem was solved by substituting sturdier ABS plastic 3-bladed propellers. No further blade breakages were recorded after the installation of these propellers. However, some anemometer maintenance (replace bearings, replace tachometers, re-orientation of support poles, etc.) was still required.

4.7 MONOSTATIC ACOUSTIC VORTEX-SENSING SYSTEM

The MAVSS was designed to require minimal operator interaction; however, there remain several tasks which require the attention of the operator. Since only one side of the runway is populated with MAVSS sensors, data are collected only when the crosswind is appropriate for transporting the vortices over the sensors. In general, if the crosswind is positive, the vortices will move toward the northwest side of the runway and the MAVSS need not be turned on. The operator can get some indication of the vortex transport by monitoring the GWVSS display. The operator must also start and stop the analog tape recorder (it had been determined that in an airport environment the MAVSS does not track vortices for longer than 2 minutes after an aircraft detection).

In the original plans for installation of the vortex sensors at Toronto it was expected that the tests would be conducted during the summer and fall months. Therefore, no provisions were made to operate the MAVSS during periods when snow would accumulate in the antennas. When the test program was extended through the winter, protection against snow accumulation was accomplished using wooden covers over the antennas. When the snowfall subsided and it was desired to collect data with the MAVSS, the operators would have to remove each cover.

4.8 DIAGNOSTICS

Once the operator has determined there is a problem with one of the components in the field, a preliminary diagnostic was done using the DIAGNOSTIC command. When the operator enters this mode, all the multiplexed data-channel voltage levels are displayed in zones 2 and 3 as shown in Figure 36. The operator may than inspect the voltages from each anemometer as well as the aircraft-detector and reference voltages. To initiate this mode the keyword DIAGNOSTIC is typed followed by a hardware device number:

DATA BOX	DEVICE NUMBER
0	1B
1	2B
2	3B
3	1A
4	2A
5	3A
6	Met Tower

Data acquisition is continued by typing RECORD.

4.9 DEBUG

At times it became necessary to modify some of the fundamental parameters of the system; e.g., the number of photos taken, the threshold of the aircraft detector, the timing between photos, etc. In order to do this, modification of the system software was required. This was accomplished by using the Data General DEBUG software routine which is initiated by typing DEBUG.

The EXECUTIVE program transfers control to DEBUG and then only DEBUG commands are recognized. In this mode direct examination and alteration of the computer memory may be performed.

4.10 LOG SHEETS

A major responsibility of the operator is to maintain a daily activity log. A sample log sheet is shown in Figure 37. Several of the entries are self-explanatory (Date, Weather, Tape No., A/C

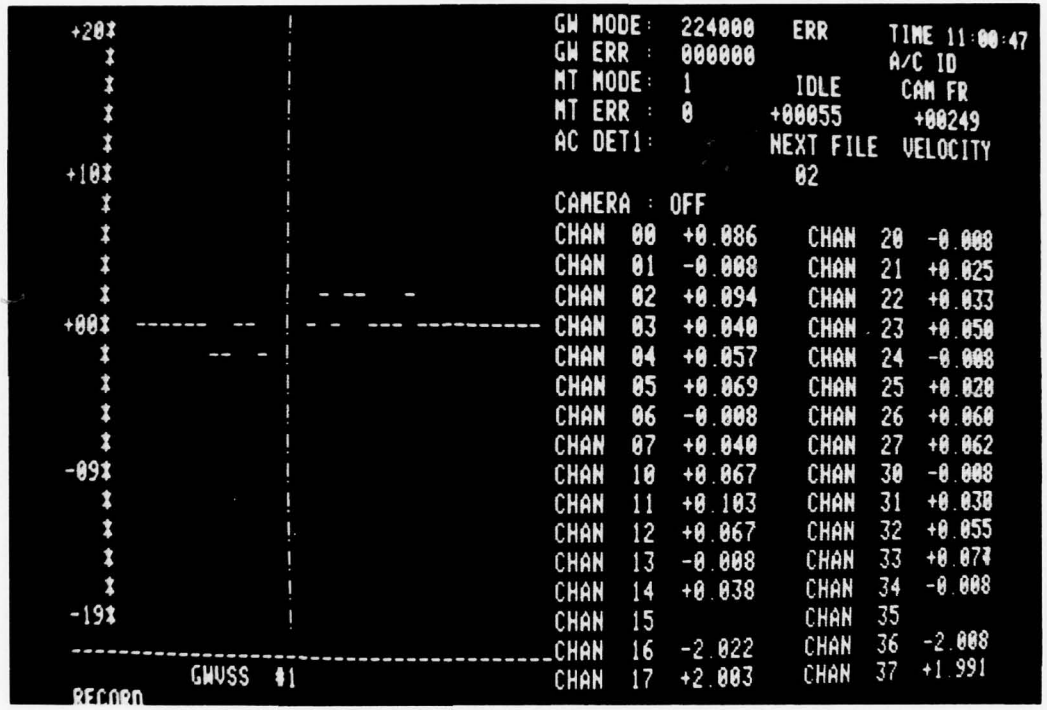


FIGURE 36. DISPLAY OF DIAGNOSTIC DATA

TORONTO INTERNATIONAL AIRPORT VORTEX TEST SITE ACTIVITY LOG

DATE: MAY 23 1977 SYSTEM STATUS: MAVSS OFF

WEATHER: OVERCAST HAZY OTHER SYSTEMS NORMAL

TAPE NO: 00089 FILE 00 FILM PACK 30

Run No.	A/C Type	Time Hour	Min.	Sec.	U V	Comments	
1	DC9	09	10	13		FILE 00 FILM PACK 30 CAM FR 182	
	B727	09	12	26	+2 +4	ONLY AC DET NOS. 1&3 FIRED	C +21.0
	B727	09	14	03		ONLY AC DET NO. 3 FIRED	
	B727	09	15	28		ONLY AC DET NOS. 1&3 FIRED	
5	B727	09	21	06	+2 +2	CAM FR 166	C +21.7
	DC9	09	28	16			
	DC8	09	30	28			
	DC9	09	36	06			
	B727	09	44	26			
10	L1011	09	49	57	+4 +2	CAM FR 146	C +22.7
	DC9	09	52	55			
	L1011	09	59	05			
	DC9	10	01	19		ONLY AC DET NO. 3 FIRED	
	B727	10	04	59			
15	DC10	10	06	57	+1 +1	CAM FR 126 ONLY AC DET NOS. 1&3 FIRED	C +23.3
	DC9	10	15	15			
	DC9	10	21	33		ONLY AC DET NO. 1 FIRED	
	L1011	10	24	21		ONLY AC DET. NOS, 1& 3 FIRED	
	L1011	10	28	59		ONLY AC DET NOS. 1&3 FIRED	
20	DC8	10	35	19	+3 -1	CAM FR 106 MAVSS ON	C +25.5

FIGURE 37. LOG SHEET

Type, and Time). The "system status" region allows for general system comments such as defective anemometers, camera status, defective components, etc. The "comments" column allows for recording activities which may be changing from run to run. The wind and its components are recorded four or five times a page and were helpful to the data analyst. The general weather conditions are recorded at least twice per page in the right-hand margin in the form of a one letter code:

CODE	WEATHER
S	Sunny
C	Overcast
R	Rain
W	Snow
L	Sleet
H	Hail
N	Night

In addition, when the condition is Sunny, an indication of the approximate percentage of cloud cover is recorded (e.g., S/4 means Sunny with 40 percent cloud cover). The remainder of the comments is used for general observations which may assist the data analysis performed at TSC such as:

- aircraft detectors which did not trigger
- MAVSS ON/OFF Status
- false trigger of an aircraft detector
- sensor malfunction
- tape-recorder malfunction
- software malfunction.

4.11 LASER DOPPLER VELOCIMETER

The first series of LDV measurements examined the behavior of vortices from aircraft passing over the ravine to a landing on runway 05R and from aircraft departing on runway 23L.

4.11.1 Data Collection in the Ravine

The mobile LDV system was set up in the ravine on the approach to runway 05R. The intent was to conduct a brief series of measurements to determine the effect of the ravine on vortex behavior. The van was parked between approach-light stations approximately 330 feet (110 m) from the runway threshold and 23 feet (7 m) from the extended runway centerline. The topography of the area near the site is shown in Figure 38. The aircraft were about 83 feet (25 m) above the van.

The van arrived in Toronto on 3 July 1976 and was positioned and set up in the ravine on 4 July. Due to problems with the rented power generator, the system was not operable until 9 July. The van was manned from 0700 to about 1900 between 9 and 19 July. During this period only 18 aircraft landed on 05R (5 B-727s, 1 B-737, 2 B-747s, 6 DC-8s, 3 DC-9s, and 1 LearJet). These aircraft landed between 1537 and 1620 on 9 July.

4.11.2 Finger-Scan Tracking of Vortices

On the afternoon of 19 July 1976 the laser van was moved from the ravine to the location shown as laser site 2 on Figure 28 for tracking vortices from departing aircraft. Data collection took place in two sessions: 20 July through 23 July and 13 August through 31 August. A total of 723 takeoffs were monitored: 186 B-727s, 12 B-737s, 30 B-747s, 88 DC-8s, 270 DC-9s, 20 DC-10s, 19 B-707s, 57 L-1011s, and 41 other (including VC-10s DC-3s, CV-580s, Learjets, and unidentified two-engine propeller aircraft).

4.11.3 Second Series of LDV Measurements

Analysis of the GWVSS data was affected by the impossibility of detecting vortices over the runway. At times one vortex was either not observed or was observed to move back over the runway. Since the presence (or absence) of this vortex could not be ascertained, nothing could be said concerning its life and/or its importance to interdeparture spacings. To track vortices when they were

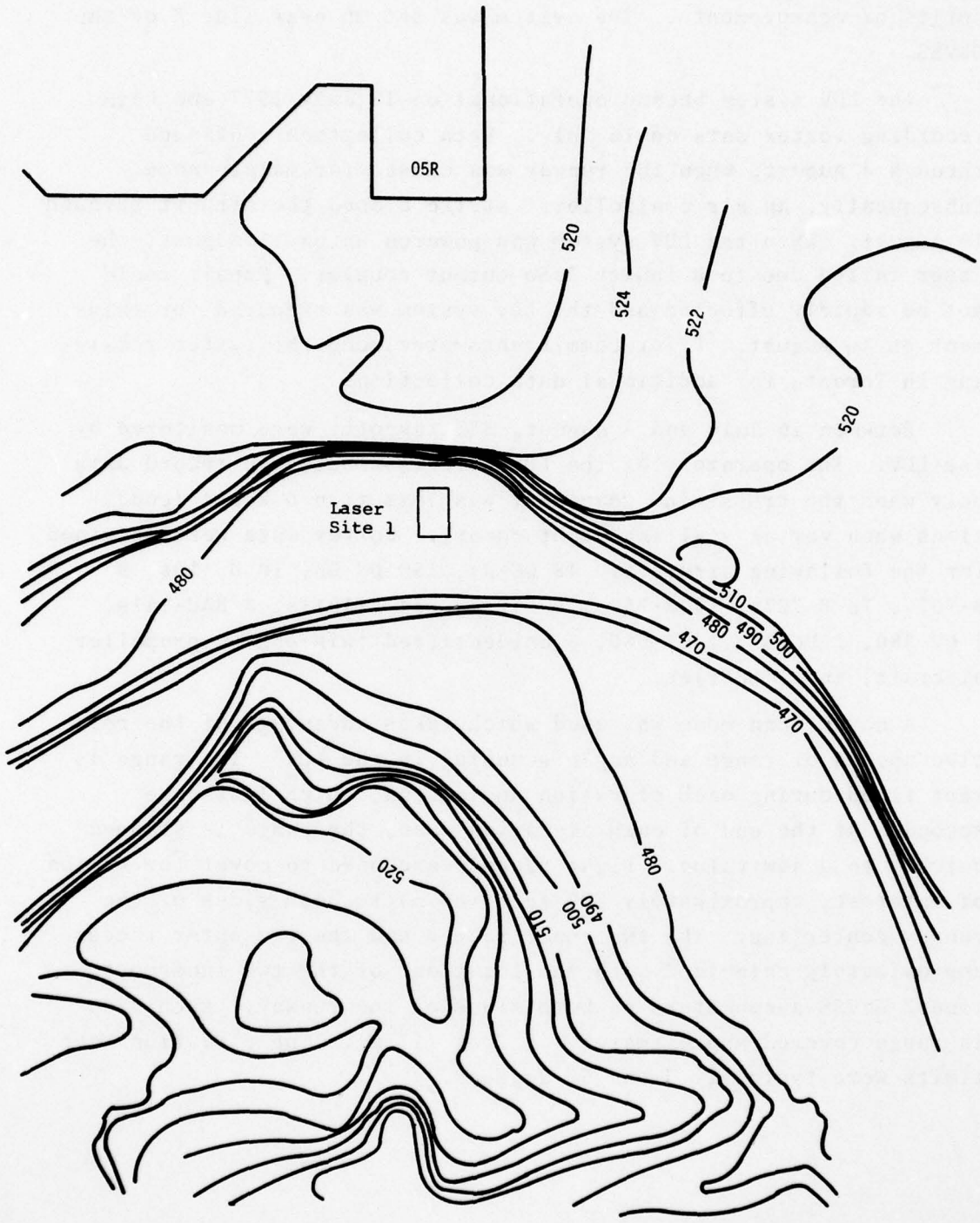


FIGURE 38. TOPOGRAPHY OF LASER SITE NO. 1

above the runway, the LDV was returned to Toronto for an additional series of measurements. The system was set up near line 2 of the GWVSS.

The LDV system became operational on 15 July 1977 and began recording vortex data on 16 July. Data collection continued through 4 August, when the runway was closed for maintenance. Subsequently, an air controllers' strike closed the airport through 10 August. When the LDV system was powered up on 11 August, the laser failed due to a faulty ZeSe output coupler. Repair could not be rapidly effected and the LDV system was prepared for shipment on 16 August. Prior commitments precluded the system remaining in Toronto for additional data collection.

Between 16 July and 4 August, 353 takeoffs were monitored by the LDV. The operators of the LDV were instructed to record data only when the cross-wind component was less than 6 knots (conditions when vortex stalling might occur). Vortex data were obtained for the following aircraft: 48 DC-8s, 150 DC-9s, 10 DC-10s, 9 B-707s, 78 B-727s, 14 B-737s, 5 B-747s, 24 L-1011s, 4 BAC-111s, 1 CV-880, 2 DC-3s, 1 CV-580, 6 unidentified twin-engine propeller aircraft, and 1 Learjet.

A novel scan mode was used which takes advantage of the relative speeds of range and angle scanning in the LDV. The range is kept fixed during each elevation angle scan, which lasts one second. At the end of each elevation scan, the range is stepped quickly to a new value. Eight ranges were used to cover the region of interest, approximately 200 feet (60 m) to both sides of the runway centerline. The two inner ranges and the two outer ranges approximately coincided with the locations of the two innermost line 2 GWVSS anemometers on both sides of the runway. Each step in range covered approximately 55 feet (17 m). The elevation scan limits were typically 3 and 50 degrees.

5. DATA PROCESSING

Some of the data processing was performed by the NOVA minicomputer at the test site. GWVSS and MET anemometer voltages were converted to wind speeds, temperature-sensor voltages were converted to temperatures and lapse rates were calculated, and start-of-run (SOR) marks and aircraft velocities were obtained from aircraft-detector voltages. The resultant digital tapes and the MAVSS analog tapes were sent to TSC where the major portion of the data processing was performed.

5.1 MONOSTATIC ACOUSTIC VORTEX-SENSING SYSTEM

The data obtained from the monostatic acoustic sensors received some signal processing (filtering, time-variable gain, etc.) before being recorded on tape. The analog tapes are then shipped to TSC for the final data processing and analysis.

The major steps in the processing are outlined in the block diagram of Figure 39. The output of the analog tape is sent to a real-time spectrum analyzer which resolves the signal into 28 frequency components, 14 on either side of the transmitted frequency. Since the transmitted frequencies of two adjacent sensors were separated by 600 Hz and the maximum expected Doppler shift was 300 Hz, it is possible to use one spectrum analyzer to process the signals from two adjacent sensors. One complete spectrum is obtained for each range gate. The signal is then passed through an analog squaring module which produces the spectral power density. The analog output of the squaring module is converted to a 9-bit digital signal and input to a Varian 620/L minicomputer, where the digital processing is performed. A block diagram of the hardware involved is given in Figure 40.

Two separate passes through the minicomputer are required. On the first pass, velocity components are calculated and stored on a digital data tape. On the second pass, the vortex parameters are calculated and output to a digital tape. The initial step in

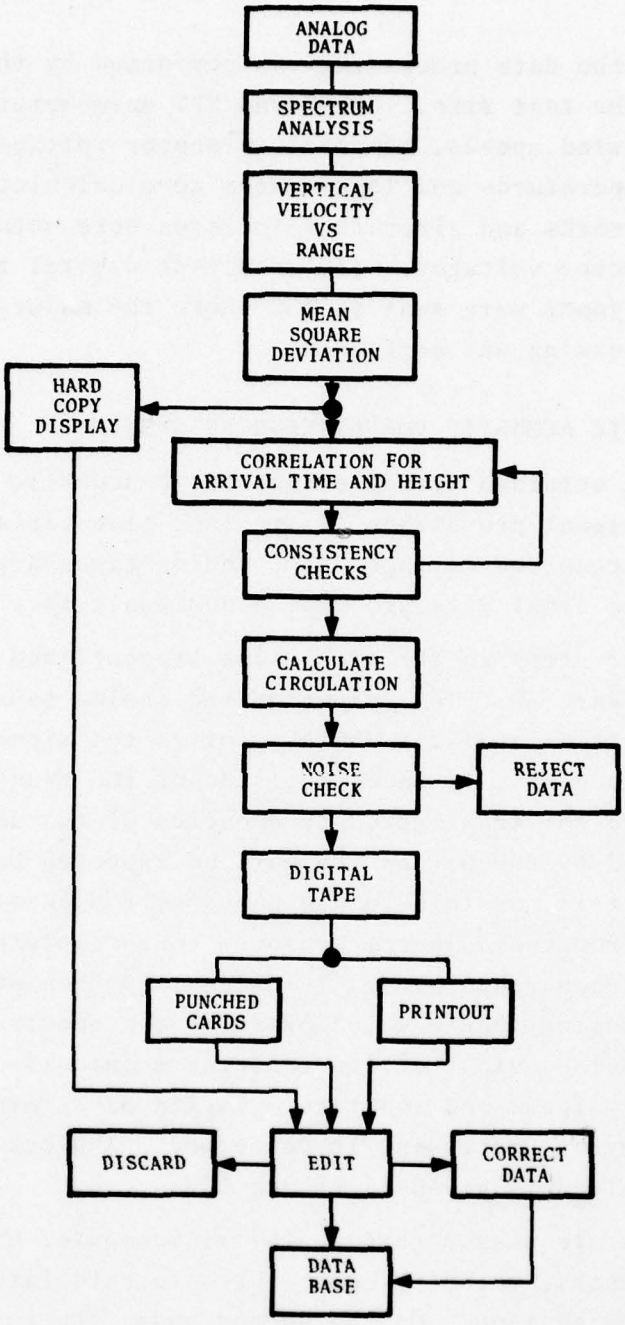


FIGURE 39. MONOSTATIC ACOUSTIC SYSTEM DATA FLOW

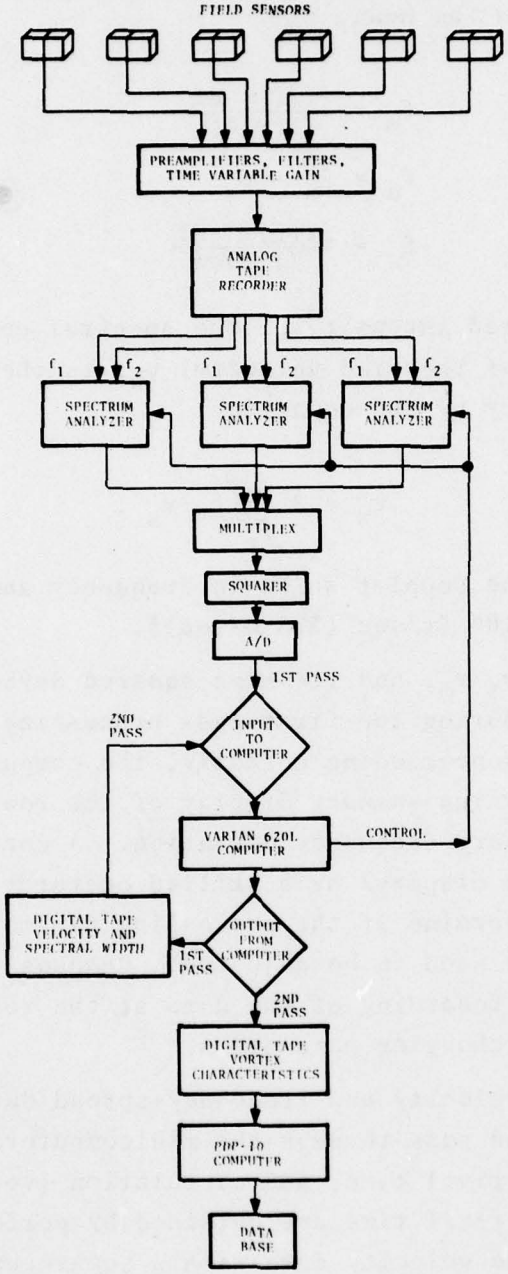


FIGURE 40. MONOSTATIC ACOUSTIC SYSTEM HARDWARE

the first-pass assembly-language computer program is the calculation of the mean frequency, f_m, and the mean-square-deviation of the spectrum from the mean, f_d:

$$f_m = \frac{\int I(f) f \, df}{\int I(f) df}$$

and

$$f_d = f_m^2 - f_s$$

where

$$f_s = \frac{\int I(f) f^2 \, df}{\int I(f) df} \quad .$$

I(f) is the squared intensity of the spectral component. The vertical component of the wind velocity, v_w, is then calculated from the mean frequency by the equation:

$$v_w = 2 \frac{f_m - f_t}{f_t} \; v_s \; ,$$

where $f_m - f_t$ is the Doppler shift in frequency and v_s is the velocity of sound [1100 ft/sec (335 m/sec)].

The velocity, v_w, and its mean-squared deviation are stored on digital tape during the first-pass processing. As a check that the processing is proceeding normally, the computer generates a CRT and hard-copy run-summary display of the raw spectrum, velocity, or mean-square frequency deviation. A certain amount of analysis of these displays by a skilled operator is required at this point to determine if the processing parameters (gains, mixing levels, etc.) need to be adjusted. Changes in weather conditions during the recording of the data at the test site are the major reason for changing parameters.

The stored velocity and frequency-spread data are then processed in a second pass through the minicomputer to calculate the vortex height, arrival time, and circulation (vortex strength). The height and arrival time are obtained by performing a running correlation of the velocity data with a square-wave function that is a first approximation to the expected vortex signature. The height (range gate) and arrival time are defined to be the points

where the most positive and most negative correlations are obtained. Several consistency checks are performed at this time: (1) it is required that the first vortex (defined as the vortex that enters the sensed volume with an upward velocity component) appear before the second; (2) to reduce the identification of a large unidirectional velocity-noise component as a vortex, it is required that each side of the vortex contribute at least 20 percent of the correlation; and (3) the correlation must be above an empirically determined, operator-defined threshold. Starting and stopping times for the correlation process are provided by dividing the expected maximum and minimum vortex transport velocities, respectively, by the distance of the sensor from the runway centerline.

An indication of the vortex strength is obtained by calculating the average circulation:

$$\Gamma' = \frac{\pi \int_{-R}^{R} r \, v_w \, dr}{R} .$$

The radial distance from the center of the vortex, r in the integral, is obtained by assuming the transport velocity (V_T) of the vortex is constant and therefore relates to the elapsed time:

$$r = V_T \, t .$$

The transport velocities are calculated using the start-of-run aircraft-detector signal and the calculated vortex arrival times at the respective sensors. In general, the higher the number of sensors which detect the vortex, the more reliable the calculation of the transport velocity and hence the circulation. The average circulation is calculated for four values of R: 5, 10, 20 and 30 meters (17, 33, 66, 99 feet).

A comparison of the display hard copy and the data summary print-out results in either rejection of bad data, adjustments to correctable data, or no action. The final step is the inclusion of the data into a data base.

5.2 METEOROLOGICAL AND GROUND-WIND VORTEX-SENSING SYSTEM

Each MET and GWVSS data sample (GWVSS anemometer voltage, time code, aircraft ID code, etc.) is converted to a 16-bit word and scaled to engineering units. The NOVA assembles these words into arrays called "frames" according to the format given in Tables 5 and 6. The frames are then grouped into "records" which consist of an integral number of frames and a maximum of 2048 words. Near the end of a record, if the next frame to be recorded would result in the record exceeding 2048 words, the current record is filled with zeros and this frame of data is inserted in the next record. This insures tape synchronization and error recovery capability in the data reduction process. The data were then recorded on 9-track digital tape with a limit of 4500 records to assure control of the amount of tape used on each 2400-foot (730-m) reel.

The data from the MET subsystem and the GWVSS are collected at a rate of 5 frames/second. The MET data are recorded continuously when the system is on. Recording of GWVSS data begins with the first trigger from any of the three aircraft detectors and terminates by a computer-controlled time-out. A clock, initiated with the first trigger, is reinitiated with any subsequent trigger (at least 20 seconds later) from another aircraft detector and terminates the recording of data after an elapsed time of 240 seconds. Experience from previous test sites has shown this to be an upper time limit for the detection of vortices.

Each new data tape is prefaced with a fixed format ASCII record identifying the site (YYZ), the tape number, the date the tape was started, and the name of the site operator. This record may be followed by optional ASCII message records (up to 80 characters) through which pertinent information is passed on to the data reduction and analysis system (e.g., sensor failures). When data collection was stopped, an End-of-File (EOF) mark was placed on tape. An optional ASCII message could then be written on tape preceding the restart of data collection. The format of the data tape is shown in Figure 41.

TABLE 5. GWVSS NINE-TRACK DATA-FRAME FORMAT

WORD NO. (OCTAL)	16-BIT WORD	COMMENTS
0	FRAME ID	NO. 5
1	ARRAY NO.	1,2,3
2	-1600ft (484m)	0.1 knot/1sb
3	-1500ft (455m)	
4	-1400ft (424m)	
5	-1300ft (393m)	
6	-1200ft (363m)	
7	-1100ft (333m)	
10	-1000ft (303m)	
11	-900ft (272m)	
12	-800ft (242m)	
13	-700ft (212m)	
14	-600ft (182m)	
15	-500ft (152m)	
16	-450ft (136m)	
17	-400ft (121m)	
20	-350ft (106m)	
21	-300ft (91m)	
22	-250ft (76m)	
23	-200ft (61m)	
24	-150ft (45m)	
25	+150ft (45m)	
26	+200ft (61m)	
27	+250ft (76m)	
30	+300ft (91m)	
31	+350ft (106m)	
32	+400ft (121m)	
33	+450ft (136m)	
34	+500ft (152m)	
35	+600ft (182m)	
36	+700ft (212m)*	*not included in
37	+800ft (242m)*	array No. 3
40	days	3 4-bit BCD characters
41	hours/mins.	4 4-bit BCD characters
42	sec./0.1sec.	4 4-bit BCD characters
43	A/C det/A/C ID	2 8-bit bytes 0=nominal -1=new a/c
44	velocity	1 knot/1sb
45	camera frame no	250-0
46	error code	0=no error; ≠ 0=error number

TABLE 6. METEOROLOGICAL NINE-TRACK DATA-FRAME FORMAT

WORD NO. (Octal)	16-BIT WORD	COMMENTS
0	FRAME ID	NO. 6
1	MET #1	
2	U 100ft (30m)	0.1 knot/1sb
3	V 100ft (30m)	
4	W 100ft (30m)	
5	U 20ft (6m) P	
6	V 20ft (6m) P	
7	W 20ft (6m) P	
10	U 20ft (6m) S	
11	V 20ft (6m) S	
12	W 20ft (6m) S	
13	spare	
14	lapse rate	0.01°C/100ft (30m)/1sb
15	temp.	0.1°C/1sb
16	days	3 4-bit BCD characters
17	hours/mins.	4 4-bit BCD characters
20	sec./0.01sec.	4 4-bit BCD characters
21	error	0=no error; -1 = error

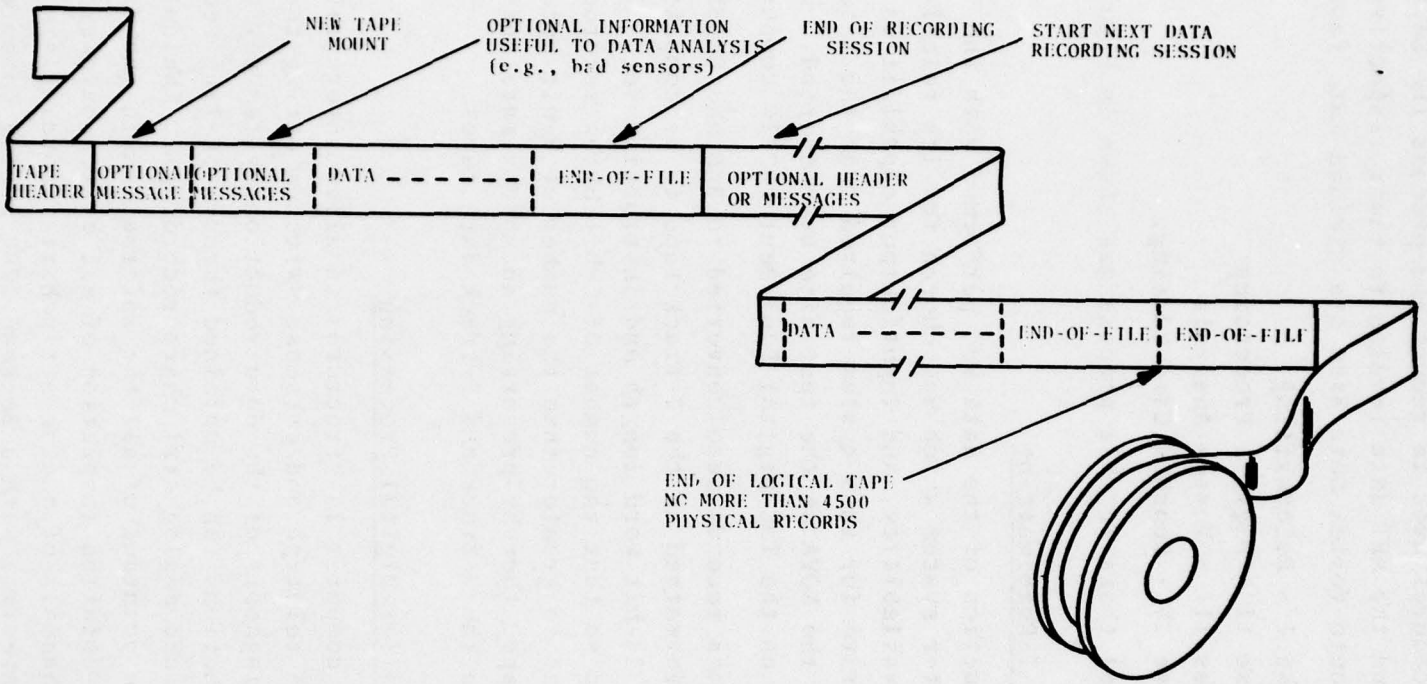


FIGURE 41. DIGITAL TAPE FORMAT

The procedures used to reduce and process the GWVSS anemometer data and the MET data leading to their respective entries into the Toronto Vortex Data Base are divided into four phases:

a. Phase I - Reformatting
b. Phase II - Digital Processing
c. Phass III - Vortex Analysis
d. Phase IV - Punched Card Editing.

The individual tasks in this process are shown in Figure 42.

5.2.1 Phase I-Reformatting

The reduction of the data was performed with the TSC XDS-9300 hybrid computer system which was chosen for its relatively low cost, high availability, and input/output capabilities. The 7-track tape drive for this system required that the 9-track tapes generated by the NOVA at the test site be converted. This was accomplished on the TSC Digital Equipment PDP-10 computer system.

ASCII data records were converted to BCD and GWVSS and MET data were reformatted on the 7-track tape to be compatible with the XDS-9300 24-bit word length and instruction set. The data were repacked so that the number of 6-bit bytes recorded on 7-track tape was no greater than the number of 8-bit bytes recorded on 9-track tape, thereby preserving an approximate one-to-one match between the 9-track and 7-track data tapes.

5.2.2 Phase II - Digital Processing

The XDS computer is structured to allow interactive operator inputs from a teletype and/or sense switches during the processing of tapes. Diagnosis of the data reduction system performance and system malfunctions can be obtained through on-line requests of data "dumps" and analog stripchart recordings. The data dump consists of a printout of all the information in the data stream and allows a detailed inspection of all system parameters. Sixteen selectable channels of analog stripchart recording are available through an interface with a Beckman 2200 analog computer. The

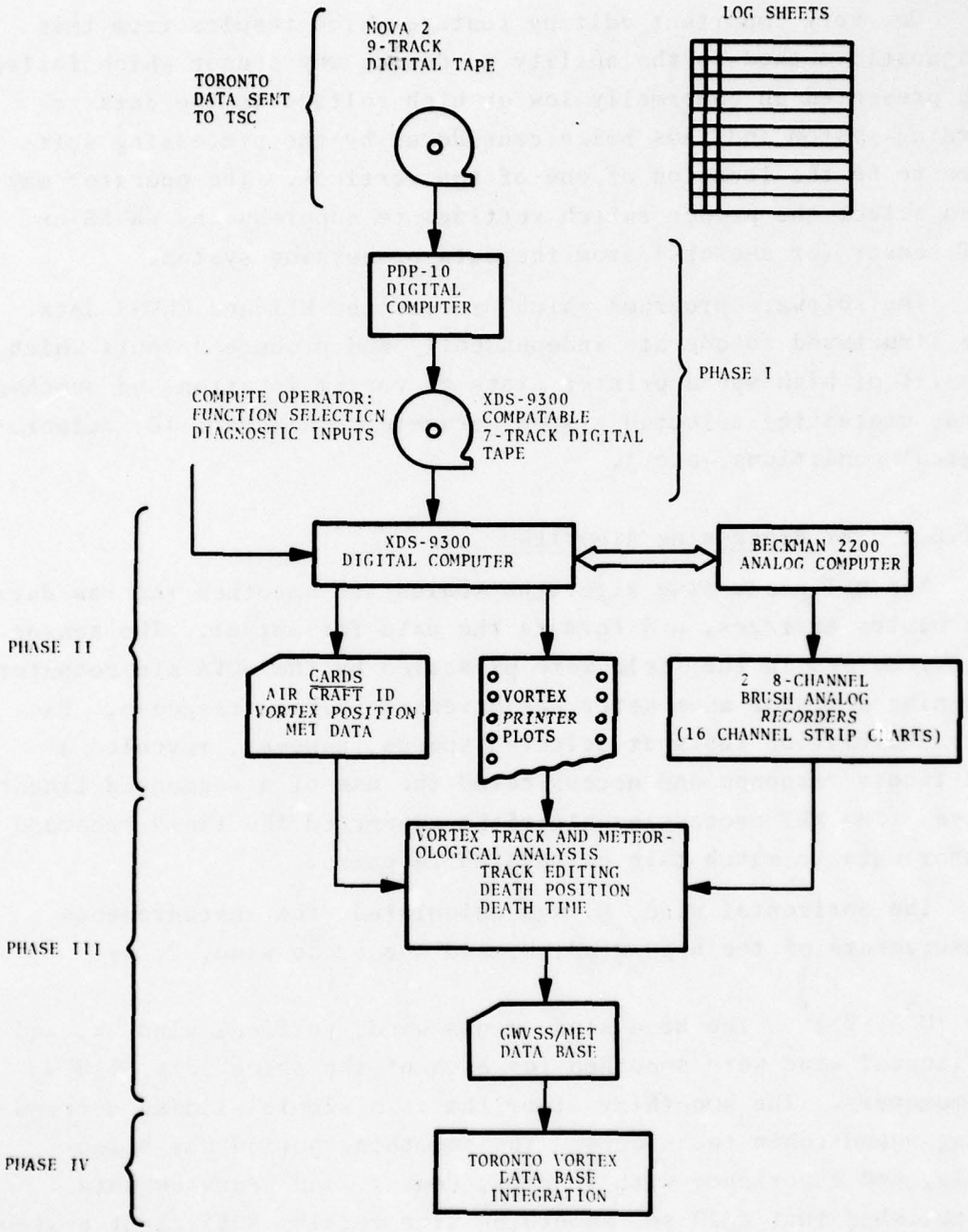


FIGURE 42. DIGITAL-TAPE PROCESSING SEQUENCE

AD-A068 925 TRANSPORTATION SYSTEMS CENTER CAMBRIDGE MASS F/G 1/2
AIRCRAFT WAKE VORTEX TAKEOFF TESTS AT TORONTO INTERNATIONAL AIR--ETC(U)
FEB 79 T SULLIVAN, J HALLOCK, B WINSTON

UNCLASSIFIED TSC-FAA-79-9 FAA-RD-78-143 NL

2 OF 3
AD
A068925



channels to be strip recorded from either the GWVSS or MET subsystems are operator selectable.

One very important editing feature which results from this diagnostic method is the ability to detect any sensor which failed and presented an abnormally low or high voltage to the data recording system and thus being considered by the processing software to be the location of one of the vortices. The operator may then select the proper switch settings to suppress any GWVSS or MET sensor (or sensors) from the data processing system.

The software programs which process the MET and GWVSS data are structured to operate independently and produce outputs which consist of high-speed printer plots of vortex location and punched cards containing selected system parameters (aircraft ID, meteorological conditions, etc.).

5.2.2.1 MET Processing Algorithm

The MET processing algorithm scales and smoothes the raw data, calculates averages, and formats the data for output. The sensor data recorded in the field were prescaled by the NOVA minicomputer assuming a linear anemometer speed versus voltage response. Factory calibration tests at selected speeds, however, revealed a non-linear response and necessitated the use of a segmented linear curve. The MET processing algorithm converted the field-recorded sensor data to match this calibrated response.

The horizontal wind, H, was calculated from instantaneous measurements of the head wind, U, and the cross wind, V, as $H = (U^2 + V^2)^{\frac{1}{2}}$. The head wind, cross wind, vertical wind, W, and horizontal wind were smoothed for each of the three sets of UVW anemometers. The smoothing algorithm is a simple sliding average using round-robin techniques. The smoothing period was selectable, and experience with Kennedy, Denver, and Heathrow data established that a 20-sec smoothing time retains sufficient system dynamic response to track the average winds. If either U or V were suppressed due to a failed sensor, the H calculation was automatically suppressed.

Since the MET processing is continuous, it is difficult to tabulate and save all the MET data associated with the presence, motion, and life of a vortex. As a consequence, a single representative set of MET parameters is generated and used to characterize the MET conditions for the analyses. A mean and standard deviation are calculated for the smoothed MET data collected during the first 60 seconds of each run (or until the end of the run if less than 60 seconds). In the event of data dropouts, the 60 seconds of data must be collected within the first 90 seconds of the aircraft run or a flag will be generated informing the operator that the data are too noisy to be considered valid. The operator, once having diagnosed the problem, could suppress further MET processing, and continue to generate vortex tracks. During the processing of each aircraft run, the results of the smoothing and the turbulence calculation are tabulated at 5-second intervals at the end of each run. These tabulations aid in understanding anomalies in the MET data, such as gusts moving through the anemometer system.

5.2.2.2 GWVSS Processing Algorithm

The GWVSS processing algorithm is divided into two parts. The run-mark and header processing algorithm controls the start and termination of each vortex-track printout, initiates the master clock, and formats the run-header data for printout. The first aircraft detector to trigger initiates a clock for its respective baseline and the master clock from which all other timing is referenced. Each subsequent aircraft-detector trigger initiates a clock for its respective baseline as is indicated by the line of delta (Δ) symbols on the sample vortex track of Figure 43. If an aircraft detector does not trigger, the clock for that particular line and the delta symbols are omitted from the printout as shown in Figure 44. Only the first trigger of each detector is accepted during the first 20 seconds of each run to suppress multiple triggers. The header information which is formatted for printing includes the time code at which the first aircraft detector triggers, aircraft type, temperature, lapse rate, aircraft speeds, cammera-frame counter, and separation time between aircraft.

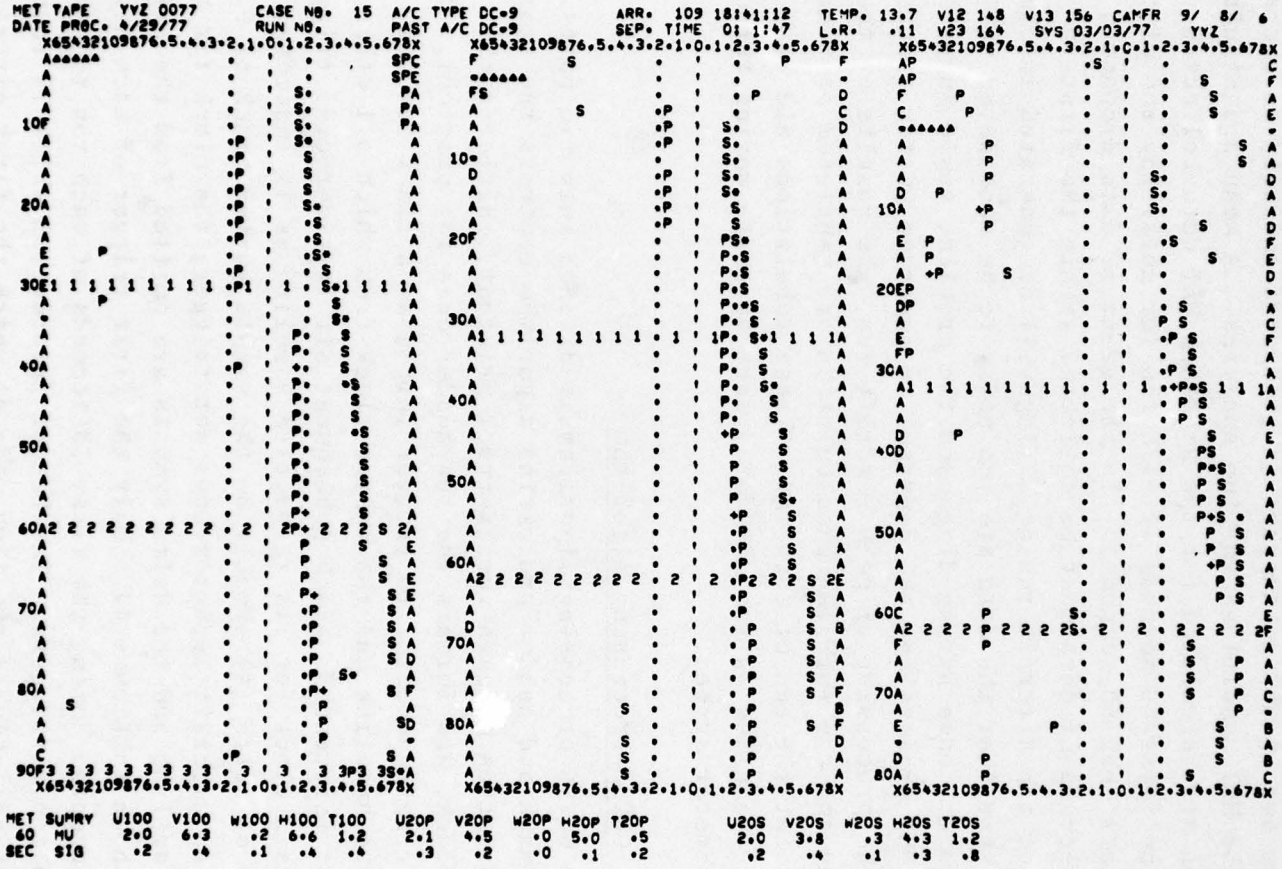


FIGURE 43. SINGLE-RUN COMPUTER OUTPUT

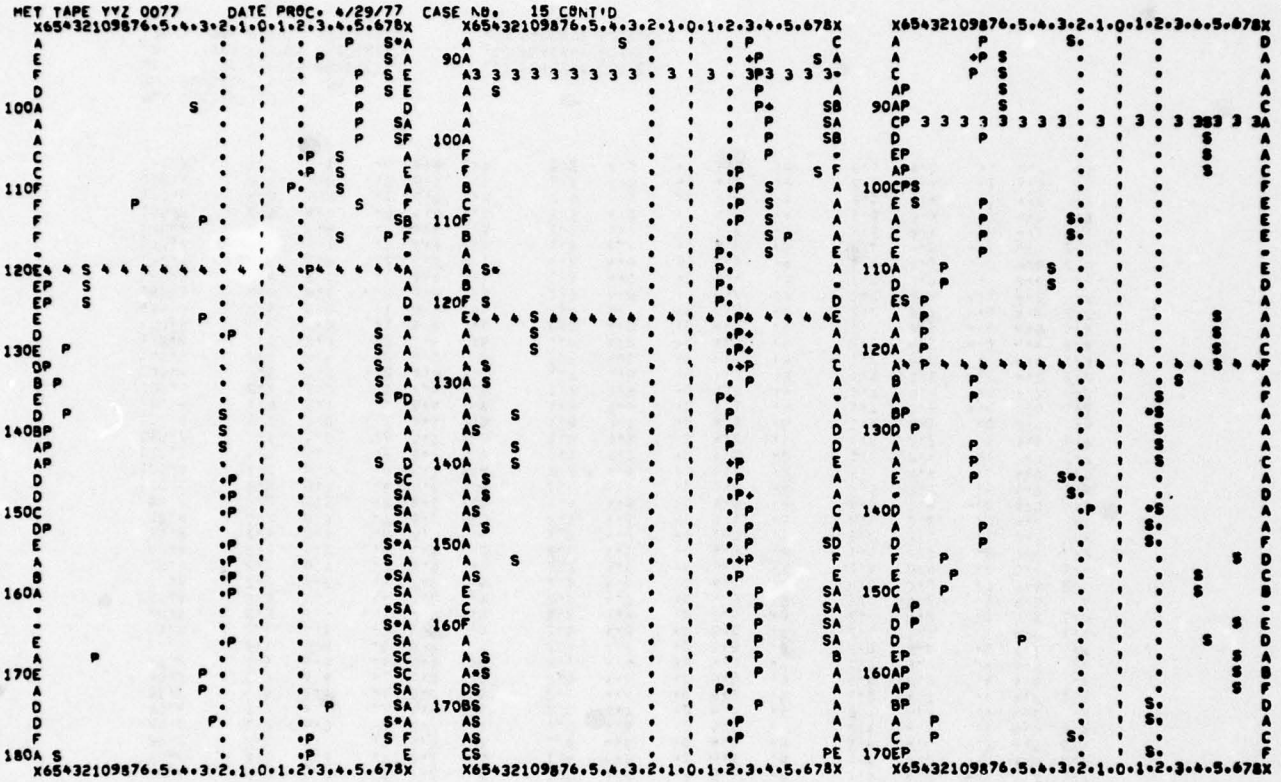


FIGURE 43. SINGLE-RUN COMPUTER OUTPUT (CONTINUED)

TIME	U100	V100	W100	H100	T100	U20P	V20P	W20P	H20P	T20P	U20S	V20S	W20S	H20S	T20S
.2	1.8	6.0	.4	6.2	.4	1.7	4.9	.0	5.1	.3	1.7	4.2	.1	4.5	.2
5.4	1.9	6.0	.3	6.2	.6	1.6	5.0	.0	5.2	.4	1.5	4.5	-.0	4.7	.8
10.6	2.0	5.9	.3	6.2	1.5	1.5	4.9	.0	5.1	.3	1.4	4.5	-.1	4.7	1.7
15.6	2.0	5.8	.3	6.1	1.3	1.4	4.6	.0	4.8	.6	1.6	4.2	.0	4.5	3.7
20.6	2.0	5.7	.3	6.0	.8	1.8	4.6	.0	4.9	.3	1.9	4.0	.2	4.5	1.4
25.6	1.8	6.0	.2	6.2	1.7	2.0	4.6	.0	5.0	.7	2.1	4.0	.4	4.5	2.5
30.6	1.7	6.2	.1	6.4	1.1	2.0	4.7	.0	5.1	.4	2.1	4.0	.4	4.5	.2
35.8	1.8	6.4	.1	6.6	1.8	2.1	4.8	.0	5.2	.5	2.0	4.3	.4	4.7	1.2
40.8	1.8	6.6	.1	6.8	1.2	2.0	4.6	.0	5.0	.3	1.9	4.2	.4	4.6	.6
45.8	1.9	6.5	.1	6.8	1.6	2.1	4.4	.0	4.9	.7	1.9	3.9	.4	4.3	.6
50.8	2.1	6.6	.2	6.9	.5	2.4	4.2	.0	4.8	.3	2.0	3.6	.5	4.1	.8
55.8	2.2	6.6	.3	6.9	.9	2.5	4.3	.0	5.0	.8	2.1	3.4	.4	4.0	1.1
60.8	2.3	6.6	.4	7.0	1.0	2.5	4.4	.0	5.0	.8	2.2	3.3	.3	3.9	1.0
65.8	2.3	6.7	.4	7.0	.7	2.5	4.2	.0	4.9	.5	2.0	3.2	.3	3.8	.6
70.8	2.2	6.7	.4	7.0	.5	2.4	4.1	.0	4.7	.2	2.0	3.0	.3	3.6	2.1
75.8	2.3	6.5	.3	6.9	1.1	2.2	4.0	.0	4.6	.3	1.8	2.9	.2	3.4	1.4
80.8	2.3	6.1	.4	6.5	2.2	2.1	4.1	.0	4.5	.2	1.8	2.9	.2	3.4	1.3
85.8	2.4	5.8	.6	6.3	1.4	2.2	4.4	.0	4.9	.7	2.2	3.0	.1	3.7	.4
90.8	2.3	5.7	.7	6.1	1.0	2.3	4.6	.0	5.1	.5	2.5	3.2	.0	4.0	.0
95.8	2.2	5.7	.7	6.0	1.2	2.4	4.8	.0	5.3	.4	2.6	3.5	-.0	4.3	.0
100.8	2.0	5.7	.4	6.0	1.5	2.4	4.8	.0	5.3	.4	2.3	3.6	.0	4.3	1.8
105.8	2.0	5.5	.3	5.8	2.6	2.2	4.4	.0	4.9	.2	2.1	3.4	.1	4.0	2.0
110.8	1.9	5.4	.2	5.7	3.3	2.1	4.0	.0	4.5	.2	1.9	3.4	.1	3.9	1.7
115.8	1.7	5.5	.2	5.7	1.3	1.9	3.8	.0	4.2	1.1	1.8	3.2	.1	3.6	1.9
120.8	1.9	5.9	.2	6.1	2.3	1.8	3.7	.0	4.1	.6	1.8	3.1	.0	3.6	.4
125.8	2.0	6.1	.1	6.4	.8	1.8	3.6	.0	4.1	.4	1.7	3.2	-.0	3.6	1.2
130.8	2.2	6.0	.1	6.4	1.8	1.7	3.9	.0	4.2	.4	1.7	3.3	.0	3.7	.3
135.8	2.5	5.8	.2	6.3	1.0	1.7	3.9	.0	4.2	.3	1.8	3.6	.0	4.0	1.0
140.8	2.5	5.4	.2	6.0	.9	1.7	4.1	.0	4.4	.5	1.8	4.0	.0	4.4	1.3
145.8	2.5	5.3	.2	5.9	.6	1.8	4.2	.0	4.5	.5	2.0	4.1	-.2	4.6	2.3
150.8	2.7	5.6	.1	6.2	.6	2.0	4.0	.0	4.5	.6	2.3	3.9	-.2	4.5	1.8
155.8	2.6	5.9	.1	6.4	1.0	2.0	4.1	.0	4.5	.3	2.2	3.7	-.1	4.4	2.2
160.8	2.6	6.1	-.0	6.6	.6	1.9	4.0	.0	4.4	.4	2.2	3.6	-.1	4.2	.7
165.8	2.6	6.1	.0	6.6	1.1	1.8	4.0	.0	4.4	.5	2.0	3.7	.1	4.2	.0
170.8	2.7	5.8	.2	6.3	2.1	1.7	4.3	.0	4.6	.4	1.9	4.1	.0	4.5	1.0
175.8	2.8	5.7	.3	6.3	1.8	1.8	4.3	.0	4.6	.5	2.1	4.2	-.1	4.7	2.5
180.8	2.7	5.8	.3	6.4	1.8	2.0	4.1	.0	4.6	.3	2.2	3.8	-.0	4.4	1.1
185.8	2.8	6.0	.3	6.6	1.6	2.3	4.0	.0	4.6	.4	2.5	3.4	.0	4.2	1.9
190.8	2.6	6.2	.1	6.7	.6	2.3	4.1	.0	4.7	.8	2.5	3.4	.1	4.2	.2
195.8	2.5	6.2	.2	6.7	.9	2.2	4.3	.0	4.8	.6	2.3	3.6	.1	4.3	.3
200.8	2.5	6.1	.1	6.6	1.7	2.2	4.5	.0	5.0	.5	2.4	4.0	.1	4.7	.3

RUN STATISTICS
RUN PULSE AT REC. 954
L1: 1006 FRAMES PROCESSED .00 PERCENT EDITED
L2: 987 FRAMES PROCESSED .00 PERCENT EDITED
L3: 960 FRAMES PROCESSED .00 PERCENT EDITED

FIGURE 43. SINGLE-RUN COMPUTER OUTPUT (CONTINUED)

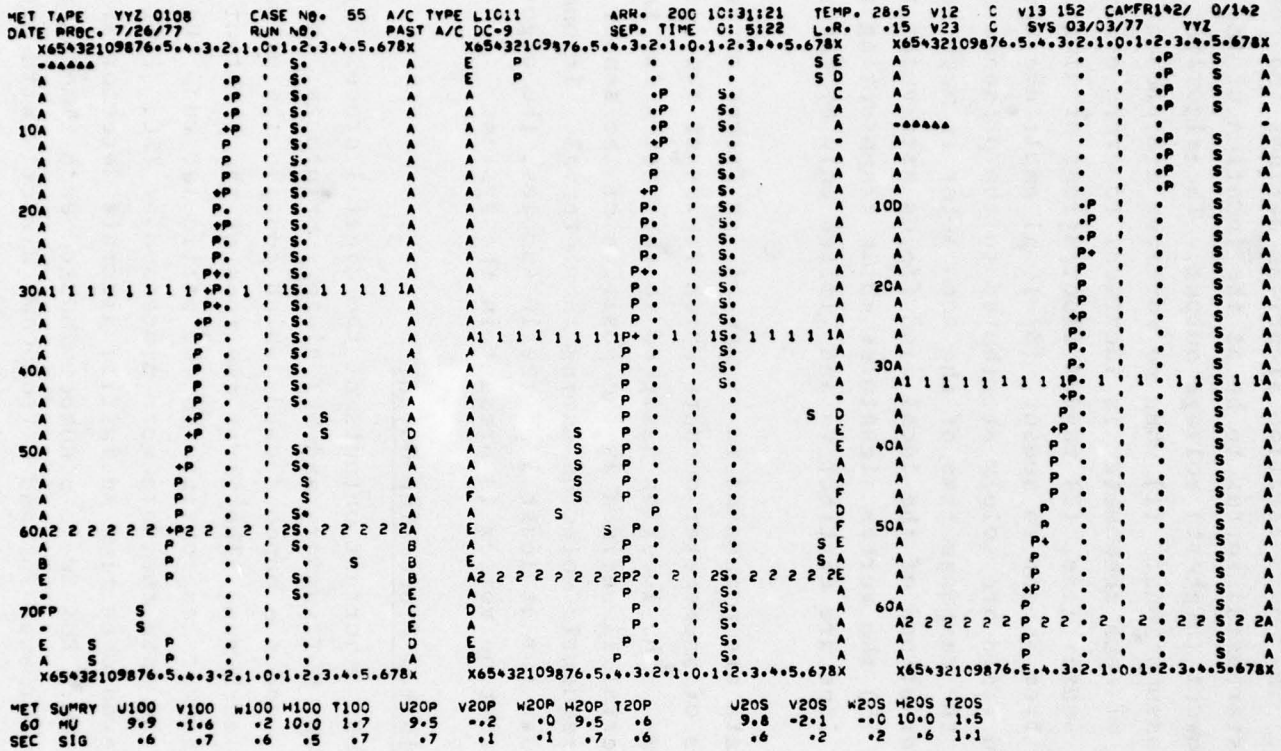


FIGURE 44. VORTEX TRACK WITH MISSING START-OF-RUN MARK

The location of a vortex is determined each time a complete set of sensor voltages is viewed from each of the anemometers in a baseline. The GWVSS location algorithm defines the position of the port (starboard) vortex to be at the location of the sensor with the lowest (highest) voltage output. The algorithm makes the following assumptions: (1) when no vortices are present, the statistics of each anemometer is identical to every other anemometer on a sensor line, (2) random fluctuations of wind are uncorrelated from sensor to sensor, (3) local amplitude deviations of the wind field are solely attributed to the presence of vortices, (4) the response time of the anemometer is much faster than the variations of the local wind fields attributed to vortices, and (5) the vortex signatures while tranpsorting through the sensor line are distinctive and limited only by the sample rate.

The data are processed in groups of ten frames or ten consecutive sets of anemometer outputs which represent two seconds of elapsed time. The location assigned to the vortex for this two-second interval is defined as the position of the sensor which was most frequently selected during the interval. If one sensor is not chosen for at least 5 of the 10 samples, the algorithm concludes that no vortex is present in the system.

5.2.2.3 Digital Processing Output

The most important outputs of the digital processing are the vortex track, MET summary and MET history printouts, (shown in Figure 43), and the punched cards which contain the primary parameters for each run. The first two rows of the printout contain header parameters appropriate to the particular run. DATA PROC indicates the date the data were processed at TSC. CASE NO is a number indexed each time an initial aircraft detector trigger has been received. RUN NO is a number indexed each time an aircraft departs from runway 23L and corresponds directly with the run number recorded on the log sheets. These numbers should be the same but false triggers from extraneous sources such as aircraft departing from other runways result in extra triggers which must

be mannually expunged. SYS indicates the latest revision date of the data reduction software.

The vortex-track printout is oriented with GWVSS line 1 to the left, line 2 in the center, and line 3 to the right. Each track is a time history of the port and starboard vortices as indicated by the vortex-location algorithm. The vortex positions are printed at two-second increments with the port vortex assigned the character "P" and the starboard vortex the character "S." Whenever the indicated vortex location is distributed across two adjacent sensors, a "+" is associated with the port vortex and a "*" is associated with the starboard vortex.

The alphabetic characters (A, B, C, etc.) running down the page on both sides of the tracks correspond to a validity-weighting assigned to the port (left column) and starboard (right column) vortex indication. The number of times a particular location is chosen during the 2-second interval is an estimate of the confidence of the decision and is coded as follows:

Code	Number of times a location is chosen during a two-second interval (10 samples)
A	10
B	9
C	8
D	7
E	6
F	5
-	< 5

When the chosen location contains less than five out of the ten samples, a "-" code is listed and no vortex location is indicated. This level of confidence is used in the data analysis when a decision must be made as to whether the observed signals truly represent the existence of a vortex or are due to fluctuations in the ambient wind.

The apostrophes in the center of each track represent the location of the runway centerline. The dots to the left and right

of the apostrophes represent a ± 200-foot (±60-m) corridor. The numbers (sometimes separated by dots) at the top and bottom of each track represent the sensor positions which are quantized at 50-foot (15-m) increments up to ± 450 feet (±137 m) and then at 100-foot (30-m) increments. A series of 1's, 2's, 3's and 4's are printed to show the 30-, 60-, 90- and 120-second elapsed-time marks, respectively, on each track and are used in the data analysis.

An a priori logic was formulated which used the master clock to set reference 30-, 60-, 90- and 120-second timing marks for baselines whose aircraft detector did not trigger. Table 7 illustrates the elapsed-time offset (in seconds) when baseline "x" contained the first aircraft trigger and baseline "y" is an untriggered baseline.

TABLE 7. ELAPSED TIME OFFSET FOR UNTRIGGERED BASELINES (SEC.)

x \ y	1	2	3
1	0	+4	+10
2	-4	0	+6
3	-10	-6	0

The summary of meteorological parameters for each run appears in the last two lines on the first page of the run printout under the heading MET SUMRY (Figure 43). The 60 SEC entry on the left indicates that data have been averaged for 60 seconds. The data are grouped into three divisions containing the U, V, W, H, and T (turbulence, discussed in Section 6.3) for each of the three MET sensors 100 feet (30 m), 20 feet (6 m) port and 20 feet (6 m) starboard. The top line labeled MU is the time-averaged data and the bottom line labelled SIG is the standard deviation of the averaged data.

The track continues until 200 seconds have elapsed on all baselines or until the aircraft detectors are triggered by the

following aircraft in a time less than 200 seconds. Following each vortex track is a printout of the averaged meteorological conditions at 5-sec increments. This list is useful to analyze and to interpret anomalous meteorological data such as gusts passing through the system or unusual vortex behavior.

The column immediately to the right of each baseline is reserved for error flags. An "S" in this column indicates an error in data transmission detected by the NOVA acquisition system such as missing sensor data (data dropouts) and power-supply voltages out of specification. When a data dropout is detected, the entire frame for that sensor line is rejected.

A printout of a summary of all the important parameters is listed at the end of each processed tape as shown in Figure 15. A column is available for the data analyst to manually insert the test site run number (which may differ from the CASE number). The CODE entry is a numerical code of the aircraft type. The SOR entry is a numerical code to indicate which aircraft detectors triggered. If a detector triggered, the number of the corresponding baseline will be printed (e.g., "23" implies that only detectors on lines two and three triggered). The REC entry indicates the data tape record number when the collection of data started. DURATION is the difference in successive record numbers.

5.2.3 Phase III Vortex Track Analysis and MET Verification

The vortex track analysis consists of two subtasks as follows:

- Identifying the time and position at which the vortex-location algorithm indicates the demise of a vortex.
- Confirming the position of the vortex as defined by the vortex-location algorithm at the 30-, 60-, 90- and 120-second reference times.

The first subtask is the most important step in the data analysis; it required analysts who had a great deal of experience with similar data from other vortex data collection sites. The analyst must use information from several sources to judge when the

RUN SUMMARY

4/29/77 YYZ 0077 YYZ

CASE	RUN	ARR. TIME	A/C TYPE	CODE	SBR	V12	V13	V23	CAMERA FRAME	SEP. TIME	REC.	DURATION
1		109 17:32:54		0	100	0	0	0	240/ 0/ 0	99:99:99	5	▲ 5
2		109 17:40:20	DC-9	6	123	144	144	148	58/ 58/ 58	0: 7:26	102	▲ 97
3		109 17:42:52	DC-10	7	123	160	148	140	57/ 56/ 54	0: 2:32	153	▲ 51
4		109 17:46:36	L1011	8	100	0	0	0	53/ 0/ 0	0: 3:44	227	▲ 74
5		109 17:54:59	L1011	8	3	0	0	0	49/ 0/ 49	0: 8:23	326	▲ 99
6		109 17:57: 9	DC-9	6	123	148	148	0	45/ 44/ 42	0: 2:10	370	▲ 44
7		109 17:58:39	DC-9	6	123	140	148	156	41/ 39/ 38	0: 1:30	400	▲ 30
8		109 18: 4: 5	DC-9	6	123	152	152	0	37/ 36/ 34	0: 3:26	494	▲ 94
9		109 18: 5:47	727	2	23	0	0	148	33/ 34/ 31	0: 1:42	528	▲ 34
10		109 18:11:24	VC-10	9	123	224	204	192	29/ 28/ 26	0: 5:37	621	▲ 93
11		109 18:13:35	727	2	23	0	0	152	25/ 26/ 23	0: 2:11	665	▲ 44
12		109 18:32: 0	747	4	123	132	132	0	21/ 19/ 18	0:18:25	792	▲ 127
13		109 18:37:54	DC-9	6	3	0	0	0	17/ 0/ 17	0: 5:54	888	▲ 96
14		109 18:39:25	DC-9	6	123	156	160	164	13/ 12/ 10	0: 1:31	918	▲ 30
15		109 18:41:12	DC-9	6	123	148	156	164	9/ 8/ 6	0: 1:47	954	▲ 36
16		109 18:45:25	DC-9	6	100	0	0	0	5/ 0/ 0	0: 4:13	1038	▲ 84
17		109 18:46:21	DC-9	6	123	152	156	0	1/ 0/ 0	0: 0:56	1057	▲ 19
18		109 18:48: 9	DC-9	6	3	0	0	0	0/ 0/ 0	0: 1:48	1093	▲ 36
19		109 18:50:23	747	4	123	144	144	140	0/ 0/ 0	0: 2:14	1137	▲ 44
		109 18:51: 2	TAPE OFF	33							1151	▲ 14
20		110 7:29:21	DC-9	6	123	140	144	148	250/250/250	99:99:99	1167	▲ 16
21		110 7:34: 6	DC-9	6	3	0	0	0	249/ 0/249	0: 4:45	1258	▲ 91
22		110 7:36:29	727	2	123	136	136	132	245/243/242	0: 2:23	1306	▲ 48
23		110 7:38: 9	DC-9	6	123	160	160	156	241/240/238	0: 1:40	1340	▲ 34
24		110 7:40:47	DC-9	6	123	152	156	0	237/236/234	0: 2:38	1392	▲ 52
25		110 7:44:13	DC-9	6	100	0	0	0	233/ 0/ 0	0: 3:26	1461	▲ 69
26		110 7:47:48	DC-9	6	123	156	160	0	229/228/226	0: 3:35	1532	▲ 71
27		110 7:49:44	727	2	123	136	136	140	225/223/222	0: 1:56	1571	▲ 39
28		110 7:52:27	727	2	123	148	148	144	221/220/218	0: 2:43	1626	▲ 55
29		110 7:59:32	727	2	100	0	0	0	217/ 0/ 0	0: 7: 5	1724	▲ 98
30		110 8: 6: 3	DC-9	6	123	152	156	0	213/212/210	0: 6:31	1818	▲ 94
31		110 8: 7:50	DC-9	6	123	148	152	156	209/208/206	0: 1:47	1854	▲ 36
32		110 8:10: 3	727	2	123	164	156	152	205/204/202	0: 2:13	1898	▲ 44
33		110 8:11:52	DC-9	6	123	156	156	0	201/200/198	0: 1:49	1934	▲ 36
34		110 8:18:40	727	2	123	128	136	140	197/195/194	0: 6:48	2032	▲ 98
35		110 8:20:37	DC-8	5	123	120	132	144	193/191/190	0: 1:57	2071	▲ 39
36		110 8:23: 3	DC-8	5	123	152	152	0	189/188/186	0: 2:26	2119	▲ 48
37		110 8:49: 6	DC-8	5	100	0	0	0	185/ 0/ 0	0:26: 3	2268	▲ 149
38		110 8:58:18	OTHER	10	100	0	0	0	181/ 0/ 0	0: 9:12	2369	▲ 101
39		110 9: 3:32	DC-8	5	123	128	144	156	177/175/174	0: 5:14	2459	▲ 90
40		110 9: 5:43	DC-8	5	123	144	144	0	173/171/170	0: 2:11	2503	▲ 44
41		110 9: 8:59	DC-9	6	3	0	0	0	169/ 0/170	0: 3:16	2568	▲ 65
42		110 9:10:35	L1011	8	123	152	156	0	165/164/162	0: 1:36	2600	▲ 32
43		110 9:14:11	DC-9	6	123	152	160	168	161/160/158	0: 3:36	2663	▲ 63
44		110 9:15:58	727	2	123	140	136	0	157/155/154	0: 1:47	2698	▲ 35
45		110 9:17:22	727	2	123	148	148	0	153/152/150	0: 1:24	2727	▲ 29
46		110 9:19: 8	727	2	123	156	156	152	149/148/146	0: 1:46	2762	▲ 35
47		110 9:21: 4	DC-9	6	123	148	148	0	145/144/142	0: 1:56	2801	▲ 39

FIGURE 45. PARAMETER SUMMARY COMPUTER PRINTOUT

location algorithm has ceased tracking the vortex. This defines the "death time" and "death position" of the vortex. The cessation of tracking could be due to several sources: (1) the vortex decays to a point where it is no longer distinguishable from the ambient wind, (2) the vortex rises to a height where it is out of the intrinsic range of the sensor, (3) the vortex stalls directly over the runway where there are no sensors, or (4) organized vortex flow has ceased and only a gust-like movement of air remains. Some of the aids which the analyst uses in making the decision are the validity-weighting factors (A, B, C, etc.) at the sides of the vortex track printouts, the meteorological parameters (head wind, cross wind, and turbulence), the aircraft type, and the aircraft height. An example of an analyst decision of a vortex death on each of the three baselines is given by the check (V) notation in Figure 46. There are many interactive factors which must be considered by the analyst when making this decision and it is often a difficult task.

The analyst must also correct obvious errors of the vortex-location algorithm at the 30-, 60-, 90-, and 120-second reference times. The location of the port vortex on line 2 at 120 seconds in Figure 47 was selected by the location algorithm to be at -450 feet (-137 m). It is obvious that the actual position should be approximately -1200 feet (-366 m) and was so indicated by the analyst.

The measured meteorological parameters were verified by the data analyst. The winds at the MET tower are compared with those reported on the log sheets and discrepancies were analyzed. Consistency among the U, V, W measurements at the two tower levels was checked. The data were reviewed with respect to long-term (hours) and short-term (seconds) variation and continuity. Finally, the MET data were reviewed with respect to the vortex tracks; a general correlation should exist between the vortex transport characteristics and the meteorological conditions. A block diagram of the vortex track analysis and MET verification process is given in Figure 48.

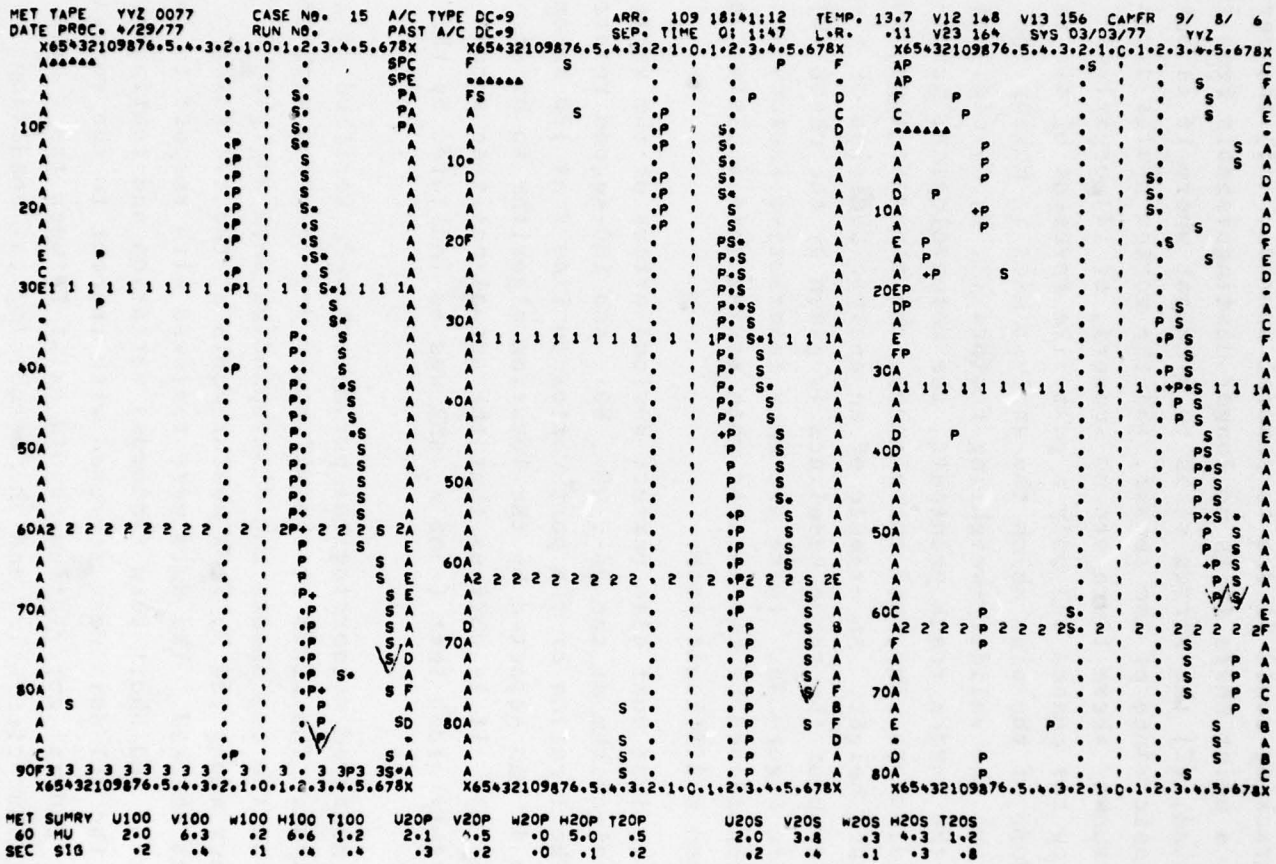


FIGURE 46. VORTEX DEATH NOTATION

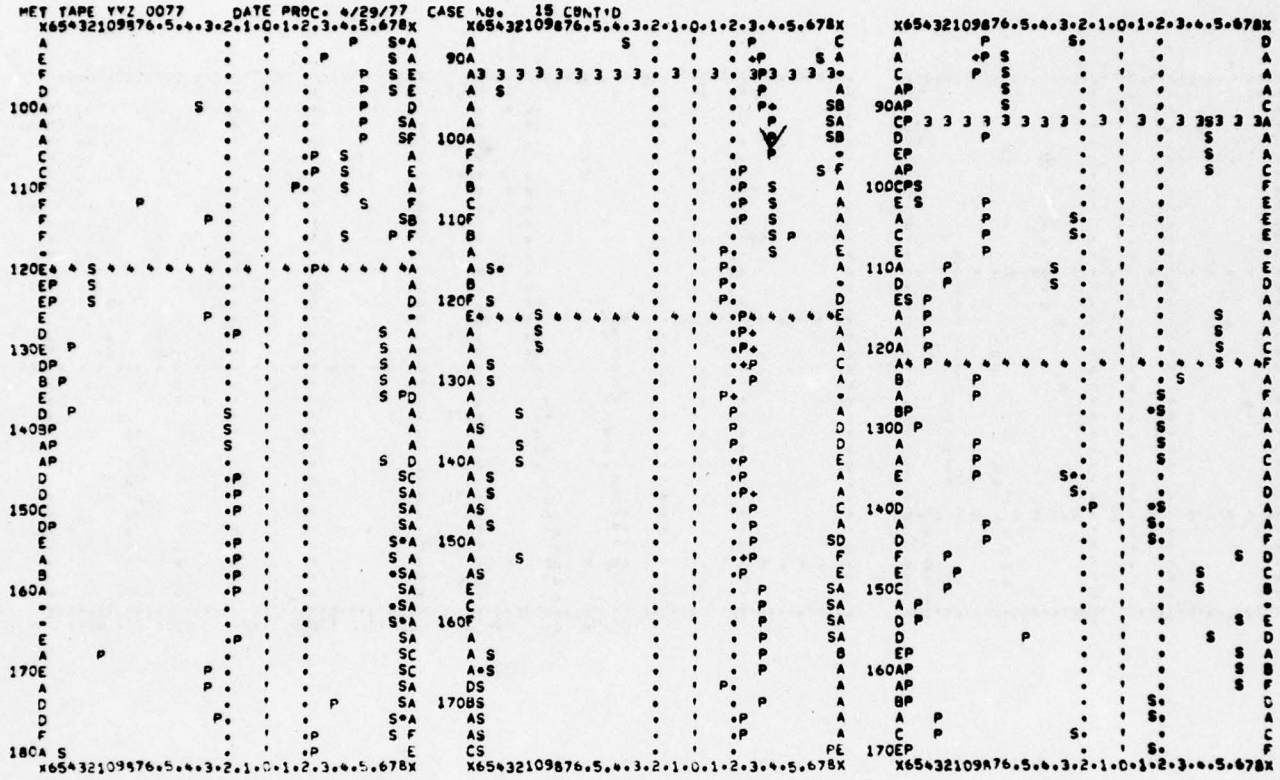


FIGURE 16. VORTEX DEATH NOTATION (CONTINUED)



FIGURE 47. CORRECTION OF VORTEX LOCATION ALGORITHM ERRORS

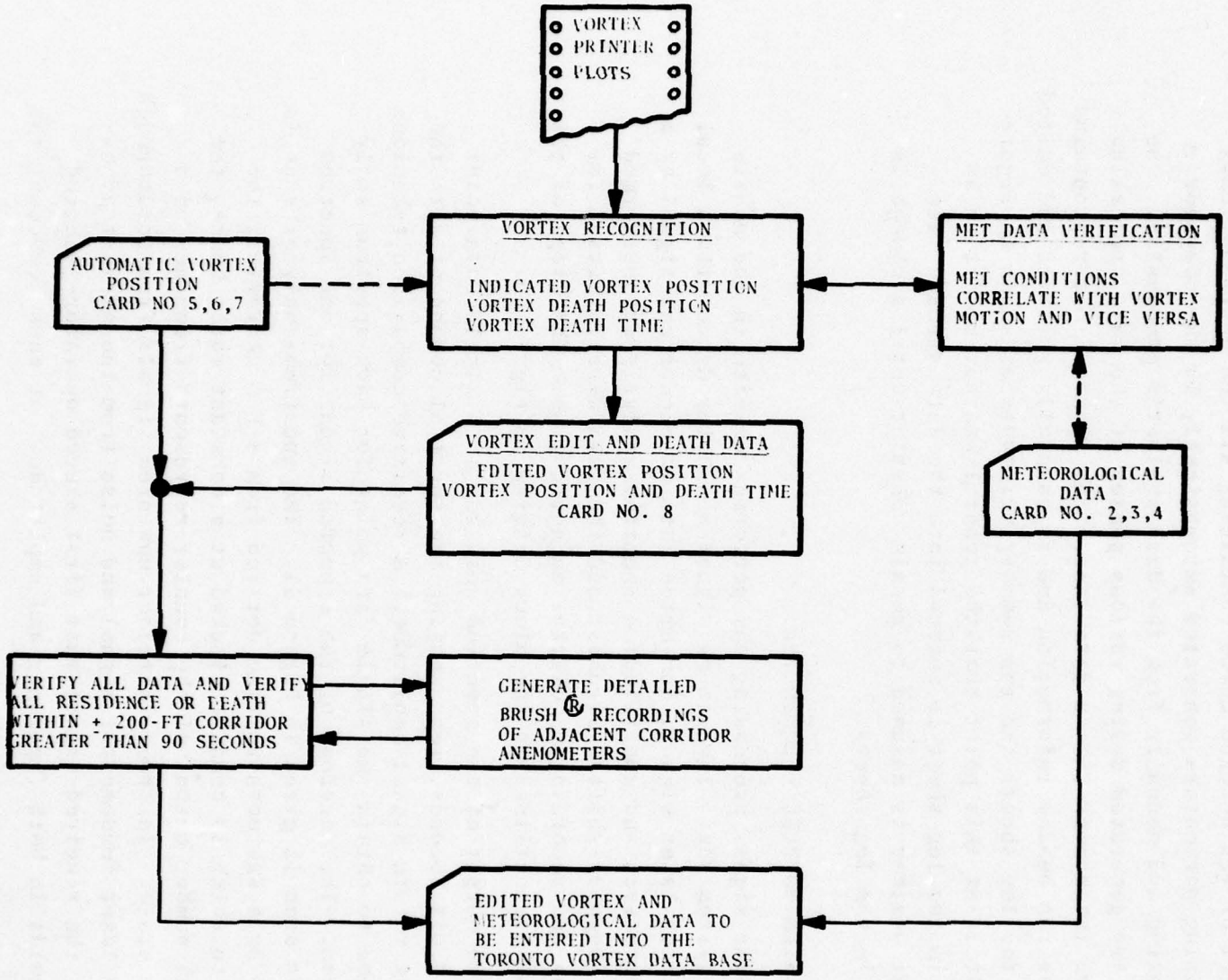


FIGURE 48. VORTEX TRACK ANALYSIS AND METEOROLOGICAL DATA VERIFICATION

5.2.4 Phase IV-Punched Card Editing

A second output from the GWVSS and MET data processing system is a set of ten punched cards containing all the pertinent data processing parameters generated automatically in the computer processing and manually from the data analyst's processing. The cards are generated during various phases of the data processing and are integrated into a data base. The "Number 1" card contains all the run header information and is carefully verified and edited using the log sheets and run summary printouts as shown in Figure 49. It is at this point that the general weather condition as noted in the log sheet is entered into the data stream. The general weather is assumed to remain constant until a change is noted in the log sheets.

5.3 LASER DOPPLER VELOCIMETER

Some signal processing was performed on-site in the mobile laser system van. The return signal was heterodyned with a local oscillator laser signal, converted into an electrical signal by a photodetector, and amplified; a spectrum analysis was performed on the Doppler-shifted signals; and the data were formatted for display and recording on digital magnetic tape. The steps of this process are outlined in the block diagram in Figure 50.

The output of the spectrum analyzer is a single data point every 0.014 seconds, representing the spectral component with the highest return signal amplitude. A recursive comparison technique was used to obtain the single data point for each spectrum analyzer scan. The envelope of the expected signal for one spectrum analyer scan is given in Figure 51. The spectrum analyzer scan is driven by a sawtooth voltage derived from a D/A converter, the input to which is counter clocked at a constant rate; hence, the digital number output of the counter represents frequency on a linear scale. In order to reject unwanted signals from feedthrough of the laser fundamental signal and noise from the ambient atmosphere, the received signal must first exceed operator-selected thresholds in both frequency and amplitude. At each new count the

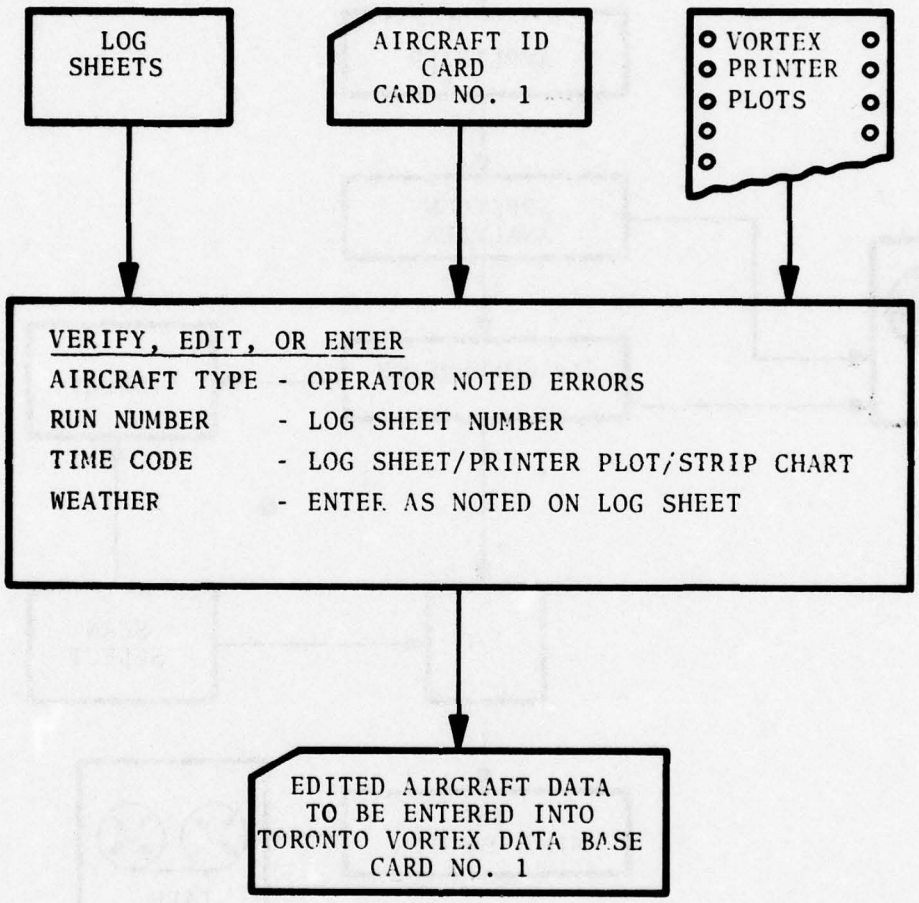


FIGURE 49. EDITING OF NUMBER ONE DATA ANALYSIS CARD

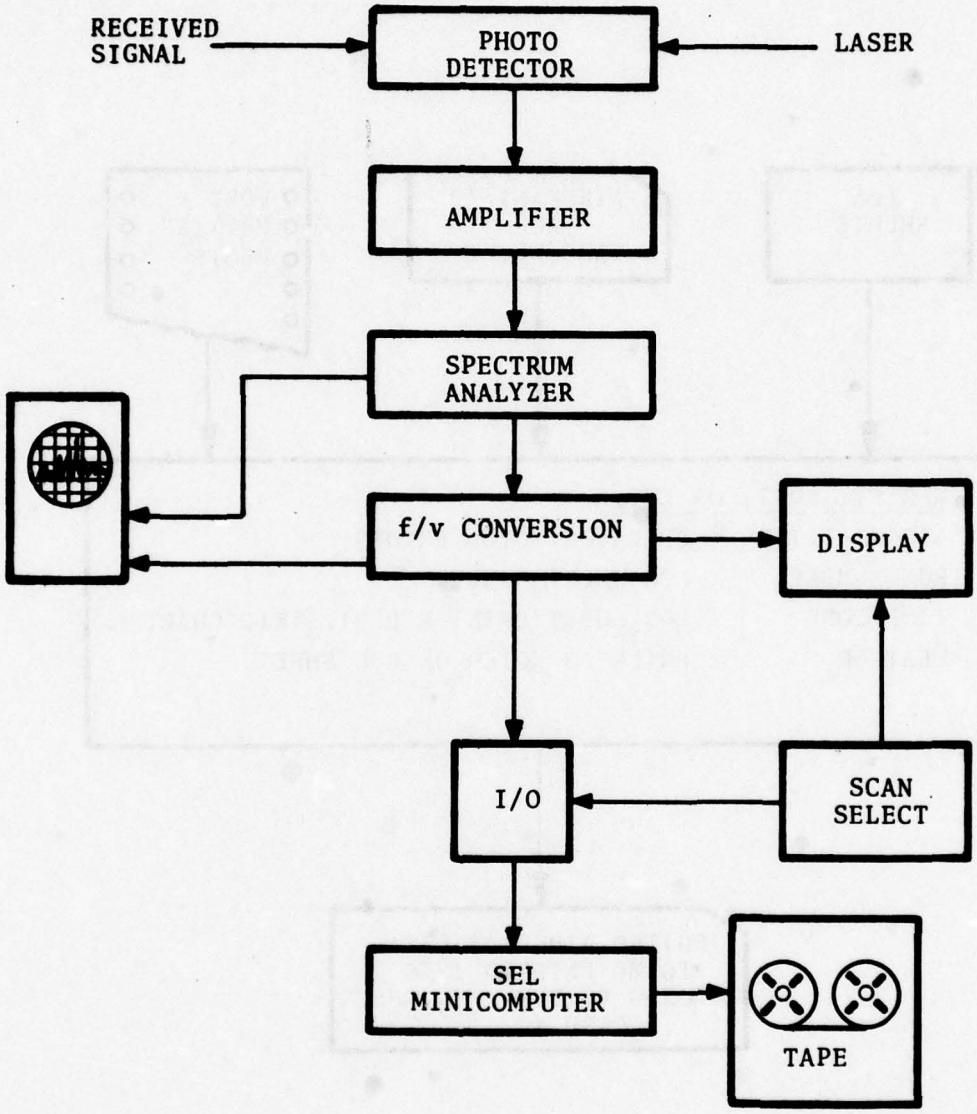
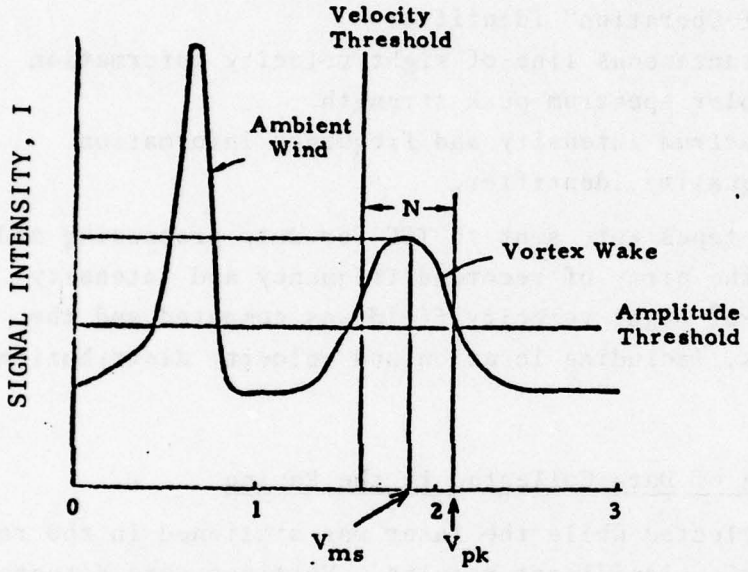


FIGURE 50. LASER DOPPLER VELOCIMETER HARDWARE

N = bandwidth

V_{pk} = velocity of highest channel above amplitude threshold

V_{ms} = velocity of the channel having the peak signal



Typical Vortex Spectrum

FIGURE 51. LASER DOPPLER VELOCIMETER VORTEX SPECTRUM

spectrum analyzer output was compared with that obtained on the previous count. If the current sample is larger, it and its corresponding frequency were stored; if it was smaller, the previous value was stored. At the end of the sweep the number stored corresponded to the highest signal power observed (i.e., the peak in the spectrum). The SEL 810A minicomputer formatted the data for recording on magnetic tape. The data logged by the computer included:

a. All scan volume location parameters
b. "Mode of Operation" identifier
c. The instantaneous line-of-sight velocity information
d. The Doppler spectrum peak strength
e. Full spectrum intensity and frequency information
f. A data quality identifier.

The digital tapes were sent to TSC for data processing and analysis. From the array of recorded frequency and intensity points, the line-of-sight velocity field was computed and the vortex parameters, including location and velocity distribution, were determined.

5.3.1 Processing of Data Collected in the Ravine

The data collected while the laser was stationed in the ravine yielded very little significant results. Vortices were detected and tracked for 11 landings (4 B727s, 1 B-737, 2 B-747s, 3 DC-8s, and 1 DC-9). Most of the undetected vortices (5) occurred at the end of the time period; the wind had increased in intensity by then and landings were switched to runways 23L/R.

The signatures for the detected vortices appeared normal but exhibited an unusually fast breakup. Even with a cross-wind component, the vortices never drifted more than about 150 feet (45 m) from the extended runway centerline. The vortices did descend below the level of the plateau, but only by about 10 or 15 feet (3 or 4 m).

Although only 11 vortex pairs were detected, the early breakup of the vortices was apparent and was attributed to the

geography. The wind flow apparently separated at the lip of the ravine; the van was in the near wake of the wall of the ravine. It is postulated that the shearing action of the near wake flow caused the breakup of the vortices, at least in the region above the laser system. What is not known is the effect of the breakup of the vortices at this location on the vortices both closer to the runway threshold and further out.

5.3.2 LDV Data Collected Between Lines 1 and 2

The data were collected in the finger-scan mode where both the range and elevation of the focal volume are continuously changing. Typical range scans were between 3 and 30 degrees at a 1.0-Hz rate. The resulting locus of the moving focal volume sweeps out a lobed pattern resembling pointing fingers. The advantage of this scan mode is that it covers a large region; the disadvantage is that the greatest concentration of the data comes from the limits of the range and elevation scans.

In general, the signatures of the vortices resembled signatures obtained elsewhere (Ref. 8) for landing aircraft. However, the highest velocity measured for the takeoff vortices was approximately 35 ft/sec (10 m/sec) whereas landing vortices often yielded velocities in excess of 50 ft/sec (15 m/sec).

5.4 PHOTOGRAPHIC SYSTEM

The processed film was sent to the Applications Research Corporation (ARC) in Philadelphia, PA, in the form of 33-ft (10-m) continuous rolls of 24 mm x 36 mm ectachrome positives (slides). The film was displayed on a surface about 7 feet (2 m) from the projector. The coordinates of the aircraft and the coordinates of fixed landmarks which coincided with the line of sight from the camera to the intersections of each of the first two sensor lines and the runway were read from a scaled screen. The aircraft coordinates (X, Y), along with aircraft status information such as tape and run numbers, date, time and aircraft type were keypunched for input into the ARC computer program ACSTAT which

calculated the height of the aircraft over each of the three sensor lines. Figure 18 shows a typical four-photo sequence of a departing aircraft.

The ACSTAT program first converted the projected coordinates of the aircraft into displacement L along the runway and height H above the runway. Using the geometry of Figure 52, H and L (in feet) are given by:

$$H = h\,\frac{1750}{f \cdot m}\,\frac{\cos\left(\frac{d \cdot m - (BF + AB)}{f \cdot m}\right)}{\cos\left[\tan^{-1}\left(\frac{1250}{1750}\right) - \tan^{-1}\left(\frac{d \cdot m - AB}{f \cdot m}\right) + \tan^{-1}\left(\frac{d \cdot m - (AB+BF)}{d \cdot m}\right)\right]},$$

$$L = 1250 - 1750 \cdot \tan\left[\tan^{-1}\left(\frac{1250}{1750}\right) - \tan^{-1}\left(\frac{d \cdot m - AB}{f \cdot m}\right) + \tan^{-1}\left(\frac{d \cdot m - (AB+BF)}{d \cdot m}\right)\right],$$

where M is the projection scale factor which relates projected measurements to displacements on the film,

$$m = \frac{\text{Length of projected frame (inches)}}{\text{36 mm (length of film frame)}},$$

h is the altitude of the aircraft in inches, AB is the measured distance (projected) from the edge of the film to the first sensor line landmark (in inches), BF is the measured longitudinal distance to the aircraft from the first sensor line landmark (in inches), d is one-half the film frame longitudinal axis (equal to 18 mm for the Olympus camera), and f is the focal length (in mm).

In general there were four sets of coordinates (X, Y) for each takeoff run corresponding to the four photographs taken. The first photograph was triggered by the passage of the aircraft over the first sensor line. The others followed in sequence 1.5 seconds apart. The four sets of coordinates were then fitted to a second-order polynomial trajectory as shown in Figure 53. The program calculated the coefficients of the polynomial using a least-squares

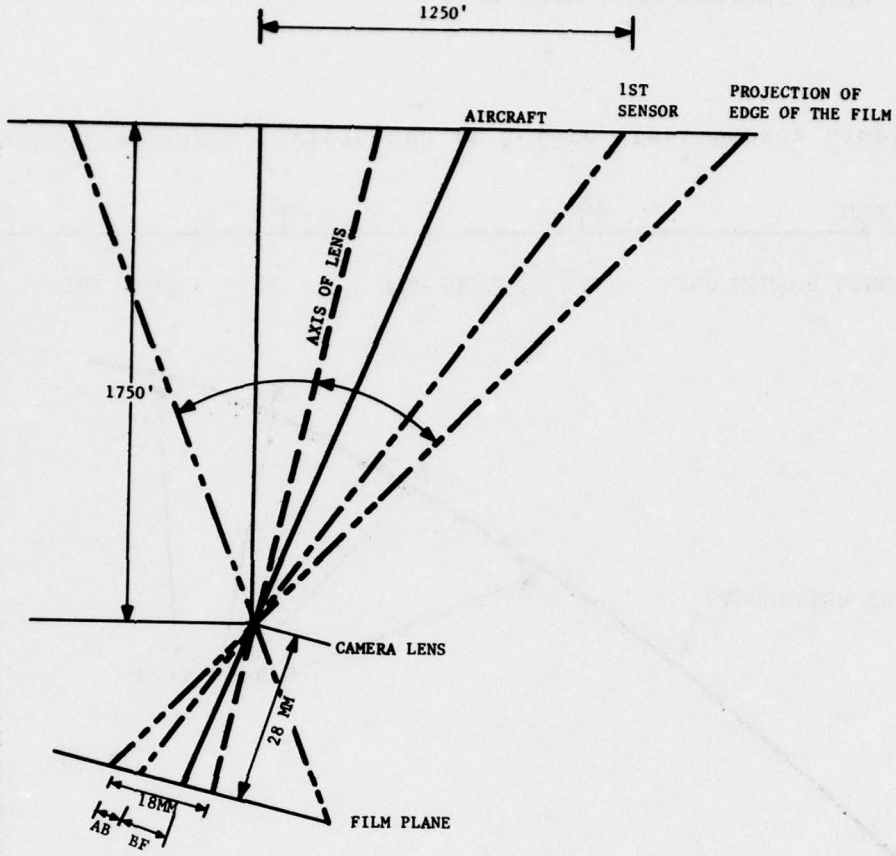


FIGURE 52. CAMERA GEOMETRY

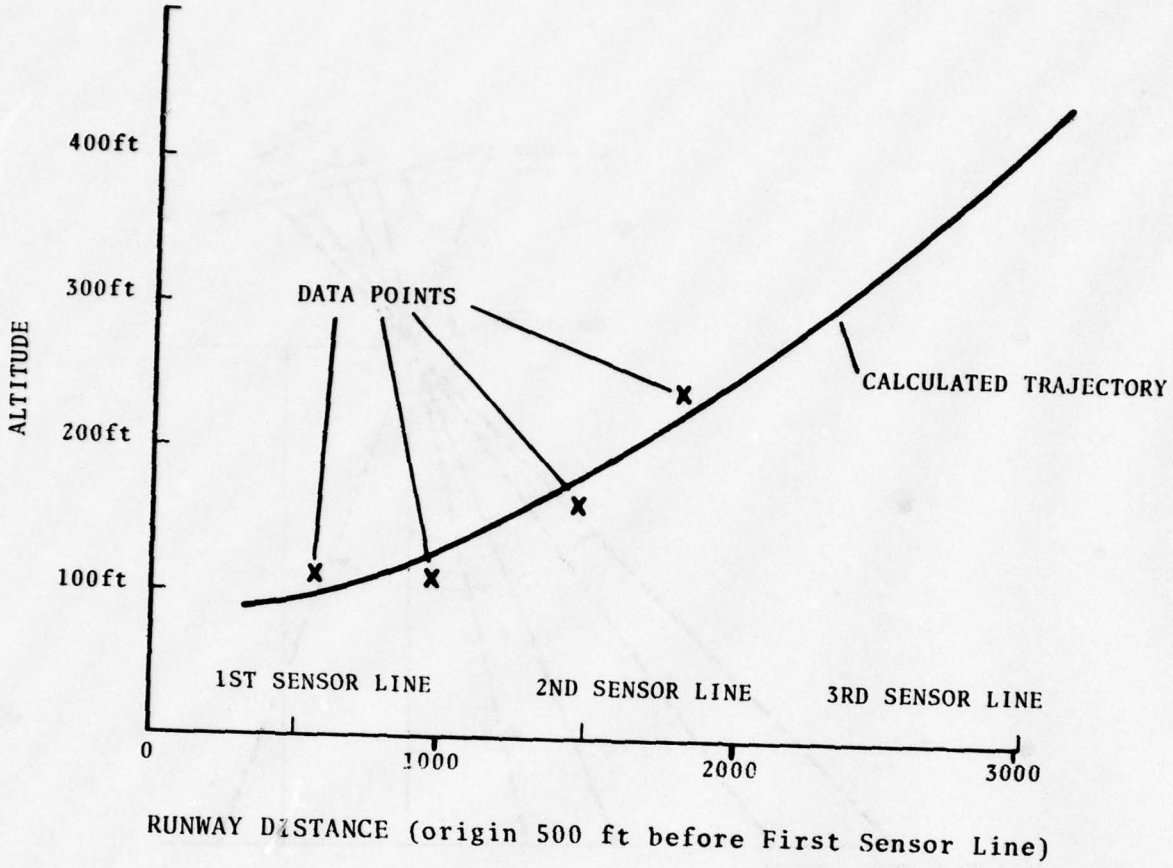


FIGURE 53. TRAJECTORY CALCULATED FROM PHOTOGRAPHIC DATA

fitting routine. If the equations for the polynomial coefficients were consistent and the second derivative of the trajectory curve was positive, the position of the aircraft over each of the sensor lines was estimated. When either the second derivative of the trajectory curve was negative or the estimated altitude of the aircraft over successive sensor lines did not increase, the results were flagged and the data for that takeoff were rechecked.

It usually turned out that the flagged data were the result of misreading the coordinate values in one of the photographic frames and the corrected values produced consistent altitudes.

In all, photographs for about 2030 takeoff runs were processed. The sensor-line altitude, as well as aircraft status data (tape and run number, aircraft type, time date, etc.) were key punched and sent to TSC along with a computer printout of the information. A typical printout is shown in Figure 54. The computer cards were used to enter the altitude data into the TSC data base.

MONTH	DAY	TAPE NO.	RUN NO.	HR	MIN	SEC	AIRCRAFT TYPE	DIST. OF 1ST SENSOR LINE FROM RUNWAY THRESHOLD IN FEET	AIRCRAFT ALT. ABOVE 1ST SENSOR LINE IN FEET	DIST. OF 2ND SENSOR LINE FROM RUNWAY THRESHOLD IN FEET	AIRCRAFT ALT. ABOVE 2ND SENSOR LINE IN FEET	DIST. OF 3RD SENSOR LINE FROM RUNWAY THRESHOLD IN FEET	AIRCRAFT ALT. ABOVE 3RD SENSOR LINE IN FEET
7	28	110	34	7	16	17	DC-9	5800.0	54.1	6800.0	124.7	8300.0	272.1
7	28	110	35	7	17	36	DC-8	5800.0	60.7	6800.0	109.7	8300.0	265.1
7	28	110	36	8	8	6	DC-9	5800.0	50.1	6800.0	116.8	8300.0	257.7
7	28	110	38	8	14	29	DC-9	5800.0	65.8	6800.0	134.5	8300.0	299.5
7	28	110	39	8	24	30	DC-9	5800.0	42.9	6800.0	113.0	8300.0	285.3
7	28	110	40	8	29	36	B-727	5800.0	95.5	6800.0	186.1	8300.0	418.3
7	28	110	41	8	32	0	DC-8	5800.0	28.0	6800.0	72.8	8300.0	251.2
7	28	110	42	8	34	22	DC-8	5800.0	112.9	6800.0	220.2	8300.0	406.8
7	28	110	44	8	51	25	B-727	5800.0	41.2	6800.0	73.4	8300.0	289.8
7	28	110	45	8	59	45	DC-9	5800.0	43.1	6800.0	131.0	8300.0	261.3
7	28	110	46	9	1	36	B-727	5800.0	42.7	6800.0	127.6	8300.0	302.9
7	28	110	47	9	3	12	DC-8	5800.0	22.1	6800.0	49.4	8300.0	192.8
7	28	110	49	12	59	14	DC-9	5800.0	162.4	6800.0	260.7	8300.0	450.7
7	28	110	51	13	21	28	DC-9	5800.0	95.7	6800.0	171.6	8300.0	337.3
7	28	110	52	13	23	58	OTHER	5800.0	121.0	6800.0	207.9	8300.0	461.5
7	28	110	53	13	50	30	DC-9	5800.0	114.5	6800.0	257.8	8300.0	499.1
7	28	110	55	14	10	5	B-727	5800.0	47.4	6800.0	125.7	8300.0	330.1
7	28	110	57	14	14	0	DC-8	5800.0	84.6	6800.0	179.7	8300.0	417.2
7	28	110	58	14	24	49	DC-9	5800.0	143.8	6800.0	288.9	8300.0	574.7
7	28	110	59	14	30	31	DC-8	5800.0	27.7	6800.0	54.8	8300.0	224.8

FIGURE 54. PHOTOGRAPHIC TRAJECTORY SUMMARY

6. METEOROLOGY

Analysis of the data collected at other wake vortex tests sites strongly indicates that the most important parameter for determining vortex transport characteristics is the ambient wind. In this section some of the characteristics of the ambient wind measured during the data collection at Toronto Airport are reported.

6.1 WIND MEASUREMENTS

Three UVW, three-axis wind sensors were mounted on a 100-ft (30-m) tower, one at the 100-ft (30-m) level and two sensors at the 20-ft (6-m) level. As mentioned in Section 2.5, two sensors were required at the 20-ft (6-m) level to eliminate the effects of tower shadowing. Fig. 55 shows an overhead sketch of the tower cross section and the placement of the booms which held the sensors. It can be seen that winds coming from the general direction of W_1 will result in the tower shadowing the port sensor and, likewise, winds coming from a general direction of W_2 will result in the tower shadowing the starboard sensor. For analysis purposes the measurement by the port sensor is used whenever the cross-wind component, V, is positive, and the measurement by the starboard sensor is used whenever the cross-wind component is negative.

In order to assign a single value to the wind components which represents the wind over the duration of the test run, a one-minute running average is used. A sixty-second averaging was chosen for the following reasons: (1) it is approximately the average lifetime of a vortex, (2) previous studies using Kennedy and Heathrow data (Ref. 3) have shown that 60-second averages give consistent and reproducible characterization of vortices, and (3) the influence of wind gusts is minimized.

The MET data presented in this section were collected only when aircraft were taking off on runway 23L and only when the test site was manned. A linear interpolation was performed on the wind

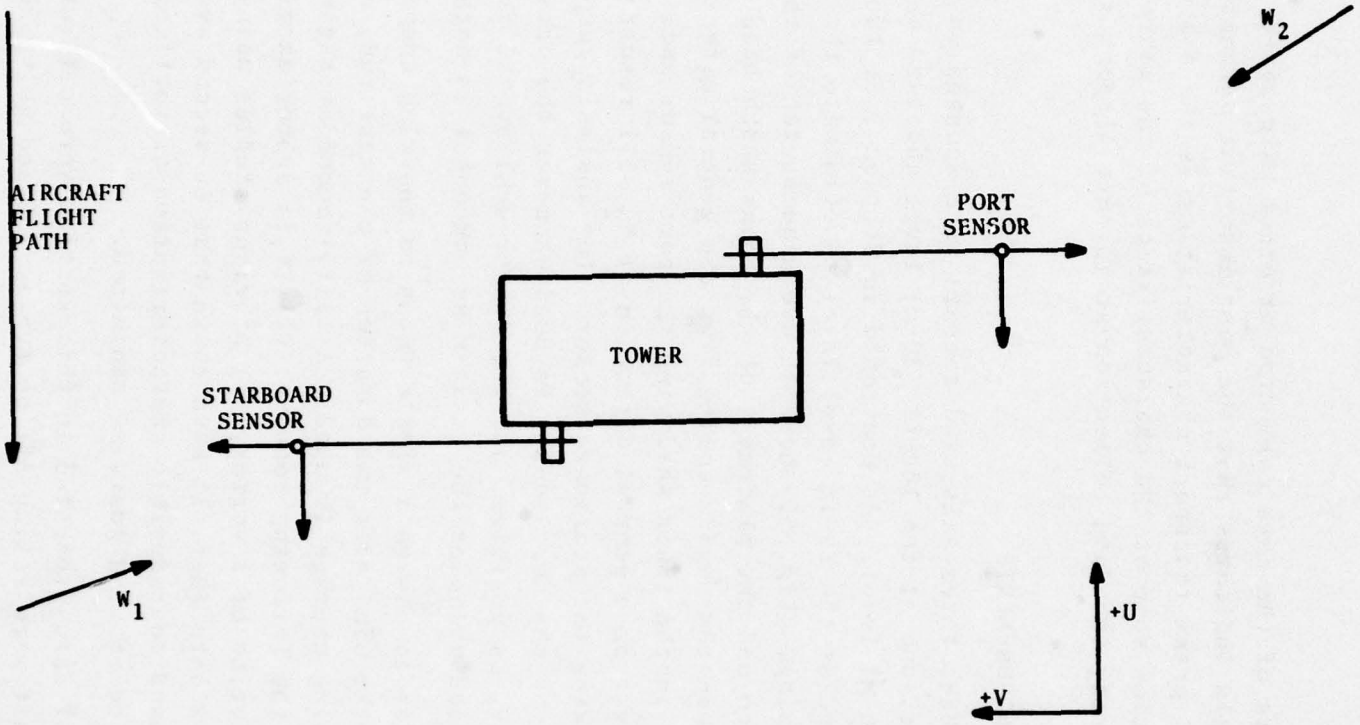


FIGURE 55. SENSOR TOWER-SHADOWING EXAMPLE

measured at the 20-ft (6-m) and 100-ft (30-m) levels to obtain a representative wind at the 50-ft (15-m) level. This was done so that comparisons could be made with the characteristics of vortices observed in previous tests. Fig. 56 shows the overall distribution of the interpolated 50-ft (15-m) horizontal wind and the cross wind. The wind rose obtained during the times runway 23L was in use for departures and data were being collected at the test site is given in Fig. 57.

6.2 VERTICAL WIND SHEAR

The differences between the measurements of the 100-ft (30-m) sensor and the selected 20-ft (6-m) sensor are an indication of low-level vertical wind shear. A summary of these results is given in Table 10, where H is the total horizontal wind magnitude and θ is the wind direction. A superscript represents the height of the sensor in feet and the subscript represents the height in meters (e.g., H_{30}^{100}, θ_{6}^{20}). In general, the results were as expected with the wind magnitude difference increasing and the wind direction difference decreasing with increasing wind magnitude. The higher wind magnitude differences at $25 \leq H_{30}^{100} < 30$ knots and 30 knots $< H_{30}^{100}$ may be attributed to the relatively few data points (these measurements are not statistically significant). As expected, the angular variations are highest for the very low winds.

The mean wind shear was 2.9 kts/100-ft (2.9 kts/30 m) during the data collection. The shear exceeded 5 kts/100 ft (5 kts/30 m) for 7% of the departures. No observations were recorded when the shear exceeded 10 kts/100 ft (10 kts/30 m).

6.3 TURBULENCE

Assigning a meaningful definition of the turbulence of the ambient wind is not a simple task. In previous tests (Refs. 2, 3, and 9) it has been shown that the parameter ε, the equilibrium rate of turbulent eddy dissipation, correlates well with the lifetime of vortices, and is given by the expression

$$\varepsilon^{1/3} = 0.398\, H^{2/3}\, T^{-1/3}\, \sigma_T ,$$

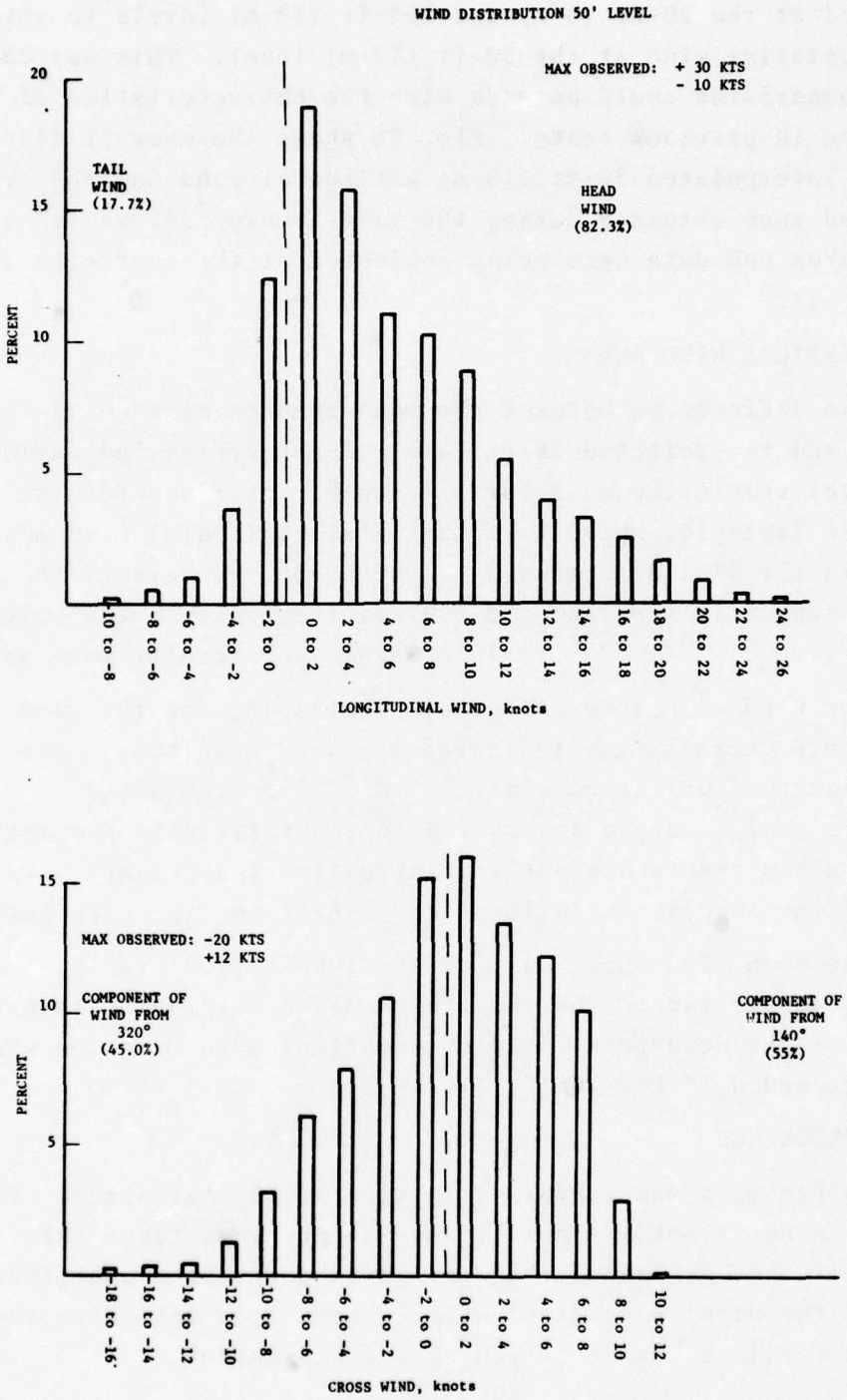


FIGURE 56. DISTRIBUTION OF ONE-MINUTE AVERAGED WINDS

ALL A/C

V50	V80 (KNOTS)																									
	-14	-12	-10	-8	-6	-4	-2	0	2	4	6	8	10	12	14	16	18	20	22	24	26	28	30	TCNT	TPER
-20	0	0	0	0	0	0	0	0	0	0	0	0	1	0	0	0	0	0	0	0	0	0	0	1	.0
-19	0	0	0	0	0	0	0	0	0	0	0	0	0	0	0	0	0	0	0	0	0	0	0	0	.0
-18	0	0	0	0	0	0	0	0	0	0	0	0	0	0	0	0	0	0	0	0	0	0	0	0	.0
-17	0	0	0	0	0	0	0	0	0	0	0	0	0	1	0	0	0	0	0	0	0	0	0	1	.0
-16	0	0	0	0	0	0	0	0	0	0	2	2	0	0	0	0	0	0	0	0	0	0	0	4	.1
-15	0	0	0	0	0	0	0	1	0	0	0	5	0	1	0	0	0	0	0	0	0	0	0	7	.1
-14	0	0	0	0	0	0	0	0	0	0	0	2	1	1	0	0	0	0	0	0	0	0	0	4	.1
-13	0	0	0	0	0	0	1	0	1	1	1	5	1	1	1	0	0	0	0	0	0	0	0	12	.2
-12	0	0	0	0	0	1	0	0	2	2	2	3	1	0	0	0	0	0	0	0	0	0	0	11	.2
-11	0	0	0	0	0	0	0	1	3	6	1	4	3	4	4	0	1	0	0	0	0	0	0	27	.5
-10	0	0	0	0	0	0	0	1	9	4	7	4	8	6	5	3	1	0	0	0	0	0	0	48	.9
-9	0	0	0	0	0	0	1	5	9	6	13	8	12	12	9	4	2	0	1	0	0	0	0	82	1.5
-8	0	0	0	0	0	0	0	7	7	9	9	14	14	13	9	9	3	4	2	0	0	0	0	100	1.8
-7	0	0	0	0	0	0	3	9	7	19	13	32	20	16	13	7	6	4	2	0	0	0	0	151	2.7
-6	0	0	0	0	0	0	4	23	9	20	10	27	37	18	15	6	13	5	3	0	0	0	0	190	3.4
-5	0	0	0	0	0	2	6	21	11	20	22	29	22	14	13	13	11	10	3	1	0	0	0	198	3.6
-4	0	0	0	0	0	1	3	19	27	24	37	40	28	18	18	12	11	7	3	0	0	0	0	248	4.4
-3	0	0	0	0	0	2	2	18	36	48	46	66	18	14	22	11	8	6	2	1	0	0	0	290	5.0
-2	0	0	0	0	0	0	2	17	35	48	43	53	47	24	11	17	9	9	2	3	2	0	0	322	5.7
-1	0	0	0	0	0	2	4	25	43	34	29	49	42	15	14	20	14	6	5	2	1	0	0	309	5.4
0	0	0	0	0	0	4	20	62	74	65	45	53	67	42	29	28	28	14	6	2	1	1	1	542	9.6
1	0	0	0	0	0	7	28	34	69	47	73	57	70	39	13	18	15	9	7	3	2	1	1	499	8.8
2	0	0	0	0	0	2	24	55	54	76	61	31	42	26	15	8	7	10	1	0	1	0	0	413	7.3
3	0	0	1	0	2	3	19	53	62	102	69	47	20	18	9	7	6	3	1	1	0	0	0	419	7.4
4	0	0	0	1	3	4	10	43	83	71	47	33	17	10	7	3	4	1	4	0	0	0	0	341	6.1
5	0	0	0	3	8	3	10	56	109	67	26	14	8	8	4	6	1	0	1	0	0	0	0	324	5.8
6	0	0	0	1	4	9	22	78	137	67	17	7	6	5	1	6	0	1	0	1	0	0	0	362	6.4
7	0	0	0	0	10	9	15	78	120	67	26	8	3	0	0	0	0	0	0	0	0	0	0	329	5.9
8	0	0	0	0	5	7	14	50	90	45	18	5	3	0	0	0	0	0	0	0	0	0	0	237	4.2
9	0	0	0	0	0	2	14	29	47	21	4	1	1	0	0	0	0	0	0	0	0	0	0	119	2.1
10	0	0	0	0	0	0	4	6	14	11	3	0	3	1	0	0	0	0	0	0	0	0	0	42	.7
11	0	0	0	0	0	0	1	0	2	3	0	0	0	1	0	0	0	0	0	0	0	0	0	7	.1
12	0	0	0	0	0	0	0	0	0	1	0	0	0	0	0	0	0	0	0	0	0	0	0	1	.0
13	0	0	0	0	0	0	0	0	0	0	0	0	0	0	0	0	0	0	0	0	0	0	0	0	.0
14	0	0	0	0	0	0	0	0	0	0	0	0	0	0	0	0	0	0	0	0	0	0	0	0	.0
15	0	0	0	0	0	0	0	0	0	0	0	0	0	0	0	0	0	0	0	0	0	0	0	0	.0
16	0	0	0	0	0	0	0	0	0	0	0	0	0	0	0	0	0	0	0	0	0	0	0	0	.0
17	0	0	0	0	0	0	0	0	0	0	0	0	0	0	0	0	0	0	0	0	0	0	0	0	.0
18	0	0	0	0	0	0	0	0	0	0	0	0	0	0	0	0	0	0	0	0	0	0	0	0	.0
19	0	0	0	0	0	0	0	0	0	0	0	0	0	0	0	0	0	0	0	0	0	0	0	0	.0
20	0	0	0	0	0	0	0	0	0	0	0	0	0	0	0	0	0	0	0	0	0	0	0	0	.0
TCNT	0	0	1	5	32	54	207	691	1060	884	620	576	495	308	212	178	140	89	43	14	7	2	2	5620	
TPER	.0	.0	.0	.1	.6	1.0	3.7	12.3	18.9	15.7	11.0	10.2	8.8	5.5	3.8	3.2	2.5	1.6	.8	.2	.1	.0	.0		100.00

FIGURE 57. WIND ROSE

TABLE 8. VERTICAL WIND SHEAR

HORIZONTAL WIND (knots)	$\lvert H_{30}^{100} - H_{6}^{20} \rvert$ (knots)		$\lvert \theta_{30}^{100} - \theta_{6}^{20} \rvert$ (Degrees)		DATA POINTS
	MEAN	σ	MEAN	σ	
$0 \leq H_{30}^{100} < 3$	0.6	0.5	33.4	41.9	485
$3 \leq H_{30}^{100} < 5$	0.9	0.7	12.8	21.5	733
$5 \leq H_{30}^{100} < 10$	1.6	0.9	5.6	6.1	2569
$10 \leq H_{30}^{100} < 15$	2.4	1.0	4.3	4.3	1087
$15 \leq H_{30}^{100} < 20$	3.4	1.1	3.8	3.4	506
$20 \leq H_{30}^{100} < 25$	4.4	1.0	3.9	3.8	206
$25 \leq H_{30}^{100} < 30$	5.1	1.2	6.4	6.5	30
$30 \leq H_{30}^{100}$	5.3	0.6	6.8	2.2	4
ALL H_{30}^{100}	1.8	1.3	8.5	17.3	5620
ALL $H_{30}^{100} \geq 5$	2.1	1.2	5.0	5.4	4402

where H is the horizontal wind. T is a selectable characteristic time constant and was chosen to be 5 seconds. σ_T is the RMS angular variation and is given by

$$\sigma_T = \left(\frac{\sum_{i=1}^{N} W_i^2 - \frac{1}{N} (\bar{W}_5)^2}{N-1} \right)^{1/2} \cdot \frac{57.3}{H} ,$$

where W_i is the vertical component of the wind sampled seven times per second. W_5 is the 5-second mean value of the vertical wind, and N = 35 (7 samples/sec for 5 sec).

Table 11 gives the turbulence values measured at Toronto for all cross winds and then subdivided into positive and negative cross winds. Fig. 58 shows the total wind distribution as a function of turbulence (e.g., when the turbulence is in the region $0 \leq T < 2$, 34% of the data were recorded with a total wind less than 12 knots).

The significance of these turbulence values can be demonstated by referring to Reference 10. Turbulence levels are reported as units of a parameter R which is related to ε by

$$R = \left(\frac{\rho}{\rho_o} \right)^{1/3} \varepsilon^{1/3} ,$$

where ρ/ρ_0 is the ratio of the air density at the test site to that at sea level. For Toronto $(\rho/\rho_0)^{1/3} \approx 1$ and $R \approx \varepsilon^{1/3}$. Turbulence values between 0.8 and 1.9 are considered "light," between 1.9 and 4.5 "moderate," and between 4.7 and 10.7 "heavy." These subjective values refer to pilot responses in flight conditions.

TABLE 9. TURBULENCE DISTRIBUTIONS

$\varepsilon^{1/3}$ ($cm^{2/3}$ sec^{-1})	ANY V (number)	V>0 (number)	V<0 (number)
0.0-0.9	627	298	286
1.0-1.9	1384	902	455
2.0-2.9	1588	1005	570
3.0-3.9	990	519	464
4.0-4.9	562	237	323
5.0-5.9	234	87	145
6.0-6.9	98	61	37
7.0-7.9	25	12	12
8.0-8.9	13	6	7
9.0-9.9	12	4	8
10.0-10.9	15	8	7
11.0-11.9	7	2	4
12.0-12.9	8	1	7
13.0-13.9	2	0	2
14.0-14.9	7	1	6
15.0-15.9	2	0	2
16.0-16.9	2	1	1
17.0-17.9	4	1	3
18.0-18.9	3	0	3
19.0-19.9	1	0	1
GT20	36	17	18
TOTAL	5584	3145	2343
MEAN	2.69	2.53	2.97
STD. DEVIATION	1.81	1.51	2.11

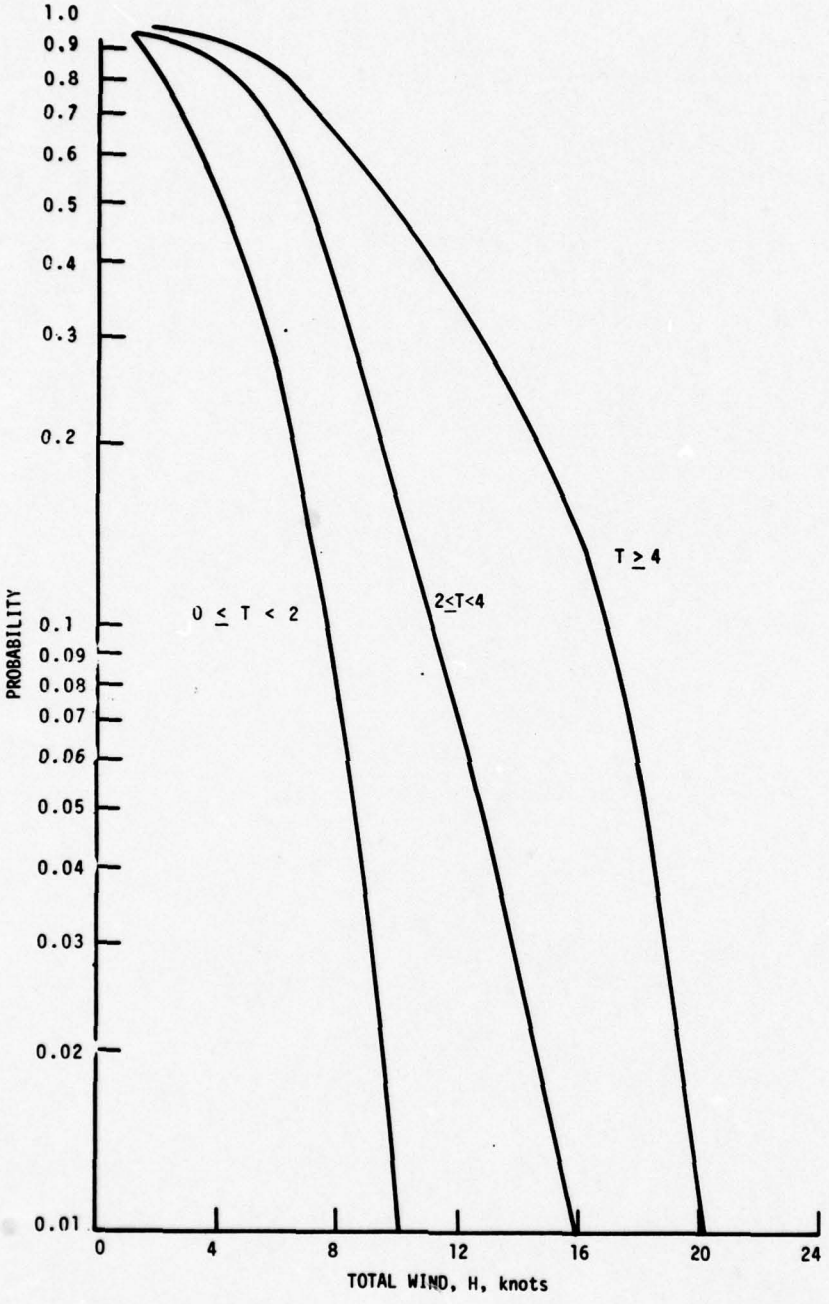


FIGURE 58. TURBULENCE DISTRIBUTIONS BY HEAD WIND

7. DATA ANALYSIS

The final approach and early takeoff stages are the two regions where an aircraft wake vortex has the highest hazard potential to a following aircraft. Here, aircraft are close to the ground with minimal capabilities to maneuver and are using control capabilities to keep the aircraft on the desired course. Historically, landing is the more dangerous situation since most of the vortex-related accidents in the United States occurred with one aircraft landing behind another aircraft. One reason for this might be that on final approach all landing aircraft follow essentially the same path and hence the probability of vortex encounter is greater. The takeoff phase, however, remains a potentially hazardous vortex-encounter area due to the density of aircraft operations.

7.1 AIRCRAFT TYPES

A total of 5633 takeoffs were monitored during the test period. The distribution by aircraft type was as follows:

AIRCRAFT TYPE	NUMBER OBSERVED
707	164
727	1388
737	214
747	106
DC-8	742
DC-9	2236
DC-10	108
L-1011	358
VC-10	12
Other	167
BAC-111	138
TOTAL	5633

7.2 REFERENCE CORRIDOR

Since vortices usually move away or dissipate before a following aircraft arrives, the vortex track data were analyzed in terms of how soon they exit a "reference corridor". Previous test results (Heathrow (Ref. 3), etc.) have defined a "safety zone" of ±150 ft (±45 m) about the runway centerline with no height restriction. This zone was determined from analysis of data from aircraft-vortex encounter simulations and photographs of aircraft deviation from the instrument flight path at Denver's Stapleton Airport. It was not practical to use this ±150-ft (±45 m) corridor in the Toronto tests due to the lack of sensors over the runway. A ±200-ft (±60-m) corridor was chosen as the smallest corridor which could be used considering the Toronto sensor geometry.

The region is referred to as a "reference corridor" and not a "safety zone" since the former is necessarily larger than the latter (primarily for data analysis reasons) and not from considerations of safe aircraft operations. However, similar to the safety zone, if both vortices are clear of the reference corridor, they cannot pose a threat to a following aircraft on the same runway. The existence of a vortex within the reference corridor when a following aircraft arrives does not mean that a hazardous condition exists; it is a necessary but not a sufficient condition (the vortex could decay to a non-hazardous level, aircraft paths could be separated by 400 ft (120 m) even with both aircraft within the corridor, etc).

7.3 VORTEX RESIDENCE

A vortex which can be detected within ±200 ft (±61 m) of the runway centerline is defined to be "resident" in the reference corridor. A vortex which is first detected within the corridor normally ceases to be resident by one of two means: a) the vortex transports out of the corridor, or b) the vortex decays to a state where it is no longer detectable within the corridor. However, at the Toronto test site a third mechanism must be considered. Vortices which stall directly over the runway may not be detected since the first vortex sensors are located ±150 ft (±45 m) from

the runway centerline.

The data were analyzed in a manner which allowed for determining vortex residency characteristics at four time-reference points: 30, 60, 90 and 120 seconds after start-of-run (SOR). Fig. 59 shows the probability of finding a vortex resident in the corridor equal to or longer than the specified elapsed time (e.g., on all three lines, 10 percent of the runs indicated a vortex inside the corridor boundaries 90 seconds after the passage of the aircraft). This figure is a composite of all the aircraft and meteorological conditions. There is no significant difference in the data among the three baselines except at the 30-second point. Here, residence times for line 1 appear to be longer than for line 2, which in turn are longer than for line 3. This can be explained by considering that ground effect is the mechanism which causes vortices to stall and the vortices from the higher aircraft are blown out of the corridor before being affected.

The data can be compared to the results obtained from the tests on landing aircraft at Heathrow (Ref. 3), but an adjustment must be made to compensate for the smaller ±150-ft (±45-m) safety corridor chosen in the Heathrow analysis. In order to scale the data, the assumption is made that vortex transport velocities are essentially constant and there exists a linear distribution of velocities between 0 and V_{max}, the velocity at which the vortex would transport 200 ft (60 m) in 30 seconds [6.7 ft/sec (20m/sec)], as shown in Fig. 60. This may be seen to be a reasonable assumption by carrying the analysis one step further. From the graph one may also postulate that 50 percent of the vortices have velocities greater than that required to transport 200 ft (60 m) in 60 seconds [200 ft (60 m) in 60 seconds = 2.33 ft/sec (0.7 m/sec)], the next time reference. Fig. 59 confirms this hypothesis by showing that approximately 50 percent (27/62 = 44 percent) of the vortices remain resident at 60 seconds. Thus, for comparison purposes, the assumption is made that 75 percent of the vortices resident in the ±200-ft (±60-m) corridor would be resident in a ±150-ft (±45-m) corridor and the data for line 1 are compared to the Heathrow results in Fig. 61.

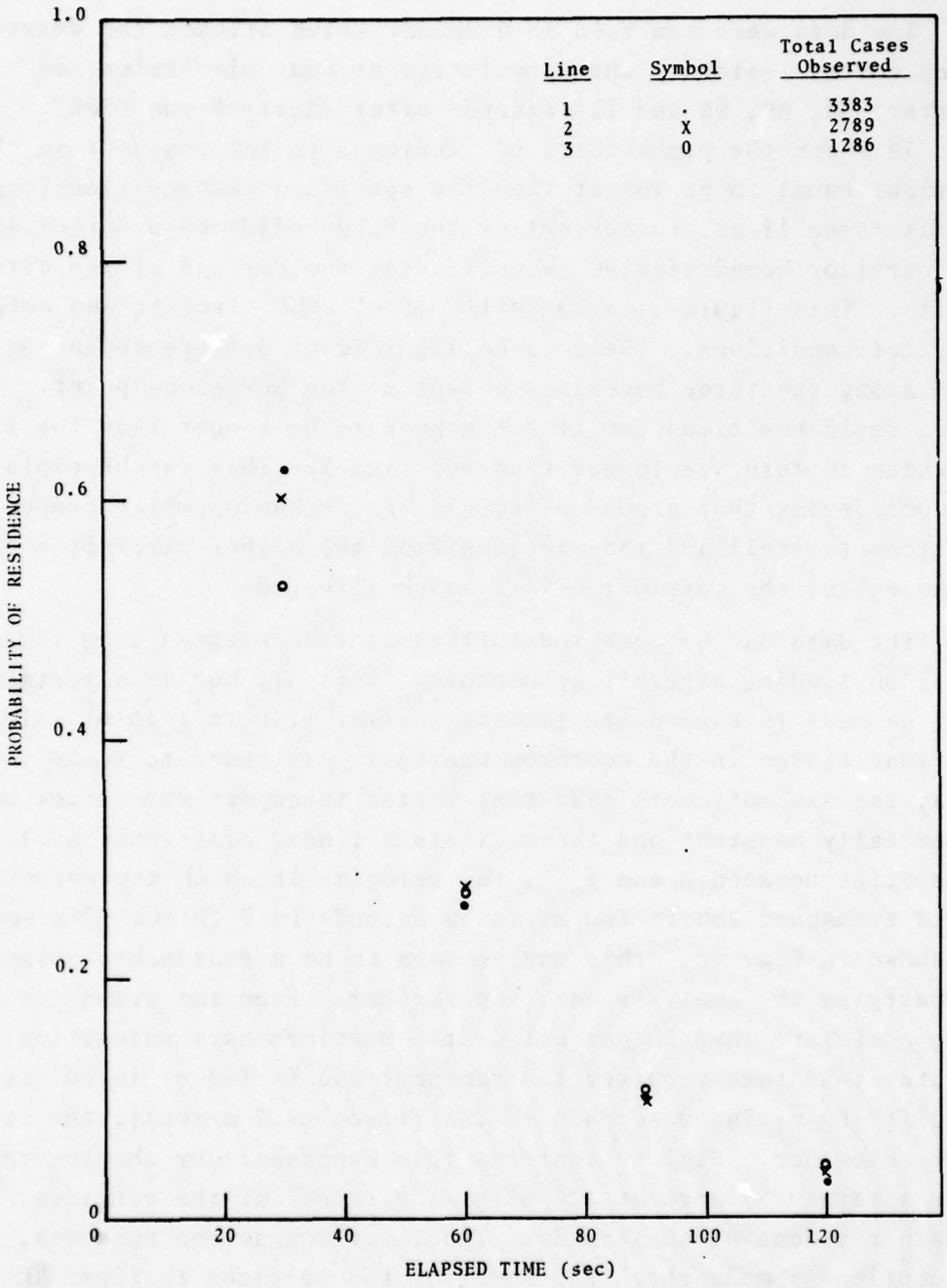
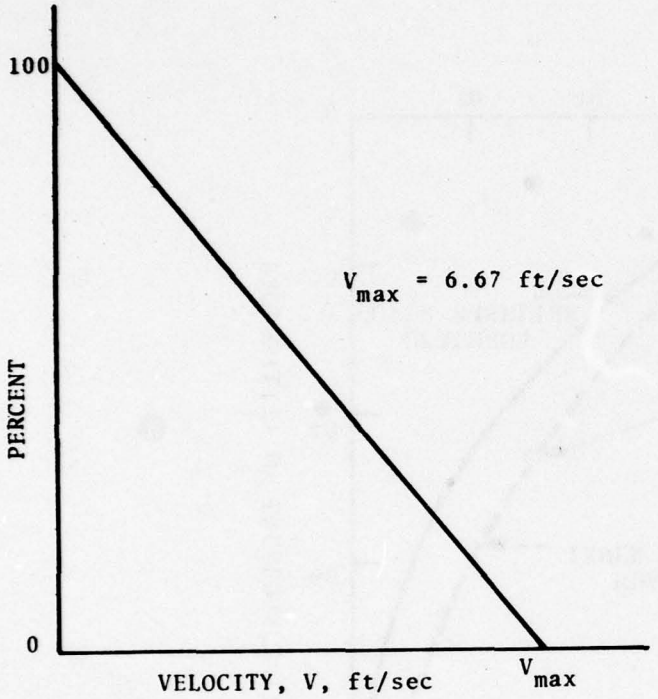
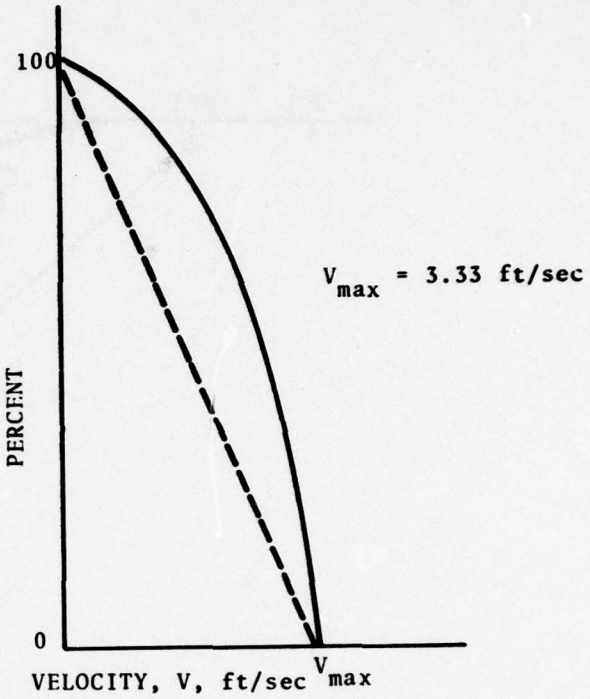


FIGURE 59. PROBABILITY THAT A VORTEX REMAINED IN THE REFERENCE CORRIDOR AS A FUNCTION OF ELAPSED TIME



Percentage of vortices resident for at least 30 seconds whose velocities exceed V



Percentage of vortices resident for at least 60 seconds whose velocities exceed V

FIGURE 60. VORTEX VELOCITY PROFILES

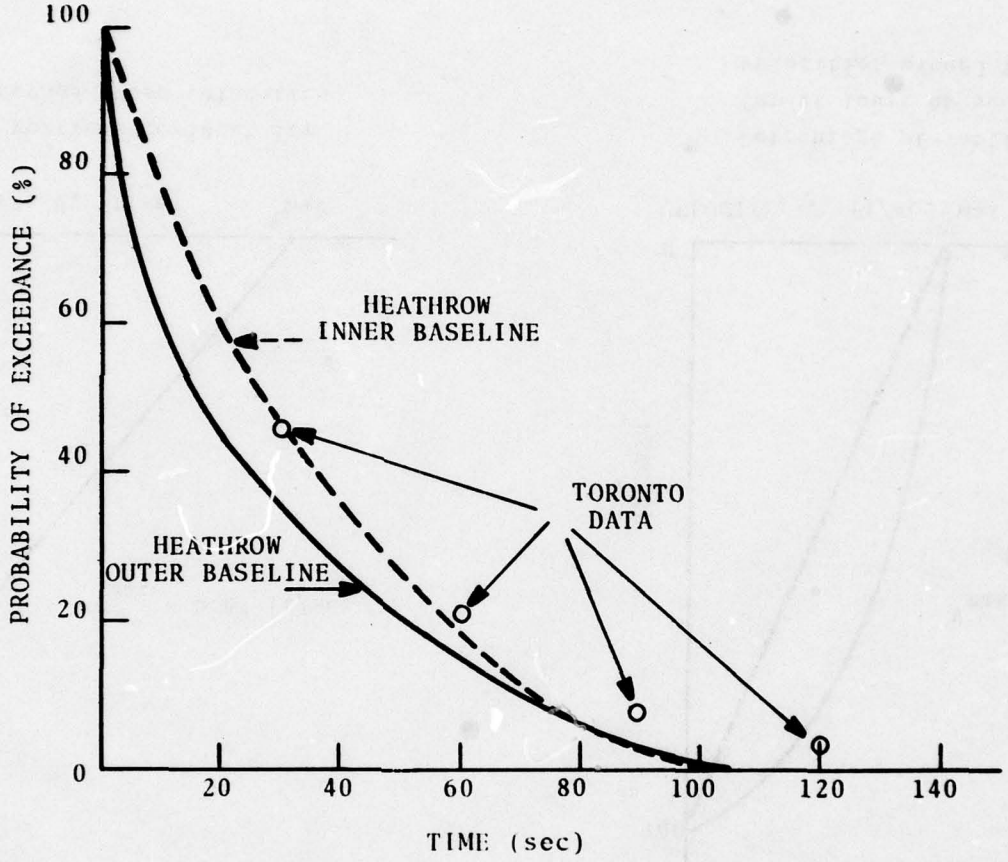


FIGURE 61. PROBABILITY THAT A VORTEX WILL REMAIN IN THE REFERENCE CORRIDOR LONGER THAN A GIVEN TIME AND COMPARED TO HEATHROW DATA

The results of this analysis show that vortex behavior for the shorter residence times is similar in both experiments. However, a noticeable difference esists at the higher residence times; a number of data points were observed where vortices remained in the corridor for longer than 90 seconds (10 percent) and 120 seconds (4 percent). As might be expected, the contribution from the Heavy aircraft (B-707, B-747, DC-8, DC-10, L-1011) is disproportionately high. (The B-707 and DC-8 were included in the Heavy category for this report; for a discussion see Section 7.9). Table 12 lists the results of separating the residence-time statistics so that a percentage is found by dividing the number of cases where a vortex from a Heavy aircraft is observed in the corridor into the total number of Heavy aircraft observed. Likewise, the number of cases of a vortex from a Non-heavy aircraft is divided into the total number of Non-heavy aircraft observed. These data are plotted in Fig. 62. It should be noted that in Table 12 and Figure 62 the Jumbo aircraft were intentionally isolated from the heavy class to emphasize their characteristics.

A total of 180 cases were observed where a vortex from a Heavy aircraft remained in the $\pm$200-ft ($\pm$60-m) corridor for longer than 120 seconds, the required air traffic control time separation for a non-Heavy aircraft following a Heavy aircraft. It should be remembered, however, that these data were obtained from the ground wind anemometer system where the analysis contained virtually no information about the vortex strength. It is highly probable that the detected long-lived vortices are only very weak vortex remnants. This proposal is further substantiated by the fact that there were no reports of an aircraft encountering the turbulence from the vortex of another aircraft during the entire series of the tests.

7.4 VORTEX LIFETIMES

From the beginning of its life, a vortex pair undergoes three forms of decay. The first form is a viscous decay which leads to a gradual vortex demise. The two other decay mechanisms, core bursting and sinuous instability, are catastrophic and result in a very rapid change of vortex state. Decay mechanisms develop through

TABLE 10. VORTEX RESIDENCE AS A FUNCTION OF AIRCRAFT TYPE AND GROUND-WIND SENSOR LINE

Type of Aircraft	30 Seconds Line 1	2	3	TOTAL	60 Seconds Line 1	2	3	TOTAL
JUMBO	71	69	68	70	40	37	41	39
HEAVY	69	67	63	67	34	35	37	35
NON-HEAVY	59	57	47	56	22	23	21	22
COMBINED	62	60	53	60	26	27	27	26

Type of Aircraft	90 Seconds Line 1	2	3	TOTAL	120 Seconds Line 1	2	3	TOTAL
JUMBO	20	20	22	21	8	11	11	10
HEAVY	16	17	19	17	6	8	10	8
NON-HEAVY	7	6	6	6	2	2	2	2
COMBINED	10	10	10	10	3	4	5	4

Note: Jumbo aircraft are segregated from the heavy type to emphasize their long residence times. The percentage is obtained by dividing the number of vortices observed resident by the total number of vortices observed for the type of aircraft.

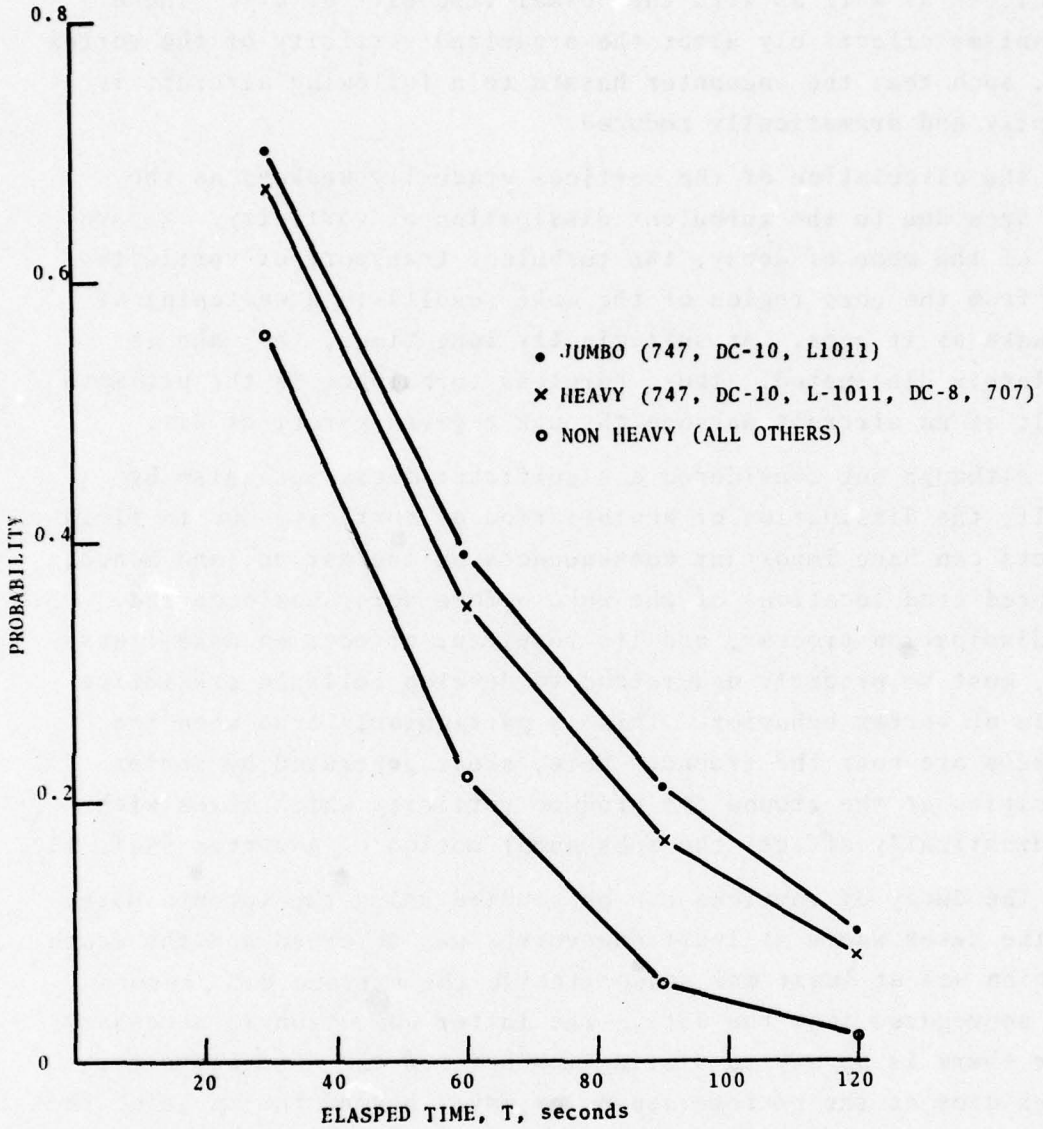


FIGURE 62. PROBABILITY THAT A VORTEX WILL REMAIN IN THE CORRIDOR FOR A TIME LONGER THAN ELAPSED TIME, T

Note: Jumbo aircraft are segregated from the heavy type to emphasize their long residence times.

coupling with atmospheric, aircraft-induced and self-induced turbulence as well as with the normal viscosity of air. These mechanisms effectively alter the organized vorticity of the vortex pair, such that the encounter hazard to a following aircraft is abruptly and dramatically reduced.

The circulation of the vortices gradually weakens as the wake ages due to the turbulent dissipation of vorticity. Regardless of the mode of decay, the turbulent transport of vorticity away from the core region of the wake results in a weakening of the wake as it ages. At sufficiently long times, the wake is completely dissipated. Thus, harmless turbulence is the ultimate result of an aircraft passage through a given parcel of air.

Although not considered a significant decay mechanism by itself, the dissipation or annihilation of vorticity due to fluid effects can have important consequences on the motion (and hence, the predicted location) of the wake before decay has occurred. The dissipation process, and its resultant effects on wake transport, must be properly understood to develop reliable predictive models of vortex behavior. This is particularly true when the vortices are near the ground. Here, shear generated by vortex velocities at the ground can produce vorticity which mixes with the drastically affects the subsequent motion of a vortex (Ref. 11).

The decay of vortices can be studied using the Toronto data. All the cases where at least one vortex was observed and the death position was at least one sensor inside the extreme end sensors were segregated from the data. The latter condition is necessary since there is no way to distinguish between the case where the vortex dies at the extreme sensor or moves beyond the range of the sensor line. It is not possible, however, to determine which mechanism caused the vortex decay using only GWVSS data.

7.4.1 Vortex Decay Time

Studies have shown that it is the total wind which correlates best with the decay of vortices. Fig. 63 shows the distribution of the death times for the oldest vortex of the pair. The data are

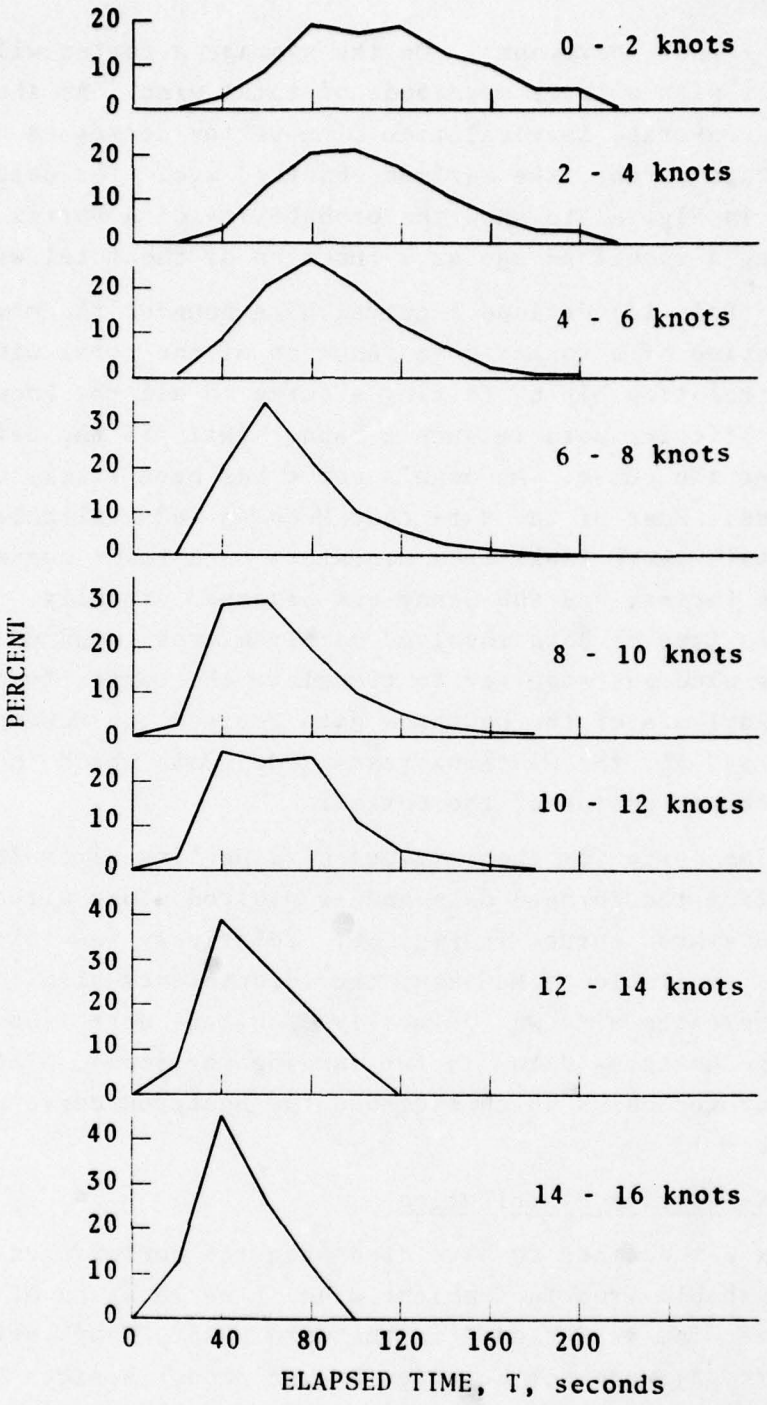


FIGURE 63. VORTEX DEATH TIME DISTRIBUTION AS A FUNCTION OF TOTAL WIND WHEN BOTH VORTICES ARE OBSERVED, THE OLDER VORTEX TIME IS USED

divided into 2-knot increments. On the average a vortex will survive longer with a lower magnitude of total wind. As the wind increases, the average survival time of a vortex decreases as well as, to a certain extent, the maximum observed age. The data are also plotted in Fig. 64 to show the probability of a vortex lifetime exceeding a specified age as a function of the total wind.

McGowan (Ref. 12) devised a curve which bounded the maximum observed lifetime of a vortex as a function of the total wind. He obtained the relationship by fairing a curve to all the known (in 1970) vortex lifetime data in such a manner that all the data were included under the curve. McGowan's curve has been widely used in the literature. Most of the data that McGowan had available came from tower tests where smoke from canisters on a tower became imbedded in the vortex, and the decay was assessed visually. By necessity this type of data involved mainly a cross-wind component since a cross wind was required to translate the vortex to and past the tower. Analysis of the Heathrow data revised the McGowan curve as shown in Fig. 65; the Heathrow tests added data which included winds along the direction of the vortex.

A lifetime curve for the vortices of departing aircraft may be obtained from the Toronto data and is plotted along with the McGowan and Heathrow curves in Fig. 66. Relatively few takeoff vortices were available to McGowan; the Toronto data also include situations where the wind was primarily along the direction of flight (as the Heathrow data did for landing vortices). The wind conditions for the cases which exceeded the Heathrow curve are listed in Table 13.

7.4.2 Vortex-Position Distribution

A vortex was defined to have died when the vortex signal was not distinguishable from the ambient wind. The location of the vortex when it died is included in the data base. Many vortices (about 40 percent) were not detected by the sensor systems and thus have no definable death position. This result could be attributed to several causes: (1) aircraft were extremely high

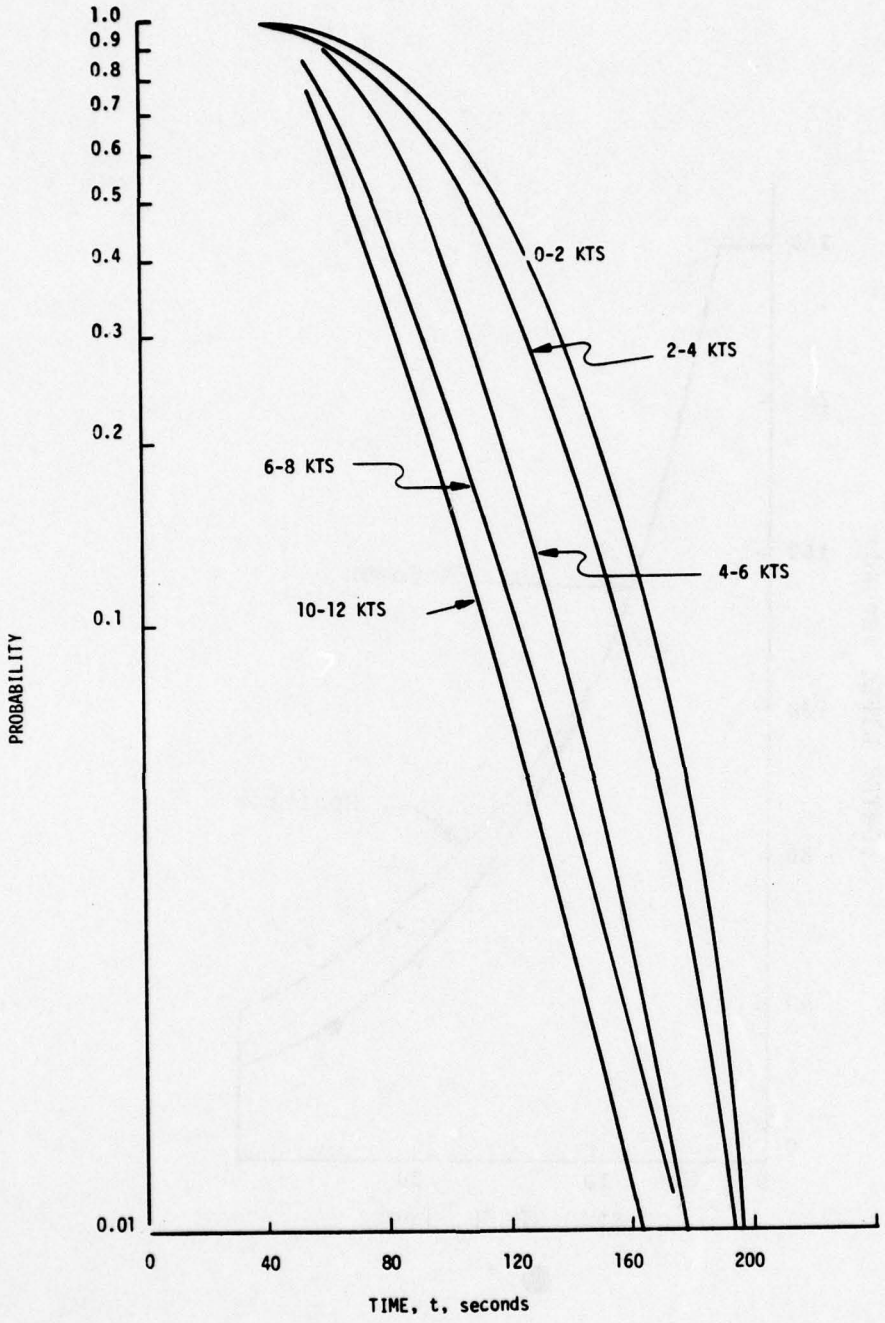


FIGURE 64. PROBABILITY FOR A VORTEX NOT TO DECAY AS A FUNCTION OF TOTAL WIND. DATA FROM ALL AIRCRAFT ARE INCLUDED

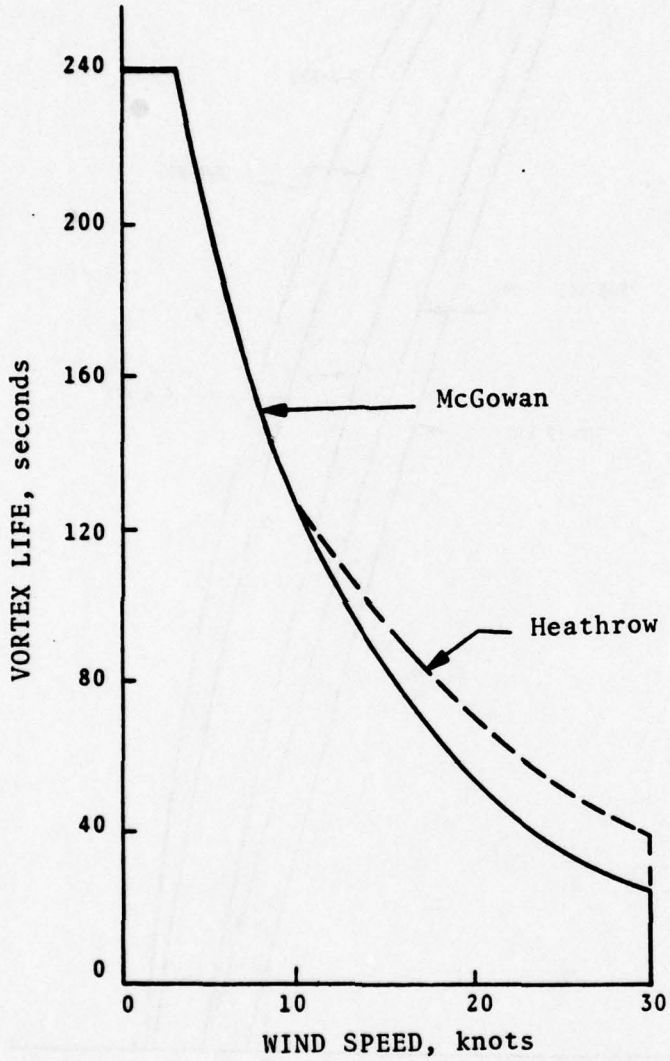


FIGURE 65. MCGOWAN CURVE OF MAXIMUM OBSERVED VORTEX LIFETIMES AS A FUNCTION OF WIND SPEED

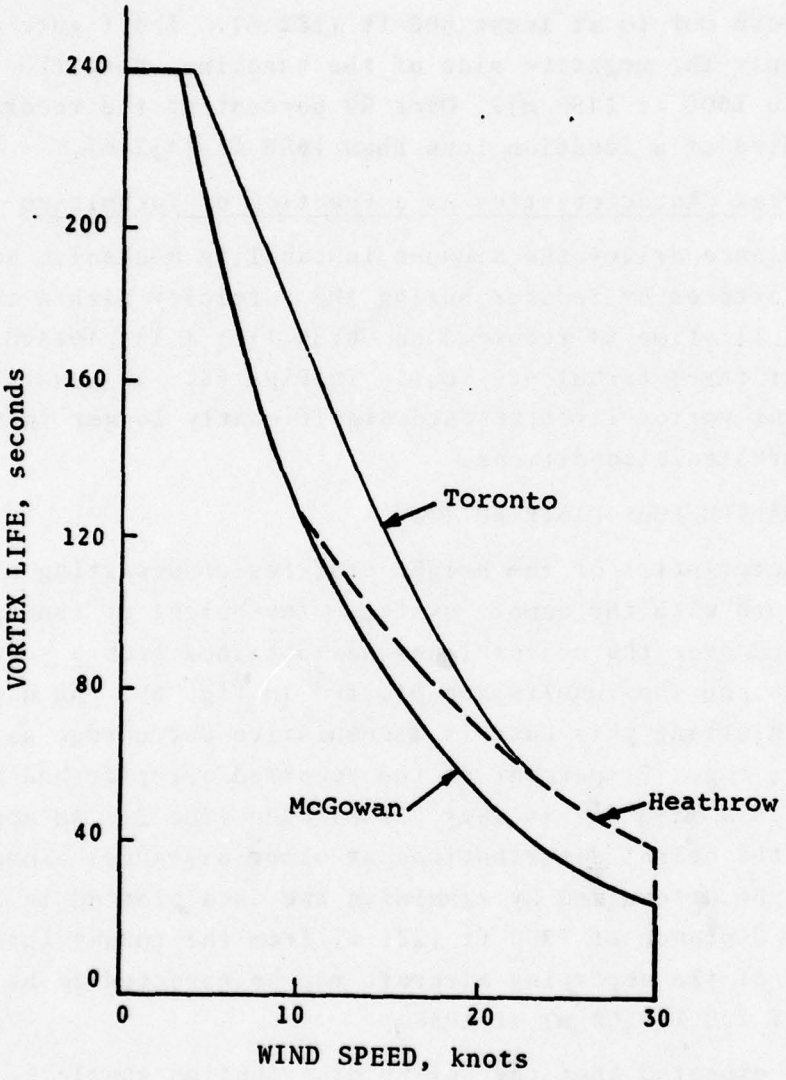


FIGURE 66. MCGOWAN CURVE OF MAXIMUM OBSERVED VORTEX LIFETIMES AS A FUNCTION OF WIND SPEED REVISED TO INCLUDE TORONTO DATA

when they passed the baselines, (2) high winds and their associated higher turbulence (see Fig. 58) resulting in early decay of the vortices, and (3) the lack of sensors in the area directly over the runway. The distribution of death positions for all aircraft on all baselines combined is given in Fig. 67, e.g., 39 percent of the cases where at least one vortex was recorded by the GWVSS had a vortex move out to at least 600 ft (182 m). The figure contains data for only the negative side of the baseline where the sensors extended to 1600 ft (455 m). Over 99 percent of the recorded vortices died at a location less than 1600 ft (455 m).

7.4.3 Vortex Characteristics as a Function of Turbulence

Turbulence drives the sinuous instability mechanism and acts to erode vortices by redistributing the vorticity within the vortex. The vortex lifetime as recorded on GWVSS line 1 is plotted as a function of three turbulence levels in Fig. 68. In general, it can be seen that vortex lifetimes are significantly longer in the lighter turbulence conditions.

7.5 AIRCRAFT-HEIGHT DISTRIBUTIONS

Characteristics of the height profiles of departing aircraft were obtained with the camera system. The height of the aircraft as it passed over the sensor lines was obtained from a sequence of photographs and the results are plotted in Fig. 69. An alternative method of plotting this data is a cumulative percentage as shown in Fig. 70; e.g., 71 percent of the recorded aircraft had a height less than 75 m (250 ft) as they passed over line 2. An approximation of the height distributions at other distances along the runway may be determined by examining the data plotted in Fig. 71; e.g., at a distance of 7300 ft (221 m) from the runway threshold, 36 percent of the departing aircraft may be expected to be at an altitude of 200 ft (60 m) or less.

It is expected that the height distribution should be a function of the head wind, with the aircraft altitude being higher as the head wind increases. This effect was observed and the data are plotted in Fig. 72; there exists a noticeable shift toward the

TABLE 11. DATA POINTS OUTSIDE OF MCGOWAN CURVE REVISED TO INCLUDE HEATHROW DATA

R_y, Knots	θ, Degrees	Lifetime, Seconds
19.5	358	72
8.3	359	150
11.6	348	132
16.9	358	98
8.6	20	146
8.1	359	162
6.0	1.5	200
11.7	351	140
9.7	5.7	142
12.6	18	136
16.5	29	96
5.7	6.4	190
9.5	8.3	140
9.9	7.6	172
8.7	12.7	178
10.5	0.3	130
8.7	357	148
8.7	357	144
7.1	338	188
7.1	338	182
7.1	338	186
12.2	347	114
9.1	339	152
9.1	339	172
19.5	18	74
10.7	355	152
12.1	3.1	128
6.0	103	200
10.5	18	146
9.3	11	170
6.0	1.5	200
9.2	1.3	148
8.1	355	166
6.9	14	202
6.7	39	180
7.3	21	184

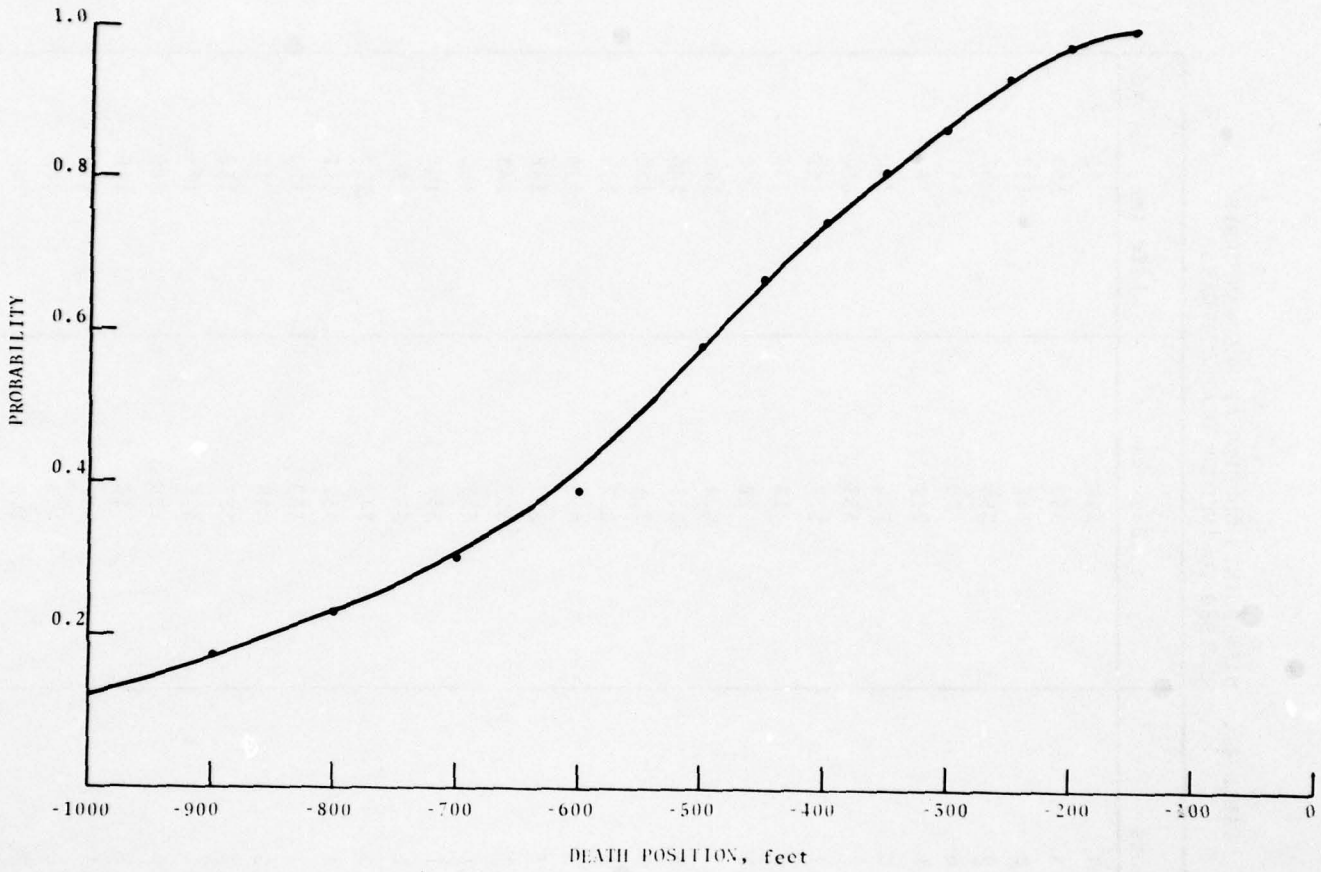


FIGURE 67. PROBABILITY THAT THE DEATH POSITION OF THE VORTEX FURTHER FROM THE CENTER LINE WAS LESS THAN OR EQUAL TO DP. All sensor lines are combined

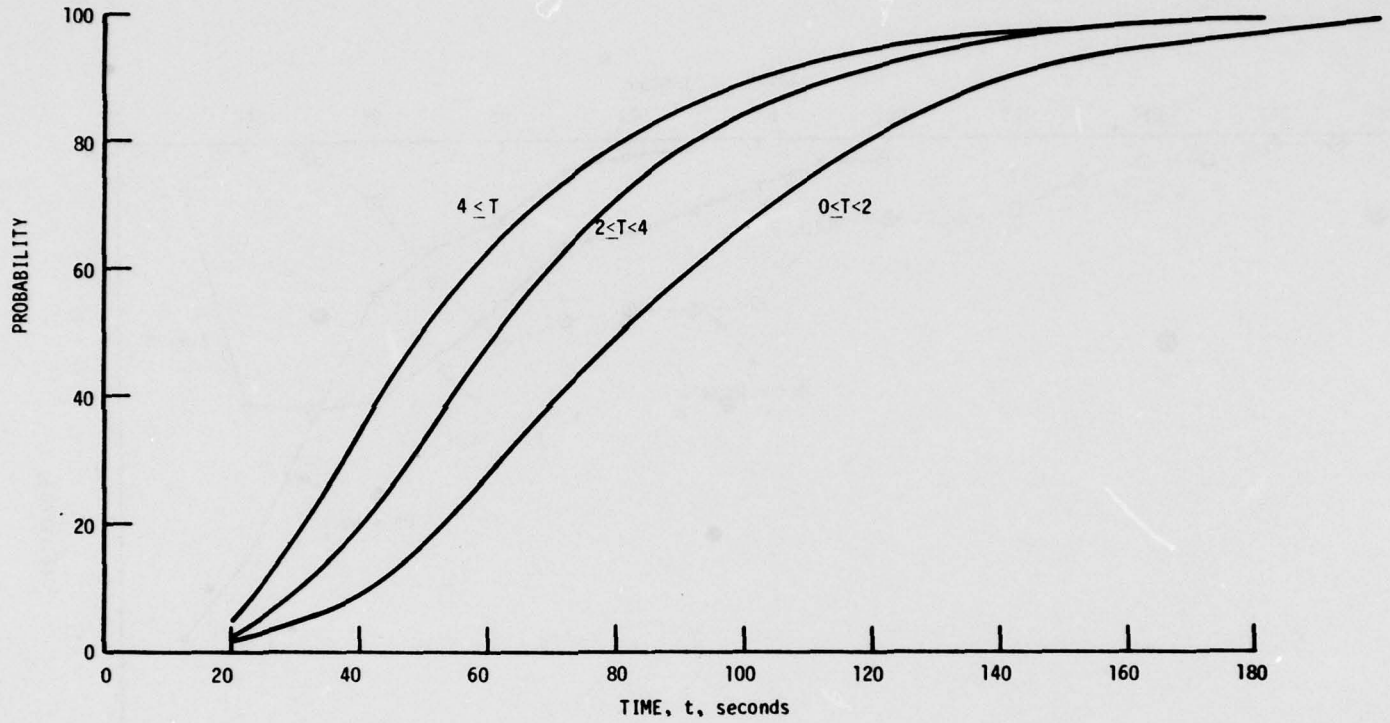


FIGURE 68. PROBABILITY THAT AN OBSERVED VORTEX HAS DECAYED IN A TIME LESS THAN t, AS A FUNCTION OF TURBULENCE. All sensor lines and all winds are included

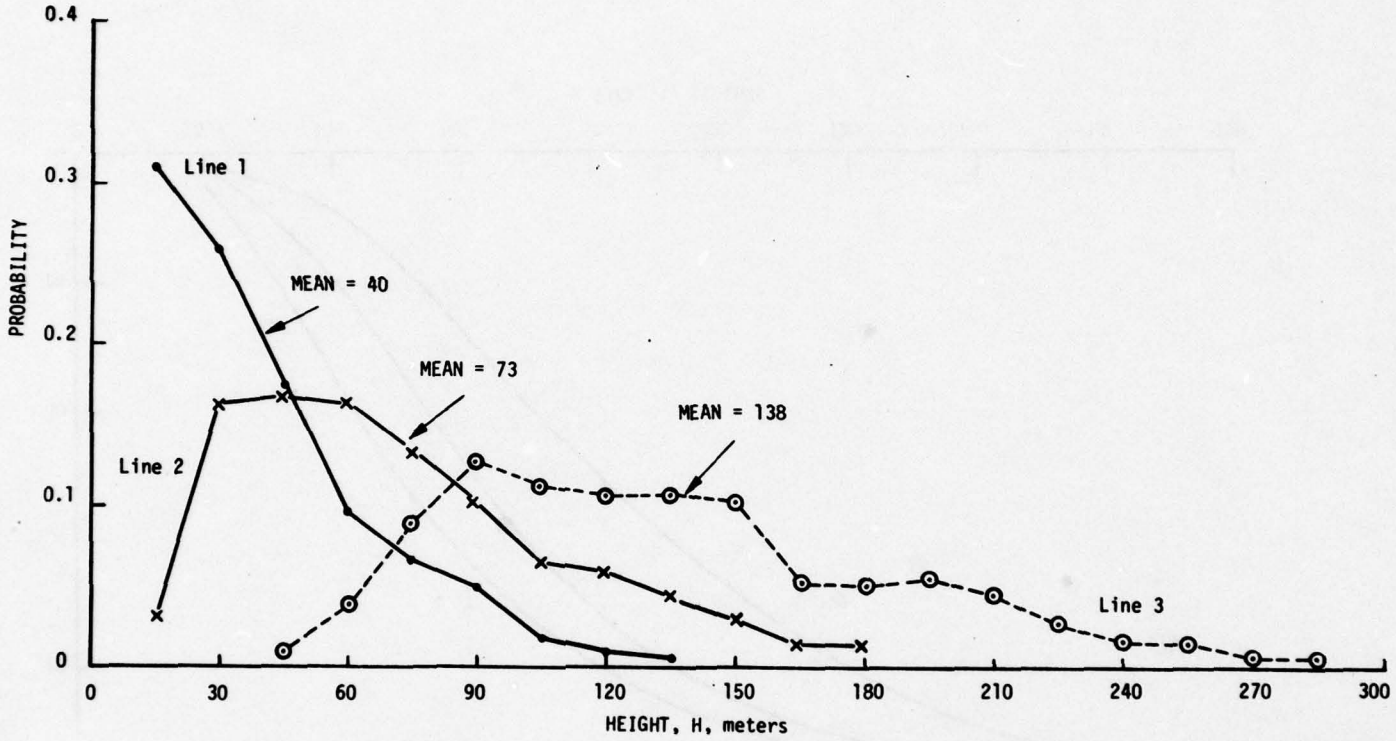


FIGURE 69. PROBABILITY THAT THE AIRCRAFT HEIGHT WAS BETWEEN h-15 AND h

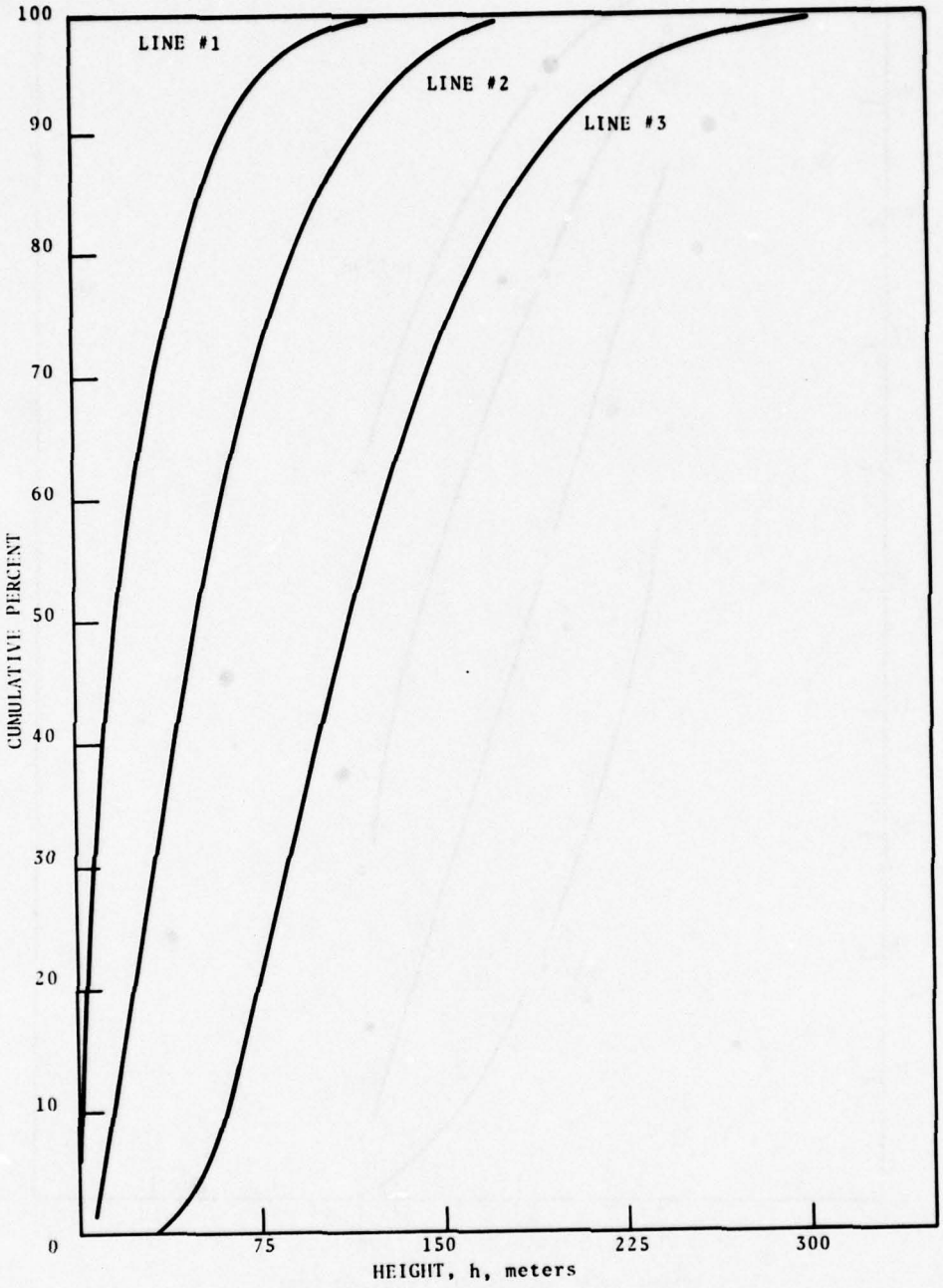


FIGURE 70. CUMULATIVE PERCENTAGE OF AIRCRAFT WHOSE HEIGHT IS LESS THAN h. All aircraft are included

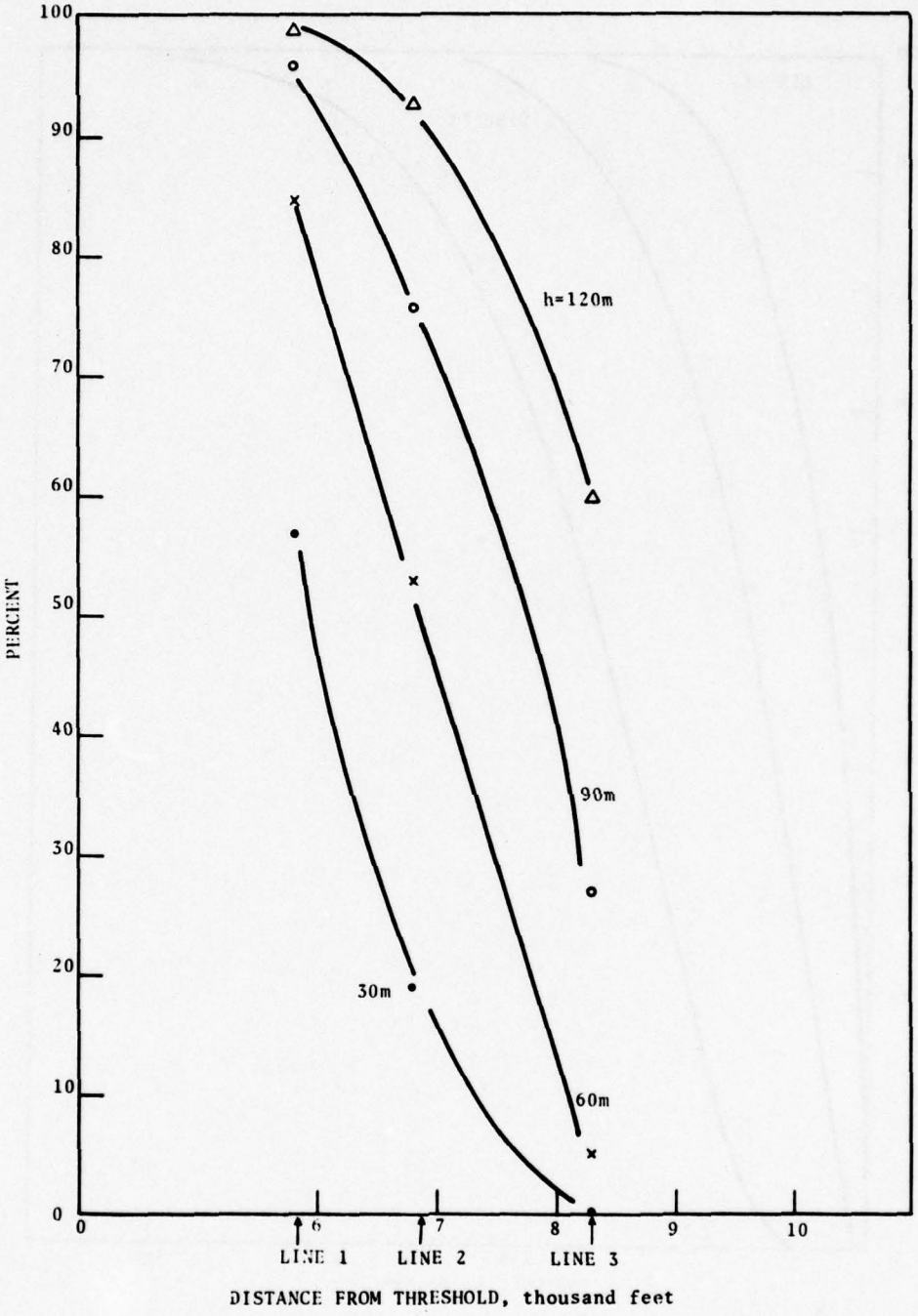


FIGURE 71. PERCENTAGE OF AIRCRAFT WHOSE HEIGHT IS BELOW h AS A FUNCTION OF DISTANCE FROM RUNWAY THRESHOLD

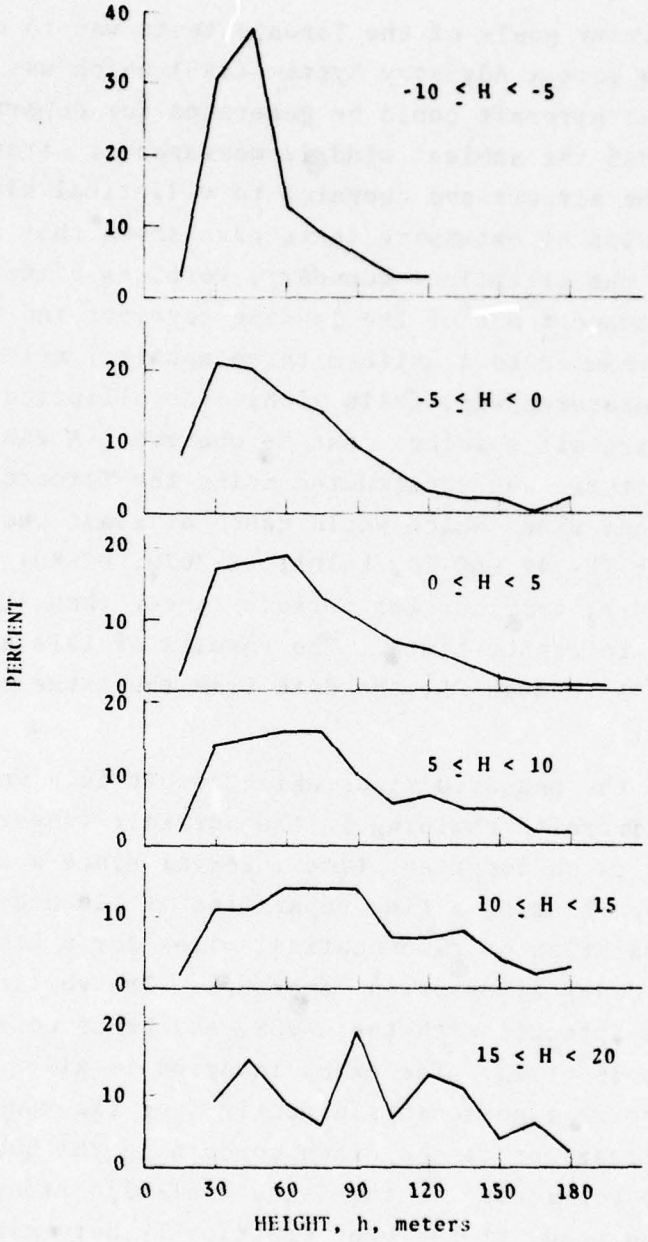


FIGURE 72. PERCENTAGE OF AIRCRAFT WHOSE HEIGHT IS BETWEEN h-15 AND h AS A FUNCTION OF THE HEAD WIND

higher altitudes as the total wind increases.

7.6 PREDICTIVE CAPABILITY AND SYSTEMS

One of the primary goals of the Toronto tests was to determine if an analog to the Vortex Advisory System (VAS) which was developed (Ref. 4) for arrival aircraft could be generated for departure aircraft. In the VAS the ambient wind is measured at strategic locations around the airport and compared to elliptical wind criteria. The results of extensive tests have shown that if the wind falls outside the elliptical boundary, vortices either decay very quickly or transport out of the landing corridor and the separation may be reduced to a uniform three nautical miles for all aircraft. If the measured wind falls within the elliptical boundary, normal aircraft spacings must be oberved. A VAS-type elliptical wind criteria was constructed using the Toronto data to determine the ambient winds which would cause at least one vortex of a Heavy aircraft (B-747, DC-10, L-1011, B-707H, DC-8H) to remain in the $\pm$200 ft ($\pm$60-m) corridor for periods longer than the 60-, 90- and 120-second reference times. The results of this analysis are shown in Fig. 73 through 75; the data from the three baselines have been combined.

Fig. 73 shows the measured winds which result in a vortex from a Heavy category aircraft remaining in the corridor longer than 120 seconds. This is an important time interval since a controller is given the option of using a time separation of 120 seconds or a radar distance separation of five nautical miles for a Large aircraft following a Heavy aircraft on departure. The vortices discussed herein were detected with the GWVSS, and hence no measure of vortex strength is given. The exact location is also not definable since there were no sensors directly over the runway. Therefore, no implications can be drawn concerning the hazard potential of these vortices. If the 5-nautical-mile radar separation criteria are used, it has been empirically determined that the time between takeoffs is in the region of 80 seconds. Since the data base does not permit obtaining results similar to Fig. 73 for 80 seconds, the closest possible value, 90 seconds, is plotted

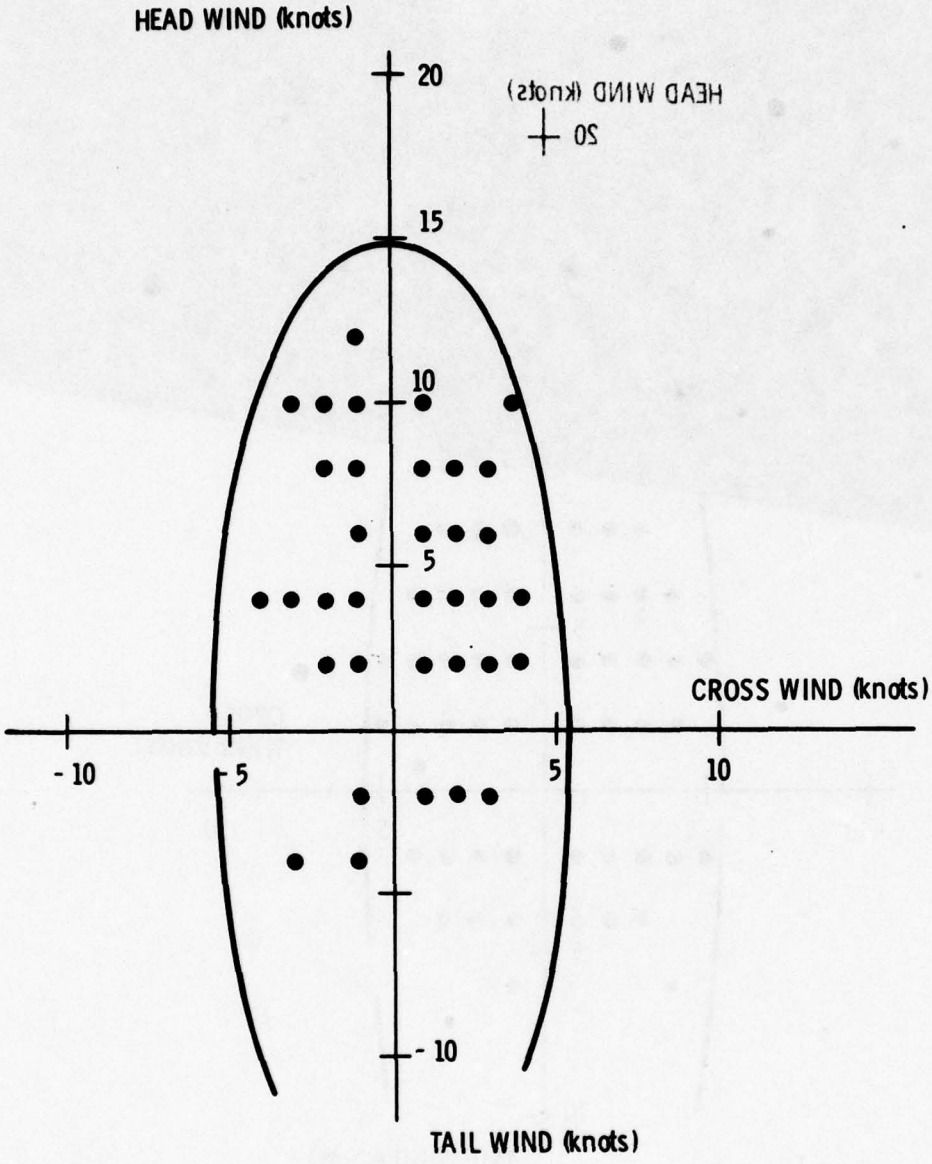


FIGURE 73. WIND CONDITIONS WHICH LED TO RESIDENCE TIMES IN EXCESS OF 120 SECONDS

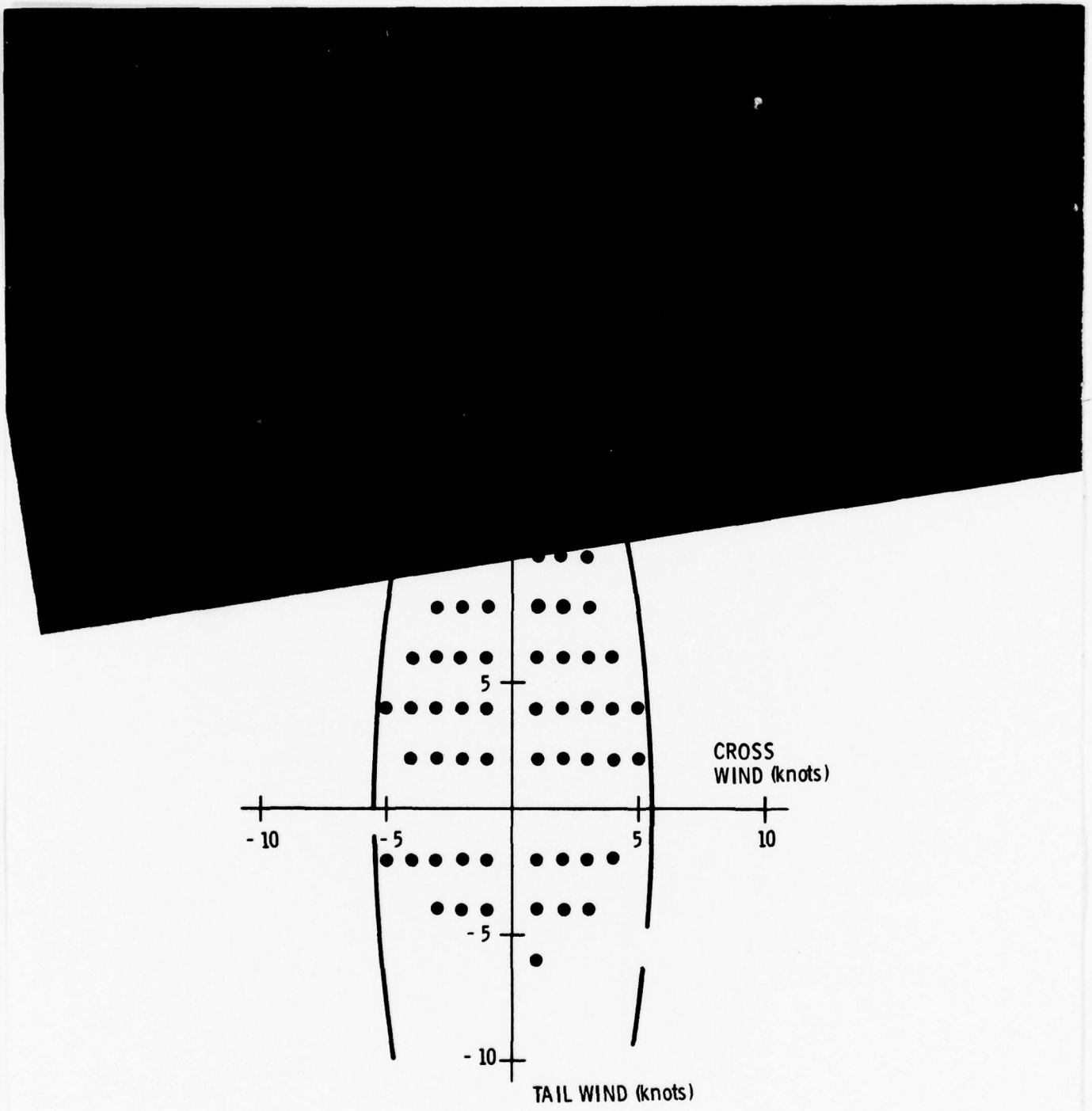


FIGURE 74. WIND CONDITIONS WHICH LED TO RESIDENCE TIMES IN EXCESS OF 90 SECONDS

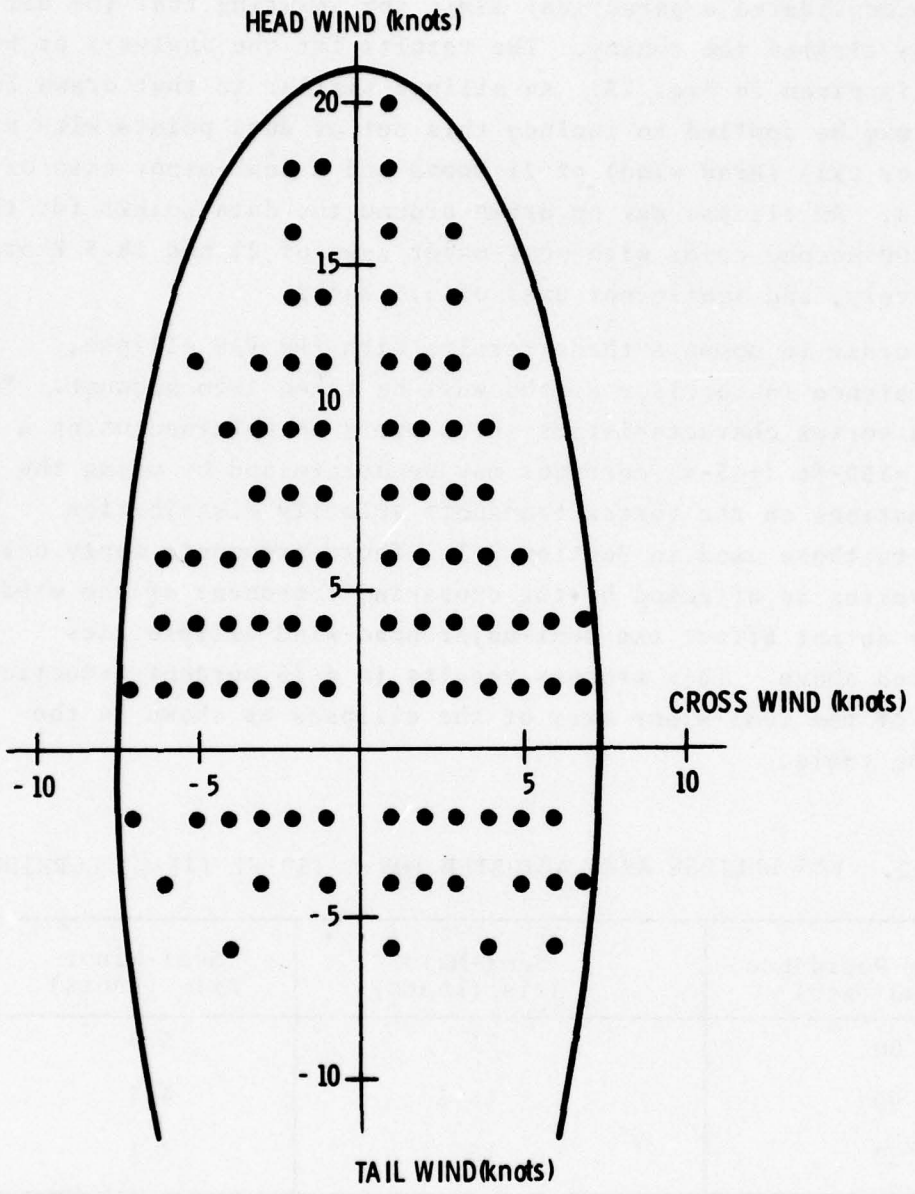


FIGURE 75. WIND CONDITIONS WHICH LED TO RESIDENCE TIMES IN EXCESS OF 60 SECONDS

in Fig. 74. Finally, if one were to consider reducing the separation time below 80 seconds, a logical choice would be 60 seconds which is considered a paractical limit for insuring that the aircraft has cleared the runway. The results for the analysis at 60 seconds is given in Fig. 75. An ellipse similar to that drawn for the VAS may be applied to include this set of data points with a semi-major axis (head wind) of 21 knots and a semi-minor axis of 7.5 knots. An ellipse may be drawn around the data points for the 60- and 90-second cases with semi-major axes of 21 and 18.5 knots, respectively, and semi-minor axes of 5.5 knots.

In order to compare these results with the VAS ellipse, the difference in corridor widths must be taken into account. The expected vortex characteristics which would be obtained using a smaller ±150-ft (±45-m) corridor may be determined by using the approximations on the vortex transport velocity distribution similar to those used in Section 7.3. These arguments apply only to the vortex as affected by the crosswind component of the wind and thus do not affect the semi-major head-wind ellipse axes calculated above. This process results in a 25 percent reduction in size of the semi-minor axes of the ellipses as shown in the following table:

TABLE 12. VAS ELLIPSE AXES ADJUSTED FOR A 150-FT (45-M) CORRIDOR

Vortex Residence Time (sec)	Semi-Major Axis (knots)	Semi-Minor Axis (knots)
60	21	5.6
90	18.5	4.1
120	15	4.1

If the data are plotted superimposed on the wind rose (Fig. 57), it can be shown that approximately 44 and 25 percent of the recorded winds lie outside the boundary enclosing the data points for the 90- and 60-second cases, respectively.

The probability of having a vortex from a Heavy aircraft remain in the corridor can be determined as a function of head-wind component. The total number of cases where the two vortices from the Heavy aircraft were observed with measured head winds and tail winds were 1534 and 476, respectively. The total number of cases where one vortex of this set was observed to remain in the corridor for at least 60 seconds with measured head winds and tail winds was 652 and 186, respectively. Therefore, the probability that a vortex will remain in the corridor for longer than 60 seconds is 0.43 (652/1534) for head-wind conditions and 0.39 (186/476) for tail-wind conditions. The following table lists this result together with those obtained for 90 and 120 seconds.

TABLE 13. PROBABILITY THAT A VORTEX WILL REMAIN IN THE CORRIDOR

TIME (seconds)	P_{head}	P_{tail}	P_{tail}/P_{head}
60	0.43(652/1534)	0.39(186/476)	0.91
90	0.20(313/1534)	0.19(90/476)	0.95
120	0.037(56/1534)	0.107(51/476)	2.89

The result of the analysis at 120 seconds corresponds with the result obtained from the tests on landing aircraft (P_{tail}/P_{head} = 1.6 (Heathrow) and 4.0 (Kennedy/Stapleton)). The results at 60 and 90 seconds, however, differ importantly from the landing tests with almost equal probability of a stalled vortex for both head and tail winds.

7.7 CROSSING VORTICES

Residence times are referenced to a 200-ft (60-m) corridor at each baseline. Because aircraft are at different altitudes over

each of the GWVSS baselines and because the lateral transport of vortices depends on both vortex height and cross wind, a vortex could exit the corridor on one side of the runway at one baseline and on the other side of the runway at another baseline.

The GWVSS data base was interrogated to find those cases where a vortex was on opposite sides of the runway at different baselines. The data were examined 30, 60, 90, 120, and 150 seconds after the aircraft passed the sensor lines. Instances of vortices detected on opposite sides of the runway occurred for 7.3 percent of the takeoffs after 30 seconds, 2.7 percent after 60 seconds, 0.6 percent after 90 seconds, 0.2 percent after 120 seconds, and never after 150 seconds. The maximum cross-wind component (V at 100-ft (30-m) height) was 10.7 knots at 30 seconds, 5.8 knots at 60 seconds, 4.2 knots at 90 seconds, and 2.3 knots at 120 seconds. MAVSS data for the 60-second and older cases were not available (cross wind in wrong direction for most of these cases), but the inherent longitudinal stretching of the vortex may be expected to weaken these vortices.

The VAS analog discussed in Section 7.6 indicates a cross-wind criteria in excess of the 5.8 knots found for the 60-second crossing. It is of note that the maximum cross-wind components for the crossing cases occurred for the Heavy category aircraft (primarily the B-747).

7.8 VORTEX BOUNCING

Vortex bouncing is the term applied to the situation where one vortex begins to rise shortly after being formed while the other vortex descends and levels off at about half a wingspan above the ground. Theories (Refs. 11, 13, and 14) speculate that a cross-wind shear is somehow responsible.

The MAVSS data were searched for thoses cases where a vortex was detected over at least three MAVSS sensors and photographic data were available to give the height of the aircraft as it passed the MAVSS array. The number of such cases was small as not only must the cross-wind component be such as to blow the vortex over

at least three sensors, but the aircraft must be low enough for the vortex to be detected and the vortex must not decay too quickly.

Fig. 76 to 78 show the variation in height of the vortices as a function of vortex age where the height of the aircraft as it passes the MAVSS array is denoted by h_o and the vortex height above the MAVSS antennas is denoted by h. When $h-h_o$ is positive, the vortex has ascended above the height of the vortex-generating aircraft. Four domains of h_o are considered: between zero and half the wingspan of the vortex-generating aircraft, between half and one wingspan, between one and two wingspans, and between two and three wingspans. Whenever h_o was at least two wingspans, the vortices always descended and began to level off at an altitude of about half a wingspan above the ground. Whenever h_o was between one and two wingspans, the vortices descended but at a slower rate (because the vortices are closer to the ground) and leveled off. Whenever h_o was between half and one wingspan, the vortices initially descended but then began to rise and sometimes rose above h_o. For the L-1011 cases shown, h_o equaled one wingspan; one vortex descended and the other initially descended but then began to rise. Whenever h_o was less than half a wingspan, the vortices consistently rose above h_o.

The closer the vortices are generated to the ground, the more the tendency for a vortex to rise. The rising of the low altitude vortices might be attributed to the downwash behind the aircraft acting as a reflector.

7.9 AIRCRAFT SEPARATIONS

The interdeparture time spacings were determined from the difference in successive triggers in the aircraft detectors. Presentation of the analysis depends on properly dividing the aircraft into classes which are meaningful in air traffic control (ATC). The Canadian ATC uses a system very similar to the U.S. as defined by Table 1. One difference is the definition of a "Heavy" and in particular for the DC-8 and B-707 aircraft. Rather than use the qualifier "capable of" a gross take-off weight in

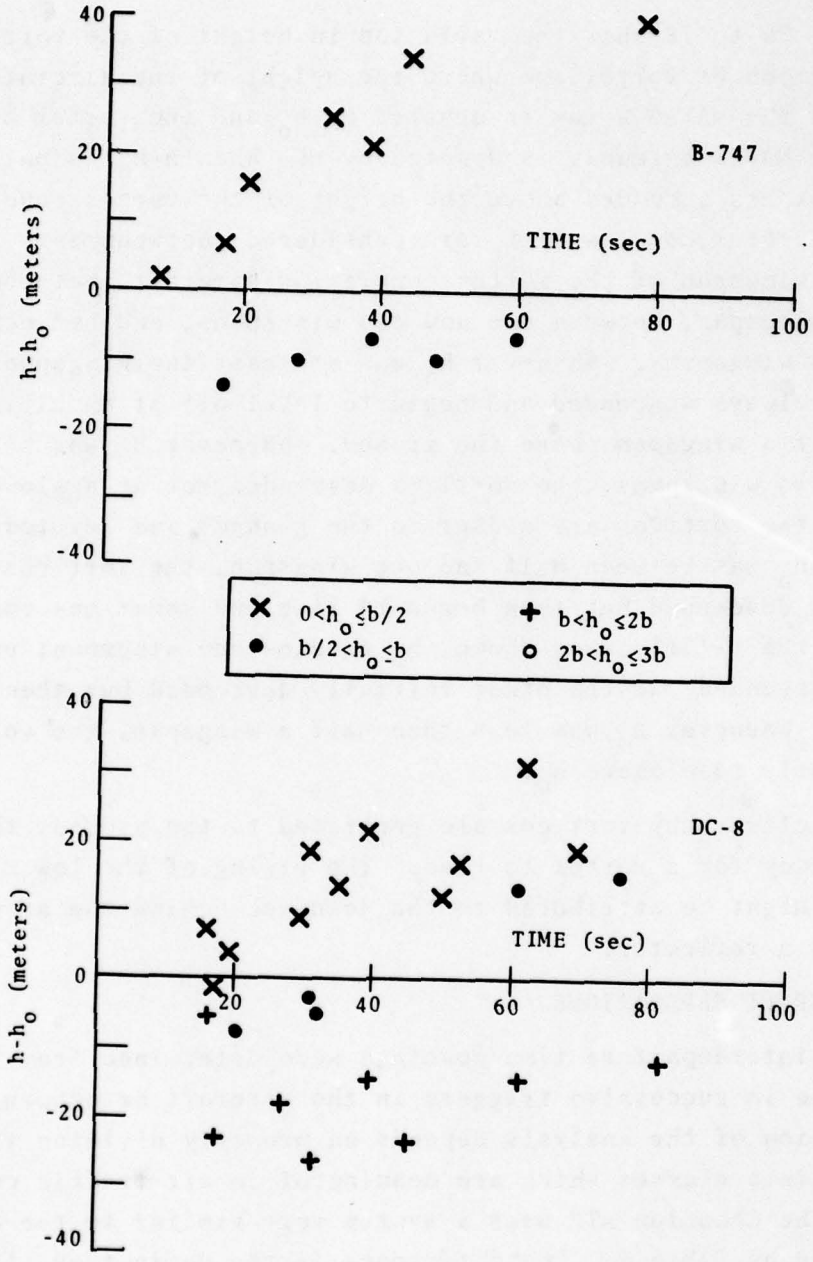


FIGURE 76. VORTEX HEIGHT VERSUS AGE FOR THE B-747 AND DC-8

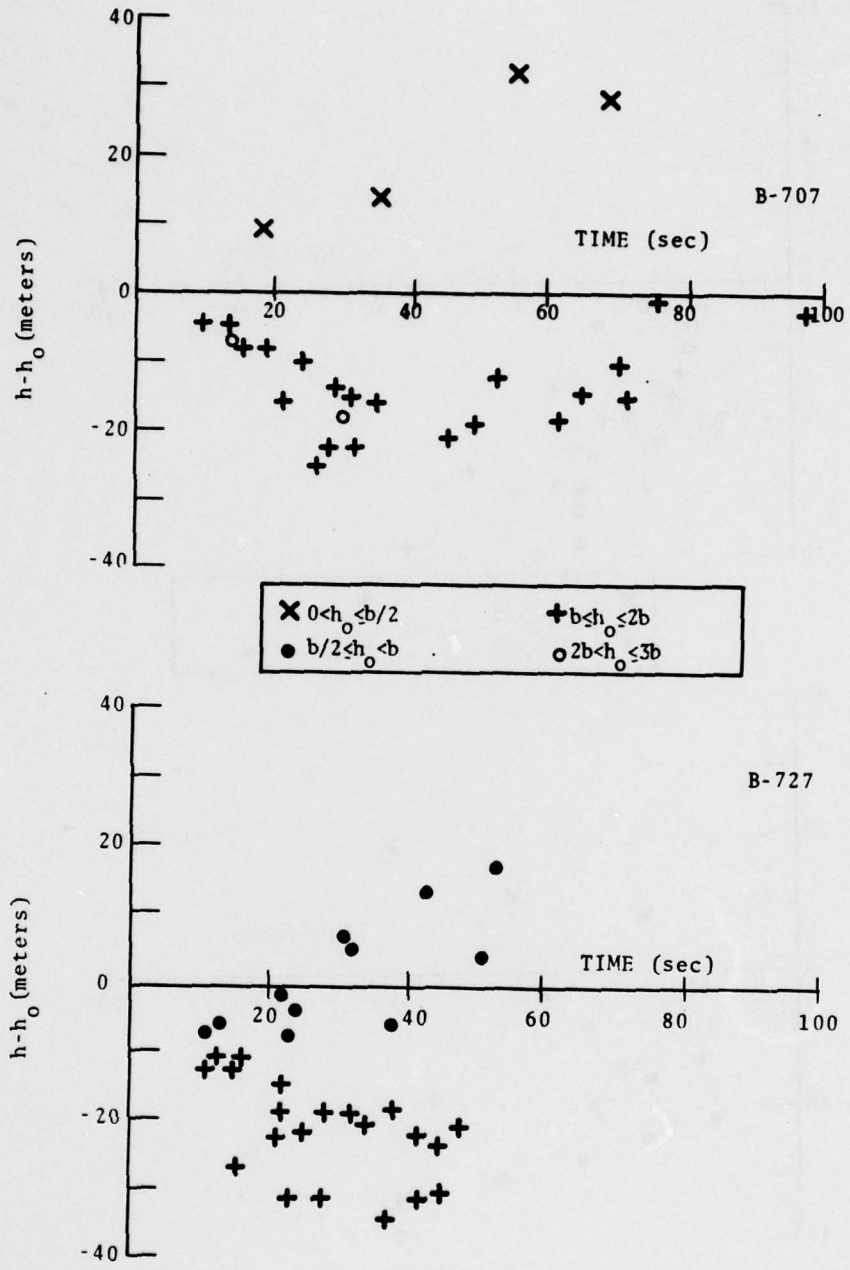


FIGURE 77. VORTEX HEIGHT VERSUS AGE FOR THE B-707 AND B-727

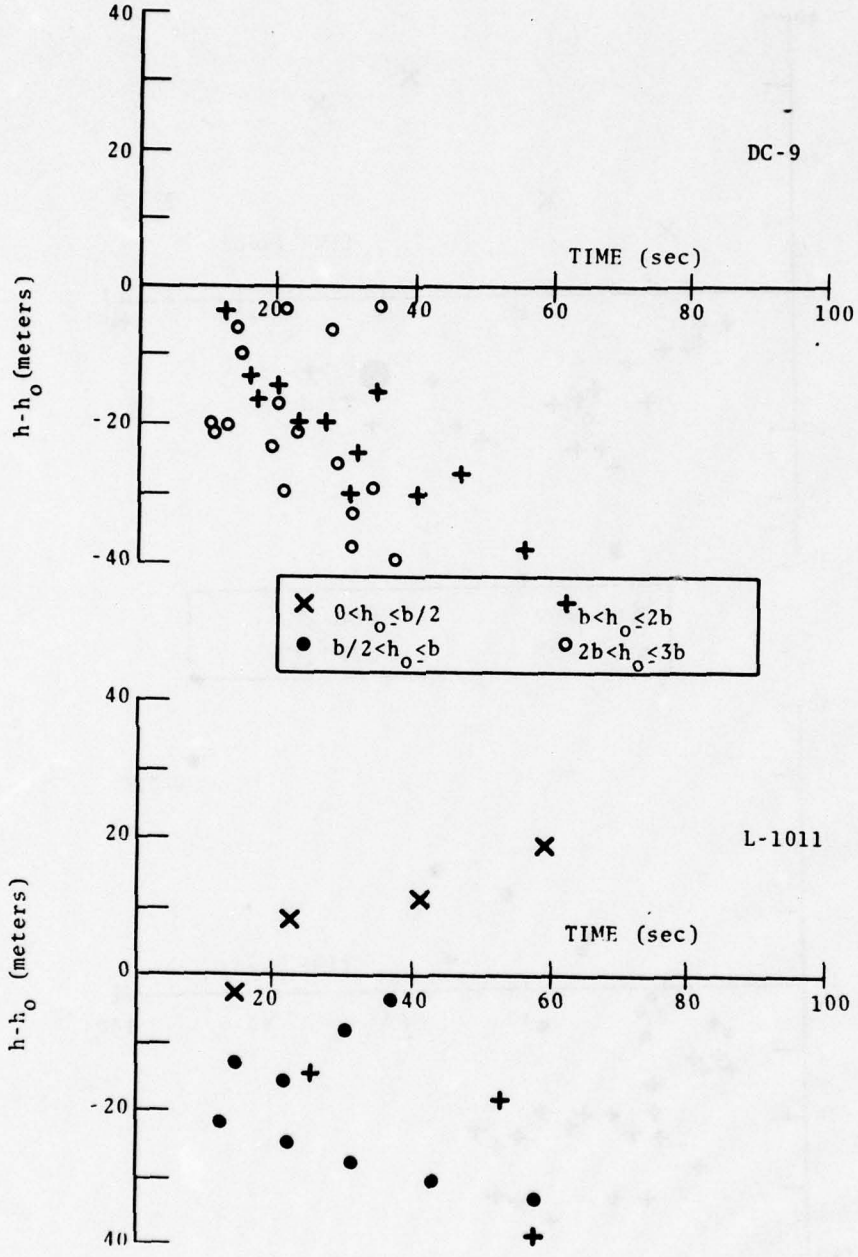


FIGURE 78. VORTEX HEIGHT VERSUS AGE FOR THE DC-9 AND L-1011

excess of 300,000 lbs (136,000 kgms), the Canadian ATC uses the criteria that the actual in situ weight of the aircraft must be in excess of 300,000 lbs (136,000 kgms). Thus, similar to the operations in the U.S., all "jumbo" aircraft (B-747, L-1011, DC-10) fall into the "Heavy" class but B-707's and DC-8's are divided into Heavy and Large. The 707-DC8 class difference was not available at the Toronto test site and as a result all B-707's and DC-8's were placed in the Heavy class for data analysis (it was empirically determined that Canadian air traffic controllers treat all departing B-707's and DC-8's as Heavies unless the pilot specifically alerted the tower that his aircraft qualified to be treated as a non-Heavy). The distribution of aircraft separation times is shown as a cumulative distribution in Figs. 79 and 80; the B-707 and DC-8 are included as Heavy aircraft.

7.10 VORTEX DECAY

The MAVSS was deployed to study the decay of vortices. Whenever a vortex passed over a MAVSS antenna, the vertical velocity field of the vortex was measured. The average circulation or strength of the vortices parameterizes the degree of hazard to a following aircraft; the average circulation may be used to quantitatively determine roll moments and roll rates an aircraft would experience if inadvertently caught in a vortex.

7.10.1 Average or Effective Strength

The measured vertical velocity distributions are used to calculate an "effective strength"--the strength of a line vortex which produces the same torque on an aircraft as the measured velocities produce. In other words, the first moment of the measured vertical velocity distribution is defined to be equal to the first moment of a potential or line vortex (Ref. 15):

$$\int_{-b/2}^{b/2} V_{\text{line vortex}} \cdot r \, dr = \int_{-b/2}^{b/2} V_{\text{doppler}} \cdot r \, dr$$

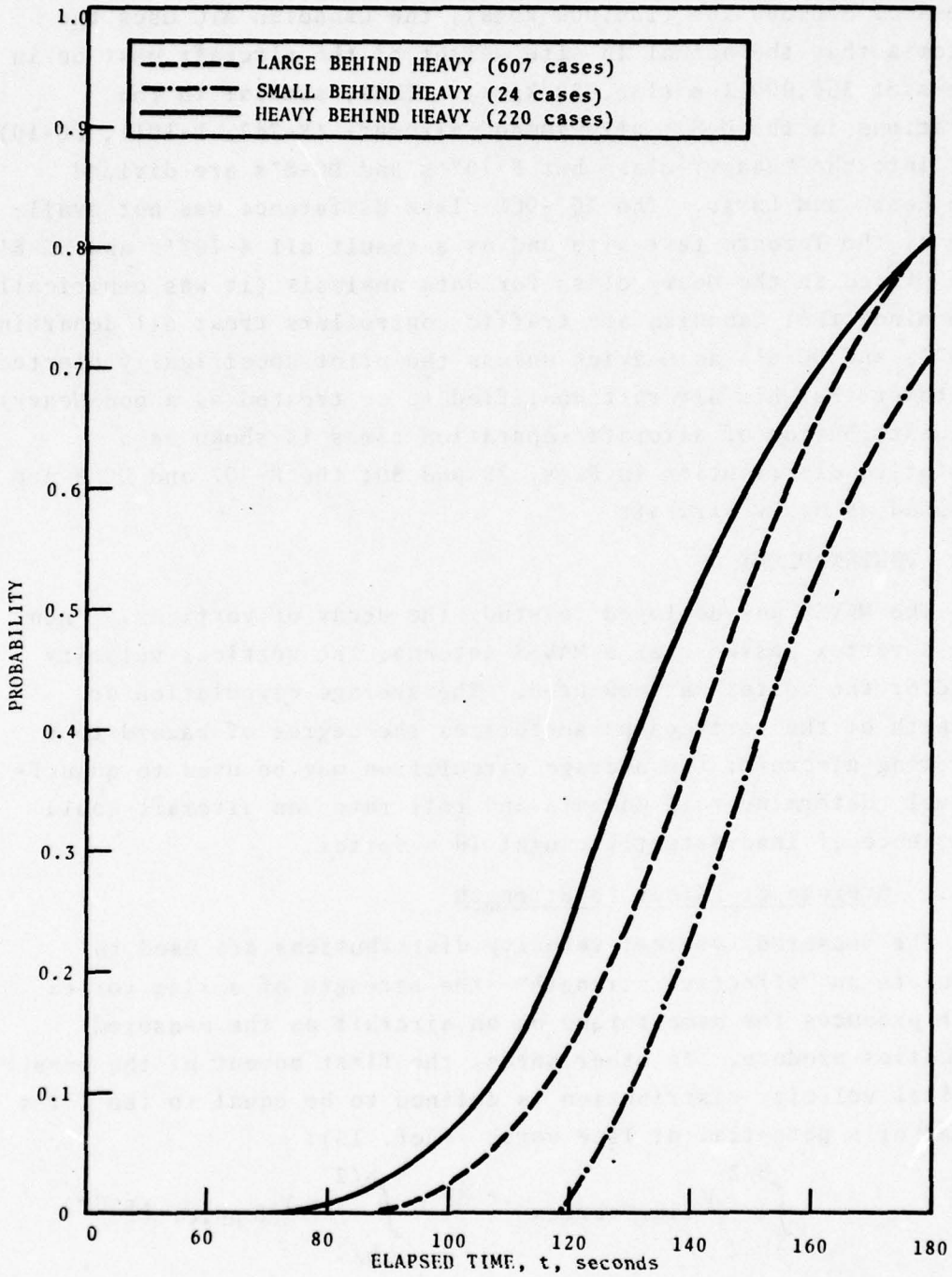


FIGURE 79. PROBABILITY THAT THE SEPARATION BETWEEN AIRCRAFT IS LESS THAN t FOR THE CASES WHERE A HEAVY WAS THE LEAD AIRCRAFT

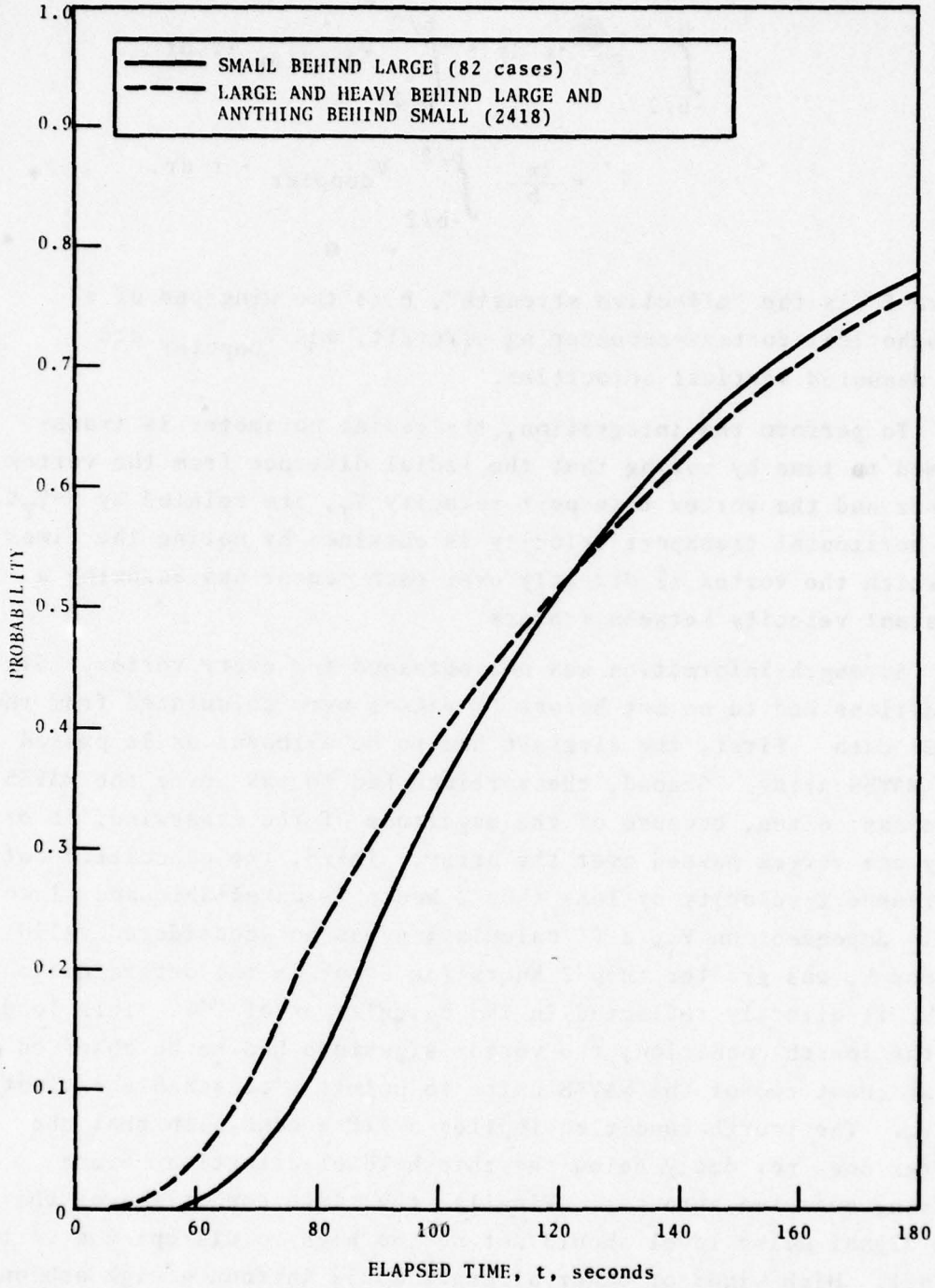


FIGURE 80. PROBABILITY THAT THE SEPARATION BETWEEN AIRCRAFT IS LESS THAN t FOR THE CASES WHERE THE LEAD AIRCRAFT IS EITHER LARGE OR SMALL

$$\int_{-b/2}^{b/2} \frac{\Gamma'}{2\pi r} \cdot r \, dr = \int_{-b/2}^{b/2} V_{doppler} \cdot r \, dr$$

$$\Gamma' = \frac{2\pi}{b} \int_{-b/2}^{b/2} V_{doppler} \cdot r \, dr,$$

where Γ' is the "effective strength", b is the wingspan of a hypothetical vortex-encountering aircraft, and $V_{Doppler}$ are the measured vertical velocities.

To perform the integration, the radial parameter is transformed to time by noting that the radial distance from the vortex center and the vortex transport velocity V_T, are related by $r=V_T t$. The horizontal transport velocity is obtained by noting the times at which the vortex is directly over each sensor and assuming a constant velocity between sensors.

Strength information was not obtained for every vortex. Six conditions had to be met before Γ' values were calculated from the MAVSS data. First, the aircraft had to be airborne as it passed the MAVSS array. Second, the vortices had to pass over the MAVSS antennas; often, because of the magnitude of the crosswind, no or only one vortex passed over the array. Third, the calculation of a transport velocity of less than 2 knots is unreliable and since Γ' is dependent on V_T, a Γ' calculation was not considered valid unless V_T was greater than 2 knots (an error in the determination of V_T is directly reflected in the calculation of Γ'). This leads to the fourth condition; the vortex signature had to be observed by at least two of the MAVSS units to permit a reasonable estimate of V_T. The fourth condition implies a fifth condition that the vortex does not decay below the threshold of detection before passing over two antennas. Finally, the sixth condition was that the signal noise level should not be too high to disrupt the vortex signal. High winds or other aircraft could introduce high ambient noise levels.

TABLE 14. MAVSS DATA BASE

AIRCRAFT TYPE	Number of Cases with Γ′ Evaluated at:			
	5 Meters	10 Meters	20 Meters	30 Meters
B-707	117	117	114	103
B-727	529	528	468	405
B-737	72	72	58	53
B-747	81	80	75	67
DC-8	480	478	438	375
DC-9	468	468	391	327
DC-10	60	60	56	51
L-1011	196	196	184	161
BAC-111	30	30	26	22
Other	7	7	7	7
TOTALS	2040	2036	1817	1571

Even with these limitations, Γ' data were obtained for 2040 aircraft (36 percent of the total number of aircraft recorded). Table 14 indicates the Γ' data by aircraft type. The table shows the number of cases for Γ' evaluated with b/2 of 5,10,20, and 30 meters (17,33,66, and 100 feet). The number of valid cases with b/2 of 30 m (100 ft) is usually less than the number for b/2 of 5 m (17 ft) as the signals from the outer portions of a vortex were sometimes indistinguishable from noise or corrupted by the presence of the other vortex.

Figure 81 shows a composite of all the B-707 Γ' data for the four selected b/2 values. If both vortices passed over four antennas, then eight data points will appear in the plot (four for the port vortex and four for the starboard vortex). Unless otherwise noted, the Γ' data to be discussed herein will be for b/2 of 20 m.

Figures 82 and 83 show the Γ' data for the various aircraft types. In general, it is noted that the average Γ' for a given time t increases with b/2. This indicates that the velocity field of a vortex extends to at least b/2 from the vortex center. These composite plots begin to indicate vortex decay; the older the vortex vortex, the lower the Γ'. Fig. 84 to 87 group the Γ' data into 20-second intervals and show the mean, maximum, and minimum values of Γ' in these 20-second intervals. The numbers above the maximum values are the number of cases in that interval. At least three cases were required. The mean values show the decay of strength with time. Note that for a given time interval the heavier the aircraft, the larger the mean Γ'. Gross takeoff weight appears to correlate strongly with the magnitude of Γ', as expected.

7.10.2 Vortex Decay Modes

Fig. 88 to 91 show individual cases of the decay of vortices. Γ' values are shown for b/2=5 m (the triangles), 10 m (the plus signs), 20 m (the X signs), and 30 m (the diamonds). The top graph in Fig. 88 exhibits a gradual decay with a halving of strength approximately every 60 seconds. The dissipation varies as t^{-1} and is probably a turbulent or viscous diffusion process.

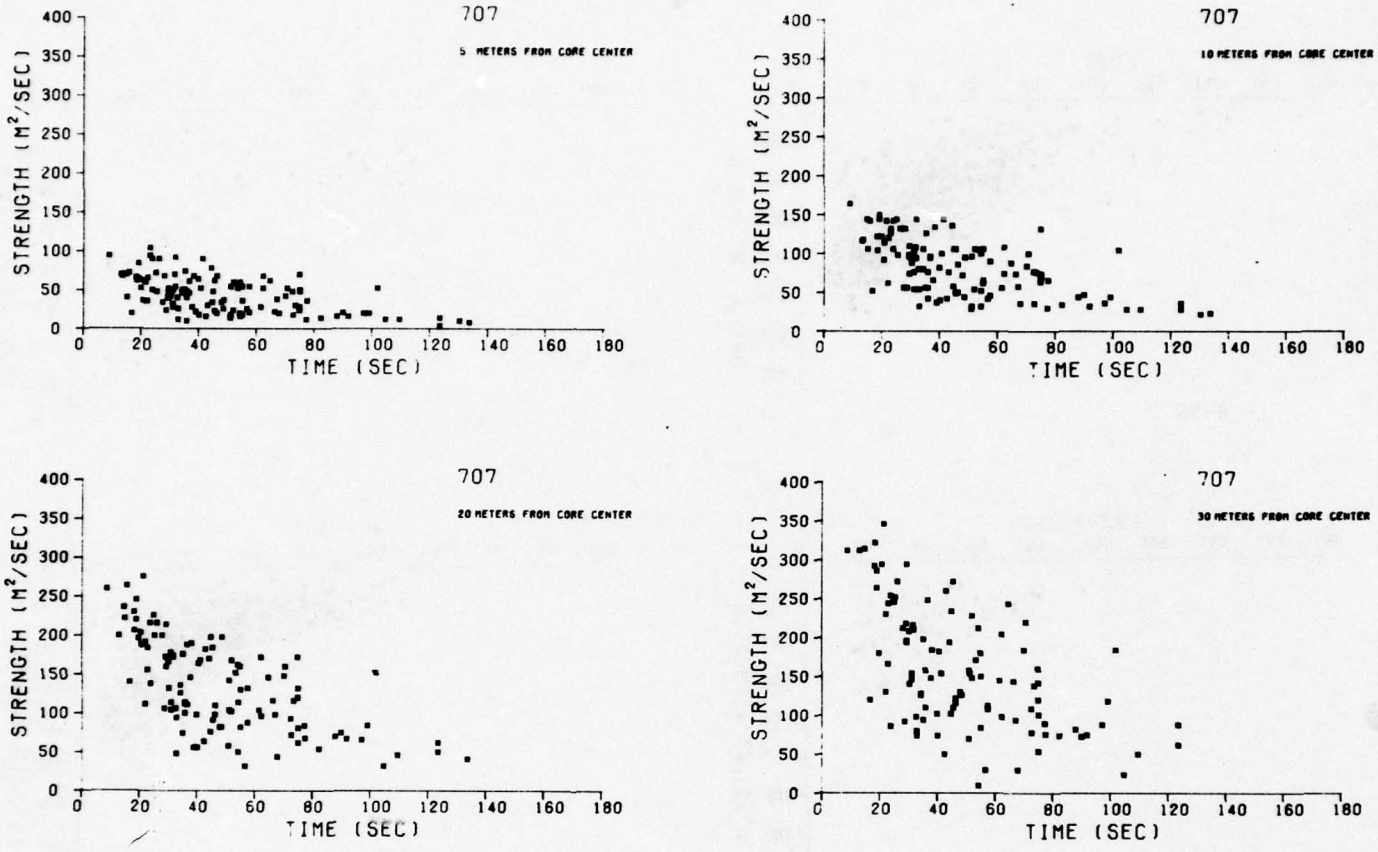
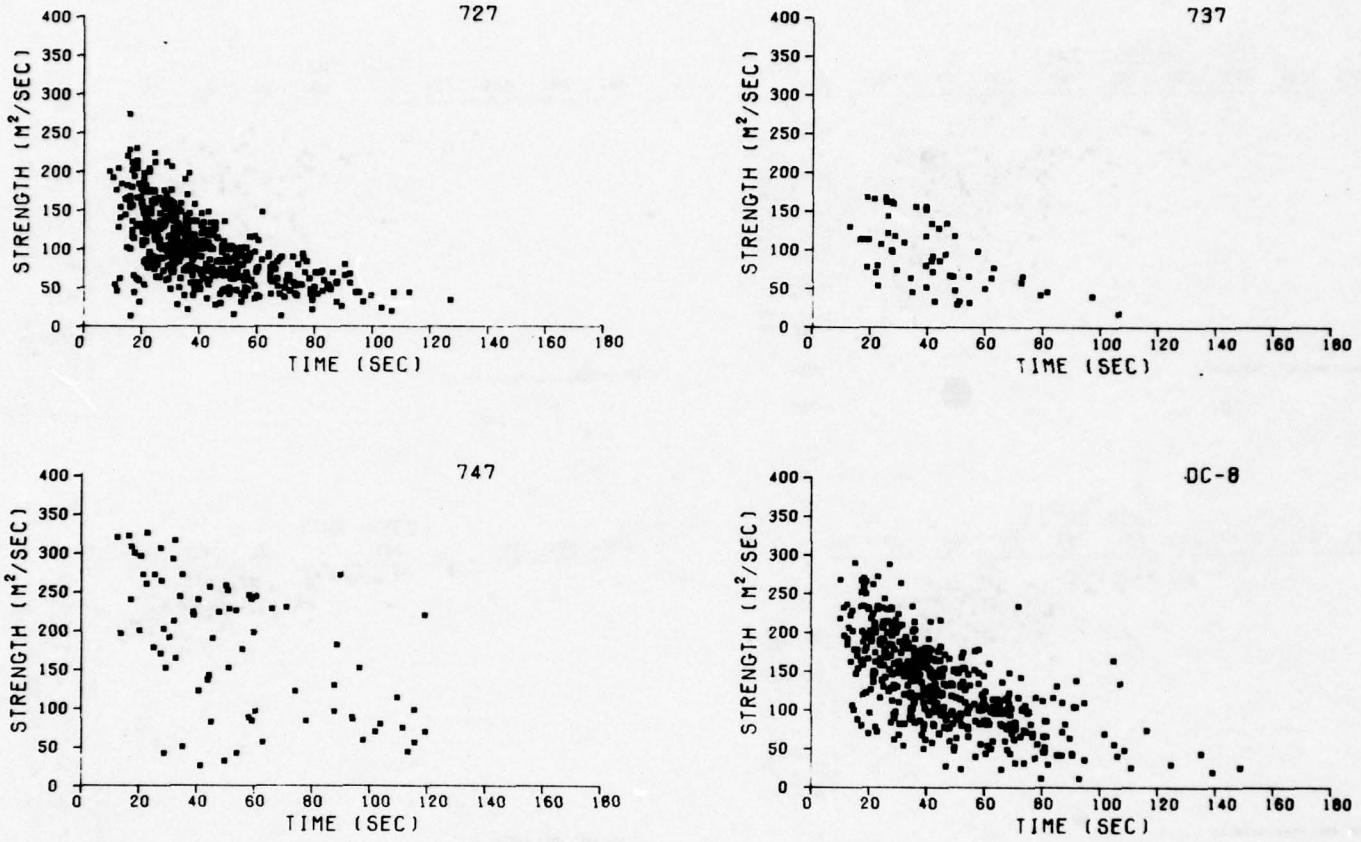


FIGURE 81. B-707 CIRCULATION FOR FOUR VALUES OF b/2



FIGUR E 82. CIRCULATION FOR THE B-727, B-737, B-747, AND DC-8, AVERAGED OVER A 20-METER RADIUS

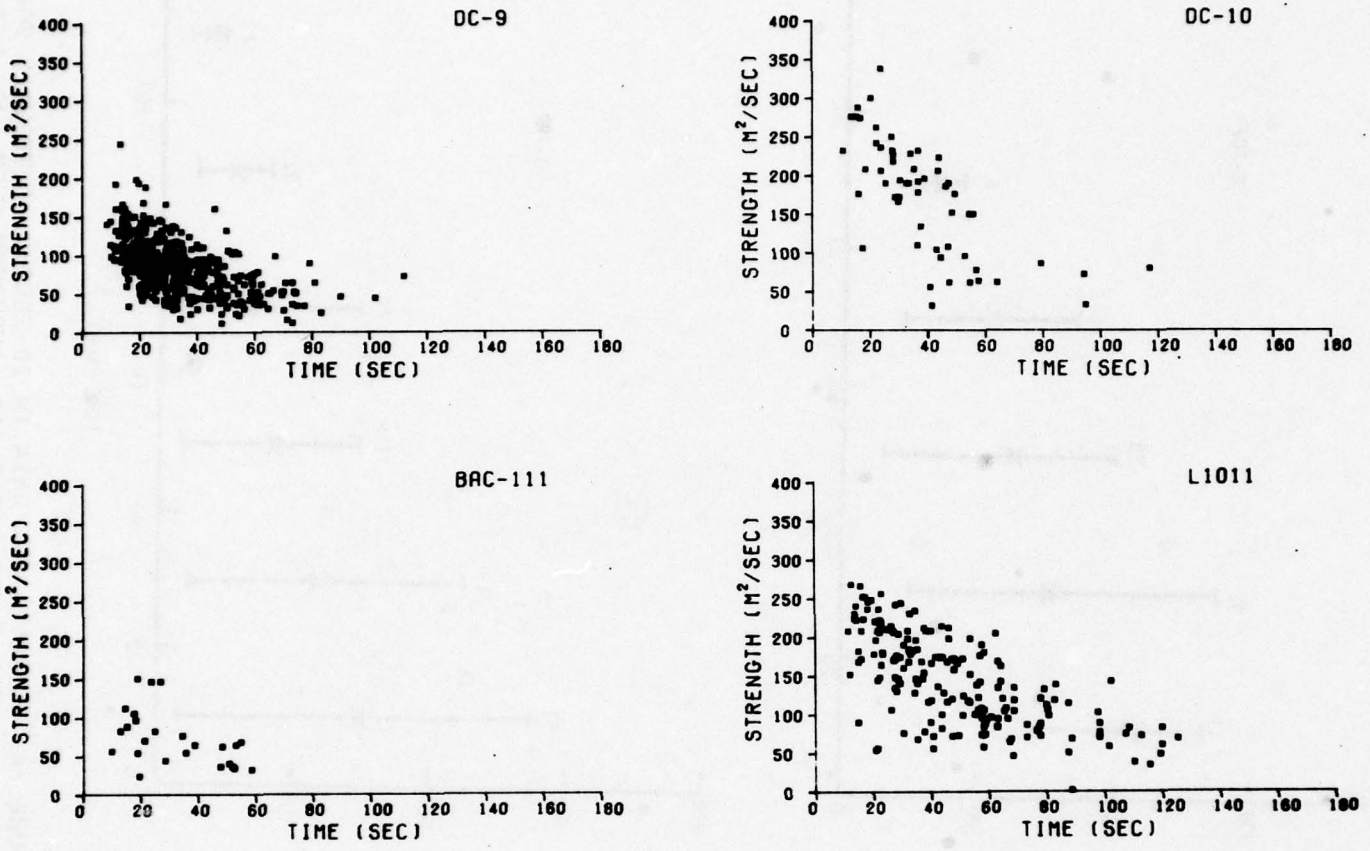


FIGURE 83. CIRCULATION FOR THE DC-9, DC-10, BAC-111, AND L-1011, AVERAGED OVER A 20-METER RADIUS

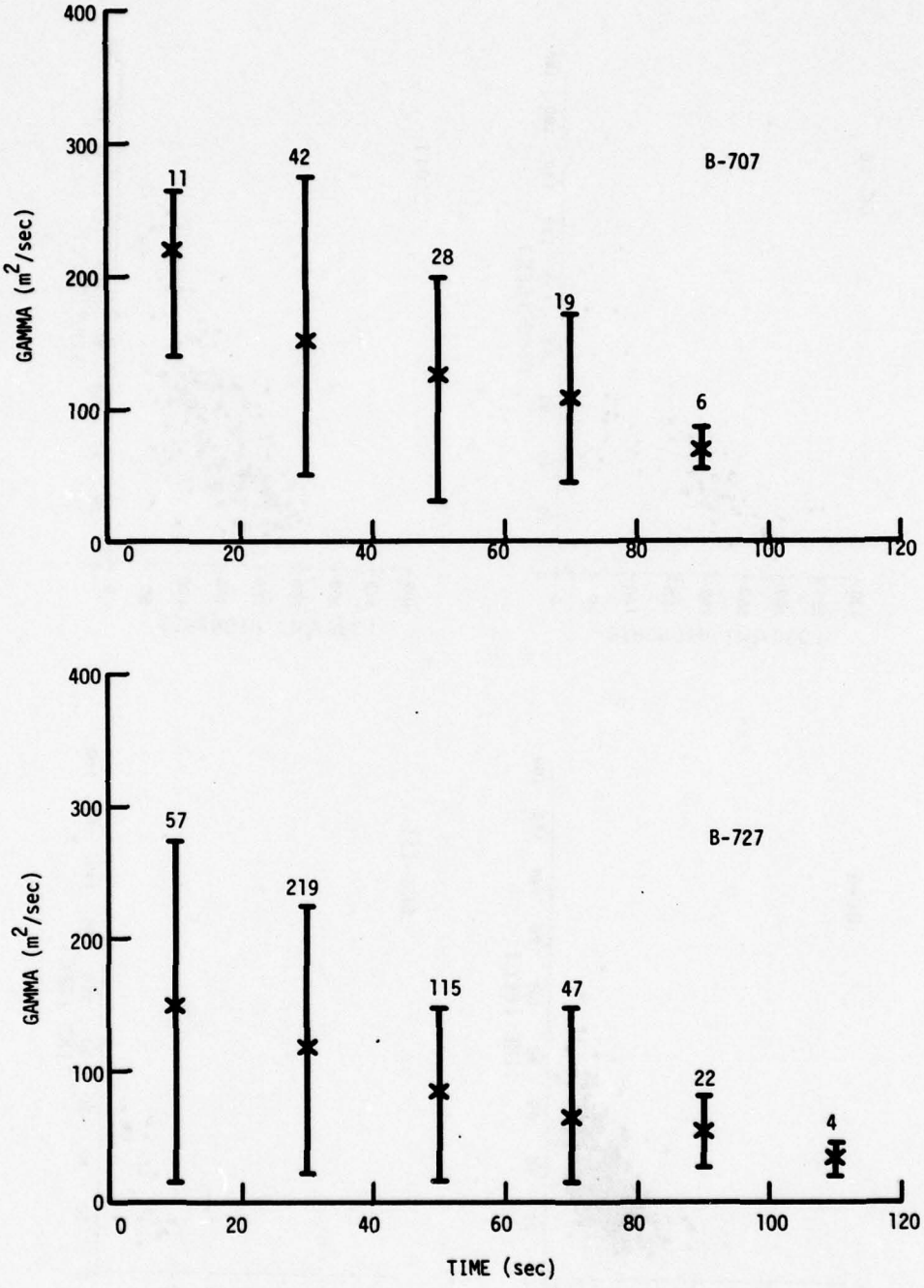


FIGURE 84. CIRCULATION DATA IN 20-SECOND INTERVALS FOR THE B-707 AND B-727, AVERAGED OVER A 20-METER RADIUS

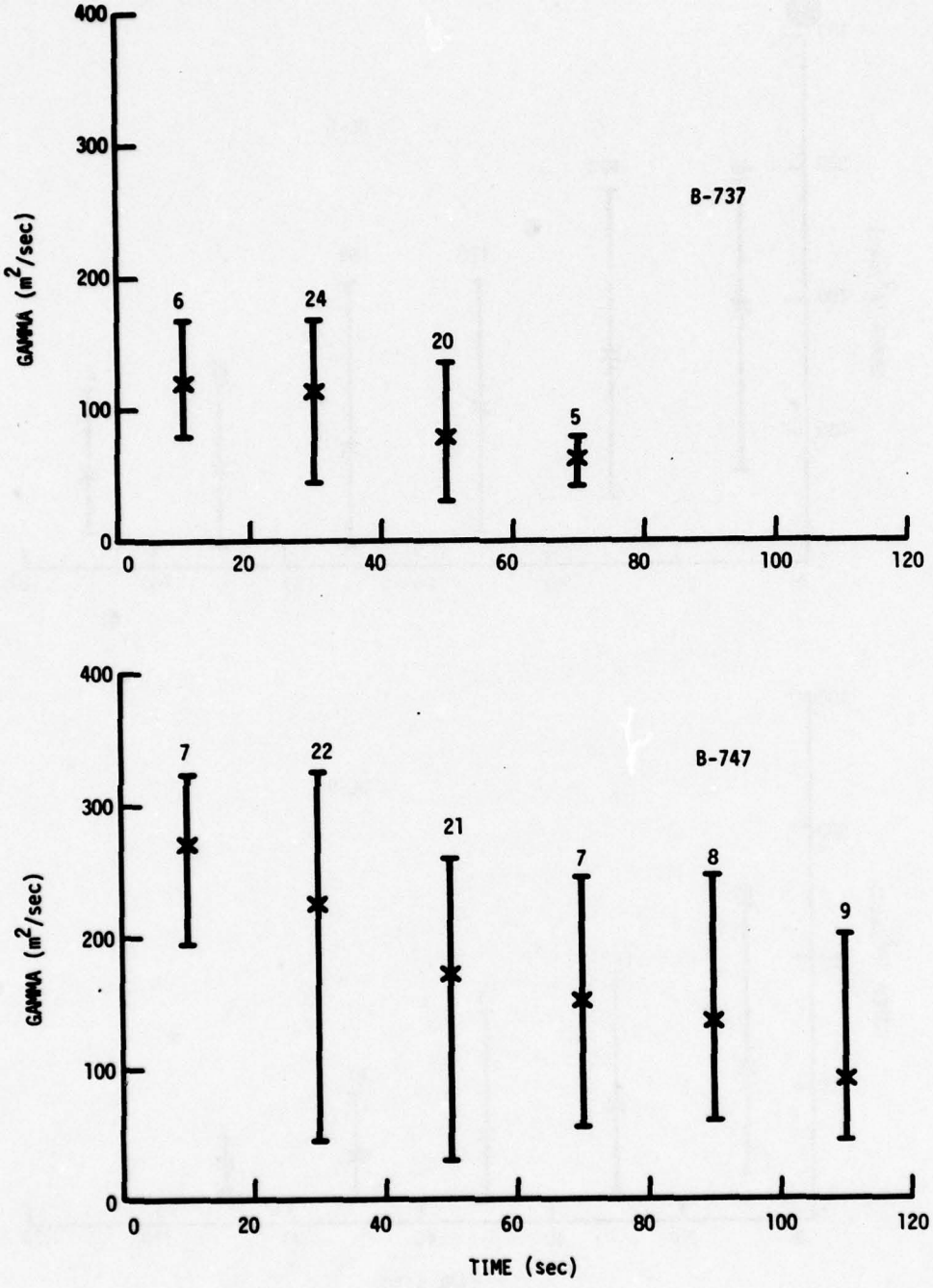


FIGURE 85. CIRCULATION DATA IN 20-SECOND INTERVALS FOR THE B-737 AND B-747, AVERAGED OVER A 20-METER RADIUS

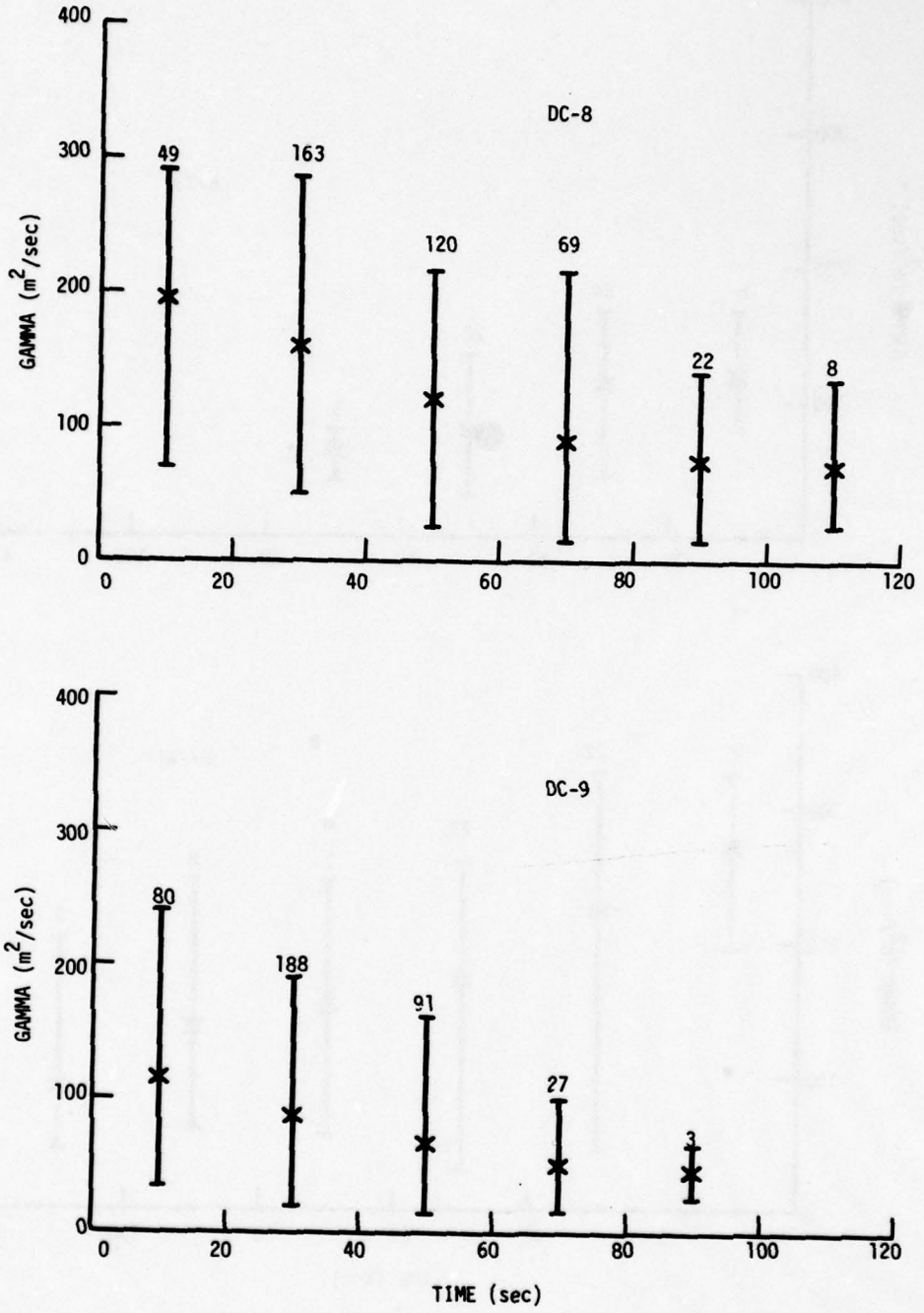


FIGURE 86. CIRCULATION DATA IN 20-SECOND INTERVALS FOR THE DC-8 AND DC-9, AVERAGED OVER A 20-METER RADIUS

But, note that the larger the b/2, the faster the decay--the decay is apparently taking place at the outer portions of the vortex. This is contradictory to current turbulent decay theories which predict decay to proceed from the inner portions to the outer portions. This inward decay was prevalent among the various cases and is an important new mechanism of vortex decay. Decay, here, refers to the change in strength for a given b/2 value. The total strength or energy of the vortex may not be decreasing, but the organized vorticity is spreading outward from the outer portions of the vortex. Thus, to an aircraft penetrating the vortex at various times, the vortex is effectively decaying.

The bottom graph of Fig. 88 displays a case where the strength rapidly decays. The strength decreases by a factor of two in approximately 15 seconds. It is suggested that this rapid decay may be caused by a sinusoidal instability in which the vortex has linked with its image vortex.

The top graph of Fig. 89 exhibits a third decay mode: the vortex undergoes a rapid decay which is curtailed leaving a relatively constant, but weaker, vortex in its stead. It is postulated that vortex breakdown, or core bursting, has occurred, leaving behind a remnant which interacts weakly with the atmosphere. The strength of the remnant correlates with the size of the vortex-generating aircraft: B-727 remnants (top of Fig. 89) are weaker than L-1011 remnants (bottom of Fig. 91).

Reference 15 found that the three decay modes (turbulent decay, sinusoidal instability, and breakdown) were about equally probable for landing aircraft. Although subject to much interpretation (and imagination), it appears that for takeoff vortices turbulent decay was the most probable form of decay followed by breakdown and sinusoidal instability; the probabilities were about 1/2, 1/3, and 1/6, respectively.

7.10.3 General Decay Model

The strength or circulation of a vortex decays with distance behind the vortex-generating aircraft, and the decay is influenced

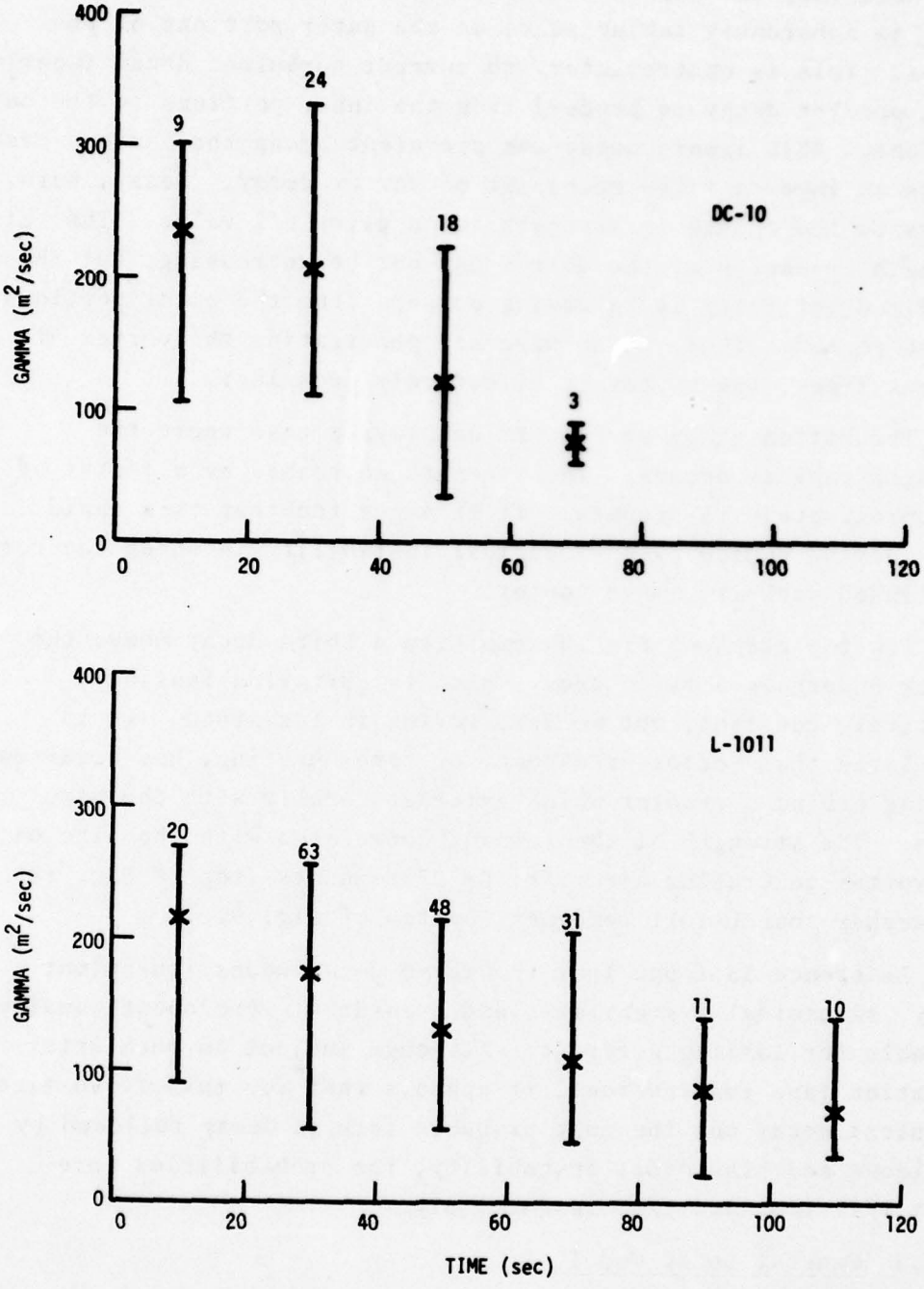


FIGURE 87. CIRCULATION DATA IN 20-SECOND INTERVALS FOR THE DC-10 AND L-1011, AVERAGED OVER A 20-METER RADIUS

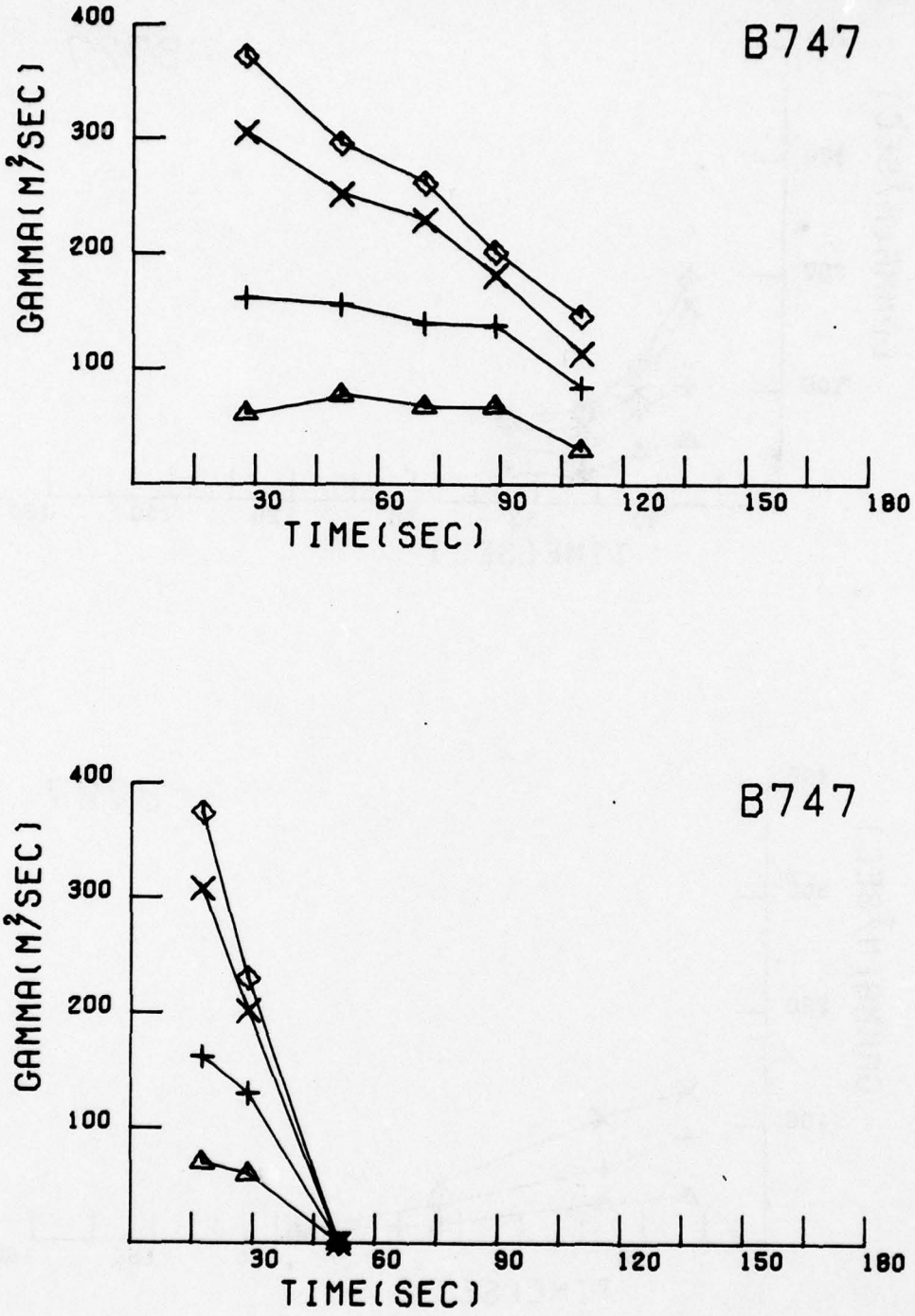
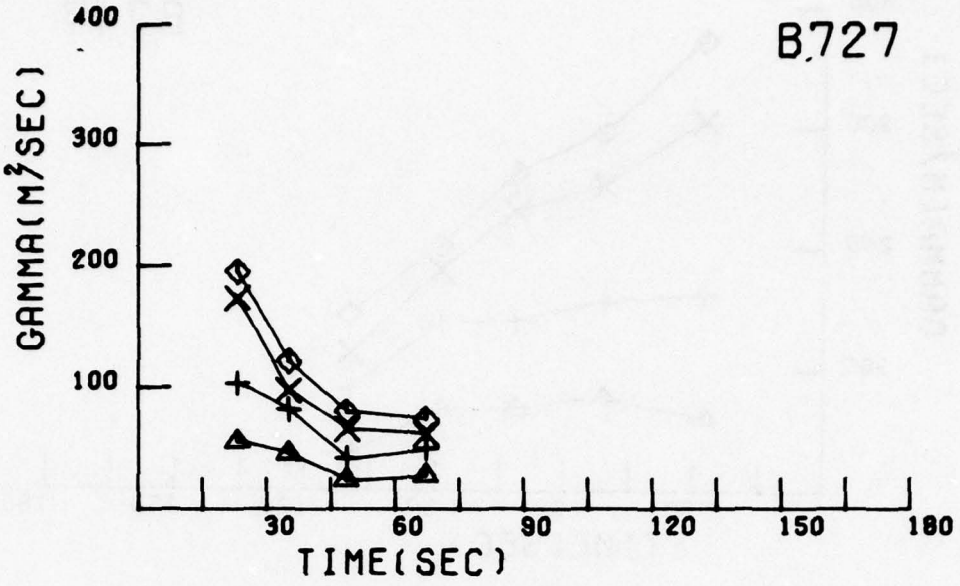


FIGURE 88. TWO EXAMPLES OF B-747 VORTEX DECAY. The four curves are for an average radius of 5, 10, 20, and 30 meters



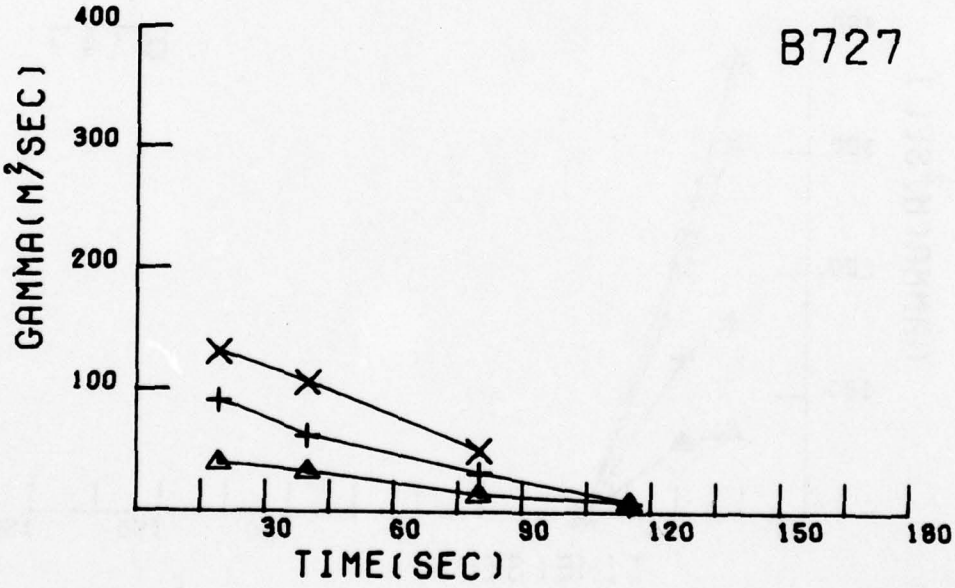
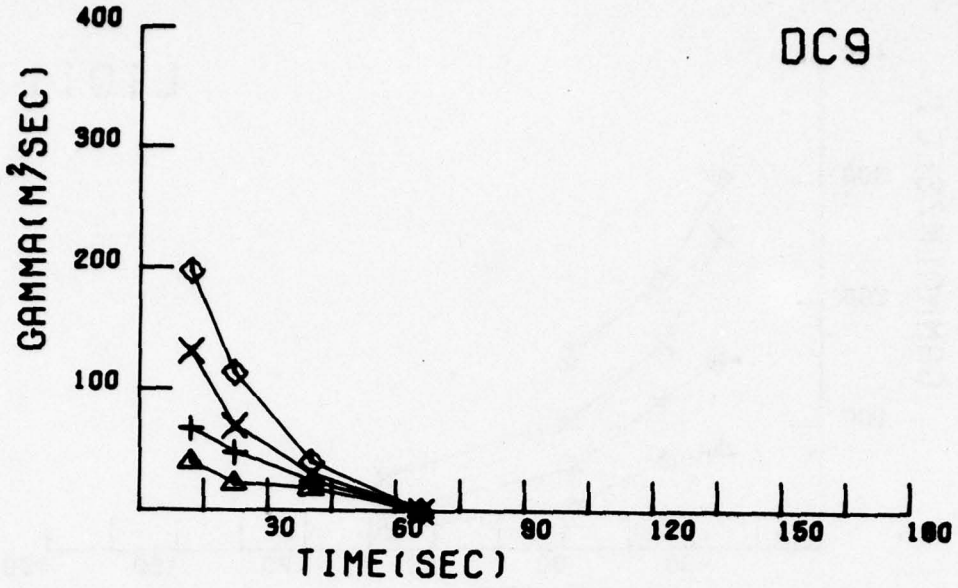


FIGURE 89. TWO EXAMPLES OF B-727 VORTEX DECAY.
The four curves are for averaging radii of 5, 10, 20 and 30 meters



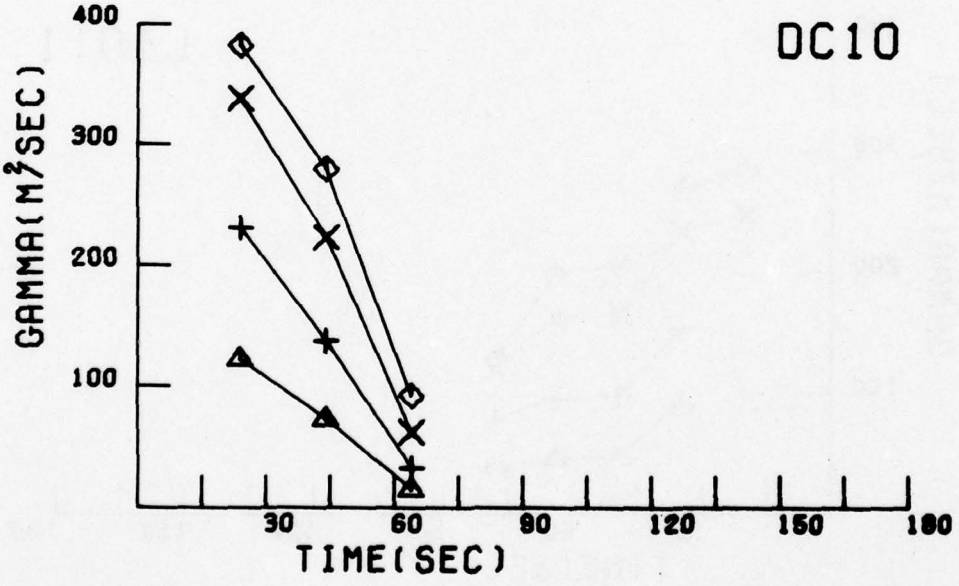
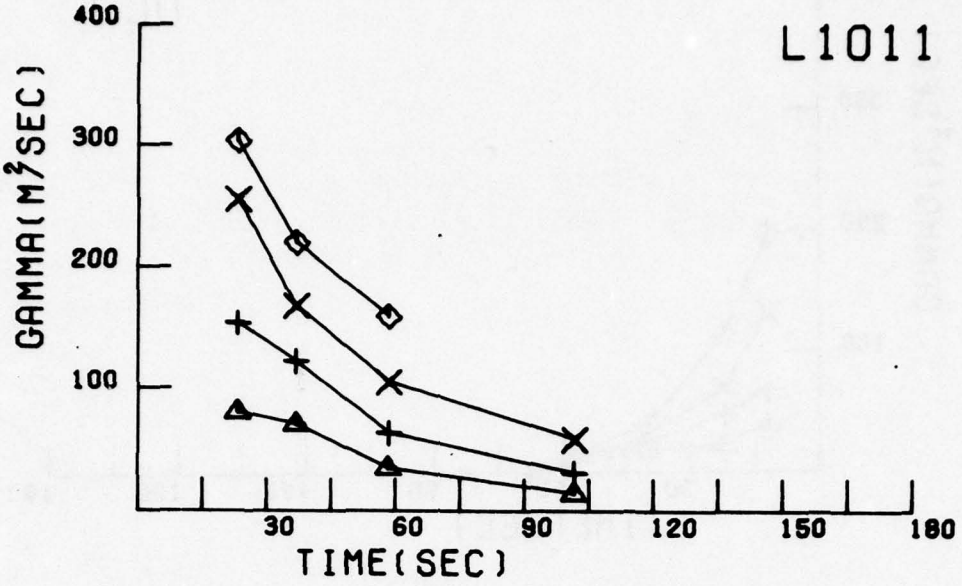


FIGURE 90. EXAMPLES OF DC-9 AND DC-10 VORTEX DECAY. The four curves are for averaging radii of 5, 10, 20, and 30 meters



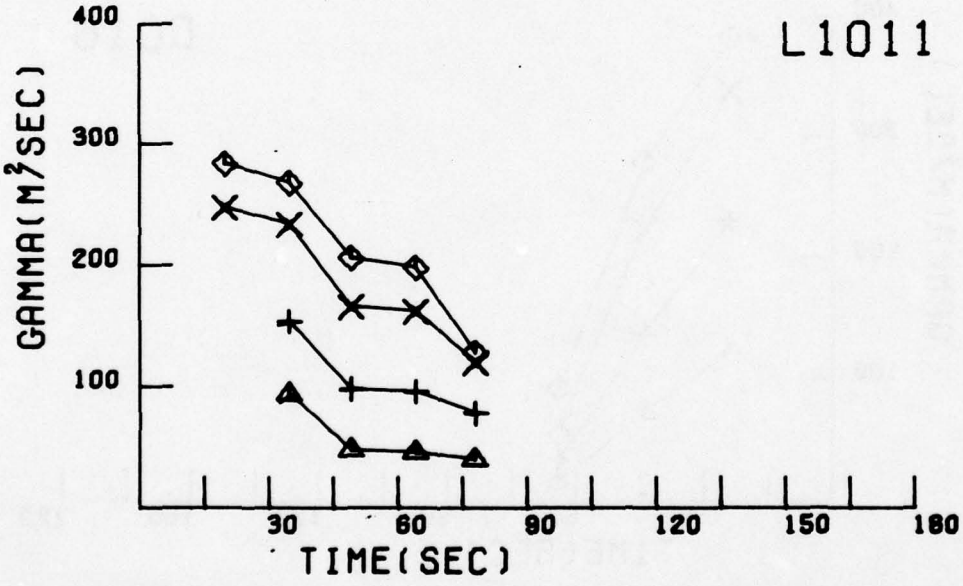


FIGURE 91. TWO EXAMPLES OF L-1011 VORTEX DECAY, The four curves are for averaging radii of 5, 10, 20, and 30 meters

by many factors. Close behind the aircraft the initial dispersion of the wake is governed by aircraft configuration, which includes aerodynamic geometry (particularly engine and flap placement) and thrust and flap settings. While the initial vortex-decay rate is configuration-sensitive, ultimately the decay rate must be determined by self-decay of the vortex pair coupled with atmospheric shear, turbulence, and stratification.

The MAVSS data were examined to see if a general decay function or model could be derived. Only the takeoffs for which three or more Γ' values were obtained were considered. Many functions were tried, but one model did fit the data quite well.

The circulation calculated for the vortex as it passes over the MAVSS sensor closest to the runway is defined as Γ_o . All circulation values are then normalized to Γ_o. The distance behind the vortex-generating aircraft is non-dimensionalized by multiplying the distance d by the aircraft's lift coefficient C_L and dividing by the product of the aspect ratio A and the wingspan b. By non-dimensionalizing the problem, the characteristics of each aircraft type are included as a normalization in the model. The distance d behind the aircraft is given by the speed of the aircraft (liftoff speed) times the vortex age as the vortex passed over the MAVSS sensor. The best data fit, in a least-squares sense, is

$$\frac{\Gamma'}{\Gamma_o} = \begin{cases} 1.0 & \frac{dC_L}{b\,A} \leq 10.0 \\ 10.0 \left(\frac{d}{b} \cdot \frac{C_L}{A} \right)^{-1} & \frac{dC_L}{b\,A} > 10.0 \end{cases}$$

Thus, Γ' is constant for dC_L/ba 10.0 (corresponding to a distance of up to 50 wingspans) after which Γ' dissipates as d^{-1} or $(\text{time})^{-1}$.

Constant circulation at short times/distances followed by a $(\text{time})^{-1}$ dependence was also found for the core circulation of a B-747 in landing configuration (Ref. 16). The "break" for the B-747 measurements occurred at about 33 wingspan lengths, somewhat

closer to the vortex-generating aircraft than the "break" found for the takeoff vortices. Other investigators (several papers in Ref. 17) have found slightly different shaped curves, but the main feature of constant circulation followed by decay appears consistent with all observations. Takeoff vortices, however, seem to begin to decay later than vortices shed by landing aircraft.

7.10.4 Probability Models for Vortex Decay

To determine the probability that a vortex will decay to a given Γ' in time t, the strength data were segregated by aircraft type and treated as an ensemble. The calculated values were connected by straight lines as in Figs. 88 to 91. The lines were extrapolated to t=0 by setting Γ' at t=0 equal to the first calculated Γ' value. By noting the time it took for the vortex to pass over the last two MAVSS sensors where the vortex was detected, the time when the vortex should have passed over the next sensor was extrapolated. The Γ' at this extrapolated time was defined as zero and a line was connected between this point and the last calculated Γ'. To calculate the decay probability, the ensemble of the straight-line segmented decay curves was examined in 10-second intervals.

The number of vortices having a Γ' greater than a limiting circulation, Γ_A, divided by the total number of cases of each aircraft type is defined as the probability fraction, $F(t,\Gamma_A,b)$, which depends on the vortex age and aircraft wingspan. The probability fraction is plotted for four values of Γ_A (50, 100, 150 and 200 m^2/sec) in Figs. 92 and 93. As an example, the probability that the strength of a B-707 vortex is at least 100 m^2/sec after 70 seconds is 0.22. After some initial time, the probability curves assume the form of a single straight line which can be represented by the exponential e^{-Bt}, where B is the decay rate. The slopes of the curves are approximately the same, regardless of aircraft type. Thus it appears that the decay rate of takeoff vortices is only weakly (if at all) dependent on the aircraft which generated the vortices. However, the initial time at which the probability

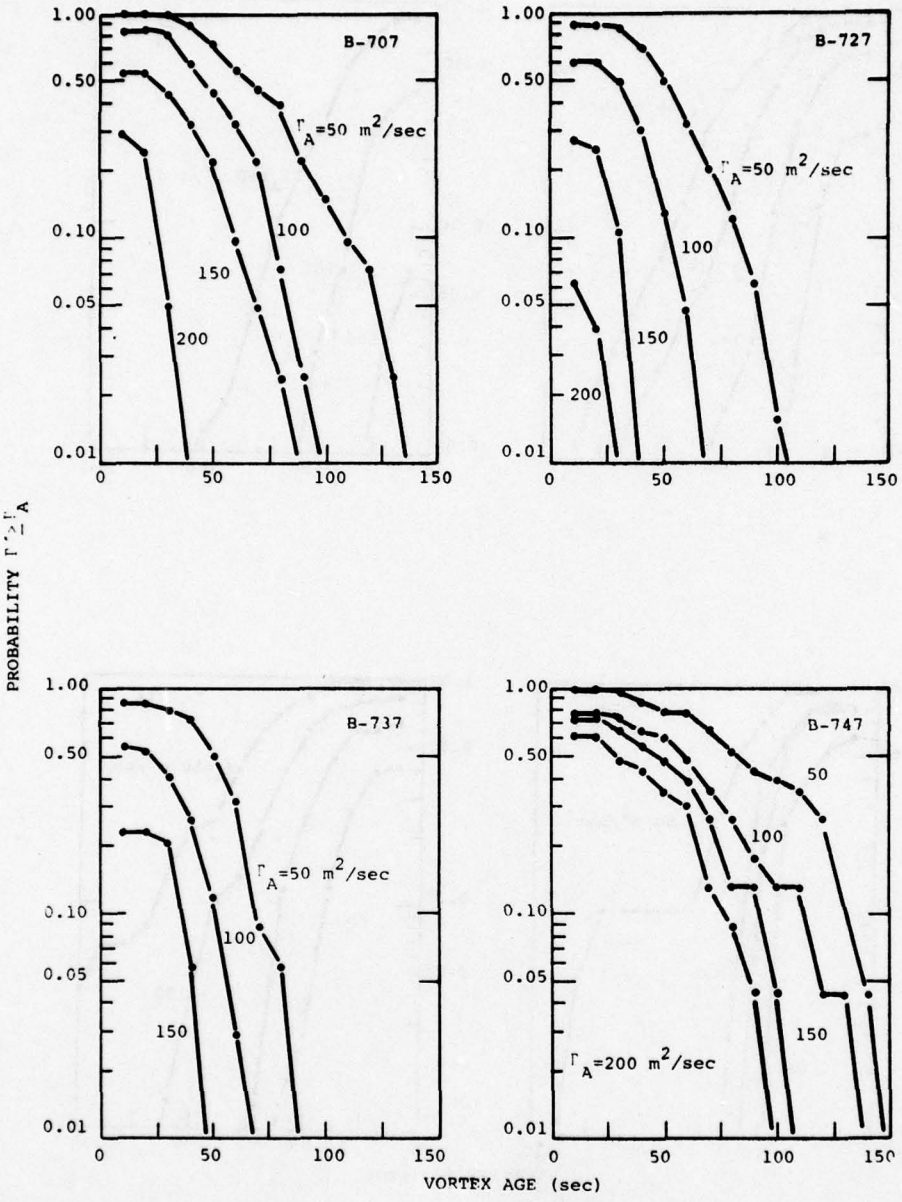


FIGURE 92. VORTEX-STRENGTH PROBABILITY OF DECAY VERSUS TIME FOR B-707, B-727, B-737, AND B-747

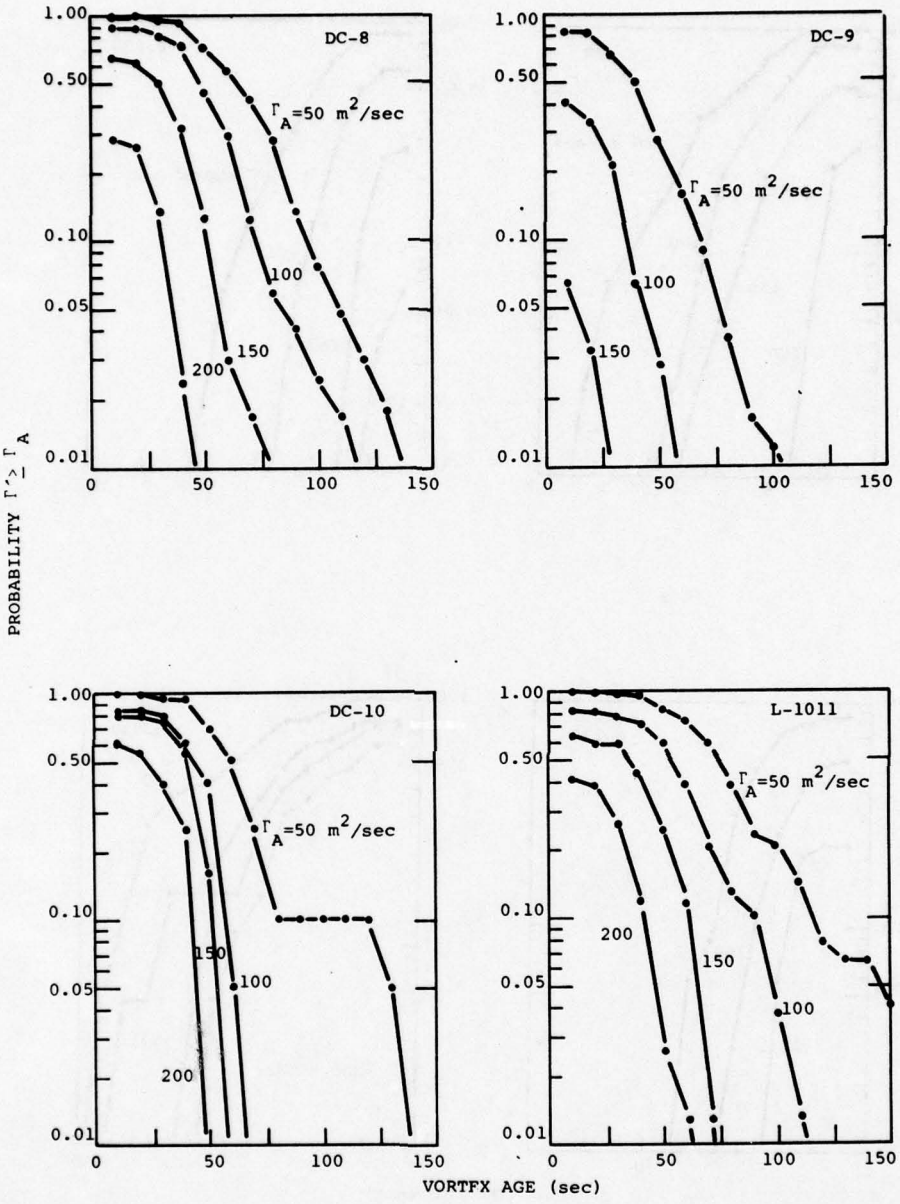


FIGURE 93. VORTEX-STRENGTH PROBABILITY OF DECAY VERSUS TIME FOR DC-8, DC-9, DC-10, AND L-1011

curves could be approximated with a straight line does depend on the aircraft type--the heavier the aircraft, the older the vortex before the onset of the final exponential decay. For example, the final exponential decay for Γ_A=100 m^2/sec begins at about 110 seconds for the B-747, 70 seconds for B-707, and 40 seconds for the B-727. (The discontinuity in the DC-10 curve for Γ_A=50 m^2/sec can be attributed to poor statistics--there were only 3 cases where Γ' exceeded 50 m^2/sec between 80 and 110 seconds).

An indication of the functional dependence of the initial portions of these curves can be obtained by plotting the probability function as a function of the square of the age as shown in Fig. 94. These curves also tend to take the form of a straight line leading to the conclusion that $F(t,\Gamma_A, b)$ has the form $\exp(-B\Gamma_A t^2)$ for this region of the curve.

7.11 LASER DOPPLER VELOCIMETER

In general very little quantitative information was obtained from the three series of laser tests conducted at Toronto Airport.

7.11.1 Ravine Site

The lack of data yielded no reportable quantitative results from the analysis of the data collected at this site.

7.11.2 Finger-Scan Tests

Vortex tracks were generated for many of the takeoffs. Since the van was midway between two of the GWVSS lines, there was little information to be obtained by comparing tracks from two systems. In addition, the time period was at the beginning of the program before all the subsidiary equipment was operating properly. Since reduction of the laser data was time consuming (both labor and computer time), the reduction and subsequent analysis were limited.

Circulation values were calculated for a few cases as a cross check on the MAVSS. Vortices were noted to stall in the vicinity of the runway, but analysis of stalling vortices was postponed until the second series of LDV measurements.

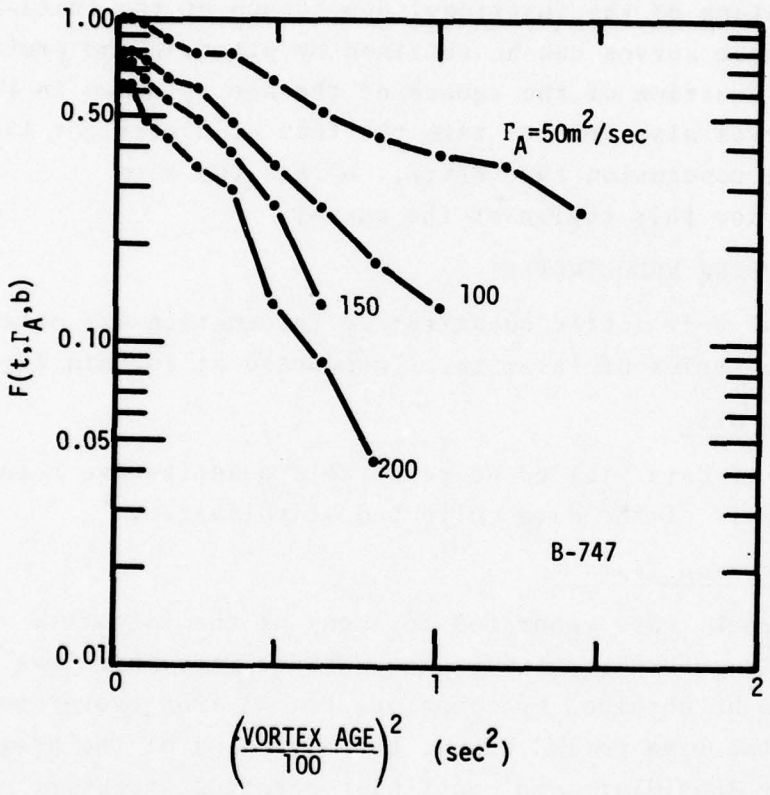


FIGURE 94. FRACTION OF VORTICES WITH A Γ' GREATER THAN A LIMITING CIRCULATION

7.11.3 Arc-Scan Tests

The GWVSS data were analyzed first to determine which LDV runs to analyze. Eighty-eight stalling or partial stalling cases were identified from the GWVSS data, and the corresponding LDV runs were processed.

It was difficult to distinguish a stalled vortex when the nonstalling vortex was moving toward the LDV. In this situation, the laser beam passed through the translating vortex to a focal volume at the stalled vortex, and the back-scattered energy returned through the moving vortex to the LDV. Perhaps the spectra from the two vortices are mixed enough to make signatures difficult to recognize.

The partial stalling cases were examined first. A partial stalling case is one where a vortex is first detected by the GWVSS on one side of the runway, then the vortex apparently moves back over the runway and sometimes appears to emerge on the other side of the runway. The cases where the vortices apparently crossed over the runway according to the GWVSS data were shown by the LDV data to have indeed done just that. The LDV data confirmed the GWVSS analysis. At times the vortex did not reappear after the signal was lost by the anemometer nearest the runway; the LDV data showed that about half the time the vortex moved over the runway and decayed. The estimate of the vortex life for these cases based on GWVSS data alone was found to be about 20 seconds too short on the average. For the other half of the time, the vortex apparently decayed over/near the anemometer nearest the runway.

The stalling cases were examined next. These cases were characterized in the GWVSS data by one vortex moving off (away from the runway) and the other vortex never being detected. The LDV data showed that a vortex was present near or over the runway and, hence, not sensed by an anemometer. In this situation, the longest time that the LDV continued to detect a vortex was 65 seconds. Although this is a relatively short time, the few cases do not rule out the possibility that vortices could persist in the area for longer times.

8. CONCLUSIONS

The Toronto joint TSC/FAA/MOT project must be considered a success. Over 5000 takeoffs were monitored and the data produced valuable information on vortex dynamics and decay. A wind criterion analogous to that of the Vortex Advisory System has been tentatively identified which could permit reduced longitudinal spacings between departing aircraft. Since the project examined vortex behavior in a regime where only meager information existed (takeoffs), it is not surprising that new effects were also found.

Capacity restrictions due to wake-vortex-imposed separations are a major contributor to traffic delays at the large airports. The Vortex Advisory System should decrease delays through reduced interarrival times; the data collected at Toronto indicate that a similar system for reducing inter-departure times is possible. Additional data will be required, however, as the over 5000 takeoffs do not contain a sufficient number of Heavy aircraft to be statistically significant for a safety-related program.

The study of vortex decay has indicated that the same decay mechanisms are taking place for takeoff vortices as for landing vortices, but the relative frequencies of the three mechanisms are different. Turbulent decay seems to be the dominant mechanism; a new finding which will revise interpretation of turbulent decay theories is that the decay takes place from the outer portions of the vortex towards the center (not vice versa as existing theories predict). The McGowan vortex lifetime curve, which has been extensively employed in the literature, has been revised as a result of the Toronto tests.

Takeoff vortices appear, on the average, to last longer and, hence, to move farther than landing vortices. This result was not unexpected as departing aircraft are heavier, with a corresponding stronger vortex, than landing aircraft. There have been few takeoff accidents attributed to wake vortices; it was thus postulated that the various departure paths and distribution in heights of

AD-A068 925 TRANSPORTATION SYSTEMS CENTER CAMBRIDGE MASS F/G 1/2
AIRCRAFT WAKE VORTEX TAKEOFF TESTS AT TORONTO INTERNATIONAL AIR--ETC(U)
FEB 79 T SULLIVAN, J HALLOCK, B WINSTON

UNCLASSIFIED TSC-FAA-79-9 FAA-RD-78-143 NL

3 OF 3
AD
A068925



END
DATE
FILMED
6-79
DDC

the departing aircraft alleviated the vortex problem. The Toronto measurements confirm this postulate; the heavier and stronger vortex-producing aircraft usually are lower at a given location than the more vortex-prone lighter aircraft.

The only incomplete part of the data collection was the inability to monitor the region above the runway. If a vortex was not observed, it was not known whether it decayed or stalled over the runway. The laser velocimeter attempted to answer the question, but the limited data and the difficulty and expense in reducing and analyzing the laser data precluded a definitive response to the question.

8. CONCLUSIONS

The Toronto joint TSC/FAA/MOT project must be considered a success. Over 5000 takeoffs were monitored and the data produced valuable information on vortex dynamics and decay. A wind criterion analogous to that of the Vortex Advisory System has been tentatively identified which could permit reduced longitudinal spacings between departing aircraft. Since the project examined vortex behavior in a regime where only meager information existed (takeoffs), it is not surprising that new effects were also found.

Capacity restrictions due to wake-vortex-imposed separations are a major contributor to traffic delays at the large airports. The Vortex Advisory System should decrease delays through reduced interarrival times; the data collected at Toronto indicate that a similar system for reducing inter-departure times is possible. Additional data will be required, however, as the over 5000 takeoffs do not contain a sufficient number of Heavy aircraft to be statistically significant for a safety-related program.

The study of vortex decay has indicated that the same decay mechanisms are taking place for takeoff vortices as for landing vortices, but the relative frequencies of the three mechanisms are different. Turbulent decay seems to be the dominant mechanism; a new finding which will revise interpretation of turbulent decay theories is that the decay takes place from the outer portions of the vortex towards the center (not vice versa as existing theories predict). The McGowan vortex lifetime curve, which has been extensively employed in the literature, has been revised as a result of the Toronto tests.

Takeoff vortices appear, on the average, to last longer and, hence, to move farther than landing vortices. This result was not unexpected as departing aircraft are heavier, with a corresponding stronger vortex, than landing aircraft. There have been few takeoff accidents attributed to wake vortices; it was thus postulated that the various departure paths and distribution in heights of

9. REFERENCES

1. Gupta, V.P., "Vortex-related Accidents over the Ten-Year Period 1964-73," FAA-EM-75-6, Apr. 1975, Mitre Corp., McLean VA.

2. Hallock, J.N. and Eberle, W.R. (editors), "Aircraft Wake Vortices: A State-of-the-Art Review of the United States R&D Program," FAA-RD-77-23, Feb. 1977, DOT/Transportation Systems Center, Cambridge MA.

3. Hallock, J.N., Winston, B.P., Burnham, D.C., Sullivan, T.E., McWilliams, I.G., and Wood, W.D., "Joint US/UK Vortex Tracking Program at Heathrow International Airport, Vol. II: Data Analysis," FAA-RD-76-58.II, Sep. 1976, DOT/Transportation Systems Center, Cambridge MA.

4. Spitzer, E.A., Hallock, J.N., and Wood, W.D., "Status of the Vortex Advisory System," In: Proceedings of Aircraft Wake Vortices Conference, FAA-RD-77-68, June 1977, DOT/Transportation Systems Center, Cambridge MA, p. 326-334.

5. Little, C.G., "Acoustic Methods for the Remote Probing of the Lower Atmosphere," Proceedings of the IEEE, Vol. 57, No. 4, Apr. 1969, p. 571-578.

6. Burnham, D.C. and Sullivan, T.E., "Influence of Flaps and Engines on Aircraft Wake Vortices," J. of Aircraft, Vol. 11, No. 9, Sept. 1974, p. 591-592.

7. Hallock, J.N. and Negron, C., to be published in J. Aircraft.

8. Brashears, M.R., Lawrence, T.R., and Zalay, A.D., "Mobile Laser Doppler System Checkout and Calibration," FAA-RD-77-48, I and II, June 1977, Lockheed Missiles & Space Company, Huntsville, AL.

9. Tombach, I.H., "Observations of Atmospheric Effects on Vortex Wake Behavior," J. Aircraft, Vol. 10, No. 11, Nov. 1973, p. 641-647.

10. MacCready, P.B., Jr., "Operational Application of a Universal Turbulence Measuring System," AMS/AIAA Paper No. 66-364, Mar. 1966, AMS/AIAA Conf. on Aerospace Meterology, Los Angeles CA.

11. Brashears, M.R., Logan, N.A., and Hallock, J.N., "The Effect of Wind Shear and Ground Plane on Aircraft Wake Vortices," J. Aircraft, Vol. 12, No. 10, Oct. 1975, p. 830-833.

12. McGowan, W.A., "Aircraft Wake Turbulence Avoidance," Paper 72/6, 12th Anglo-American Aeronautical Conference, July 1971, Calgary SK, Canada.

13. Burnham, D.C., "Effect of Ground Wind Shear on Aircraft Trailing Vortices," AIAA J., Vol. 10, No. 8, Aug, 1972, p. 1114-1115.

14. Tombach, I.H., Bate, E.R., and MacCready, P.B., "Investigation of the Motion and Decay of the Vortex Wake of a Light Twin-Engine Aircraft," AV-FR-439, Oct. 1974, AeroVironment, Pasadena CA.

15. Hallock, J.N., "Monitoring Wake Vortex Strength Decay Near the Ground," J. Aircraft, Vol. 13, No. 10, Oct. 1976, p. 830-832.

16. Hallock, J.N., Burnham, D.C., Tombach, I.H., Brashears, M.R., Zalay, A.D., and Barber, M.R., "Ground-Based Measurements of the Wake Vortex Characteristics of a B747 Aircraft in Various Configurations," AIAA Paper 77-9, Los Angeles CA, 1977.

17. Hallock, J.N. (editor), "Proceedings of Aircraft Wake Vortices Conference," FAA-RD-77-68, June 1977, DOT/Transportation Systems Center, Cambridge MA.

APPENDIX A
SPECIAL HELICOPTER TESTS

The Canadian military requested that the Ministry of Transport provide them with information concerning the possible hazard due to the vortices shed from heavy helicopters, expecially in control-zone operation or operations where heavy helicopters work in close proximity to each other. It was decided that the Toronto test site could be used to obtain information on the characteristics of these vortices. The superintendent, Aerospace and Criteria, granted special permission to perform dedicated testing of helicopter vortices at the test site. A Boeing Vertol 114 (H47 Chinook) helicopter was made available by the 450 Squadron of the Canadian Armed Forces for a one-day test.

Five series of tests, each containing five passes over the sensor systems, were defined. The first four series were performed with the helicopter operating at various speeds and climbing slightly as it passed through the sensor system. The heights of the helicopter were 30-40 ft (9-12 m), 50-60 ft. (15-18 m), and 70-80 ft (21-24 m), as it passed sensor lines 1, 2, and 3, respectively. A sketch of the flight path is given in Fig. A-1. The flight path for the fifth series of tests was designed to simulate an operational helicopter landing. The aircraft crossed line 1 at an altitude of 200 ft (60 m) and continued to descend to a landing point 400 ft (121 m) past line 2, as shown in Fig. A-2. The speed and gross weight for each run are given in Table A-1.

The results from these tests clearly demonstrated that the vortices from the helicopter could be detected by both the GWVSS and MAVSS. A detailed quantitative analysis of vortex behavior is, however, not possible with these results since the number of observed cases was not statistically significant. The results are tabulated in Table A-2. The analysis of the MAVSS data shows that the calculated helicopter circulation, when heavily loaded and travelling at the slowest speed (first series), compare with the

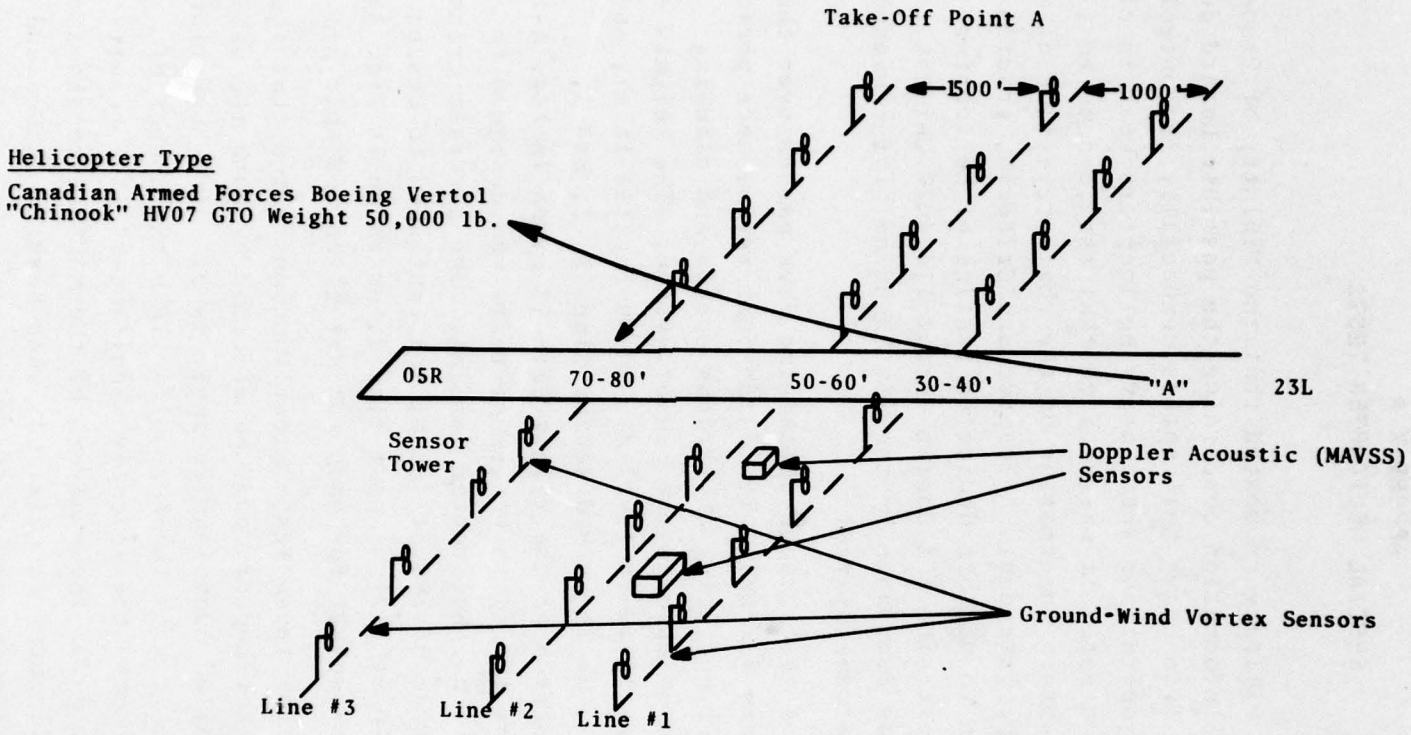


FIGURE A-1. HELICOPTER TAKEOFF FLIGHT PATH

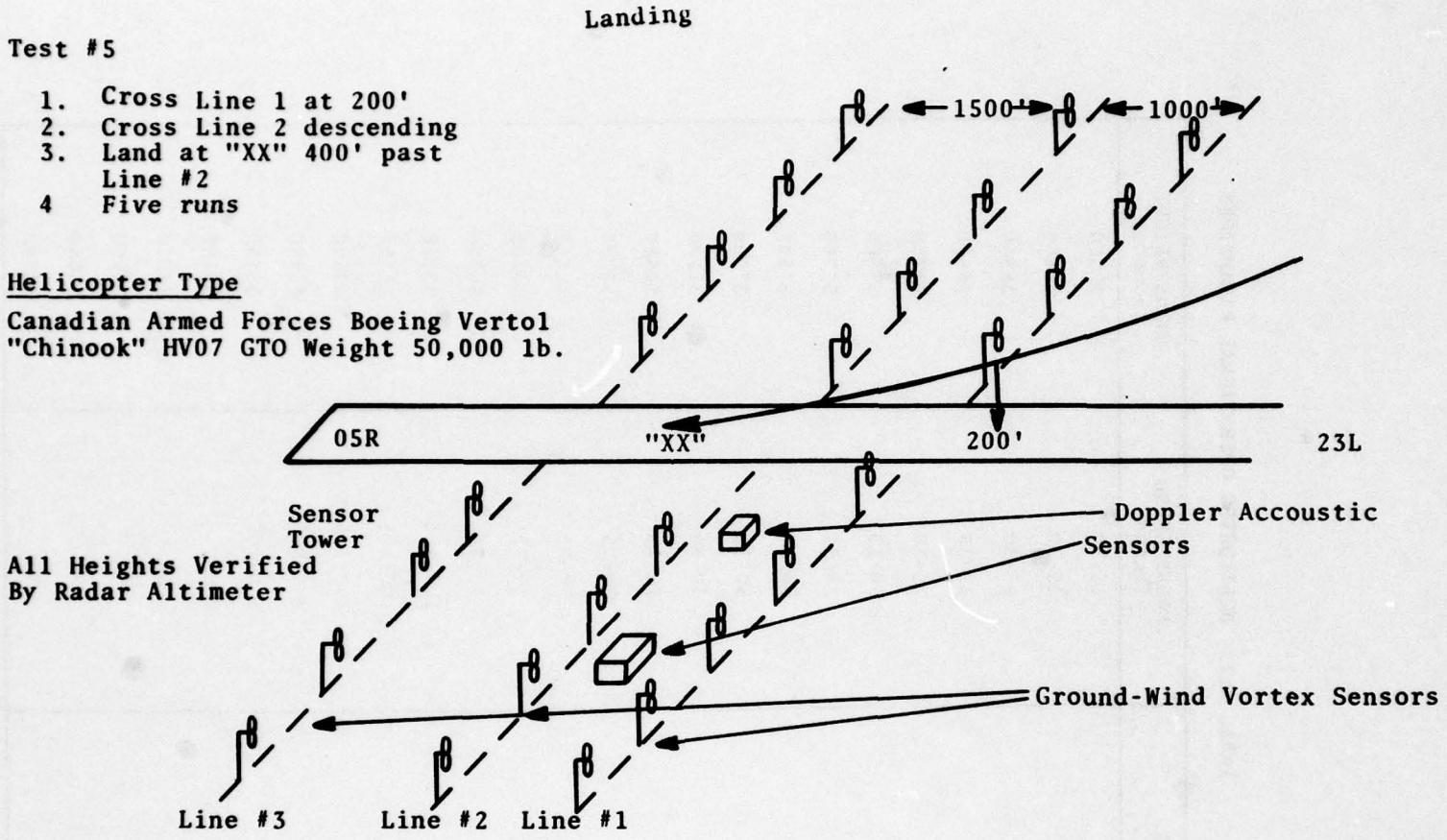


FIGURE A-2. HELICOPTER LANDING FLIGHT PATH

TABLE A-1. HELICOPTER OPERATIONAL PARAMETERS

RUN NO.	GROUND SPEED (knots)	GROSS WEIGHT (pounds)
1	25-30	39500
2	25-30	39100
3	25-30	38850
4	25-30	38600
5	25-30	38350
6	50-55	37900
7	50-55	37700
8	50-55	37500
9	50-55	37300
10	50-55	37100
11	70-75	36850
12	70-75	36700
13	70-75	36550
14	70-75	36400
15	70-75	36250
16	100-105	35850
17	100-105	35700
18	100-105	35550
19	100-105	35400
20	100-105	35250
21	NA	35100
22	NA	34950
23	NA	34800
24	NA	34650
25	NA	34500

NA: Not available.

average measured circulation of a DC-9 (from the data of Section 7.10), as shown in Fig. A-3. Heavy weight and slow speed are the conditions which are expected to produce the largest circulation as can be seen from the circulation equation (Ref. 2):

$$\Gamma = \frac{4W}{\pi \rho V b}$$

where W is the gross weight, ρ the air density, V the flight speed, and b the wingspan (the length of the rotor for helicopters).

The cases where a vortex remained in the ±200-ft (±60-m) corridor for longer than 60 seconds were isolated and are listed in Table A-3. It is surprising that the vortices remain in the corridor at relatively high crosswinds (~7 knots); it demonstrates the need for further controlled testing to investigate this phenomenon.

Analysis of the vortex tracks show two discrepancies with the logged flight parameters. First, the aircraft velocities in the first series of tests were reported to be 25-30 knots; analysis of the tracks leads to the conclusion that the velocities in this series were approximately 50 knots. A typical set of data for this series is shown in Fig. A-4. The detection of the port vortex on the third baseline clearly begins 30 seconds after the detection of the first vortex on the first baseline. Since the baselines are separated by 2500 ft (758 m), the calculated aircraft velocity is 49 knots.

Second, the detection of vortices on baseline number 3 during the last series of tests is contradictory. The flight path described in the test plan defines the helicopter landing at a point 400 ft (121 m) past baseline number 2. Since vortices cease to be generated when the aircraft touches the ground, no vortices should have been detected in line number 3.

TABLE A-2. HELICOPTER TEST RESULT SUMMARY

RUN NO.	1		2		3		4		5	
HELICOPTER SPEED (KTS)	25-30		25-30		25-30		25-30		25-30	
WIND U	-3.7		-3.6		-2.3		-2.3		-3.9	
WIND V	-3.5		-3.4		-8.3		-7.8		-6.5	
VORTEX	P	S	P	S	P	S	P	S	P	S
ANEMOMETER DATA										
LINE 1 DEATH TIME (seconds)	78	80	32	42	42	48	36	52	42	78
LINE 1 DEATH POSITION (feet)	-900	-250	-500	-150	-700	-300	-500	-250	-500	-300
LINE 2 DEATH TIME (seconds)	64	56	26	50	34	46	30	72	32	78
LINE 2 DEATH POSITION (feet)	-800	-200	-400	-200	-500	-400	-450	-450	-450	-400
LINE 3 DEATH TIME (seconds)	60	98	94	60	28	50	46	44	58	78
LINE 3 DEATH POSITION (feet)	-600	-400	-1300	-350	-450	-250	-700	-150	-700	-500

* NA - Not Available
NOV - No Observed Vortex,
** No A/C Detectors Fired For Run #17 ∴ No Data.

TABLE A-2. HELICOPTER TEST RESULT SUMMARY (CONT'D)

RUN NO.		6		7		8		9		10	
HELICOPTER SPEED (KTS)		50-55		50-55		50-55		50-55		50-55	
WIND	U	-1.2		-3.7		-2.8		-2.1		-.4	
	V	-6.4		-4.5		-4.3		-5.3		-5.0	
VORTEX		P	S	P	S	P	S	P	S	P	S
ANEMOMETER DATA											
LINE 1	DEATH TIME (seconds)	30	64	42	88	18	NOV*	22	NOV*	34	62
	DEATH POSITION (feet)	-450	-300	-500	-450	-200	NOV	-250	NOV	-400	-400
LINE 2	DEATH TIME (seconds)	36	48	30	58	24	22	56	106	24	48
	DEATH POSITION (feet)	-450	-350	-350	-200	-150	150	-450	-350	-200	-200
LINE 3	DEATH TIME (seconds)	38	82	58	80	36	84	42	44	22	36
	DEATH POSITION (feet)	-500	-300	-700	-600	-400	-400	-400	-200	-300	-200

* NA - Not Available
NOV - No Observed Vortex
** No A/C Detectors Fired For Run #17 ∴ No Data.

TABLE A-2. HELICOPTER TEST RESULT SUMMARY (CONT'D)

RUN NO.	11		12		13		14		15	
HELICOPTER SPEED (KTS)	75-80		75-80		75-80		75-80		75-80	
WIND U	-3.1		-1.9		-5.9		-4.8		-3.3	
WIND V	-6.0		-2.3		-1.8		- .7		-3.7	
VORTEX ANEMOMETER DATA	P	S	P	S	P	S	P	S	P	S
LINE 1 DEATH TIME (seconds)	30	22	44	108	54	NOV	82	NOV	30	NOV
LINE 1 DEATH POSITION (feet)	-400	150	-200	150	-500	NOV	-500	NOV	-200	NOV
LINE 2 DEATH TIME (seconds)	44	46	70	120	40	NOV	52	12	NOV	NOV
LINE 2 DEATH POSITION (feet)	-400	-200	500	450	-200	NOV	-250	200	NOV	NOV
LINE 3 DEATH TIME (seconds)	30	NOV	NOV	102	NOV	NOV	70	NOV	46	40
LINE 3 DEATH POSITION (feet)	-350	NOV	NOV	400	NOV	NOV	-450	NOV	-400	-150

* NA - Not Available
NOV - No Observed Vortex .
** No A/C Detectors Fired For Run #17 ∴ No Data.

TABLE A-2. HELICOPTER TEST RESULT SUMMARY (CONT'D)

RUN NO.		16		17		18		19		20	
HELICOPTER SPEED (KTS)		100-105		100-105		100-105		100-105		100-105	
WIND	U	-1.5		**		-.5		-.9		-1.2	
	V	-2.7				-6.7		-7.3		-5.7	
VORTEX ANEMOMETER DATA		P	S	P	S	P	S	P	S	P	S
LINE 1	DEATH TIME (seconds)	48	NOV	**	**	46	NOV	80	NOV	44	36
	DEATH POSITION (feet)	-400	NOV			-250	NOV	-1100	NOV	-500	-350
LINE 2	DEATH TIME (seconds)	22	NOV			30	NOV	98	156	38	52
	DEATH POSITION (feet)	-150	NOV			-200	NOV	-1100	-700	-600	-300
LINE 3	DEATH TIME (seconds)	28	NOV			62	26	84	22	44	NOV
	DEATH POSITION (feet)	-250	NOV			-300	-250	-350	-300	-500	NOV

* NA - Not Available
NOV - No Observed Vortex.
** No A/C Detectors Fired For Run #17 ∴ No Data.

TABLE A-2. HELICOPTER TEST RESULT SUMMARY (CONT'D)

RUN NO.	21		22		23		24	
HELICOPTER SPEED (KTS)	NA*		NA		NA		NA	
WIND U	-.3		.4		.1		.3	
WIND V	-7.7		-6.4		-5.5		-5.0	
VORTEX ANEMOMETER DATA	P	S	P	S	P	S	P	S
LINE 1 DEATH TIME (seconds)	82	62	50	58	90	42	52	50
LINE 1 DEATH POSITION (feet)	-900	-450	-600	-350	-700	-500	-500	-300
LINE 2 DEATH TIME (seconds)	70	NOV*	38	74	58	76	52	74
LINE 2 DEATH POSITION (feet)	-700	NOV	-500	-500	-500	-500	-500	-250
LINE 3 DEATH TIME (seconds)	26	NOV	22	NOV	58	30	48	NOV
LINE 3 DEATH POSITION (feet)	-350	NOV	-350	NOV	-800	-150	-600	NOV

* NA - Not Available
NOV - No Observed Vortex.
** No A/C Detectors Fired For Run #17 ∴ No Data.

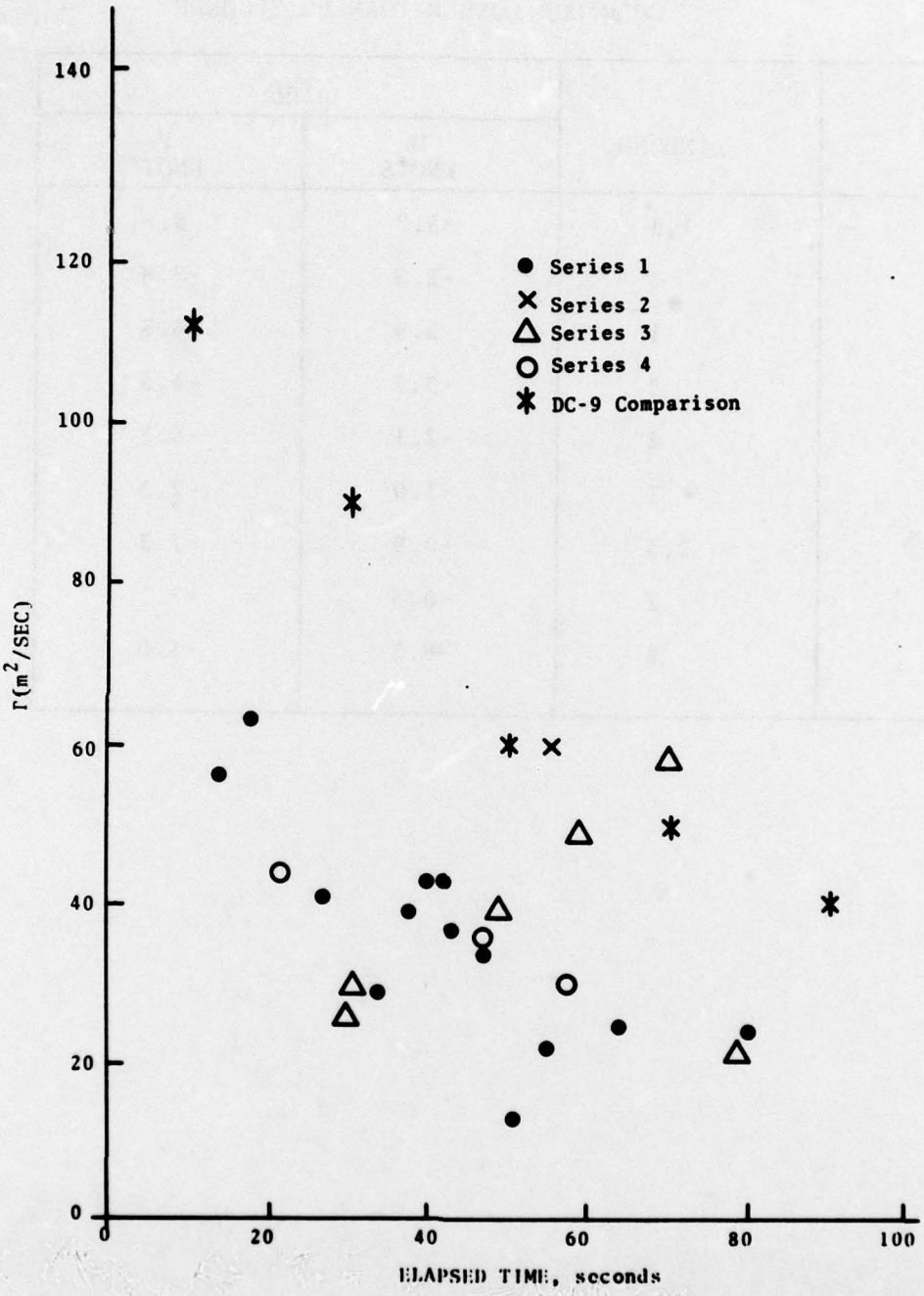


FIGURE A-3. HELICOPTER VORTEX CIRCULATION VERSUS ELAPSED TIME

TABLE A-3. HELICOPTER VORTICES WHICH WERE OBSERVED TO REMAIN IN THE REFERENCE CORRIDOR LONGER THAN 60 SECONDS

RUN NO.	LINE NO.	WIND	
		U KNOTS	V KNOTS
1	1,3	-3.7	-3.5
4	3	-2.3	-7.8
5	1	-3.9	-6.5
7	2	-3.7	-4.5
9	2	-2.1	-5.3
12	1	-1.9	-2.3
19	2,3	-0.9	-7.3
21	2	-0.3	-7.7
24	2	0.3	-5.0

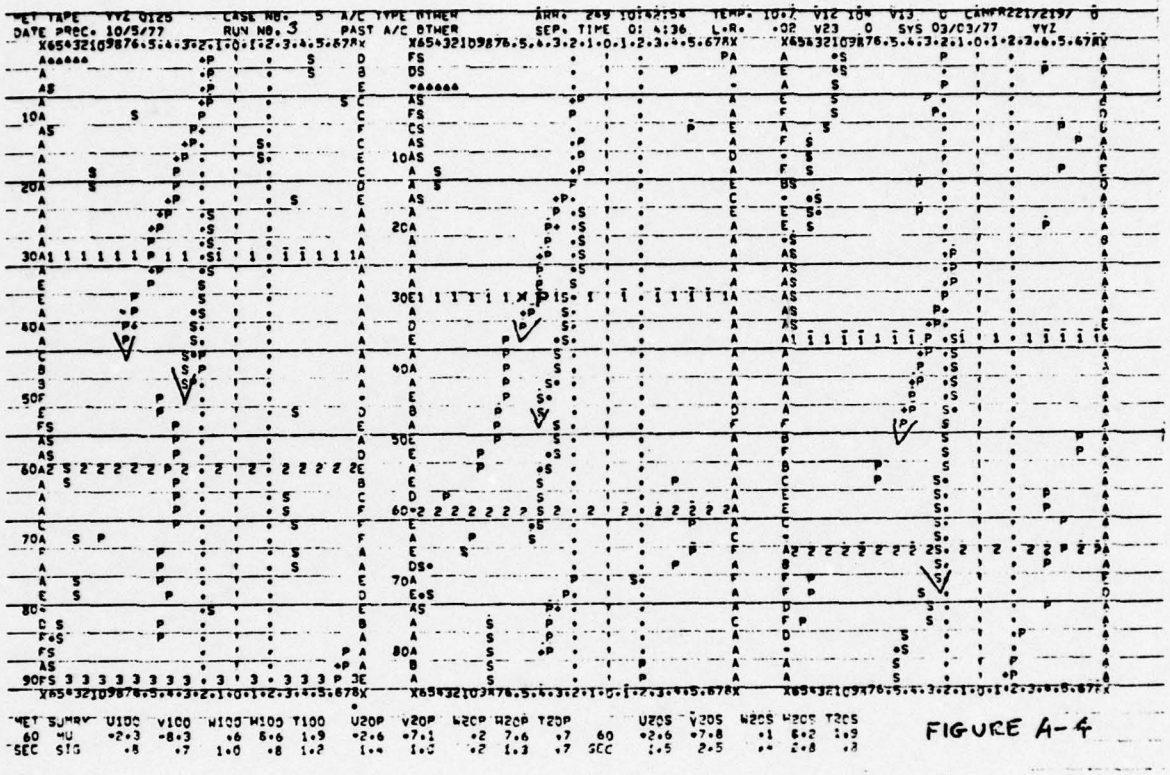


FIGURE A-4

FIGURE A-4. EXAMPLE OF A HELICOPTER GROUND-WIND TRACK

APPENDIX B

DATA BASE

All the data collected at the Toronto International Airport were reduced, converted to engineering units, and stored on magnetic tapes. These tapes formed the data base used in the data analyses. The following list indicates the information stored on the tapes.

ATTRIBUTE	EXPLANATION/COMMENT
Tape Number	GWVSS tape number
Run Number	GWVSS run number
Weather	Sunny, Cloudy, Rainy, Snowy, etc.
Aircraft Type	B-747, DC-8, etc.
Time Code	Julian Day: Hour: Minute: Second
Aircraft Speed	Speed (m/sec) measured between the three baselines
Temperature	Ambient temperature (°C)
Head Wind	60-sec average, three sensors (knots)
Cross Wind	60-sec average, three sensors (knots)
Vertical Wind	60-sec average, three sensors (knots)
Total Wind	Horizontal wind (knots)
Turbulence	In energy-dissipation rate units ($c/m^{2/3}/sec$)
σ_u	Standard deviation in 60-sec average head wind (Knots)
σ_v	Standard deviation in 60-sec average cross wind (Knots)
σ_w	Standard deviation in 60-sec average vertical wind (Knots)

σ_H	Standard deviation in 60-sec average total wind (Knots)
σ_T	Standard deviation in 60-sec average turbulence ($cm^{2/3}/sec$)
P Death Time	Lifetime of port vortex (seconds)
S Death Time	Lifetime of starboard vortex (seconds)
P Death Position	Location of port vortex when it died (meters)
S Death Position	Location of starboard vortex when it died (meters)
P1,S1	Location of vortices at 30 seconds (meters)
P2,S2	Location of vortices at 60 seconds (meters)
P3,S3	Location of vortices at 90 seconds (meters)
P4,S4	Location of vortices at 120 seconds (meters)
H1	Height of aircraft at baseline 1 (from photos) (meters)
H2	Height of aircraft at baseline 2 (from photos) (meters)
H3	Height of aircraft at baseline 3 (from photos) (meters)
MAVSS Run Number	When MAVSS data recorded
Antenna Number Location	Which antennas yielded strength data
Vortex Number	Port of starboard vortex
Vortex Age	Age of vortex at each antenna (seconds)
Transport Speed	Lateral speed of vortex crossing antenna (m/sec)
Vortex Height	Height of vortex above antenna (m)

Γ' (5 m)	Effective strength for b/2=5 m (m^2/sec)
Γ' (10 m)	Effective strength for b/2=10 m (m^2/sec)
Γ' (20 m)	Effective strength for b/2=20 m (m^2/sec)
Γ' (30 m)	Effective strength for b/2=30 m (m^2/sec)
Correlations	Numbers indicating quality of MAVSS data
Arrival Number	Number of antennas used to calculate transport speed.

250 Copies